



AD 748416

AD

AMMRC CR 66-05/31 (P)

CENTER FOR HIGH ENERGY FORMING

JUNE 1972

DR. I. R. KRAMER
Martin Marietta Corporation
Denver, Colorado

J. D. MOTE
E. F. Industries, Inc.
Louisville, Colorado

A. A. EZRA
University of Denver
Denver, Colorado

FINAL REPORT

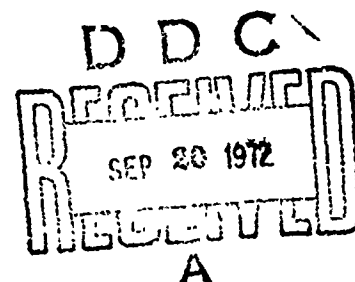
CONTRACT NUMBER DA 19-066-AMC-266(x)

Approved for public release; distribution unlimited.

Reproduced by
NATIONAL TECHNICAL
INFORMATION SERVICE
U S Department of Commerce
Springfield VA 22151

Prepared for

ARMY MATERIALS AND MECHANICS RESEARCH CENTER
Watertown, Massachusetts 02172



470

ACCESSION TAG	
NTIS	White Storage <input checked="" type="checkbox"/>
DDC	Buff Storage <input type="checkbox"/>
UNANNOUNCED	<input type="checkbox"/>
JURISDICTION	
BY	
A	

The findings in this report are not to be construed as an official Department of the Army position, unless so designated by other authorized documents.

Mention of any trade names or manufacturers in this report shall not be construed as advertising nor as an official indorsement or approval of such products or companies by the United States Government.

DISPOSITION INSTRUCTIONS

Destroy this report when it is no longer needed.
Do not return it to the originator.

Unclassified

Security Classification

DOCUMENT CONTROL DATA - R&D		
(Security classification of title, body of abstract and indexing annotation must be entered when the overall report is classified)		
1. ORIGINATING ACTIVITY (Corporate author) MARTIN MARIETTA CORPORATION University of Denver Denver, Colorado Denver, Colorado E. F. INDUSTRIES, INC., Louisville, Colo.		2a. REPORT SECURITY CLASSIFICATION Unclassified
		2b. GROUP N/A
3. REPORT TITLE CENTER FOR HIGH ENERGY FORMING-FINAL REPORT		
4. DESCRIPTIVE NOTES (Type of report and inclusive dates) FINAL REPORT		
5. AUTHOR(S) (Last name, first name, initial) Kramer, I. R., Mote, J. D., Ezra, A. A.		
6. REPORT DATE June 1972	7a. TOTAL NO. OF PAGES	7b. NO. OF REFS
8a. CONTRACT OR GRANT NO. DA 19-066-AMC-266 (X)	9a. ORIGINATOR'S REPORT NUMBER(S) AMMCR CR 66-05/31 (P)	
b. PROJECT NO. AMCMS Code 5900.21.25191	9b. OTHER REPORT NO(S) (Any other numbers that may be assigned this report)	
c.		
d.		
10. AVAILABILITY/LIMITATION NOTICES Distribution of this document is unlimited.		
11. SUPPLEMENTARY NOTES	12. SPONSORING MILITARY ACTIVITY Army Materials and Mechanics Research Center Watertown, Massachusetts 02172	
13. ABSTRACT This final report of the Center for High Energy Forming covers the work accomplished during the last year of the contract. The report includes surveys and analytical and experimental studies on various aspects of explosive metalworking. The categories covered include explosive forming, explosive welding, explosive powder compaction, explosive thermomechanical processing and a market analysis for custom metal heads.		

Unclassified
Security Classification

14 KEY WORDS	LINK A		LINK B		LINK C	
	ROLE	WT	ROLE	WT	ROLE	WT
High Energy Rate Forming Reviews Explosive Forming Shock Hardening Strain Rate Effects Plasticity Standoff Distance Ductility Explosive Welding Explosive Powder Compaction						

INSTRUCTIONS

1. **ORIGINATING ACTIVITY:** Enter the name and address of the contractor, subcontractor, grantee, Department of Defense activity or other organization (*corporate author*) issuing the report.

2a. **REPORT SECURITY CLASSIFICATION:** Enter the overall security classification of the report. Indicate whether "Restricted Data" is included. Marking is to be in accordance with appropriate security regulations.

2b. **GROUP:** Automatic downgrading is specified in DoD Directive 5200.10 and Armed Forces Industrial Manual. Enter the group number. Also, when applicable, show that optional markings have been used for Group 3 and Group 4 as authorized.

3. **REPORT TITLE:** Enter the complete report title in all capital letters. Titles in all cases should be unclassified. If a meaningful title cannot be selected without classification, show title classification in all capitals in parenthesis immediately following the title.

4. **DESCRIPTIVE NOTES:** If appropriate, enter the type of report, e.g., interim, progress, summary, annual, or final. Give the inclusive dates when a specific reporting period is covered.

5. **AUTHOR(S):** Enter the name(s) of author(s) as shown on or in the report. Enter last name, first name, middle initial. If military, show rank and branch of service. The name of the principal author is an absolute minimum requirement.

6. **REPORT DATE:** Enter the date of the report as day, month, year; or month, year. If more than one date appears on the report, use date of publication.

7a. **TOTAL NUMBER OF PAGES:** The total page count should follow normal pagination procedures, i.e., enter the number of pages containing information.

7b. **NUMBER OF REFERENCES:** Enter the total number of references cited in the report.

8a. **CONTRACT OR GRANT NUMBER:** If appropriate, enter the applicable number of the contract or grant under which the report was written.

8b, 8c, & 8d. **PROJECT NUMBER:** Enter the appropriate military department identification, such as project number, subproject number, system numbers, task number, etc.

9a. **ORIGINATOR'S REPORT NUMBER(S):** Enter the official report number by which the document will be identified and controlled by the originating activity. This number must be unique to this report.

9b. **OTHER REPORT NUMBER(S):** If the report has been assigned any other report numbers (*either by the originator or by the sponsor*), also enter this number(s).

10. **AVAILABILITY/LIMITATION NOTICES:** Enter any limitations on further dissemination of the report, other than those

imposed by security classification, using standard statements such as:

- (1) "Qualified requesters may obtain copies of this report from DDC."
- (2) "Foreign announcement and dissemination of this report by DDC is not authorized."
- (3) "U. S. Government agencies may obtain copies of this report directly from DDC. Other qualified DDC users shall request through _____."
- (4) "U. S. military agencies may obtain copies of this report directly from DDC. Other qualified users shall request through _____."
- (5) "All distribution of this report is controlled. Qualified DDC users shall request through _____."

If the report has been furnished to the Office of Technical Services, Department of Commerce, for sale to the public, indicate this fact and enter the price, if known.

11. **SUPPLEMENTARY NOTES:** Use for additional explanatory notes.

12. **SPONSORING MILITARY ACTIVITY:** Enter the name of the departmental project office or laboratory sponsoring (*paying for*) the research and development. Include address.

13. **ABSTRACT:** Enter an abstract giving a brief and factual summary of the document indicative of the report, even though it may also appear elsewhere in the body of the technical report. If additional space is required, a continuation sheet shall be attached.

It is highly desirable that the abstract of classified reports be unclassified. Each paragraph of the abstract shall end with an indication of the military security classification of the information in the paragraph, represented as (TS), (S), (C), or (U).

There is no limitation on the length of the abstract. However, the suggested length is from 150 to 225 words.

14. **KEY WORDS:** Key words are technically meaningful terms or short phrases that characterize a report and may be used as index entries for cataloging the report. Key words must be selected so that no security classification is required. Identifiers, such as equipment model designation, trade name, military project code name, geographic location, may be used as key words but will be followed by an indication of technical context. The assignment of links, rule, and weights is optional.

Unclassified

Security Classification

AMMRC CR 66-05/31 (F)

CENTER FOR HIGH ENERGY FORMING

DR. I. R. KRAMER
Martin Marietta Corporation
Denver, Colorado

J. D. MOTE
E. F. Industries, Inc.
Louisville, Colorado

A. A. EZRA
University of Denver
Denver, Colorado

June 1972

FINAL REPORT

Contract Number DA 19-066-AMC-266(x)

D/A Project ARPA NO. 720

AMCMS Code 5910.21.25191

High Energy Rate-Forming Process in Metals

Approved for public release; distribution unlimited.

Prepared for

ARMY MATERIALS AND MECHANICS RESEARCH CENTER
Watertown, Massachusetts 02172

FOREWORD

This is the final report of the Center for High Energy Forming. The report covers the work accomplished only during the seventh year's effort since the prior work has been published in previous annual reports. The work reported herein covers explosive forming, explosive welding and explosive powder compaction.

TABLE OF CONTENTS

	<u>Page</u>
Foreword	ii
Table of Contents	iii
INTRODUCTION	1
History of the Center for High Energy Forming	1
Accomplishments in the Coupling of Science and Technology	3
Present Spinoff Activities and Future Prospects	13
<u>Figures (Introduction)</u>	
1. Explosively Formed 10' Diameter Dome Out of 2014-0 Aluminum Alloy	4
2. Pipe Joint-Explosively Welded Under Simulated Field Conditions	6
3. Examples of Explosively Welded Pipe Joints	7
4. Explosive Forming Facility of NOTS-Louisville	9
5. Ti-6Al-4V Composite Structure Explosively Welded Simultaneously on Both Sides to Center Stringers	10
6. Explosive Spot Weld of Lead to Lead-Clad Steel	10
7. Copper to Steel and Aluminum to Steel Tube Explosive Welds	11
8. Small Finned Structure Explosively Welded	11
9. Aluminum Machining Chips and Bar Made From Chips by Explosive Compaction	13
10. Explosively Compacted Aluminum-Silicon Alloy and Carbide Tool Material.	13

TABLE OF CONTENTS

	<u>Page</u>
I. CLOSED DIE EXPLOSIVE FORMING	I.
Introduction	I-1
Closed Systems Explosive Forming Survey	I-2
Conclusions	I-7
II. ELEVATED TEMPERATURE EXPLOSIVE FORMING	II.
Introduction	II-1
System Requirements and Testing	II-1
Conclusions	II-4
III. EXPLOSIVE FORMING OF DOMES USING TRUNCATED CONICAL PREFORMS	III
Introduction	III-1
Preform Fabrication and Analysis	III-1
Experimental Results	III-5
Conclusions	III-18

Tables (Section III)

1. Tabulation of Theoretical Strain Values as Calculated for the Five Preform Geometries	III-6
2. Conditions of Test and Strain Resulting from Explosive Forming Tests	III-9

Figures (Section III)

1. Truncated Cone Preform	III-2
2. Layout & Dimensions for the 26° Cone Preforms	III-3
3. Theoretical Strain Values as Established For Conical Preforms with a Cone Angle Range of 45-80°	III-7
4. Maximum Values of Circumferential Cone Strain as Determined Experimentally with Respect to Preform Cone Angle	III-10
5. Average Values of Meridional Cap Strain as Determined Experimentally With Respect to Preform Cone Angle	III-12

TABLE OF CONTENTS

Page

Figures (Continued - Section III)

6. Average Values of Meridional Cone Strain is
Determined Experimentally with Respect to Preform
Cone Angle III-13
- 7a. Thickness Strain Versus Position on Cone Segment
of Preform III-15
- 7b. Thickness Strain Versus Position on Cone Segment
of Preform III-16
8. Thickness Strain of the Cap Section of the Preform
as a Function of the Cone Angle. III-17

- IV. ANALYSES OF DIE STRESS DURING EXPLOSIVE FORMING. . . . IV.
- Introduction IV-1
- Experimental Setup and Results IV-3
- Theoretical Consideration IV-11
- Energy Approach IV-11
- Pressure Approach IV-15
- Comparison of Analytical to Experimental Results . . IV-19
- Die Design Criteria. IV-19

Tables (Section IV)

1. 18% Ni Maraging Steel Data IV-12
2. Analytical Results for Maximum Compression Stress. . . IV-20
3. Analytical to Experimental Stress Ratios IV-21

Figures (Section IV)

1. Schematic of Die Test Setup IV-4
2. Block Diagram of the Instrumentation System IV-5
3. Electrical Schematic of the Instrumentation Setup
for Measuring Elastic Die Strains IV-6

TABLE OF CONTENTS

	<u>Page</u>
<u>Figure (Continued - Section IV)</u>	
4. Typical Trace of Strain Versus Time (Positive Lap - Tensile)	IV-9
5. Maximum Compressive Die Stress Vs Scandoff Distance	IV-10
6. Geometry Used in Energy Analysis	IV-16
7. Geometry Used in Pressure Analysis	IV-18
8. Unribbed, Weight Efficient Die	IV-23
 V. COMPACTION OF POWDERS USING EXPLOSIVES	 V.
Introduction	V-1
Container Studies	V-2
Density Studies	V-4
Conclusions and Recommendations	V-9
 <u>Figures (Section V)</u>	
1. Schematic Sectional View of Container and Explosive Load	V-3
 <u>Tables (Section V)</u>	
1. Weight Ratios Required to Achieve Maximum Density . .	V-8
 VI. EXPLOSIVE FORMING OF PRESSURE VESSEL STEELS	 VI.
Introduction	VI-1
Materials and Forming Procedures	VI-2
Results and Discussion of Tests on A-285 Steel . . .	VI-6
Results and Discussion of Tests on A-515 Steel . . .	VI-12
Conclusions	VI-30
Future Work	VI-31

TABLE OF CONTENTS

	<u>Page</u>
<u>Figures (Section VI)</u>	
1. Typical Strain Distribution for Explosively Free Formed Domes	VI-5
2. Typical Strain Distribution for Explosively Formed Flat Bottom Domes	VI-5
3. Results of Tensile Tests on Stress Relieved A-285 Grade C Steel	VI-8
4. Results of Charpy Impact Tests on A-285 Grade C Steel	VI-11
5. Results of Tensile Tests on A-515, Grade C, Steel . .	VI-14
6. Results of Charpy Impact Tests on A-515, Grade 70, Steel-As-Received; Cold Rolled & Explosively Formed, * = 0.045 Strain	VI-24
7. Results of Charpy Impact Tests on A515, Grade 70 Steel - As-Received; Cold Rolled & Explosively Formed, * = 0.045 Strain	VI-25
8. Results of Sub-Size Charpy Impact Tests on A-515, Grade 70, Steel Cold Rolled & Explosively Formed . . .	VI-26
9. Results of Sub-Size Charpy Impact Tests on A-515, Grade 70, Steel Cold Rolled & Explosively Formed to * = 0.35 Effective Strain And Stress Relieved at 650°C for One Hour	VI-27
<u>Tables (Section VI)</u>	
1. Chemical & Mechanical Properties Specifications for A-285, Grade C and A-515, Grade 70 Steels	VI-3
2. Results of Tensile Tests Conducted on Stress Relieved A285, Grade C Steel	VI-7
4. Results of Charpy Impact Tests on A-285, Grade C, Steel	VI-10
5. Results of Tensile Tests Conducted on A-515, Grade 70 Steel	VI-13
6. Results of Tensile Tests Conducted on Stress Relieved A-515, Grade 70 Steel	VI-15

TABLE OF CONTENTS

Page

Tables (Section VI - Continued)

7. Results of Impact Tests on Base Stock of A-515, Grade 70, Steel	VI-19
8. Results of Charpy Impact Tests on A515, Grade 70 Steel Cold Rolled to 0.04 Effective Strain	VI-20
9. Results of Charpy Impact Tests on A515, Grade 70 Steel Explosively Formed 0.04 Effective Strain	VI-21
10. Results of Charpy Impact Tests on A515, Grade 70 Steel Cold Rolled to 0.35 Effective Strain	VI-22
11. Results of Charpy Impact Tests on A515, Grade 70 Steel, Explosively Formed, 0.35 Effective Strain	VI-23
12. Temperatures at Which an Impact Strength of 40'lb. Is Obtained in A515, Grade 70 Steel - As-Received, Cold Rolled and Explosively Formed to 0.04 Strain, and Stress Relieved	VI-28
VII. EDGE PULL IN IN EXPLOSIVELY FORMED DOMES.	VII
Summary	VII-1
Introduction	VII-2
Discussion of the Problem	VII-4
Mathematical Model	VII-9
Flange Analysis	VII-12
Continuity Conditions at the Edge	VII-14
Formulation of Rate of Work	VII-16
Rate of Work in Dome	VII-16
Rate of Work in Flange	VII-19
Method of Solution	VII-21

TABLE OF CONTENTS

	<u>Page</u>
Discussion of Results	VII-28
Extension of Markov's Principle to Include Inertia Effects	VII-30
Conclusions	VII-32
Appendix	VII-33
References	VII-36

Figures (Section VII)

1. Profiles of Statically & Dynamically Die Formed 2041-0 Aluminum Domes	VII-6
2a. Circumferential Strain Distribution in Statically & Dynamically Die Formed 2014-0 Aluminum Domes	VII-7
2b. Thickness Strain Distribution in Statically & Dynamically Die Formed 2014-0 Aluminum Domes	VII-7
3. Nomenclature for Dome and Flange.	VII-8
4. Blank Pull-In vs. Draw Depth - Comparison of Theory & Experiment	VII-23
5. Parametric Curves for Blank Pull-In vs. Draw Depth.	VII-24
6. Comparison of Linearly Extrapolated Theory with Experimental Values of Pull-In	VII-25
7. Comparison of Theory & Experiment for Thickness Strain Distribution - Static Forming	VII-26
8. Comparison of Different Bulge Test Theories - Thickness Strain Distribution	VII-27

Tables (Section VII)

1. Comparison of Instability Strains	VII-29
VIII. THE DESIGN AND ANALYSIS OF EXPLOSIVE FORMING THIN SHELL DIES	VIII
Summary	VIII-1
Nomenclature	VIII-2
Introduction	VIII-3

TABLE OF CONTENTS

	<u>Page</u>
Theory	VIII-4
a. Underwater Explosion Assumptions	VIII-4
b. Shell Response	VIII-5
Comparison with Experiments	VIII-9
Conclusions	VIII-18
Acknowledgements	VIII-18
References	VIII-19
<u>Figures (Section VIII)</u>	
1. Spherical Shell Element	VIII-6
2. Lowest Non-Zero Roots of Transcendental Equation for Calculating Maximum Radial Wall Deflection	VIII-10
3a. Location of Strain Gages in Test Setup	VIII-10
3b. Strain Gage Installation	VIII-12
4. Schematic of Electronics	VIII-13
5. Oscilloscope Trace of Output from Strain Gage on Al Die	VIII-13
6. Maximum Hoop Strain Versus Charge Weight-Comparison of Theory and Experiment	VIII-15
7a. Parametric Curves for Die Strains Versus Explosion Energy - Mild Steel	VIII-16
7b. Parametric Curves for Die Strains Versus Explosive Energy - Aluminum	VIII-16
8. Percentage Alleviation Versus Radius to Thickness Ratios	VIII-17
<u>Tables (Section VIII)</u>	
1. Die Strains	VIII-11
2. Die Strains	VIII-11

TABLE OF CONTENTS

	<u>Page</u>
IX. THE MECHANICS OF ENERGY TRANSFER FROM UNDERWATER EXPLOSIONS	IX.
Introduction.	IX-1
Background.	IX-3
Scope of Work	IX-5
Dynamic Response of the Blank	IX-5
Pressure-Time History	IX-7
<u>Figures (Section IX)</u>	
1. Schematic of Setup.	IX-2
2. Coordinate System Used.	IX-6
3. Coordinate System for the Expanding Gas Sphere.	IX-10
X. THE RADIAL PISTON APPROACH TO THE DYNAMIC AUTOFRETTAGE OF THICK WALLED FORGING DIES	
Summary	X-1
Nomenclature.	X-2
Introduction.	X-3
Radial Piston Method.	X-5
Mathematical Model of the Radial Piston Configuration	X-8
Governing Equations for the Radial Piston.	X-13
Governing Equations for the Outer Cylinder.	X-15
Numerical Results	X-19
1. Initial Explosion Pressure.	X-22
2. Piston Geometry	X-22
3. Material Properties	X-23
Experimental Program.	X-30
Explosive Autofrettage - No Piston.	X-34
The Autofrettage of a Production Forging Die.	X-39

TABLE OF CONTENTS

	<u>Page</u>
Conclusions	X-40
References	X-42
 <u>Figures (Section X)</u>	
1. Radial piston autofrettage configuration.	X-6
2. Predicted system response following detonation.	X-20
3. Effect of varying the initial explosion pressure.	X-23
4. Effect of varying the piston's wall thickness	X-25
5. Effect of varying the size of the piston	X-26
6. Effect of varying the piston material.	X-27
7. Comparison of experimental and predicted values of residual hoop stresses	X-28
8. Autofrettage configuration - production forging dies .	X-35
9. Autofrettage configuration - no radial piston	X-36
10. Radial expansion at the inner diameter	X-37
XI. PRELIMINARY ANALYSIS OF THE MARKET FOR CUSTOM METAL HEADS	XI.
Introduction	XI-1
Purpose	XI-1
Procedure	XI-1
Limitations	XI-2
Summary	XI-3
Overview of the Market	XI-5
Overview of Participants	XI-5
Segmentation of Head Industry	XI-6
Custom Specialty Producers	XI-7

TABLE OF CONTENTS

	<u>Page</u>
Engineering Design Firms	XI-8
Fabricators of Metal Vessels & Tanks	XI-9
Demand Criteria	XI-9
End-User Industries	XI-10
Types of Fabricated Structures	XI-10
Size of Market	XI-11
Custom Manufactured Heads	XI-11
Vessels and Metal Tanks, Custom Fabricated at Factory	XI-13
Distribution of Product Mix	XI-15
Outside Diameter	XI-15
Rolled Thickness	XI-15
Shape	XI-16
Type Metal	XI-16
Metal Plate Prices	XI-17
Metal Forming Price Group	XI-18
Geographic Concentration of Market	XI-19
Producers	XI-19
Fabricators	XI-19
Value of Shipments	XI-19
Key Market Considerations	XI-23
Transportation	XI-23
Steel Plate Size	XI-24
Custom Production	XI-25
Seasonality	XI-25

TABLE OF CONTENTS

	<u>Page</u>
Capital Investment	XI-26
Derived Demand	XI-26
Environmental	XI-26
Competition	XI-27
Imported Steelplate	XI-27
Future Implications	XI-28
Fabricators and Head Producers	XI-28
Head Product Mix	XI-28
End-User Industries	XI-29
Growth Potential	XI-30
 <u>Figures (Section XI)</u>	
1. Map of Location of Metal Plate Fabricators	XI-22
 <u>Tables (Section XI)</u>	
1. Value of Shipments of Vessels and Metal Tanks, Custom Fabricated at the Factory	XI-14
2. Value of Shipments by Geographic Area, Metal Tanks & Vessels, Custom Fabricated at Factory	XI-21
3. Expenditures for New Plant & Equipment, Manufacturing Industries	XI-32
 <u>Appendixes</u>	
XII EXPLOSIVE THERMOMECHANICAL PROCESSING	XII.
Introduction	XII-1
Experimental Details	XII-5
Materials	XII-5
Explosive Forming & Shock Loading Procedures	XII-8
Thermomechanical Processing Schedules	XII-13
Testing Procedures	XII-15

TABLE OF CONTENTS

	<u>Page</u>
Results & Discussion	XII-16
17-7 PH Stainless Steel	XII-16
Beta III Titanium Alloy	XII-28
Summary & Conclusion	XII-35

Figures (Section XII)

1. Schematic Side View of Rectangular Explosive Stretch Forming Die	XII-9
2. Explosive Stretch Forming Workpiece Configuration . .	XII-10
3. Explosively Stretch-Formed 17-7 PH S.S. Blank	XII-12
4. Microstructure of 17-7 PH S.S. Fabricated in the Solution Treated Condition (A). (500X)	XII-23
5. Effect of Reduction by Cold Rolling in Solution Treated Condition on As-Rolled & Aged Hardness of Beta III . .	XII-34

Tables (Section XII)

1. Standard Heat Treatments for ARMCO 17-7 PH Stainless Steel	XII-6
2. Explosive Forming Parameters	XII-14
3. Hardness Data for Undeformed, Cold-Rolled, & Explosively-Formed 17-7 PH S.S.	XII-17
4. Room-Temperature Tensile Properties of 17-7 PH S.S. Following Thermal Processing, Conventional TMP, or Explosive TMP	XII-20
5. Hardness & Room-Temperature Tensile Properties of Unformed, Cold-Rolled, & Explosively Formed Beta III Ti Alloy After Aging (900° F/8 hr.)	XII-30
6. Percentage Increase in Hardness (DPH) of Beta III Ti Due to Aging After Forming to 10% Reduction in Thickness	XII-32

TABLE OF CONTENTS

	<u>Page</u>
XIII. EXPLOSIVE POWDER COMPACTION	XIII.
Introduction	XIII-1
Compaction of Ancorsteel 1,000 Iron Powder . . .	XIII-3
Experimental Procedures	XIII-7
Experimental Results and Discussion	XIII-11
Conclusions	XIII-37
Development of Explosively Compacted Tungsten . .	XIII-40
Filament Reinforced Steel Composites	XIII-40
Experimental Procedures	XIII-42
Experimental Results and Discussion	XIII-45
Conclusions	XIII-49
Studies with Udimet 700	XIII-50
Compaction of Flat Billets	XIII-61

Figures (Section XIII)

1. Photomicrograph of Ancorsteel 1000 Powders, Showing Particle Shape	XIII-4
2. Dual Square Pipe Arrangement Showing (a.) Upper and Lower Cover Plates, (b.) Iron Powder, (c.) Inner Pipe, and (d) Outer Pipe	XIII-9
3. Assembled Dual Square Pipe Arrangement	XIII-9
4. Ancorsteel Compacts Measuring 3 X 3" and Thicknesses of 1/4, 1/2, 3/4, and 1"	XIII-12
5. Percent Theoretical Density Obtained with 3 X 3" Compacts as a Function of Loading Ratio of Explosive to Ancorsteel 1000 Powder	XIII-16

TABLE OF CONTENTS

	<u>Page</u>
6. Hardness As a Function of Ratio of Explosive to Ancorsteel 1000 Powder for 3 x 3 inch Compacts	XIII-17
7. Diametral Yield Strength as a Function of Ratio of Explosive to Ancorsteel 1000 Powder for 3 x 3 inch Compacts	XIII-18
8. Hardness and Diametral Yield Strength for 6 x 6 x 1/4 inch Billets as a Function of Increasing Ratio of 40% Dynamite to Ancorsteel 1000 Powder	XIII-20
9. Hardness as a Function of Sintering Time at 2050° F for Explosively and Conventionally Compacted Ancorsteel 1000	XIII-23
10. Result of Rolling Tests Relating Sintering Time at 2050° F to Amount of Reduction for Complete Cracking	XIII-25
11. Green Conventionally Compacted Specimen Showing Large Volume of Voids	XIII-26
12. Green Explosively Compacted Specimen Showing Relatively Small Amount of Porosity (1.1:1 SWP-5).	XIII-26
13. Conventionally Compacted Specimen Sintered One Hour at 2050° F	XIII-27
14. Explosively Compacted Specimen Sintered One Hour at 2050° (1.1:1 SWP-5)	XIII-27
15. Conventionally Compacted Specimen Sintered Twelve Hours at 2050° F	XIII-28
16. Explosively Compacted Specimen Sintered Twelve Hours at 2050° F	XIII-28
17. Hardness as a Function of Sintering Temperature for one Hour for Explosively and Conventionally Compacted Ancorsteel 1000	XIII-34
18. Photomicrograph of Conventional Compacted Ancorsteel after One Hour at 800° F	XIII-35
19. Photomicrograph of Explosively Compacted Ancorsteel after One Hour at 800° F	XIII-35

TABLE OF CONTENTS

	<u>Page</u>
20. Photomicrograph of Conventionally Compacted Ancorsteel after One Hour at 1400° F	XIII-36
21. Photomicrograph of Explosively Compacted Ancorsteel after One Hour at 1400° F	XIII-36
22. Photomicrograph of Conventionally Compacted Ancorsteel after One Hour at 2400° F	XIII-38
23. Photomicrograph of Explosively Compacted Ancorsteel after One Hour at 2400° F	XIII-38
24. Effect of Sintering Temperature on the Ability of Conventionally and Explosively Compacted Ancorsteel 1000 to be Cold Rolled	XIII-39
25. Sketch of Exploded View of Double Piston Arrangement Used to Compact Steel-Tungsten Composites	XIII-43
26. Schematic Sketch of Frame for Filament-Powder Arrangement	XIII-44
27. Tungsten Filament Reinforced Ancorsteel 1000 Composite after Explosive Compaction	XIII-48
28. Tungsten Filament Reinforced Ancorsteel 1000 Composite after Sintering One Hour at 2000° F . . .	XIII-48
29. Change in Density in Sintered Udimet 700 Compacts as a Function of Time and Temperature . .	XIII-54
30. Change in Density in Sintered Udimet 700 as a Function of Varying Times and Temperatures. . . .	XIII-56
31. Explosively Compacted U-700 Sintered for One Hour at 2050° F	XIII-57
32. Explosively Compacted U-700 Sintered for 24 Hours at 2050° F	XIII-57
33. Explosively Compacted U-700 Sintered for One Hour at 2100° F	XIII-59
34. Explosively Compacted U-700 Sintered for One Hour at 2150° F	XIII-59
35. Explosively Compacted U-700 Sintered for 24 Hours at 2150° F	XIII-60
36. Explosively Compacted U-700 Sintered for One Hour at 2200° F	XIII-60

TABLE OF CONTENTS

	<u>Page</u>
<u>Tables (Section XIII)</u>	
1. Properties of Ancorsteel 1000 Iron Powder. . . .	XIII-5
2. Properties of Explosives Used in Compaction Studies.	XIII-6
3. Average Properties of Green Explosively Compacted Billets	XIII-13
4. Physical Properties of Green and Sintered Isothermally at 2050° F Ancorsteel 1000 Iron Powder Billets Explosively and Conventionally Compacted	XIII-21
5. Physical Properties of Green and Sintered Isochronally for One Hour Ancorsteel 1000 Iron Powder Billets Explosively and Conventionally Compacted	XIII-31
6. Specifications on Udimet 700 Powder.	XIII-51
7. Results of Sintering Experiments With U-700 Compacts	XIII-53
 XIV. EXPLOSIVE WELDING	
Introduction	XIV-1
Metallurgical Investigation of Explosion Welded Copper-Nickel Composites.	XIV-3
A Preliminary Investigation of Nickel, Steel and Nickel/Steel Explosion Welding	XIV-5
Nickel	XIV-6
Steel	XIV-11
The Effect of Explosive Bonding and Heat Treatment on the Mechanical Properties of 6051 Aluminum Alloy Explosion Welds	XIV-17
 <u>Figures (Section XIV)</u>	
1. Detonation Velocity of IRECO DBA-10HV Explosive as a Function of Explosive Loading on Steel. . . .	XIV-7

TABLE OF CONTENTS

	<u>Page</u>
2. Parallel Plate Explosion Welding Configuration Used for Nickel, Steel and Aluminum Welding Experiments	XIV-8
3. Sectional View of Weld Tensile Test Specimen, Loading Ram, and Support Ring	XIV-9
4. Weld Tensile Strength as a Function of Explosive Loading for 3/16 in. Thick Nickel 200. IRECO DBA-10HV Explosive, 3/32 in standoff	XIV-10
5. Nickel Explosion Welded Interface. 6.7g/in ² of IRECO DBA-10HV Explosive and 3/32 in. Standoff. . .	XIV-12
6. Nickel Explosion Welded Interface. 10.3g/in ² of IRECO DBA-10HV Explosive and 3/32 Standoff.	XIV-12
7. Nickel Explosion Welded Interface. 11.8g/in ² of IRECO DBA-10HV Explosive and 3/32 in. Standoff . .	XIV-13
8. Nickel Explosion Welded Interface. 14.9g/in ² of IRECO DBA-10HV Explosive and 3/32 in. Standoff . .	XIV-13
9. Weld Tensile Strength as a Function of Explosive Loading for 1/4 in. Thick A-515 Grade 70 Steel. . .	XIV-14
10. A-515 Steel Explosion Weld Interface. 13g/in ² IRECO DBA-10HV Explosive and 1/8 in. Standoff . . .	XIV-15
11. A-515 Steel Explosion Weld Interface. 13g/in ² of IRECO DBA-10HV Explosive and 1/4 in. Standoff. .	XIV-15
12. Detonation Velocity of Red Cross 40% Extra Dynamite as a Function of Explosive Loading on Aluminum.	XIV-19
13. Effect of Explosive Loading on the Weld Tensile Strength of 1/4 in. Thick 6061-T4 Aluminum Alloy	XIV-21
14. Effect of Explosive Loading on the Weld Tensile Strength of 1/4 in. Thick 6061-T4 Aluminum Alloy. Red Cross 40% Dynamite and 1/8 in. Standoff	XIV-22
15. Effect of Explosive Loading on the Weld Tensile Strength of 1/4 in. Thick 6061-T4 Aluminum Alloy. Red Cross 40% Dynamite and 1/8 in. Standoff	XIV-23

TABLE OF CONTENTS

	<u>Page</u>
16. 6061-0 Aluminum Explosion Weld Interface. 8g/in ² of Red Cross 40% Dynamite and 1/8 in. Standoff	XIV-24
17. 6061-T4 Aluminum Explosion Weld Interface. 10g/in ² of Red Cross 40% Dynamite and 1/8 in. Standoff	XIV-27
18. 6061-T6 Aluminum Explosion Weld Interface. 8g/in ² of Red Cross Dynamite and 1/8 in. Standoff	XIV-29
19. Weld Tensile Strength as a Function of Annealing Temperature for 1/4 in. Thick 6061-0 Aluminum Alloy. 8g/in ² Red Cross 40% Dynamite Loading and 1/8 in. Standoff	XIV-31
20. Weld Tensile Strength as a Function of Annealing Temperature for 1/4 in. Thick 6061-T4 Aluminum Alloy. 10g/in ² Red Cross 40% Dynamite Loading and 1/8 in. Standoff	XIV-32
21. Weld Tensile Strength as a Function of Annealing Temperature for 1/4 in. Thick 6061-T6 Aluminum Alloy. 8g/in ² Red Cross 40% Dynamite Loading and 1/8 in. Standoff	XIV-33
22. Brinell Hardness as a Function of Annealing Temperature for Explosion Welded, Cold Rolled and Undeformed 6061-0 Aluminum Alloy. Data for 1/4 in. Thick Plate Welded with 8/in ² Red Cross 40% Dynamite and 1/8 in. Standoff	XIV-34
23. Brinell Hardness as a Function of Annealing Temperature, Cold Rolled and Undeformed 6061-T4 Aluminum Alloy. Data for 1/4 in. Thick Plate Welded with 10g/in ² Red Cross 40% Dynamite and 1/8 in. Standoff	XIV-35
24. Brinell Hardness as a Function of Annealing Temperature for Explosion Welded, Cold Rolled and Undeformed 6061-T6 Aluminum Alloy. Data for 1/4 in. Thick Plate Welded with 8g/in ² Red Cross 40% Dynamite and 1/8 in. Standoff	XIV-36
25. 6061-0 Aluminum Explosion Weld Interface after Annealing at 650° F for 3 hr. Welded using 8g/in ² Red Cross 40% Dynamite and 1/8 in. Standoff	XIV-37

TABLE OF CONTENTS

	<u>Page</u>
26. 6061-T4 Aluminum Explosion Weld Interface after Annealing at 650° F for 3 hr. Welded using 10g/in ² Red Cross 40% Dynamite and 1/8 in. Standoff	XIV-38
27. 6061-T6 Aluminum Explosion Weld Interface after annealing at 650° F for 3 hr. Welded using 8g/in ² Red Cross 40% Dynamite and 1/8 in. Standoff	XIV-39

Tables (Section XIV)

1. Brinell Hardness of Explosion Welded 6061 Aluminum Alloy	XIV-20
--	--------

INTRODUCTION

History of the Center for High Energy Forming

In 1964, the Advanced Research Projects Agency of the Department of Defense requested teams of Universities, private companies, and Government Laboratories to propose ways and means of bringing about a direct coupling between science and technology in the field of Materials Science.

About 65 such teams responded with proposals, some of the most noteworthy being the Massachusetts Institute of Technology and Texas Instruments, M.I.T. and A.D. Little, Cornell University and General Electric, Lockheed and Stanford University. In 1965 three contract awards were made, one to the University of Denver and the Martin Marietta Corporation for research in High Energy Forming, one to Washington University at St. Louis and the Monsanto Corporation for research on polymer composite materials, and one to a team composed of the Case Institute of Technology, Bell Aerosystems and the Union Carbide Corp. for research in carbon composites. A fourth contract award was made a year later for research in corrosion to a team composed of the Naval Research Laboratory, Lehigh University, Carnegie-Mellon University, the Boeing Aircraft Company and Georgia Institute of Technology.

Three years later, the results of an official evaluation of these efforts were made public in the November 25, 1968 issue of Scientific Research (P. 13) from which the following quotation is taken:

"The one highly successful coupling experiment has been the joint effort of the Martin Marietta Corporation and the University of Denver

to develop techniques for the explosive forming of metals. The work attracted support from the Army, Navy and Air Force, and the Army is expected to expand its support soon."

The Center for High Energy Forming was operated as a team effort between the University of Denver and Martin Marietta Corporation during the first six years, with Martin Marietta Corporation as the principal contractor. During the seventh year, the application effort was subcontracted to E.F. Industries, Inc. by Martin Marietta Corporation. Before executing said subcontract several alternative approaches for perpetuating the explosive metalworking technology were examined, namely:

- "status quo"
- complete phase out by Martin Marietta Corporation
- Martin Marietta Corporation controlled subsidiary operation
- sale of technology to another company

After careful consideration and analysis Martin Marietta Corporation made the decision to sell the technology to E.F. Industries, Inc. and concomitantly subcontracted the ARPA applications effort to E.F. Industries. The reason for this approach was that E.F. Industries offered the best opportunity for hardware applications of the technology not being restricted by strict product lines.

Throughout the ARPA funded research program, a continuous effort was made to identify suitable applications for explosive forming and welding. For each promising application that was identified, the potential

user of the application was requested to provide the funds to adapt existing explosive metalworking knowledge to the application. There were two good reasons for this approach. The first was that sometimes development work is much more expensive than research work, and without independent funding, a single development program could displace several research programs. The second, more important reason was that sponsor participation during the development program provided a strong incentive to use the process when the development program was complete.

Accomplishments in the Coupling of Science and Technology

The first obvious source of applications was within the Martin Marietta manufacturing plant. Air Force funds were obtained for developing an explosive forming process to produce one-piece weld-free 10 ft. diameter domes out of 2014-0 aluminum alloy for the Titan II liquid fuel rocket. An explosively formed dome is shown in Figure 1, along with the scale model which was used to verify the process before forming the full scale dome. Another Martin Marietta generated application was a 51 inch diameter 2014-0 aluminum dome for the Sprint missile, which was being spun. Army funds were obtained for a parallel explosive forming program to produce these domes. It was found that it was cheaper to explosively form them, and a dome of better material quality and dimensional accuracy was obtained. The spinning process was discontinued, and these domes are still being produced by explosive forming.



Figure 1. Explosively Formed 10 Ft. Dia. Dome out of 2014-0 Aluminum Alloy.

Another major application that was undertaken as a joint University of Denver-Martin Marietta project was the development of an explosive method for autofrettaging cannon. This project was funded by the U.S. Army Materials and Mechanics Center, Watertown, Massachusetts. A commercial spin-off from the project was the development of an explosive method for autofrettaging forging dies, particularly for application to high velocity hot forging methods. The Sunstrand Company of Denver has successfully evaluated an explosively autofrettaged forging die, and a patent application has been filed with the U.S. Patent Office.

More recently, a process has been developed by E.F. Industries for the production of first, second and third stage domes for the Spartan missile. These domes are fabricated from thin gauge 4340 steel and will be produced on a production basis starting later this year. The process was developed directly from principles evolved on the ARPA program. The following paragraphs discuss programs that have been evolved from the ARPA funded program but have not yet been utilized in production.

Explosive welding techniques were adapted to produce fast, highly reliable connections for pipelines in the field under the sponsorship of the Humble Oil and Pipe Line Company. A field demonstration was recently conducted (Figure 2) in which 200 ft. of pipeline were laid with explosively welded joints. This pipeline was then successfully hydraulically pressure tested, sectioned (Figure 3) and examined metallogically. Patents on details of the process are being applied for.



Figure 2. Pipe Joint - Explosively Welded Under Simulated Field Conditions.

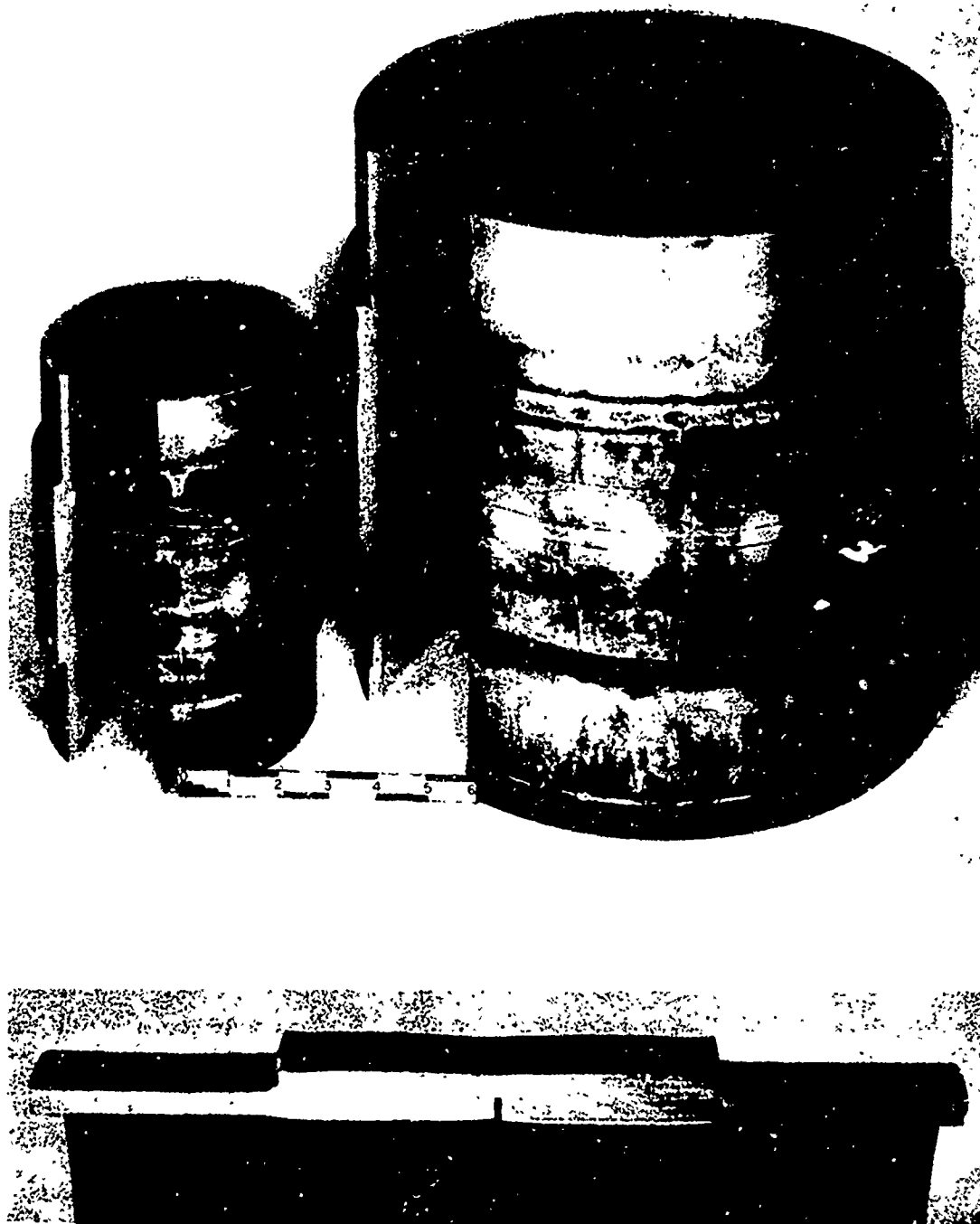


Figure 3. Examples of Explosively Welded Pipe Joints.

The Center for High Energy Forming undertook to provide an explosive forming and welding capability at the U.S. Naval Ordnance Test Station in Louisville, Kentucky. A team of engineers and technicians from N.O.T.S. was given a two week training course in explosive metalworking by the staff of the Center for High Energy Forming, who also designed an explosive forming facility for them. This explosive forming facility was built in 1969 and passed all tests (Figure 4). It has been in use for over two years, and the N.O.T.S. team trained by the Center has developed several successful applications of high energy forming to U.S. Navy needs. At present, the Center is developing, under separate contract, an explosive forming technique for fabrication of large thick hemispheres (12 ft. dia. x 6 inches thick) for the U.S. Naval Ordnance Test Station.

Explosive welding development projects have been undertaken for a variety of sponsors. Techniques were developed for the Boeing Company to explosively bond Titanium 6Al-4V skins to stringers (Figure 5). Explosive welding of lead to steel was developed for the International Lead and Zinc Organization. Examples of explosive spot welds of lead to lead-clad steel are shown in Figure 6. An example of explosively bonding a copper tube to a steel tube and an aluminum tube to a steel tube are shown in Figure 7.

Explosives can also be used to bond small parts together which are difficult to bond by conventional methods. An example is shown in Figure 8 where a small finned structure has been explosively welded together.

Reproduced from
best available copy.

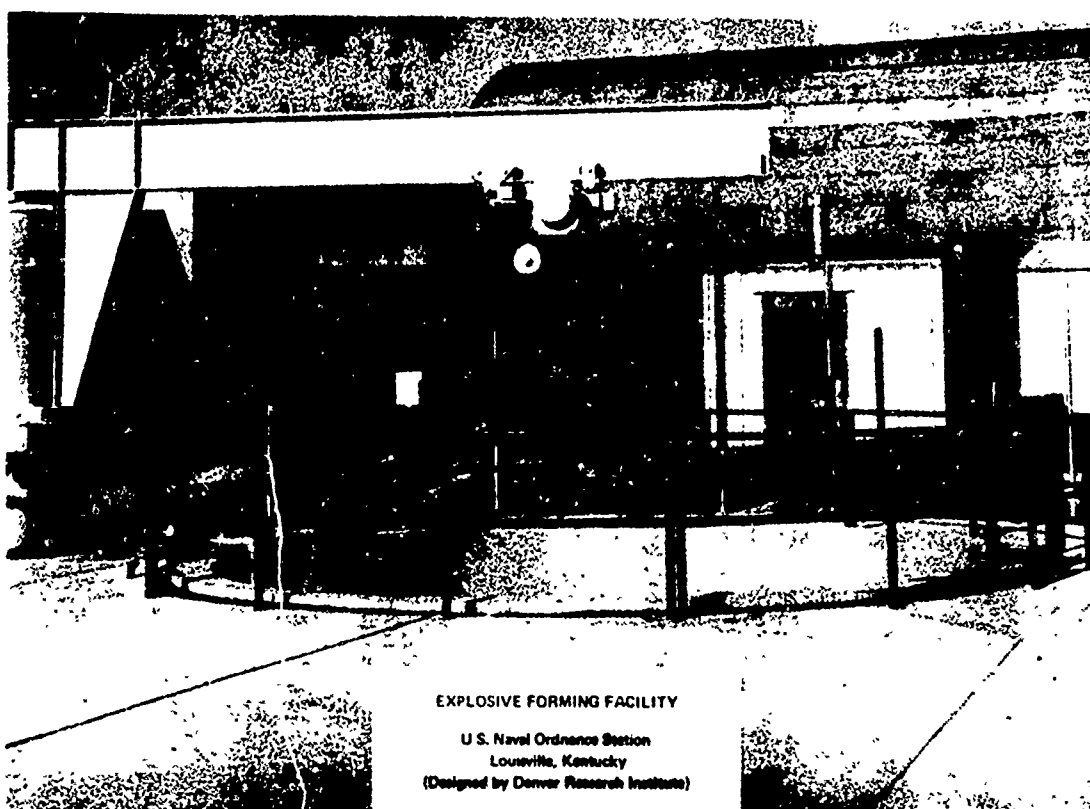


Figure 4. Explosive Forming Facility of NOTS-Louisville.

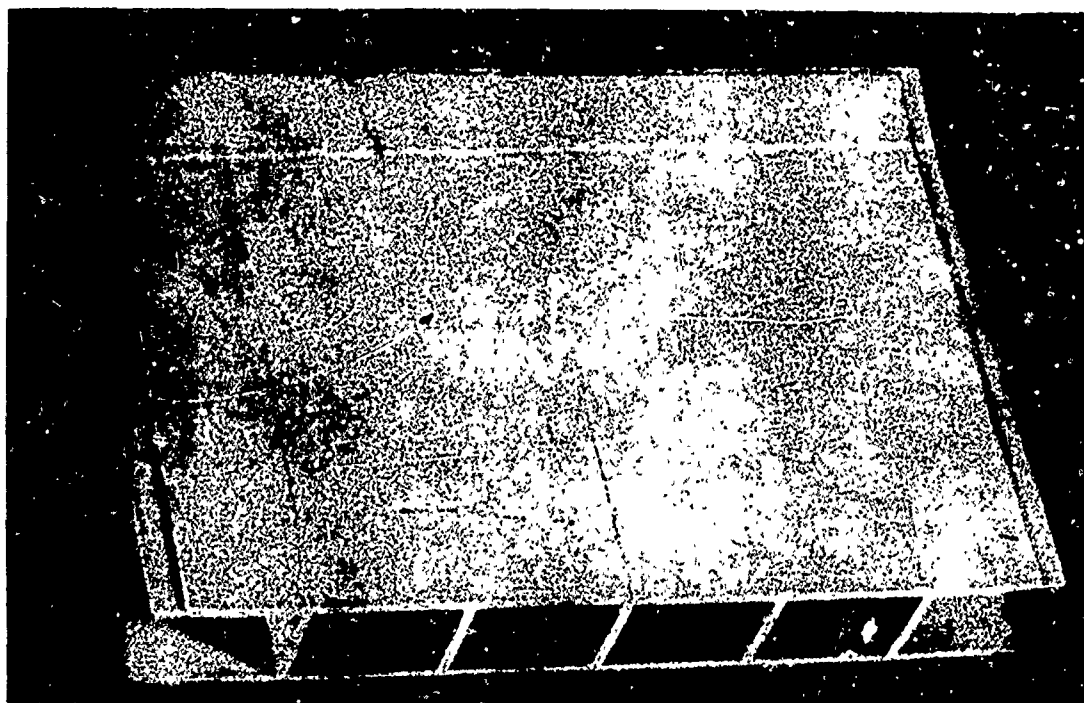


Figure 5. Ti 6Al 4V Composite Structure Explosively Welded Simultaneously on Both Sides to Center Stringers.

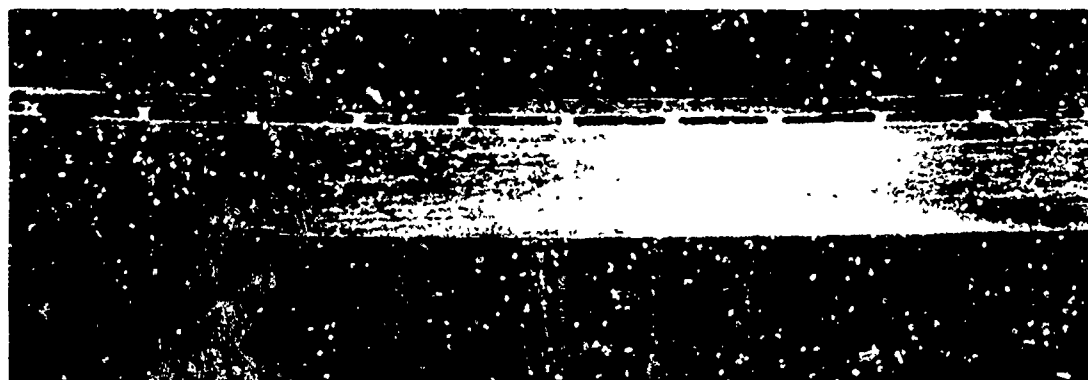


Figure 6. Explosive Spot Weld of Lead to Lead-Clad Steel.

Reproduced from
best available copy.



Figure 7. Copper to Steel and Aluminum to Steel Tube Explosive Welds.



2 3 4 5 6 7 8 9 1 2 3 4 5 6 7 8 9
THE L.S. BARRITT CO. 3 A740-1085-034
2 3 4 5 6 7 8 9 1 2 3 4 5 6 7 8 9

Figure 8. Small Finned Structure Explosively Welded.

Explosive compaction of metal powders has been undertaken with a high degree of success at the Center for High Energy Forming. An example of a bar explosively compacted from aluminum machining chips is shown in Figure 9. Explosively compacted aluminum-silicon alloy and carbide tool material are shown in Figure 10.

The results of the basic ARPA funded research programs have been presented in numerous technical papers, and in a book entitled "Principles and Practice of Explosive Metalworking" which is in press. The list of published papers is given in Appendix A.

Several graduate students, supported by the Center for High Energy Forming at the University of Denver have been awarded advanced degrees from both the Metallurgy and Materials Science Department and the Department of Mechanical Sciences and Environmental Engineering. A list of students earning advanced degrees, whose dissertations were on High Energy Forming is given in Appendix B. A list of graduate students presently enrolled is given in Appendix C.

The educational significance of the program of the Center for High Energy Forming is that each student's graduate thesis was selected to fill a technical need that had been identified in the effort to carry out a practical application. Each student was conscious of the contribution he was making in converting scientific knowledge into technology, and was left with a heightened awareness of the relationship between the two as well as the differences. It will be instructive to follow the careers of the graduate students on this program.

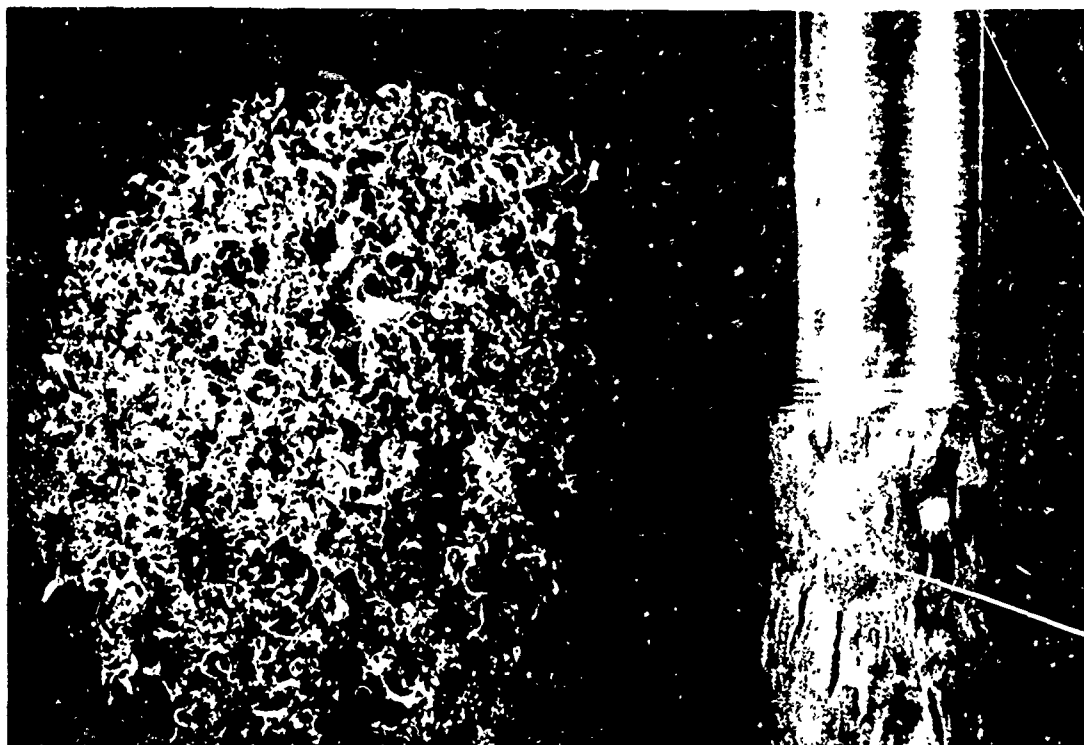


Figure 9. Aluminum Machining Chips and Bar made from Chips by Explosive Compaction.

Reproduced from
best available copy.

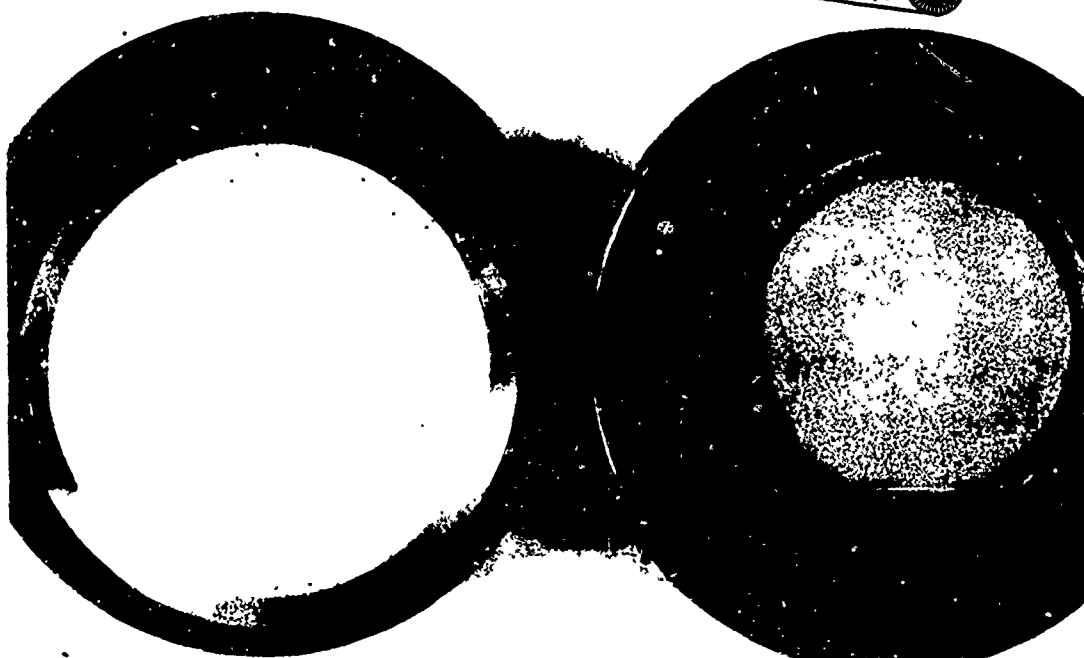


Figure 10. Explosively Compacted Aluminum-Silicon Alloy and Carbide Tool Material.

Present Spin-off Activities and Future Prospects

From its inception, the Center for High Energy Forming has sought outside sources of support to expand its activities, to find applications for its research discoveries, and to ensure the relevance of its research program to technological needs as well as to lay the groundwork for a permanent Center. Some of its previous spin-off activities were described above. Present spin-off contracts in High Energy Forming at the University of Denver are the following:

		FY72
1. Explosive Joining of Pipeline	Humble Oil & Pipe Line Company	\$85,000
2. Development of an Explosively Bonded TZM Wire Reinforced Dieless Columbium Sheet Composite	NASA, Marshall Space Flight Center	\$38,410
3. Explosive Forming of Thick Walled Domes	Naval Ordnance Station, Louisville, Kentucky	\$50,000
4. Underwater Explosive Welding	Naval Ordnance Station, Louisville, Kentucky	\$25,000
5. Impulse Welding Development Phenomenological Experiments	Department of Air Force	\$50,000
6. Effect of Dynamic Deformation on Aging of Superalloys	Naval Air Systems Command	\$42,000

These programs are intended to provide an orderly transfer from essentially full government support of the Center to other sources from both the government and private sector.

Current spin-off contracts at E.F. Industries directly related to the ARPA program include a contract with Martin Marietta Corporation for explosively welding Inconel 718 thin walled tubes to 6061 aluminum flanges

for space shuttle applications and a contract with the Army Materials and Mechanics Research Center (AMMRC) to develop the explosive welding process for making attachments to armor.

Another contract with AMMRC is designed to continue the coupling concept of the Center. This contract, to develop the explosive welding process for helicopter spars, continues the successful coupling formula of an industrial prime contractor, E.F. Industries, with a subcontract to a university, the University of Denver. Thus, the mechanism for production implementation is established at the inception of the program. Contracts of this type will enable the Center to continue in the coupling mode after the conclusion of the current contract.

I. CLOSED DIE EXPLOSIVE FORMING

L. J. Effenberger

Introduction

Explosive forming, in the past, has always been considered as a short run production or prototype method. However, higher volume production can be realized if suitable equipment is designed and fully utilized.

Only within the last ten years has the concept of an automated explosive system been considered an approachable goal from a design standpoint. The design of such machines has been undertaken and extensive research and development of semi-automatic forming tools have been carried out. For other high-energy-rate-forming processes, ie., electrohydraulic, electromagnetic and pneumatic-mechanical; production machines evolved almost simultaneously with the development of the principles and techniques of metal forming.

In order to automate the explosive process, either fully or partially, a closed system must be adopted to facilitate both the design and subsequent operation. The advantages of a closed explosive system are as follows:

1. reduction of noise level and concussion produced by the detonation of explosives,
2. increased charge efficiency, i.e., more work accomplished per unit of explosive weight, through the control of explosive energy to the work piece by means of explosives confinement and shock reflectors,
3. allows indoor operation,
4. feed and clamping mechanisms can be automated.

Closed Systems Explosive Forming Survey

Initial studies in the forming of metals using a low explosive powder charge were carried out by Lockheed in 1957. This was accomplished in a closed die using a firing head and 8-gauge shot gun shells (1 inch diameter) loaded with smokeless powder. The amount of pressure generated was limited only by the strength of the die and the firing mechanism. This system was designed for safe operation using pressures up to 50,000 psi.

Forming experiments were conducted on 4130 alloy steel and 347 stainless steel tubing. Using a female die with a closed pressure chamber and predetermined charge weights, tubing was expanded and formed to various shapes. This method utilized gas pressure applied to the inside surface of the tube to form the metal.

The Ford Motor Company also used a similar system to form jet engine inlet guide vanes in 1957. Welded preforms of .040 inch thick commercially pure titanium sheet were explosively sized. The load consisted of an 8-gauge shotgun shell calibrated for a maximum pressure of 10,000 psi. The gas pressure escaped from the firing chamber through an airfoil shaped opening in one face of the die and bulged the titanium preform outward to the final vane configuration.

The requirements for stainless steel and Hastelloy x parts for the 727 jet airplane resulted in the design and use of closed die forming. These thin wall bulged parts were fabricated by the Rohr Corporation in the early 1960's and are currently being produced by E. F. Industries. Closed

dies for diffuser, nozzle and duct parts were designed by Rohr to allow for the forming of these parts from welded tubing using 38 caliber and 12 gauge loadings of Red Dot powder. These charges are fired after the tubes are sealed in the forming dies and filled with water. In this forming method, the tubes are hydraulically bulged outward by the liquid pressure buildup in the closed system. This hydraulic pressure is produced by the expanding gaseous product which act upon the fluid "piston" contained in the sealed tube. The above parts are produced in a two shot forming sequence. A production rate of 2 to 3 parts per hour has been established for these bulged parts.

Preliminary development of a closed die system at Martin Marietta in 1965 showed the feasibility of a semi-automatic operation using chemical explosives. Two facing dies incorporating a rubber transfer media were used with the explosive being located between them. The two opposed dies allow for the production of 2 parts from one operation. The rubber pads, which were used as the energy transfer media, reduced the cycle time since the water fill operation was eliminated.

Pneumatic controls permitted opening and closing the system and part ejection was effected by bleeding air through the vacuum port of each die block. Placement of the blank and charge was accomplished manually. Semi-automated operation of this system, while forming 3 inch diameter aluminum hemispheres, yielded 24 to 36 parts per hour. Pre-packaged charges, automatic blank feed, charge feed, and part removal could easily permit the production of up to 300 parts per hour of small, simple shapes.

Subsequent development on a six-inch diameter hemispherical die system resulted in the following conclusions on this type of forming machine:

1. The rubber media does not function well for deep draw geometries since a w/d ratio of $\leq .25$ was determined to be the limit for rubber forming.
2. A vertical die arrangement, i.e., vertical tie rods, would improve die movement and clamping prior to the forming sequence.
3. The die system should be enclosed to minimize the noise level and maximize personnel safety during operation.
4. The charge feed and method of detonating the explosive present the most difficult automation problems.

The British have developed an "Explo-Forma" machine which was first reported in 1963. It was designed as an explosive forming machine which could be used to form sheets or tubes under conventional job shop conditions. Since the first prototype machine was developed, a fully automatic machine which feeds and removes the blanks and explosive charge has been developed.

The explosive charge is detonated in a completely closed, water filled cavity. As a result, an extremely low noise level, a complete absence of water splashing, and a much higher efficiency of explosive utilization is achieved.

Experience with the prototype machine showed that the major part of the cycle time was due to the time required for lowering and raising the bell off the die holder and filling it with water. Since these handling difficulties were likely to increase with a larger bell size, it was decided to invert the machine. In this position, the bell could be filled with water at all times.

This machine consists of three basic units:

1. the bell, forming the cavity within which the explosion takes place,
2. a die holder, containing the die and clamped to the bell by suitable means, and
3. an explosive holder.

A hydraulic power pack is required to move and clamp the parts. This, with a vacuum pump and simple control panel, completes the basic forming machine.

Efficiencies were calculated from strain measurements to determine the relative efficiencies of a completely open, partially closed, and a completely closed system. The calculations showed that the closed systems had the highest efficiency. The parabolic reflector shows an efficiency increase of 50% above that of an open system while the conical reflector showed an improvement of about 30%.

This machine has been used in semi-automatic operations to produce parts up to 20 inches in diameter. The bell or reflector strength limited the explosive charge size to about 24 grams of PETN.

An integrated high energy forming machine was developed under a United States Air Force contract by Vaught Aeronautics Division of L.T.V. Aerospace Corporation. The objective of the program was to increase the production capabilities of high energy forming beyond the present "state-of-the-art" by developing a new and highly mechanized HEF system. This system would be capable of fabricating sheet metal parts and materials beyond the limits of present conventional forming equipment. This was

possible by the means of integrating high explosive, hydrostatic and electrohydraulic forming processes into one system.

The resulting integral forming machine was 17 feet tall by 9 feet wide by 5 feet deep and weighed 98 tons. A 25,000 ton hydraulic clamping system is used to generate 50,000,000 pounds of clamping force. The energy chamber was designed to contain 50,000 psi with a safety factor of 2.0. Several special mechanisms were designed and constructed to permit the integration of various high energy forming systems into the basic energy chamber. These included:

1. special high pressure manifolds for introducing liquids and gases,
2. a multifiring high explosive gun,
3. a coaxial electrode and transducer for the capacitor discharge system,
4. an exhaust probe for removing the contents of the energy chamber after forming.

The forming machine operated in a semi-automatic mode and demonstrated the feasibility of a mechanized high energy forming machine. All machine functions necessary for the utilization of the integrated forming systems operated successfully except for the gas combustion process. The high pressure liquid, high explosive and electrohydraulic process showed very good integration compatibility as both singular and combined forming processes in the HEF machine. The high energy forming machine does extend its manufacturing capabilities beyond those of conventional forming equipment. It must be realized, however, that the HEF machine was not intended

to operate or to be competitive with conventional forming systems where the forming task lies within the capabilities of conventional equipment.

Conclusions

Based on the survey of closed die systems utilizing chemical explosives, the following design criteria were established:

1. The system will operate in the vertical direction only.
2. Water will be used as the transfer medium either in an open or closed system.
3. The forming tool will be designed, in most cases, with respect to one part configuration and not designed to facilitate the forming of all possible part sizes and geometries.
4. The number of parts to be produced of a given geometry and size will dictate the degree to which a given system is mechanized.
5. Manual explosive feed systems will be used for both single and multiple shot operations.

The costs involved cannot be accurately determined as there is not a general case which typifies an automated explosive forming system or "machine". Costs have ranged from a few thousand dollars for the semi-automatic machine using small dies to hundreds of thousands of dollars for a multi-energy-source system.

Production rates for standoff explosive forming operations is generally stated in the range of 1 to 4 parts per hour. Rates determined for the most automated explosive forming systems have been reported as

35 to 60 explosive operations per hour. The use of mechanized die systems of the semi-automatic type could be used to obtain a mid-range of 10-25 parts per hour. In this manner the labor to form a part can be significantly reduced, thereby, justifying the implementation of a degree of automation to an explosive forming system.

II. ELEVATED TEMPERATURE EXPLOSIVE FORMING

L. E. Jensen

Introduction

In conventional metalworking processes, materials with high yield strengths and/or low elongation are commonly worked at elevated temperatures. The increased formability of the material at elevated temperatures may reduce the number of anneals required. In explosive metalworking, the same problem of low formability is encountered when materials such as high strength steels or titanium alloys are utilized. In order to form parts from these materials at room temperatures, repetitive shots with intermediate anneals are required. In an attempt to reduce the number of processing operations, elevated temperature forming was investigated. Both a literature survey and an experimental program were undertaken to determine the feasibility of elevated temperature explosive metalworking.

System Requirements and Testing

As previously stated the high strength steels and titanium alloys represent the bulk of the low formability materials commonly formed. Temperature-elongation data for these materials were analyzed to establish the temperature requirements for the forming system. In the case of Ti 6Al-4V, it was determined that a temperature in excess of 1200° F would result in doubling the elongation experienced at room temperature. High strength steels such as 4340 tested at this temperature showed a 2.8 to 1 increase in elongation when compared to room temperature data. However, A286 steel shows a loss in elongation at

1200° F. A forming temperature in excess of 1600° F is required for increasing the elongation of A286. A design minimum of 1200° F was therefore selected with a 2000° F temperature as a design maximum. This 800° F. temperature range permits the forming of most low formability alloys.

The energy transfer media is an important parameter in an explosive metalworking system. A survey was conducted to determine which transfer media would support a minimum temperature of 1200° F. Of the available liquid lubricants, it was found that a polyphenyl ether had the highest usable temperature. This lubricant can be heated to approximately 900° F without decomposition. However, if it is heated above this temperature, thermal instability occurs and the possibility of detonating the media greatly increases.

Since a liquid lubricant was found to be unsuitable, liquid salts were investigated. All of the salts investigated showed excellent thermal properties, however, the costs seemed to be excessive and no further work was done.

Consideration was given to utilizing hot gases. It was found that temperatures in excess of 1200° F could be obtained using various heating methods. The two methods investigated were (1) to heat air and impinge it upon the work piece and (2) to burn a combustible mixture at the surface of the work piece. The hot air approach appeared to be the more promising of the two methods from an economical viewpoint.

A test fixture was constructed and several tests performed. During these tests, several major problems were encountered. The first problem was to transport the hot air from the heating unit to the surface of the workpiece. Since the air was in excess of 1200° F, most piping materials were not strong enough which led to pipe rupture. By using extra heavy wall stainless steel tubing, this problem was eliminated. The second problem arose as a direct result of solving the piping problem. It was found that the compressor used did not have an adequate volume rate. The problem was successfully solved by putting three medium volume compressors (100 CFM piston displacement) in parallel. The third problem which appeared was the most significant. Thermocouple readings indicated that temperature gradients existed over the surface of the workpiece. This problem, coupled with the long heat-up periods required, led to the exploration of the combustible gas approach. Several mixtures were tried with the existing test fixture. The results appeared encouraging, however, subsequent analysis revealed that a major redesign of the fixture was required and it was concluded that the cost was beyond the scope of this program.

The remaining transfer media are classified as solid particle media. This classification includes fine sand, finely ground alumina and small diameter steel shot. An analysis of the heat loss of the blank to the die indicated that the die had to be heated to approximately the same temperature as the blank. This increases the forming problems

since the clamping mechanism must be able to provide the necessary force at temperature. In addition, the frictional forces are greatly increased at temperature requiring the use of solid particle lubricants over the draw ring instead of the more conventional lubricants used at room temperatures.

The use of a solid particle transfer medium requires that the charge be buried in the medium at a specified distance from the blank. It can be placed on top of the transfer medium but the efficiency is decreased by greater than 50%. Placing the charge on top of the heated medium requires that the charge and initiator be adequately insulated to insure against thermal ignition or detonation of the explosives.

Conclusions

The implementation of elevated temperature forming of materials such as titanium and high strength steels presents some rather severe technical problems. As previously discussed, these materials can be incrementally formed at room temperature using intermediate anneals and multishot sequences. Thus, although somewhat tedious, the incremental forming process is easier and safer to implement. It is therefore concluded that elevated temperature forming cannot be considered feasible without considerable additional development.

III. EXPLOSIVE FORMING OF DOMES USING TRUNCATED CONICAL PREFORMS

L.J. Effenberger

L.K.W. Ching

J.D. Mote

Introduction

The explosive forming state of the art encompasses three methods of forming hemispherical or elliptical shaped domes by vastly different approaches. The selection of the method of explosive forming depends on material properties, material thickness, and diameter of the dome being formed. These methods are as follows:

1. Deep drawing using flat blanks
2. Compression forming using flat blanks
3. Sizing using a developed preform

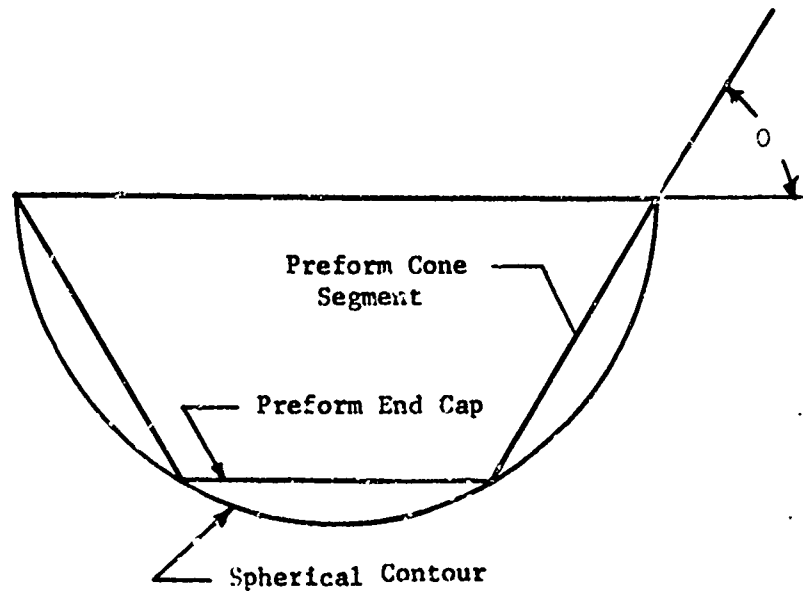
The objective of this program was to study the feasibility of producing thin walled hemispherical domes from rolled and welded conical preforms. The evaluation of varying preform geometries was made over a diameter to thickness (D/t) range of 240-445. A strain analysis was conducted comparing the theoretical and experimental strain values.

Due to its availability and ease of fabrication, 304 stainless steel was chosen as the preform material. This material was selected to minimize the effects of welding and thermal treatment.

Preform Fabrication and Analysis

The simplest developable preform shape that can be explosively sized to a hemispherical geometry is a truncated cone (see Figure 1). The conical segment is rolled and welded using the minimum number of pieces dictated by available material size. Figure 2 shows the preform

FIGURE 1
TRUNCATED CONE PREFORM



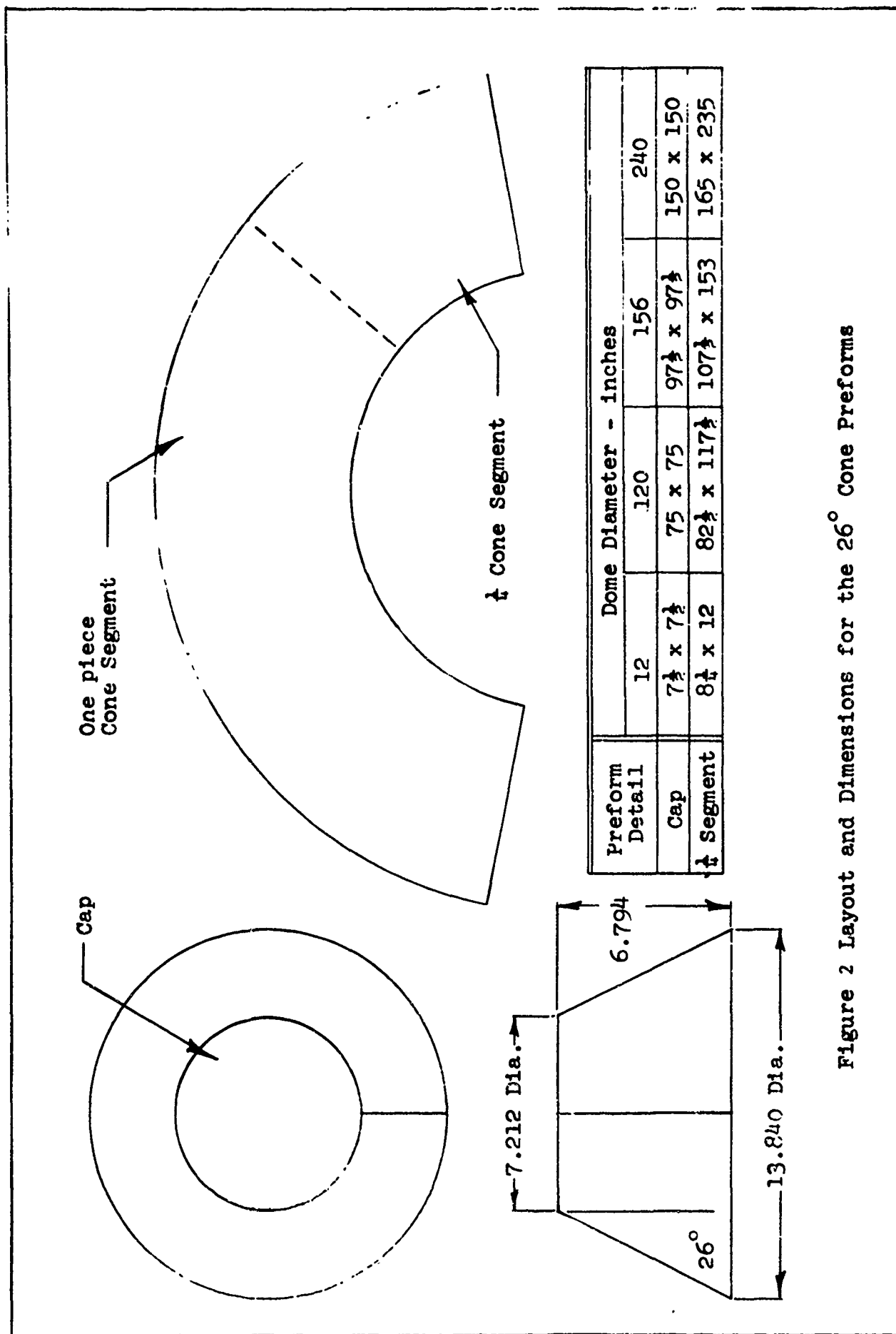


Figure 2 Layout and Dimensions for the 26° Cone Preforms

layout and dimensions for the 67° cone preform with one piece and four piece conical segments. An end cap is welded to the conical segment by a circumferential weld. The welding of the components into a preform is planar, therefore, no requirements for double curvature welding exists.

The taper of the conical segment, i.e. the angle θ , is critical since the resultant strains produced during forming contoured shapes are directly dependent upon θ . The elementary analysis of the strains induced by expanding a truncated conical preform to a hemispherical shell yield the following relationships:

Average meridional strain in cone section

$$\epsilon_m = \frac{(90-\theta)\pi}{180 \sin (90-\theta)} - 1$$

Average meridional strain in cap section

$$\epsilon_m = \frac{\pi(\theta-45)}{90 \cos (180-2\theta)} - 1$$

Maximum circumferential strain in cone section

$$\epsilon_{\text{circ}} = \frac{1}{\cos (90-\theta)} - 1$$

These relationships show that as the angle θ decreases in magnitude, the conical segment strains increase and the cap strain decreases.

The experimental strain values were calculated from the relationships:

$$\epsilon_m = \frac{l_f - l_i}{l_i}$$

$$\epsilon_{\text{circ}} = \frac{c_f - c_i}{c_i}$$

where:

ϵ_m = average meridional strain

l_i = chord length before forming

l_f = meridional length after forming

ϵ_{circ} = maximum circumferential strain

c_i = the circumference of a small circle on the cone section
before forming

c_f = the circumference of a small circle on the hemisphere
after forming

Strains were calculated for various cone angles. The meridional and circumferential strains were calculated, assuming no draw for comparison with experimental values. Table 1 shows the calculated strain values for various preform cone angles.

Figure 3 shows a plot of the strains calculated above for cone angles over the range of $45^\circ - 80^\circ$. It can be seen that for small changes in the cone angle, large changes in the circumferential cone and meridional cap strains occur. It is evident from the strain curves in Figure 3 that the most favorable preform geometry must minimize these numerically largest strains. Since the intersection of both strain curves occurs at about 64° , the preform cone angles used in the experimental phase were centered about this point.

Experimental Results

A number of tests were conducted using rolled and welded preforms to make twelve inch diameter hemispheres by explosive forming techniques.

TABLE 1
TABULATION OF THEORETICAL STRAINS VALUES AS CALCULATED FOR THE
FIVE PREFORM GEOMETRIES

Strain	Preform Cone Angle				
	70°	67°	64°	61°	56°
Average Meridional Strain, Cone	2.0%	2.69%	3.46%	4.35%	6.12%
Circumferential Strain, Max, Cone	6.42%	8.64%	11.26%	14.34%	20.62%
Average Meridional Strain, Cap	13.86%	10.49%	7.67%	5.34%	2.50%

FIGURE 3

THEORETICAL STRAIN VALUES AS ESTABLISHED FOR
CONICAL PREFORMS WITH A CONE ANGLE RANGE OF 45-80°

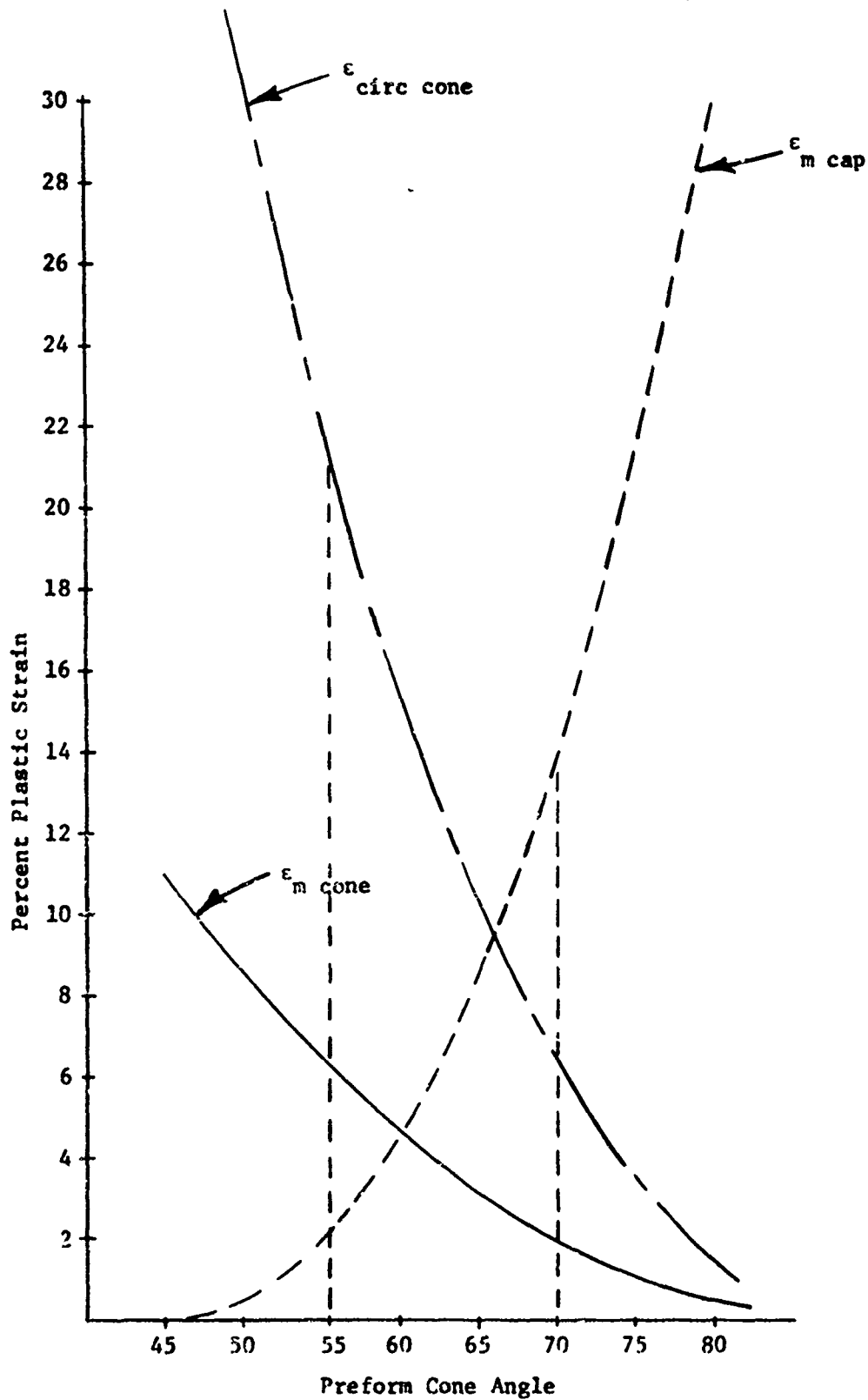


Table 2 lists some of the data taken from the above tests. In all cases, except for the 56° cone angle preforms, full hemispherical shapes were produced in one shot without weld failure.

The 61° and 56° angle preforms were annealed to improve the ductility of the weld and the heat affected zone. The welds in the stainless steel preforms failed at about 15 percent strain without stress relief. The only 56° angle preform which formed to final geometry without longitudinal weld failure was the .048 inch thick cone. This cone required two shots for complete forming.

The circumferential strain measurements were made only on the cone segment of the preform. The circumferential weld, under conditions of full preform restraint, does not undergo any circumferential strain as it is stabilized by contact on the spherical cavity surface. The only weld deformation occurs by bending as the $(90-\theta)$ angle at the weld is formed to the six inch spherical radius contour. The longitudinal weld, however, is subjected to the numerically largest strain (except for $\epsilon_{m\text{cap}}$ for 70° preform) when the preform is formed fully to the hemispherical die cavity.

The experimental values of circumferential strain in the cone section agreed quite closely with the calculated values as shown in Figure 4. The calculation of theoretical circumferential strains was based on the assumption that points on a particular circle on the cone move radially outward to a circle on the hemisphere during forming. The maximum value of strain was also assumed to occur at the mid-chord

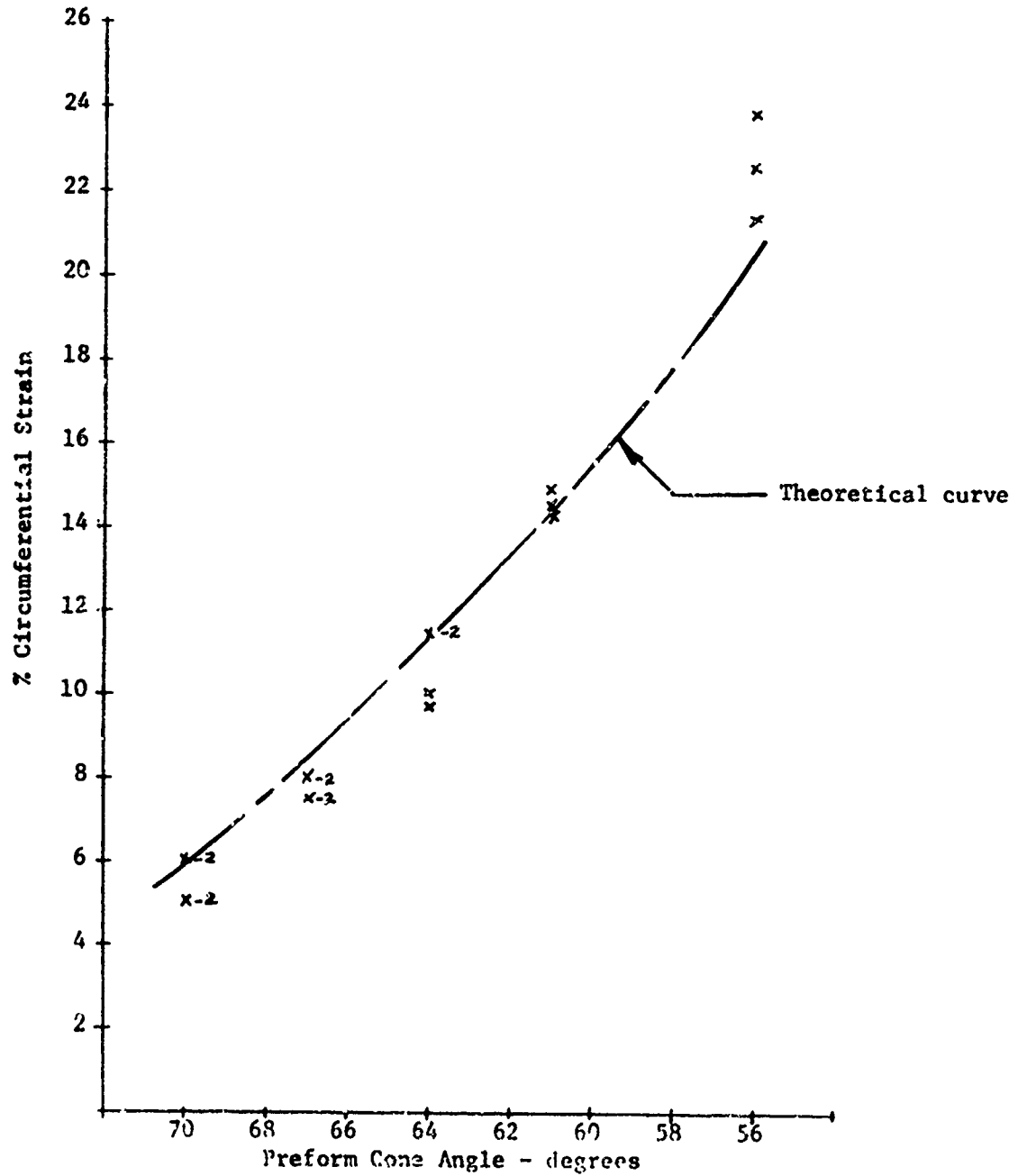
TABLE 2

CONDITIONS OF TEST AND STRAIN DATA RESULTING
FROM EXPLOSIVE FORMING TESTS

γ	Angle	Thick	E_m cone	E_m cap	E_{circ}	Comments
1A2	70°	.049	3.56	5.38	5.00	Moderate Draw
2A1	70°	.035	3.70	6.85	5.00	Moderate Draw
3A1	70°	.027	2.88	8.30	6.00	Slight Draw
3A2	70°	.027	3.25	8.14	6.00	Slight Draw
1B1	67°	.049	2.11	6.77	8.00	Slight Draw
1B2	67°	.049	2.00	7.00	7.50	Moderate Draw
2B1	67°	.035	1.11	6.30	7.50	Moderate Draw
2B2	67°	.035	3.67	10.55	7.85	No Draw
3B1	67°	.027	3.34	9.60	8.46	No Draw
1C1	64°	.049	1.64	5.67	9.70	Slight Draw
1C2	64°	.049	2.94	6.16	10.00	No Draw
2C1	64°	.035	2.89	5.72	11.50	No Draw
3C1	64°	.027	2.76	5.35	11.60	No Draw
1D1	61°	.049	3.34	5.32	14.90	No Draw
2D1	61°	.035	3.39	4.50	14.30	No Draw
3D1	61°	.027	2.92	3.67	14.50	No Draw
1E2	56°	.049	.69	1.10	21.40	Large Draw
2E3	56°	.035	2.79	3.24	23.90	Moderate Draw
3E2	56°	.027	2.12	3.87	24.40	Large Draw

FIGURE 4

MAXIMUM VALUES OF CIRCUMFERENTIAL CONE STRAIN
AS DETERMINED EXPERIMENTALLY WITH RESPECT
TO PREFORM CONE ANGLE



position, i.e. half way between preform contacts at the draw ring and the circumferential weld. Actual test showed that the strain maxima did occur in an area between the mid-chord point and 1/2 inch below the mid-point (toward the preform cap). Based on a consideration of circumferential strain, the most ideal preform shape was near a cone angle of 64.7° .

Figure 5 illustrates how the calculated average strain in the preform cap varies with the preform cone angle. The experimental data points are shown with respect to the theoretical curve.

Initial forming tests on the 70° and 67° preforms did not exhibit sufficient restraint to prevent drawing in of the preform during forming. This resulted in reducing the amount of meridional strain required to meet the final spherical contour. Data points are shown by crosses for conditions of draw and squares for no-draw conditions. As one would expect, the tendency for preform draw is much more pronounced for the steeper angle preforms. Inspection of the no-draw data shows close agreement of the experimental meridional strains with the scatterband established for the theoretical strain curve.

The meridional strain in the cone segment, as determined experimentally is shown in Figure 6. The reduction of the strains in the cone section due to part draw are not as pronounced as for the cap section. The most marked deviation was for the 56° preform where the strain values fell way below the theoretical curve. Poor preform to die fitup (undersize preform) and the use of a two shot sequence to

FIGURE 5

AVERAGE VALUES OF MERIDIONAL CAP STRAIN AS DETERMINED
EXPERIMENTALLY WITH RESPECT TO PREFORM CONE ANGLE

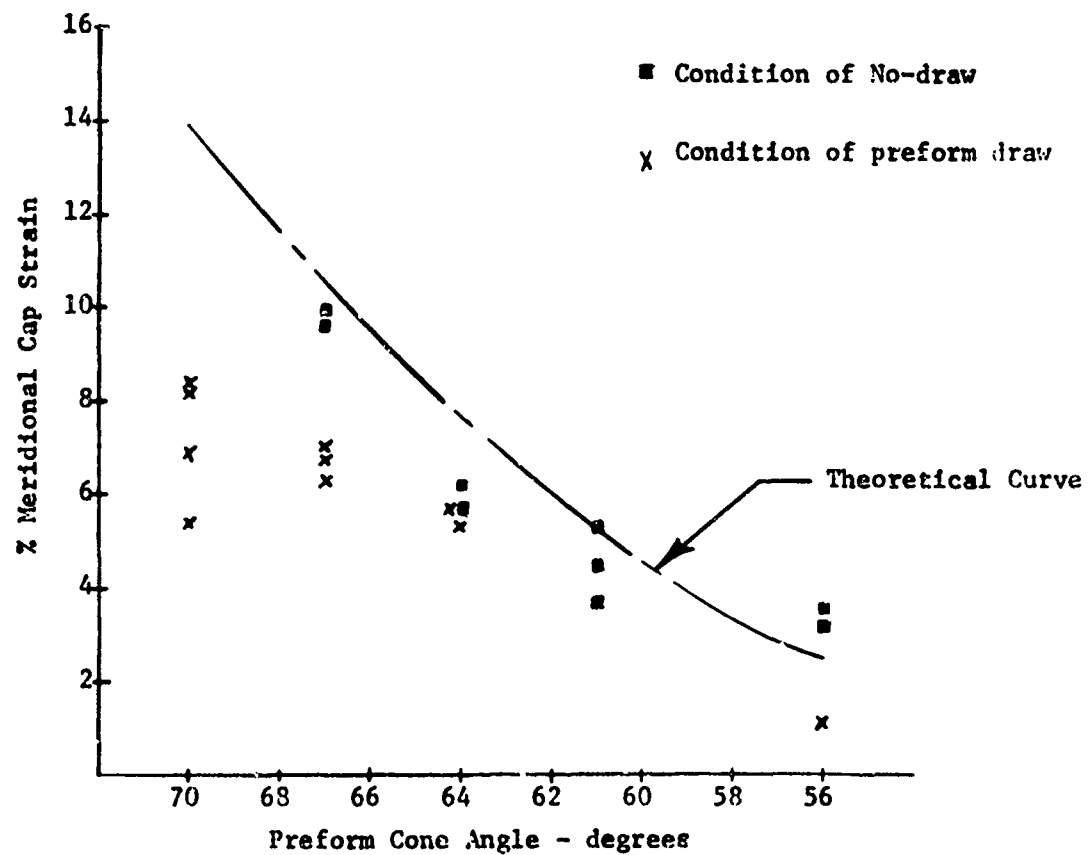
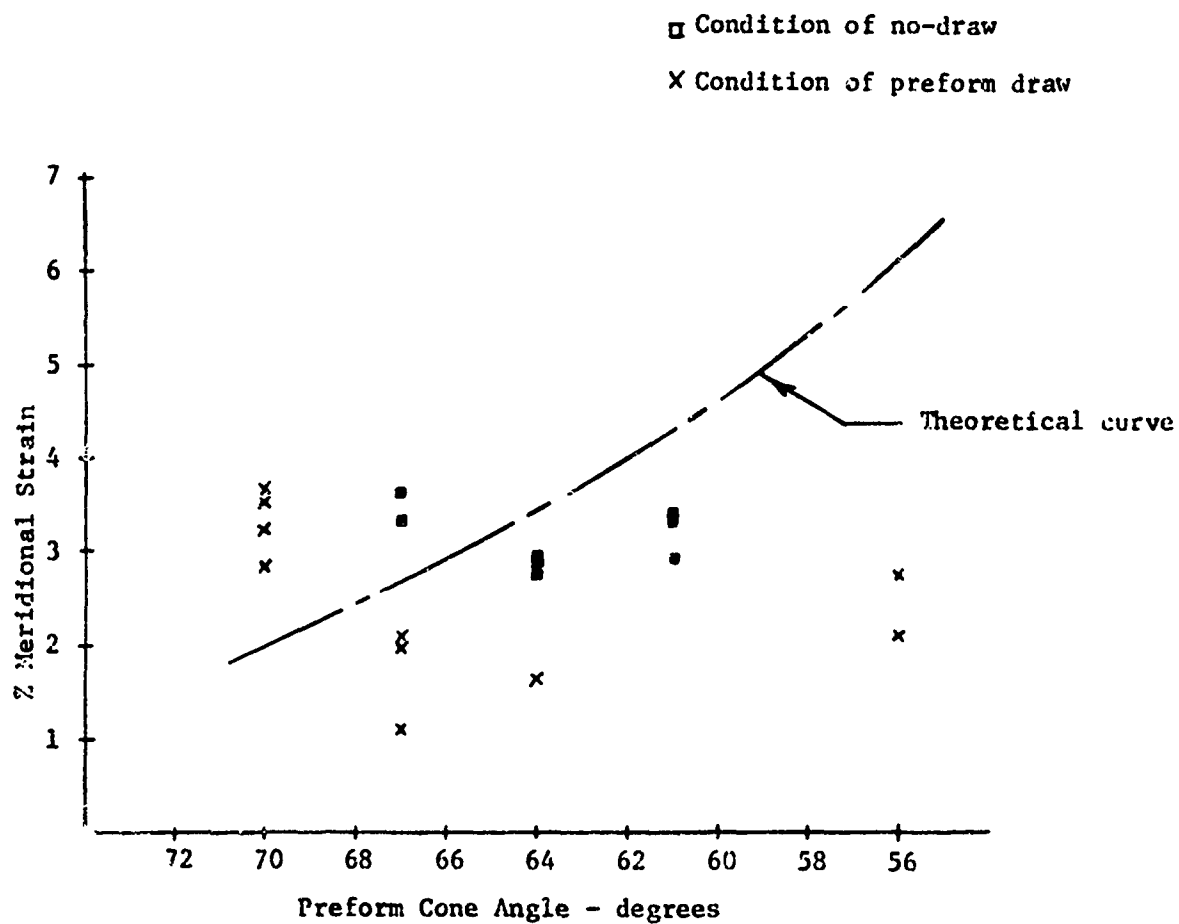


FIGURE 6

AVERAGE VALUES OF MERIDIONAL CONE STRAIN AS DETERMINED
EXPERIMENTALLY WITH RESPECT TO PREFORM CONE ANGLE



produce the hemispherical geometry allowed a large amount of part draw.

The thickness strains, as measured on sections cut from the fully formed domes, exhibited the widest range of scatter. This was due to the initial variations in sheet thickness and the dimensional changes incurred due to preform fabrication.

The thickness variation along a section of the various cone preforms can be seen in Figures 7a and 7b. The distribution on the cone is as one would expect with zero values at the die contact points. The values then increase reaching a maximum value at the mid-chord location. The maximum values occurred for the 56° preforms as the degree of deformation required for contour definition is the maximum in this case.

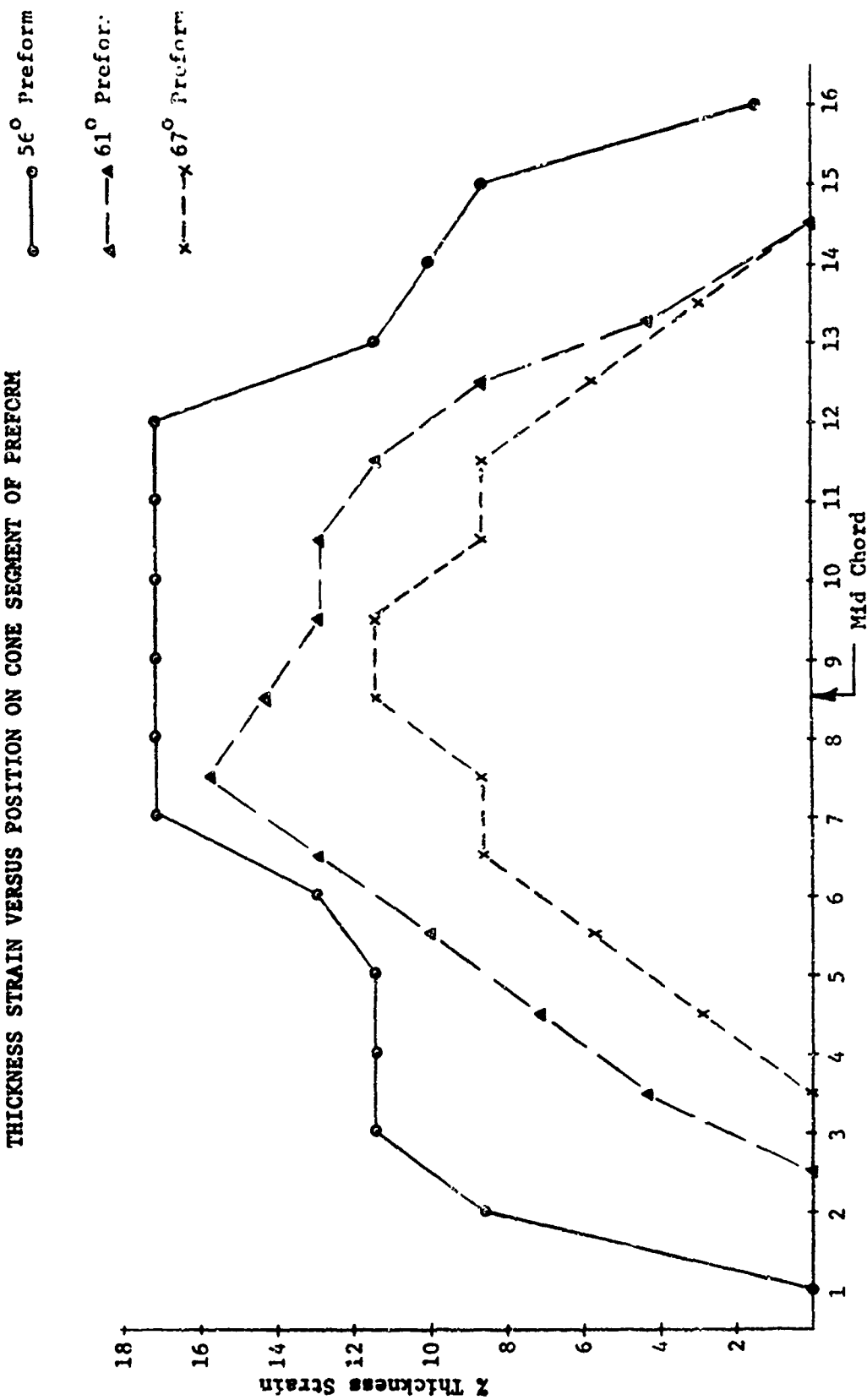
The cap thickness strains are zero at the circumferential weld location under conditions of no-draw. When preform draw occurred, compressive strain caused section thickening. Maximum thinning was found to occur, not necessarily at the center of the cap, but at locations on either side of the centerline.

As the cone angle decreased, the cap diameter decreased reducing the total strain required to contact the die contour. Figure 8 illustrates this relationship with the exception of the 70° cone data. The amount of preform draw was sufficient to lower the resultant thickness strains of the 70° cone cap to a magnitude less than the 67° cone cap.

The maximum thinout reported was 17%. Most values fell in the

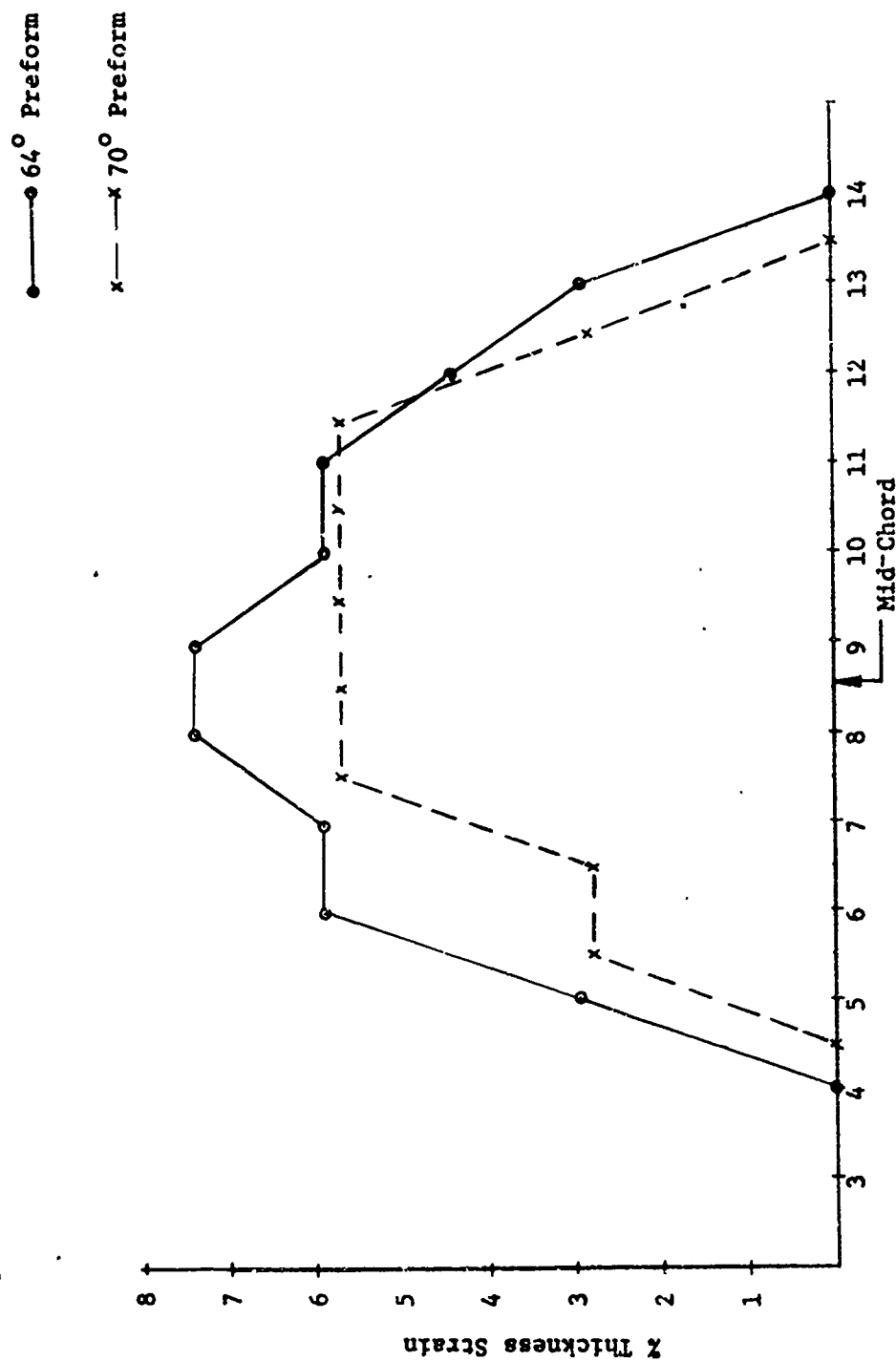
FIGURE 7a

THICKNESS STRAIN VERSUS POSITION ON CONE SEGMENT OF PREFORM



Station on Cone Segment

FIGURE 7b
THICKNESS STRAIN VERSUS POSITION ON CONE SEGMENT OF PREFORM



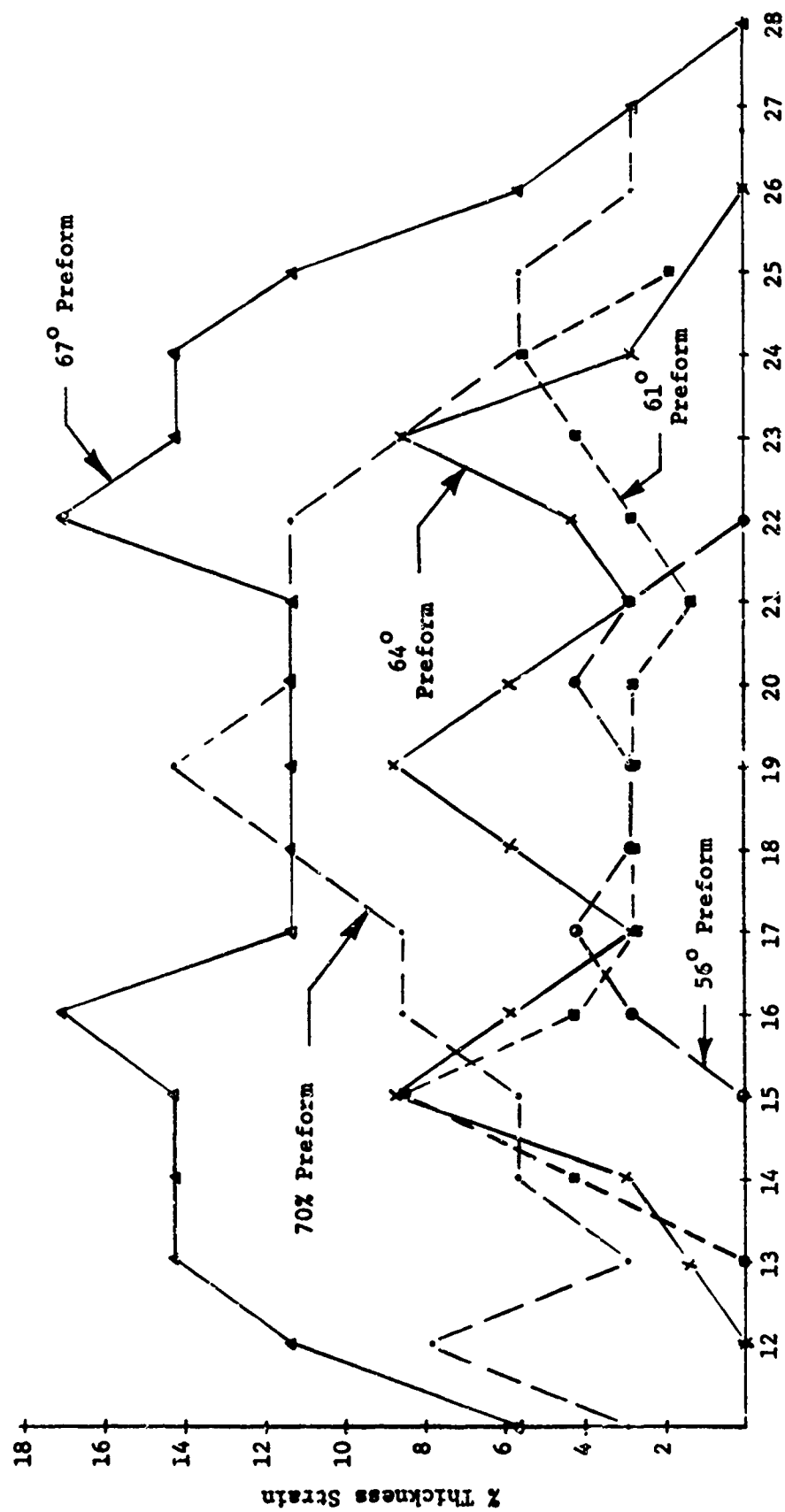


FIGURE 8

THICKNESS STRAIN OF THE CAP SECTION OF THE PREFORM AS A FUNCTION OF THE CONE ANGLE

range 2-12%. Therefore, preforms can be designed to produce shells with reduction of the amount of thinout.

Conclusions

The feasibility of the forming hemispherical shapes by the explosive sizing of rolled and welded preforms has been demonstrated. Parts of each preform geometry were formed completely to the six inch hemispherical contour.

Parts formed over the D/t range of 250-445 showed no tendency for preform wrinkling or buckling. The only reason higher D/t values were not used was because of the limitations in welding very thin stainless steel sheet material.

The experimental data for completely restrained parts agrees well with the analysis. This analysis shows the preform design, namely a cone angle of about 66° , required to minimize part strain. Further reduction of the total strain can be effected by allowing the preform to draw.

Another approach to fabricating thin shell parts, which has been demonstrated but not investigated in detail, is using a very stiff clamp ring to prevent buckling. Parts with a D/t of about 400 have been fabricated using flat blanks without face sheets. Hence, there are at least two explosive forming methods to be considered for fabricating thin shells.

IV. ANALYSES OF DIE STRESS DURING EXPLOSIVE FORMING

L. K. W. Ching

J. D. Mote

Introduction

There has been very little work done towards measuring or calculating the loads on an explosive forming die. The majority of the work accomplished in analyzing the stresses in spherical parts has been limited to static forcing functions, deformations of thin shells, or elastic solutions to stress wave loadings. None of these analyses can be easily modified for a thick shell subjected to both time and spatial varying loads. Consequently, an analytical study would have to commence from basic concepts. Difficulties such as the specification of boundary conditions could seriously hinder the analysis. Since a complete analytical approach can be ruled out as a quick solution to the problem of determining die loads, the complementary approach would be the experimental measurement of these loads. The experimentally derived results could be used to determine the accuracy of the analytical solution.

Experience has shown that dies designed for explosively fabricating 51 inch diameter aluminum head (Meehanite dies) grow under repeated shots in spite of a rather massive design. The die contour is out of tolerance after approximately 200 shots. This may be partially due to localized wear at the draw surface. However, the deviation from contour is more likely due to localized overstresses resulting in plastic growth of the die. This phenomena is extremely difficult to analyze since it is not directly related to the bulk behavior of the structure. Shell dies have been considered but the above experience indicates the analyses and experiments conducted using this concept do not reflect the actual conditions experienced in actual production explosive forming situations.

Therefore, it was the purpose of this study to determine the energy transfer to dies during explosive forming. The results of these measurements were used to develop rational die design criteria for explosive forming dies.

The subsequent sections describe the experimental techniques utilized and the results, the analytical calculations and guidelines for die designs.

Experimental Set-up and Results

The die utilized for these tests was a 6.0 inch diameter hemispherical cavity die with an outer diameter of 12.0 inches, 4.75 inch height and 3.25 inch minimum wall. The blanks were clamped to the die with a steel hold down ring and bolts torqued to a constant value. A schematic of the die set up is shown in Figure 1. All tests were performed in a hot water (135° F.) forming pool.

Annealed 2014 aluminum and 18% Ni Maraging Steel blanks 9.5 inches in diameter and .063 inches thick were used. The explosive charge was Composition A-3 pressed into a hemispherical shape. Several charge weights and standoff distances were utilized in the tests.

For the measurement of die strains, rosette gages were bonded to the circumference of the die. A watertight electrical conduit protected the instrumentation wires to the strain gages on the die. The conduit was found to be necessary since the shock wave acting upon these lead wires generated extraneous electrical signals which lead to erroneous measurements. A trigger wire beneath the explosive charge was used to disrupt an electrical circuit and establish the initiation of the test time period.

Strain measurements were recorded in a conventional fashion by the use of strain gages, wheatstone bridges, amplifiers and oscilloscopes.

A block diagram of the instrumentation system for one channel is shown in Figure 2.

A more detailed electrical schematic of the instrumentation setup for measuring die strain only is shown in Figure 3.

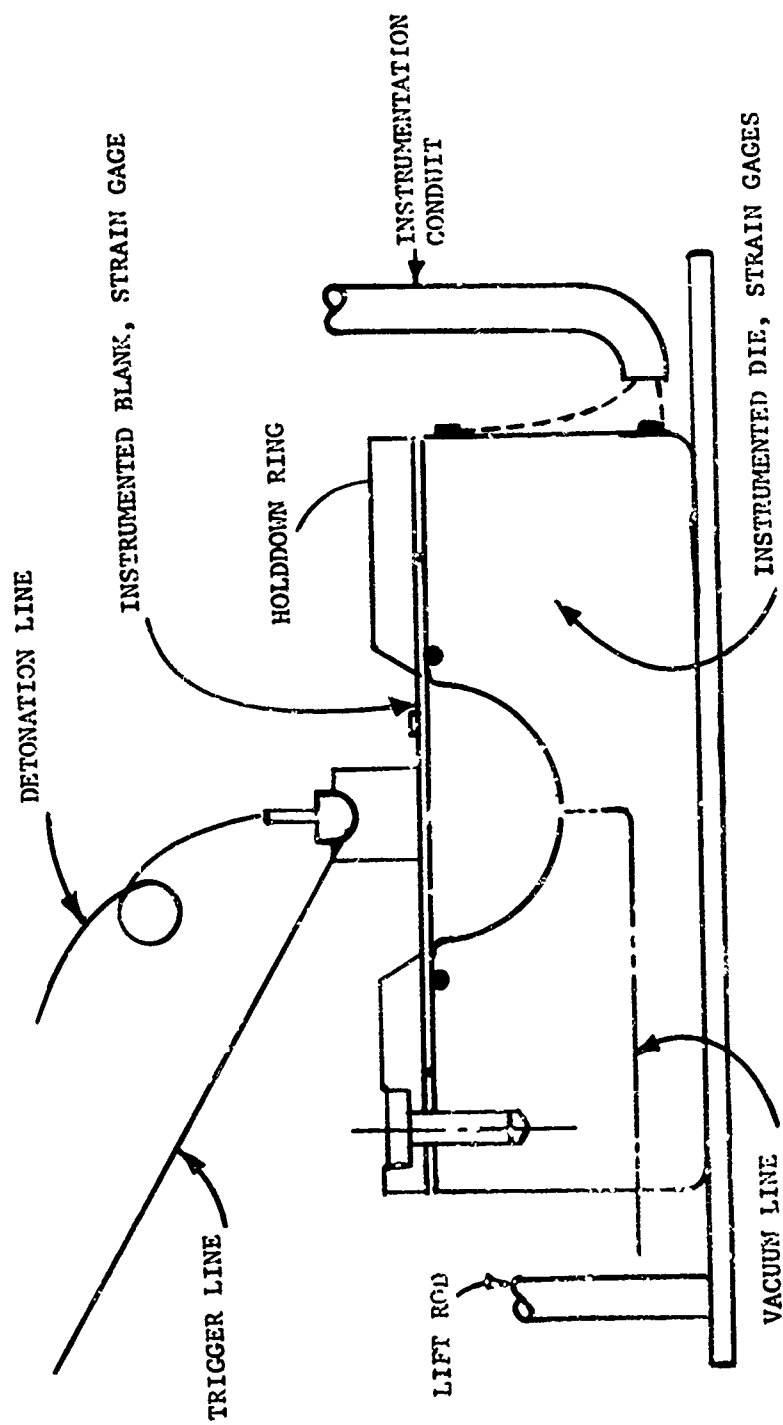


Figure 1. Schematic of Die Test Setup

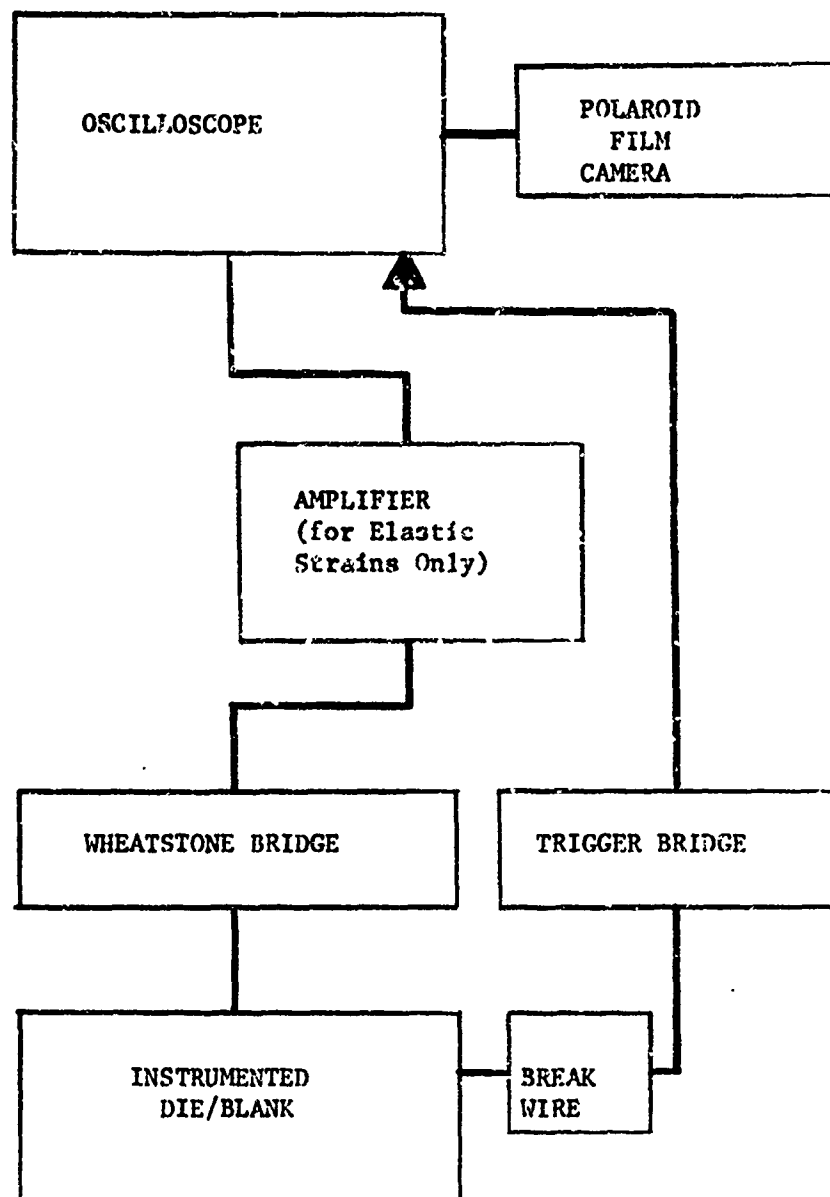


Figure 2. Block Diagram of the Instrumentation System

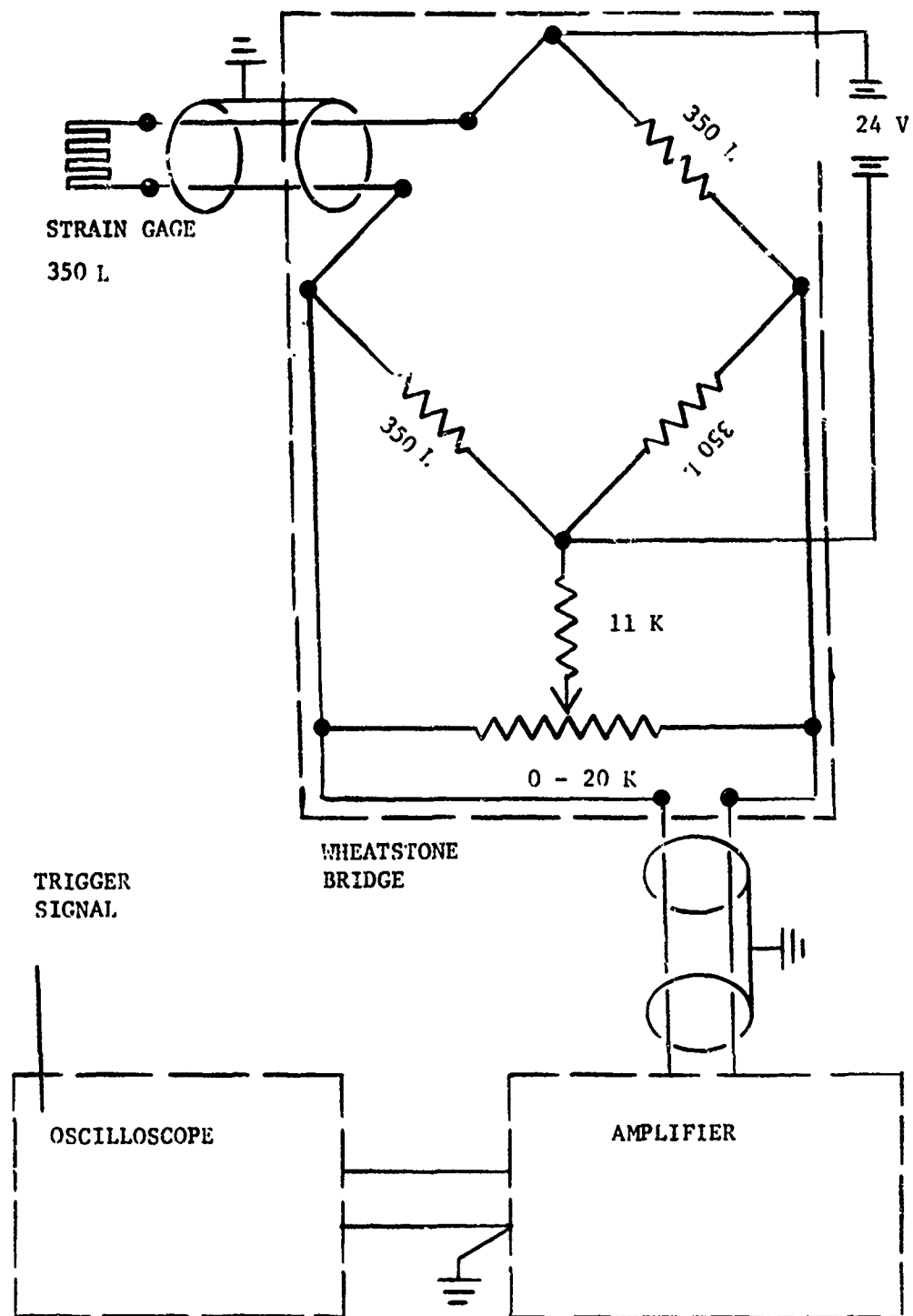


Figure 3. Electrical Schematic of the Instrumentation Setup for Measuring Elastic Die Strains

The outputs from three leg 45 degree rosettes were recorded simultaneously so that the principle stresses could be calculated. Calibration of the system was done prior to each test by shunting known resistance values across each gage while the gages were underwater. This method calibrated each circuit to a simulated static compressive strain assuming only that the manufacturer's gage factor was constant. The high excitation voltage (24 volts) was also recommended by the gage manufacturer as satisfactory to maintain a constant gage factor. The balanced bridge system of 350 ohms and 24 volt excitation was selected over the 120 ohms and 6 volt excitation system to achieve a high bridge output. Since noise was anticipated and would also be amplified, a high bridge output gave a higher signal-to-noise ratio.

Noise from several sources was found to be a problem in measuring low elastic strains as the noise could have a greater amplitude than the actual strain signal. It was possible to minimize the noise to less than 15 micro-inches per inch while measuring die strains of 200 micro-inches per inch by using water tight conduit to contain the instrumentation lead wires.

Installation of strain gages for measuring dynamic elastic die strains was performed per the instructions supplied by the gage manufacturer. The gages were annealed constantan foil mounted on a polyimide backing. The die surface was prepared using cleaning solvents from the vendor's strain gage kit. The bonding adhesive was a room temperature cure type so that the same techniques could be used on much larger dies. The waterproofing was a two part epoxy recommended by the gage manufacturer for submersion applications.

The test procedure used is outlined below:

1. Connect all instrumentation and perform a functional checkout.
2. Disconnect all instrumentation lines to the die.
3. Install charge and lower the die and charge into the pool.
4. Reconnect instrumentation lines and balance the wheatstone bridge, eliminating temperature effects.
5. Set triggering circuits for oscilloscopes and camera and detonate the charge
6. Develop Polaroid film.

A typical trace is shown in Figure 4. The results derived from the test were then reduced to digital form from the film and used as input to a computer program. This computer program then resolved the strains into principle strains and the resulting principle stresses. From the principle stress versus time tabulation, the maximum stress induced in the die was found.

The greatest minimum principle stress was of the most interest. It represented the major measured die load in all tests since this was the maximum compressive stress. Figure 5 is a plot of this maximum compressive die stress as a function of the ratio of the standoff distance to die diameter (L/D). Tests were conducted at six L/D ratios and the results recorded. After the data was reduced, the maximum compressive die stress was determined. The repeatability of the stress magnitude was checked by making several shots at a given L/D ratio. For these shots at a specific ratio, all parameters were kept constant. The repeatability of

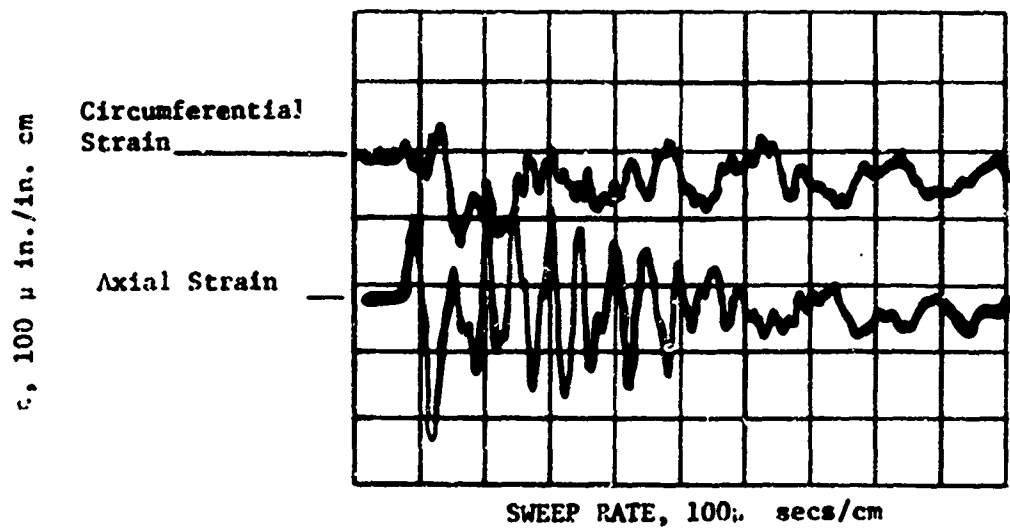


Figure 4. Typical Trace of Strain Versus Time
(Positive Lap) = Tensile)

BLANK:
2014-0 ALUMINUM
0.063 IN. THICK
 $R_0 = 9.54$ IN.
 $D^0 = 6.0$ IN.

CHARGE:
COMP. A-3
80 GRAINS
#6 F.B.C.

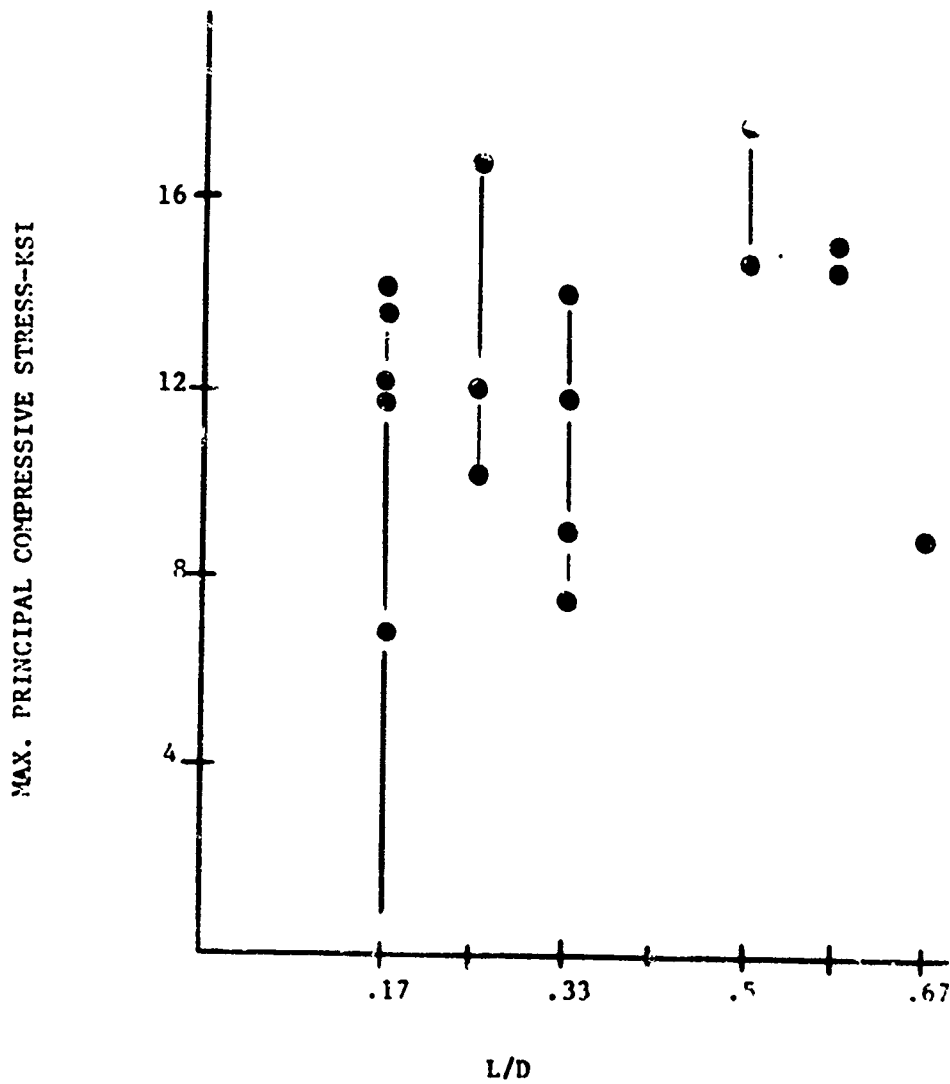


Figure 5. Maximum Compressive Die Stress Vs. Standoff Distance

stress magnitude between tests is shown to have some scatter. Testing has indicated that the load is balanced across the die. The balanced load was shown by measuring the dynamic strain of axially mounted gages which were on opposite sides of the die. In addition to those tests shown in Figure 5, two tests were performed on 18% Ni Maraging Steel domes. The results of these tests are shown in Table 1.

In addition to the maximum and minimum stress values, the data indicated that the maximum die stress is a result of the explosive shock loading. Little or no stress was induced in the die by either the reloading phenomena or the part impacting the die. However, the above statement cannot be generalized without further experimentation. The die utilized in this series of tests was a massive system and would therefore be relatively unaffected by reloading or blank impact. For a less massive die, either loading or a combination of the loadings could become the prime forcing function, as opposed to the explosive shock loading.

Theoretical Considerations

Two analyses were performed in order to correlate the explosive charge and forming geometry to the stress induced in the die. The first approach was to start with the empirical energy flux density equation while the second approach is to commence with the pressure loading of the die induced by the shock wave from the explosive. Both approaches are presented below:

Energy Approach

From the principle of conservation of energy, the strain energy in

TABLE 1
18% NI MARAGING STEEL DATA

Test No.	e (grains)	l (in.)	w (in.)	Maximum Compressive Stress (psi)
I	340	1.0	3.0	10,484
II	170	1.0	3.375	42,240

the die (E_D) is equal to the energy induced by the charge (E_C) or

$$E_D = E_C \quad (1)$$

The strain energy of the die can be calculated as work done per unit volume which is equal to the area under the stress-strain curve. Since the die strains are assumed to be elastic,

$$E_D / (\text{Vol of die}) = \frac{1}{2} \frac{\sigma_{\text{eff}}^2}{E} \quad (2)$$

where

σ_{eff} = effective stress

E = Youngs Modulus of elasticity

Equation (1) then becomes

$$\frac{1}{2} (\text{Vol of die}) \left(\frac{\sigma_{\text{eff}}^2}{E} \right) = E_C \quad (3)$$

If it is assumed that the loading for the first shot is in the axial direction, and that the die is basically a hollow cylinder, then equation (3) becomes

$$E_C = \frac{\pi h}{8E} \sigma_{\text{eff}}^2 \left[\text{O.D.}^2 - \text{I.D.}^2 \right] \quad (4)$$

The energy delivered to the die by the charge can be estimated by an equation similar to those used by Ezra.^{1*} Using this approach the energy delivered to the die by the charge is given by

$$E_C = \frac{W_e}{4} (\cos \theta_1 - \cos \theta_2) \quad (5)$$

*Refer to Bibliography at the end of this volume.

$$\text{where } \cos\theta_1 = \frac{l}{\sqrt{l^2 + (I.D.^2/4)}}$$

$$\cos\theta_2 = \frac{l}{\sqrt{l^2 + (O.D.^2/2)}}$$

W = weight of charge

e = specific energy of the explosive

l = standoff distance

I.D. = die cavity diameter

O.D. = outer die diameter

The diameters and distances are shown in Figure 6. Combining equation (5) with (4) and simplifying yields the following equation for the maximum effective stress in the die. .

$$\sigma_{\text{eff}} = \text{sqrt} \left\{ \frac{2WeE}{\pi h} \left(\frac{\cos\theta_1 - \cos\theta_2}{O.D.^2 - I.D.^2} \right) \right\} \quad (6)$$

The forming shots after the first shot, the charge is placed near the top surface of the die body or inside the die cavity. Consequently, the loading is not in the same manner as for the first shot and the assumption used previously is invalid. If it is assumed that the loading is of a spherical nature, then equation (3) becomes

$$E_C = E_D = \frac{\eta}{24E} \sigma_{\text{eff}}^2 \left[(I.D. + 2M)^3 - I.D.^3 \right] \quad (7)$$

where M = wall thickness of the die at the point of interest, (See Figure 6) and the volume of the die is calculated to be that of a hemispherical shell.

The energy transferred to the die by the charge arrives via the contact area between the blank and the die. This amount of contact cannot be specified a priori, nor can it be predicted with any accuracy. Hence, it will be assumed that all of the energy transferred to the blank is in turn transferred to the die. This assumption should yield a larger die stress than the actual case. From this assumption, the energy transferred to the die is

$$E_D = \frac{We}{4} (1 - \cos \phi_1) \quad (8)$$

Substituting equation (8) into (7) and simplifying yields the effective stress in the die wall which is

$$\sigma_{eff} = \text{sqrt} \left[\frac{6WeE (1 - \cos \phi_1)}{\pi [(I.D. + 2M)^3 - I.D.^3]} \right] \quad (9)$$

Where w = weight of explosive charge
 e = specific energy of the explosive
 E = Modulus of elasticity
 I.D. = die cavity diameter
 M = wall thickness of the die
 $\phi_1 = 90^\circ + \text{ARCTAN} \left(\frac{I.D. - 2M + 2L}{I.D.} \right)$

Pressure Approach

A second approach to calculating die stresses is to start with the free field shock pressure from the explosive charge. If it is assumed that the shock wave is acoustic and that the die acts as a rigid

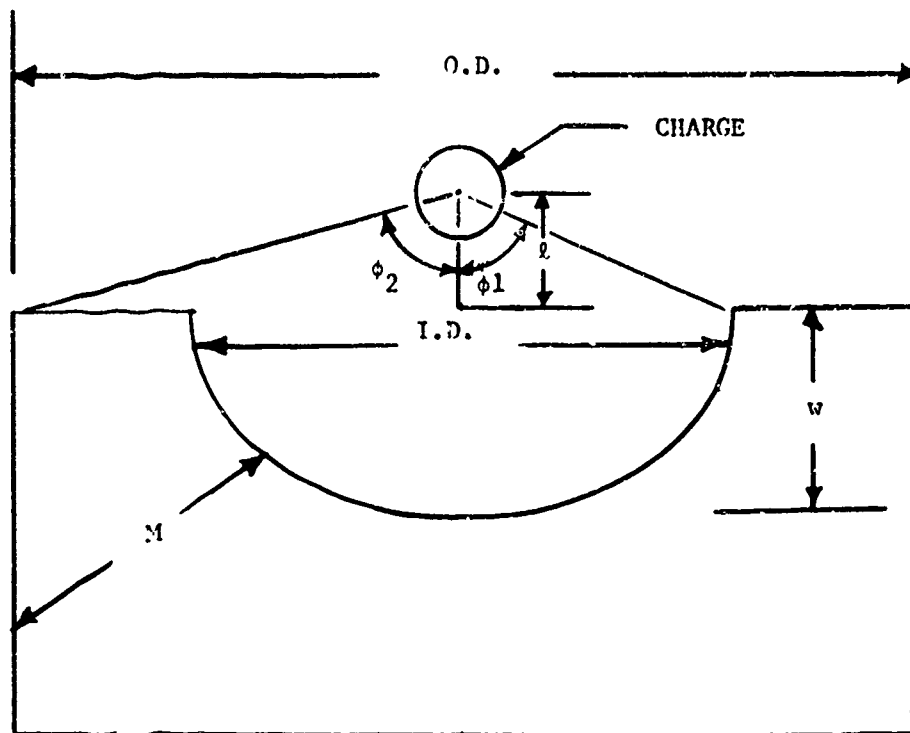


Figure 6. Geometry Used In Energy Analysis

surface, the maximum pressure that acts on the die is given by

$$P = 2P_m \quad (10)$$

The equation for the peak pressure (P_m) from an underwater explosion has been empirically determined to be ^{2*}

$$P_m = A \frac{(W^{1/3})}{R} \quad (11)$$

where A , α = constants for a given explosive

W = weight of explosive

R = distance from the explosive as defined in

$$\text{Figure 7} = \sqrt{l^2 + z^2}$$

Using the previous cylindrical assumption, the stress in the die

(σ_{eff}) is equal to

$$\sigma_{eff} = -P \quad (12)$$

from shock wave considerations. Combining equations (10), (11) and (12) yields

$$\sigma_{eff} = -2A \frac{(W^{1/3})^\alpha}{R} \quad (13)$$

Equation (13) applies to first shots only since the cylindrical assumption was used.

For forming shots after the first shot, the spherical assumption is made again. In addition if a quasistatic state is assumed, the standard Lane equations for stresses in a thick spherical shell may be used. From equation (10) and (11) the pressure is

$$P = 2A \frac{(W^{1/3})^\alpha}{R} \quad (14)$$

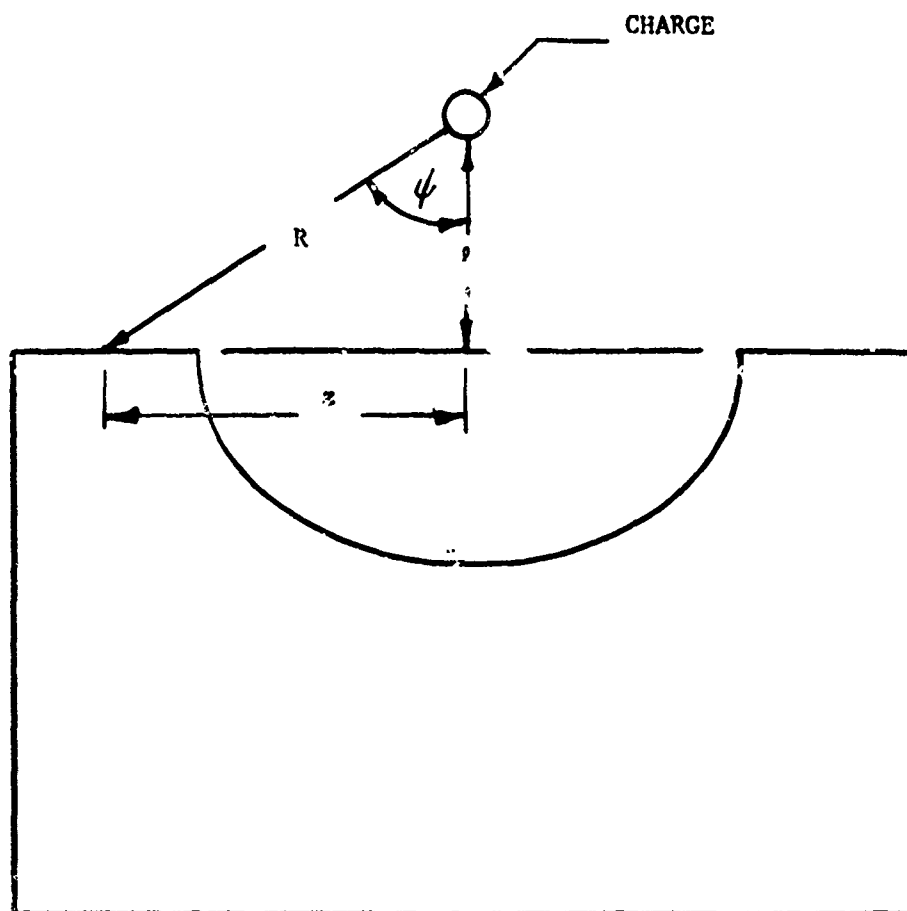


Figure 7. Geometry Used In Pressure Analysis

$$\text{where } R = \frac{I.D.}{2} + l - w$$

Substituting this pressure into the Lane equations yields

$$\sigma_{\theta} = - \frac{A(Wl/3)^{\alpha}}{R} \left[\frac{(0.5 \text{ O.D.}/r)^3 + 2}{\frac{(O.D.)^3}{I.D.} - 1} \right] \quad (15)$$

$$\sigma_r = \frac{2A(Wl/3)^{\alpha}}{R} \left[\frac{0.5 \text{ O.D.}/r^3 - 1}{\frac{(O.D.)^3}{I.D.} - 1} \right]$$

$$\text{where } r = \frac{I.D.}{2} + M$$

If equations (15) are applied to the outer boundary of the die, then it can be seen that the radial stress vanishes.

Comparison of Analytical to Experimental Results

Using the experimental parameters as given previously, various stress values were calculated using the previously derived equations. The results are shown in Table 2.

When compared to the measured results, it can be seen from Table 3 that the pressure approach consistently over predicts the die stress whereas the energy approach seems to under predict the die stress for most cases.

Die Design Criteria

The equations derived give some qualitative guide lines to the designing of dies. From these equations, it can be seen that the

TABLE 2

ANALYTICAL RESULTS FOR MAXIMUM COMPRESSIVE STRESS

		Pressure Approach	Energy Approach
2014-0	4D	Maximum Compressive Stress	Maximum Compressive Stress
		(IN KSI)	(IN KSI)
I.	1/6	18.746	10.917
II.	1/4	18.618	11.730
III.	1/3	17.932	13.683
IV.	1/2	16.800	14.282
V.	7/12	16.143	14.162
VI.	2/3	15.452	13.879
<hr/>			
18% Si. Maraging Steel			
I.	1/6	10.484	21.226
II.	1/6	42.250	45.406

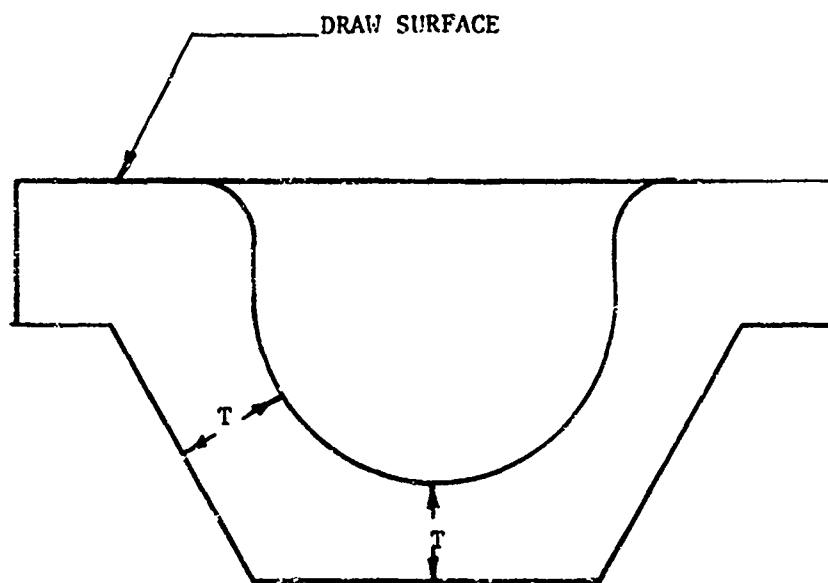
TABLE 3
ANALYTICAL TO EXPERIMENTAL STRESS RATIOS
 $\sigma_{ana}/\sigma_{exp}$ (average)

2014-0	Pressure Approach	Energy Approach
I.	1.45	0.84
II.	1.44	0.90
III.	1.69	1.29
IV.	1.04	0.88
V.	1.08	0.95
VI.	1.72	1.54
<hr/> 18% Ni. Maraging Steel <hr/>		
I.	1.55	1.30
II.	1.00	1.07

thicker the die wall is the lower the die stresses will be and hence the longer the die life. In addition, the equations and experimental results show that the charges after the first shot have a tendency of producing larger die stresses due to the increased charge efficiency. As the wall thickness of the die decreases, the die acts more like a membrane and is more likely to flex or deform when the stresses exceed the yield stress of the die material.

Based on the equations given, the most weight efficient die design would be a die whose outer contour was the same as the cavity contour. In many cases, this is impractical since contour machining of the outer surface would be expensive and would also leave an unstable surface for the die to rest on. A modification such as that shown in Figure 8 would yield a weight efficient die without the complexity of analyzing or fabricating a ribbed structure. The minimum adequate wall can be calculated using either the pressure or energy approach. If the energy approach is used, then the wall would be under designed, whereas, the pressure approach will yield a wall which is over designed. A typical die design outline is shown below.

1. Estimate the largest charge size for a signing charge and calculate the die stress based on an estimated minimum die wall.
2. Estimate the largest charge size for a first charge and calculate the die stress.
3. Iterate on steps 1 and 2 to obtain a suitable wall thickness and stress level.



T = Minimum Wall Thickness

Figure 8. Unribbed, Weight Efficient Die

4. Design basic die body.
5. Design clamping arrangement.
6. Design evacuation system if required.

BIBLIOGRAPHY

1. Ezra, A. A., "Principles and Practices of Explosive Metlworking,"
In Press.
2. Cole, Robert H., Underwater Explosions, New York: Dover Publications
Inc., 1948. "

V. COMPACTION OF POWDERS USING EXPLOSIVES

L.K.W. Ching

Introduction

There is a great deal of interest in using explosive methods for compacting metal and/or ceramic powders. This interest exists because of the high pressures that can be generated by explosives and the desire to attain significantly greater compaction densities in material systems where conventional methods produce unsatisfactory results. The most promising area for immediate use of explosive powder compaction methods is for forging preforms for compressor discs and preforms for turbine discs and turbine buckets. The potential advantage of this process is to provide greater homogeneity in the material thus eliminating the lamination problems encountered with other more conventional processes.

The amount of research done in explosively compacting powders has been minimal. A literature survey was conducted by the University of Denver to evaluate the parametric studies that have been conducted to date. Since the various compaction techniques and their advantages and disadvantages were discussed in the Fifth Annual Report of the Center for High Energy Forming, no further general discussion will be included in this paper. Additional parametric studies have also been conducted at the University of Denver. E.F. Industries, Inc. conducted a program to determine a suitable container design and explosive loadings for use with the implosion compaction techniques. This explosive compaction method required the lowest amount of capital expenditure and could also be implemented in the shortest period of time.

Two types of metal powders were utilized during this program. Iron

filings (-20 mesh) and Udimet 700 powder (-120 mesh) were used in both the container and density studies. Stainless steel tubing was used in both studies since it was readily available and easily fabricated.

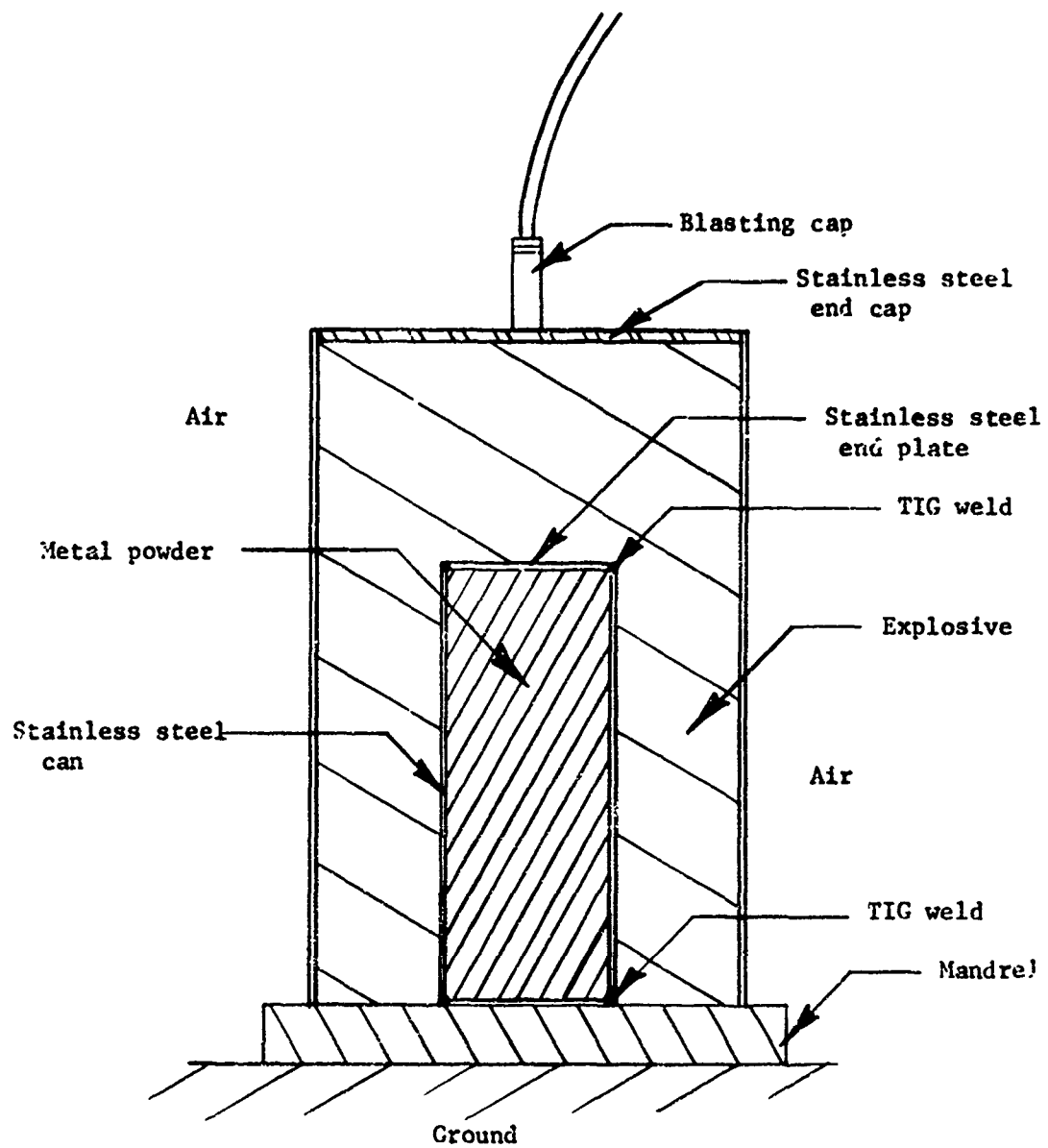
Container Studies

In order to establish a suitable container design, cylindrical powder containers were fabricated. A schematic of the container and explosive configuration is shown in Figure 1. The powder containers were fabricated using two different metal thicknesses. In order to eliminate any effects of air compression, the cans used in the container study were evacuated prior to detonation of the explosive. This series of tests indicated that there is no significant effect of container wall thickness on the compacted density as long as the tubes are thin (wall thickness to radius ratio <10). In addition, it was noted that long compacts (length to diameter ratio >5) did not yield higher compacted densities than short compacts ($l/d < 3$). It was noted, however, that the long compacts were prone to bowing and were therefore more sensitive to experimental technique. However, this bowing effect does not affect the density of the compact.

Based on the above study, the long container was selected since it would yield a large number of specimens for various destructive tests and it would also reveal the precision with which the experimental set up was made.

FIGURE 1

SCHEMATIC SECTIONAL VIEW OF CONTAINER
AND EXPLOSIVE LOAD



In order to determine if a vacuum was required for the compaction process, a series of tests was conducted. Several identical containers were fabricated and loaded with iron filings. Half of these containers were evacuated during the compaction, whereas the remaining number of containers were not evacuated. All tests performed used the identical explosive loading and configuration. Care was exercised in keeping as many variables constant such as using explosive from the same batch, Detasheet cut from the same piece and stainless steel tubing from the same tube. After compaction, samples were taken from each specimen and subjected to density determination, macroscopic examination and microscopic examination. All testing revealed that a vacuum is not required for explosive compaction of powders using the implosion technique.

Density Studies

Many parameters entered into this study and some were not varied in order to keep the program manageable. The parameters related to the study are listed below.

1. Powder to be compacted
 - a. Quantity and type
 - b. Particle size and distribution
 - c. Particle shape
 - d. Oxide layers present
 - e. Precompaction

2. Explosive

- a. Type
- b. Loading
- c. Impulse developed
- d. Angle between powder container and detonation front and other related geometry of the system
- e. Detonation velocity
- f. Method of initiation

Of the powder parameters, the type of powder, particle size and amount of precompaction were the only ones varied. As stated earlier, iron filings and Udimet 700 powders were used. The iron filings were large in size (~20 mesh) and could not be compacted to as high a density as the smaller (~120 mesh) Udimet 700 powder. The maximum compacted density for the iron filings was 86% of theoretical density, whereas, with the smaller Udimet 700 powder, densities of 99% of theoretical density were achieved. Microscopic examination of the iron compacts revealed that the voids could be closed only by gross particle deformation due to the extremely large particle sizes. However, if the compact is overpowered to achieve gross particle deformation, shock wave interactions at the center of the compact caused cracking of the compact to occur. In the case of the Udimet 700, microscopic examination revealed that the smaller particles flow more readily resulting in a denser compact. It was evident after this series of tests that:

1. Smaller particle sizes result in denser compacts

2. Less particle deformation occurs with smaller particle sizes. Work was therefore discontinued with the iron filings and the Udimet 700 powder was used exclusively for the remaining tests.

With both the container design and powder parameters fixed, investigations to determine the relationship of the explosive parameters to the compacted density commenced. Since the impulse developed by the explosive is governed by the type of explosive and its detonation velocity, it was ruled out as a primary parameter. The angle between the powder container and detonation front was also considered to be a secondary parameter because it is specified by the method of initiation, type of explosive, detonation velocity of the explosive and charge configuration. The container was cylindrical, therefore the explosive charge configuration used was cylindrical to facilitate in the set up. The method used to detonate the main explosive charge was to detonate a Detasheet charge using a blasting cap which in turn detonated a small lead-in charge. When the lead-in charge was completely detonated, detonation was occurring in a nearly planar front resulting in a collapsing cylindrical shock front then acting upon the container and metal powder thus effecting compaction of the metal powder.

Using this technique, several different explosives were evaluated as potential energy sources. Since it was the most readily available, Red Cross 60% extra dynamite (approximate detonation velocity = 12000 feet per second) was used. Visual examination of the compacts produced by this explosive revealed that minor radial macro-cracks occurred for

all explosive loadings used. Since these cracks were present, the compacted densities were much less than the theoretical density. A second series of tests performed with Composition A-3 (approximate detonation velocity = 22,000 feet per second) produced compacts with even larger radial cracks along with a hollow centered compact. In an attempt to eliminate the radial cracking and central pipe, a third series of tests was performed using Trojan 70C explosive (approximate detonation velocity = 11,000 feet per second). Compacts without either type of defect were produced using this explosive. Since the detonation velocities of the first two explosives used were higher than that of the 70C, it was concluded that the faster detonating explosives do not have a long enough pressure duration to prevent over-recovery of the compact as described in the Fifth Annual Report. If the compaction process is performed in water as opposed to air, then the faster explosives could possibly be used.

Density measurements were made on samples used in the above tests. It was found that the maximum densities occurred in a range of explosive to metal powder weight ratios of 1.2 to 2.1. The weight ratios to achieve maximum compaction for various situations are shown in Table 1. From this data it appears that for the system used in these tests the ideal weight ratio lies between 1.4 to 1.6. Data from systems using different metal powders but similar to those used here indicate that the ideal weight ratio is somewhat larger, with values from 1.4 to 1.8. It is interesting to note that in the case of Udimet 700, green compacts

TABLE 1

WEIGHT RATIOS REQUIRED TO ACHIEVE MAXIMUM DENSITY

Metal Powder	Explosive	Typical Density % Theoretical	Explosive Weight Powder Weight	Range
Iron Filings (-20 mesh)	Red Cross 60% Extra	88	1.50 - 1.60	
	Composition A-3	84	1.40 - 1.60	
Udimet 700 (-120 mesh)	Red Cross 60% Extra	92	1.25 - 1.55	
	Composition A-3	86	1.00 - 1.40	
	Trojan 70C	99	1.40 - 2.00	

produced by more conventional methods have not been reported near 100% theoretical density whereas explosive methods have produced compacts at the 99% of theoretical density level.

Conclusions and Recommendations

The explosive compaction of powders shows considerable promise as a method for fabricating forging and machining preforms. The implosion technique used in this study can be easily implemented and the densities produced using this technique warrant further research in explosive compaction.

During this study, the following results evolved:

1. The metal powder container should be of a thin wall design
2. No vacuum is required to attain compaction densities near theoretical
3. The most important powder parameter is particle size
4. The most important explosive parameters are amount and type of explosive
5. For the systems investigated, the maximum densities occurred for weight ratios from 1.4 to 1.6

The experimental work should be extended to various other geometries and materials. The geometries should include:

1. Solid disks
2. Plates and blocks
3. Hollow cylinders
4. Shells
5. Special hardware configurations

Materials which should be included are refractory metal powders, metal-ceramic powder mixtures and ceramic powders. Tests conducted on the resulting compacts should include:

1. Density measurement
2. Hardness measurement
3. Compression tests
4. Tensile tests
5. Machinability

Additionally, consideration should be given to sintering the green compacts with subsequent coining.

VI. EXPLOSIVE FORMING OF PRESSURE VESSEL STEELS

H. Otto

INTRODUCTION

Explosive forming has been applied extensively to aerospace components over the past two decades. Most of the materials that have been explosively formed are those of interest to the aerospace industry such as aluminum alloys, titanium, stainless steels, and superalloys. Some work^{1,2} has been conducted on high-strength low-alloy steels that has shown an influence of orientation upon the terminal properties. In two cases^{3,4} the hardness of a low carbon steel that was explosively formed was lower than counterparts that were statically strained to the same equivalent strain. Harris and White⁵, using a 0.05% C steel that was dynamically uniaxially strained, found a higher hardness in the dynamic stress condition. Other investigators⁶⁻⁹ using dynamic uniaxial stress conditions compared with static experiments again found the static flow stress to be less for the dynamic condition.

In a survey by Orava and Otto⁹ on the terminal properties of explosively formed materials, the terminal properties of materials were determined to be a function of the particular metal being formed. Blanket statements¹⁰ that explosive forming was detrimental to terminal properties were analyzed and could be related to one or two situations in which some degradation of a particular property in a particular material might be affected. In the same context, beneficial results were noted for other materials¹¹.

Although a limited amount of data was available on low carbon steels, the response of a steel to high energy forming would be a function of the particular steel. Any alloy addition would influence the results with respect to work hardening, response to heat treatment, original strength and structure, and morphology after forming. No single study could cover all of

the hundreds of steel alloys in use, nor could their mechanical properties be projected as a function of strain rate. In the present work, two pressure vessel steels were explosively formed and the terminal properties compared with statically strained material. It must be pointed out that the conclusions reached in this study apply only to these two steels, and any projections to other steels would be speculative.

MATERIALS AND FORMING PROCEDURES

The two steels selected for investigation were A285, Grade C, and A515, Grade 70. These two steels are used in pressure vessel applications and are covered by ASTM Designations A285-70a¹² and A515-71¹³. The A285 steel is low carbon steel for general pressure vessel applications whereas the A515 is intended for intermediate and higher temperature service. Specifications for these steels are presented in Table 1. Both steels are cross-rolled during plate production to give a relatively uniform grain size. The final rolling direction is used in delineating the orientation and does not imply that this is the only direction in which the plate was processed. Both steels were obtained in the hot rolled and normalized condition. The A285 steel was 3/8-in. thick, and the A515 was 1/2-in. thick.

Two explosive forming procedures were used: (1) forming in a flat bottom die and (2) simultaneous forming of two blanks. The latter method was developed by Altling¹⁴ and resulted in higher strains than die forming. Prior to forming, the A285 steel was sand blasted and the A515 steel surface ground on one side only so a circular photogrid could be placed on the steel. The grid system allowed measurement of the circumferential & radial strains. No attempt was made to measure the reduction or increase in thickness. For comparative purposes the effective strain was used. Assuming that a constant volume condition

Table 1. Chemical and Mechanical Properties Specifications
for A285, Grade C and A515, Grade 70 Steels

<u>Chemical Requirements</u>	<u>A285, Grade C</u>	<u>A515, Grade 70</u>
Carbon, max percent	0.28	0.31
Manganese, max	0.9	0.9
Phosphorus, max	0.035	0.035
Sulfur, max	0.045	0.04
Silicon		
Ladle analysis	---	0.15 to 0.30
Check analysis	---	0.13 to 0.33
Copper, when specified		
Ladle analysis	0.2 to 0.35	---
Check analysis	0.18 to 0.37	---
 <u>Tensile Requirements</u>		
Tensile strength, ksi	55 to 65	70 to 85
Yield strength, ksi min	30.0	38.0
Elongation, % in 8 in.	23	17
Elongation, % in 2 in.	27	21

$$\epsilon_C + \epsilon_R + \epsilon_T = 0 \quad (1)$$

exists, the effective strain is calculated using the modified Von Mises Henchy criteria

$$\epsilon^* = 2/3(\epsilon_R^2 + \epsilon_R \epsilon_C + \epsilon_C^2)^{1/2} \quad (2)$$

Engineering strains were used to calculate the effective strain even though the criteria are based upon true strain. Since the strains were used in a relative condition, converting engineering strain to true strain was not warranted. Typical strain distributions are shown in Figures 1 and 2 for the explosively formed conditions.

For comparing the A285 explosively formed steel with a static rate process, the specimen blanks were prestrained in tension to the same effective strain as the specimens selected from the explosively formed stock. A constant strain level of $\epsilon^* = 0.053$ was used.

Strain levels of 0.04 and 0.045 were selected for the A515 steel that had been die formed. The strain level of 0.04 was used for tensile tests, while the 0.045 strain was used for Charpy impact test specimens. On the free formed A515 domes a strain level of 0.35 was selected for all specimens. For comparative purposes, blanks of the A515 were alternately rolled at 90° to the same effective strain as that in the specimens selected from the domes.

Tensile tests were conducted on specimens with a 1-in. gage length. Standard size Charpy specimens were made for the A515 steel in the as-received and 0.04 strain condition. Sub-size Charpy specimens were used for the A285 steel and the A515 steel strained to 0.35 effective strain.

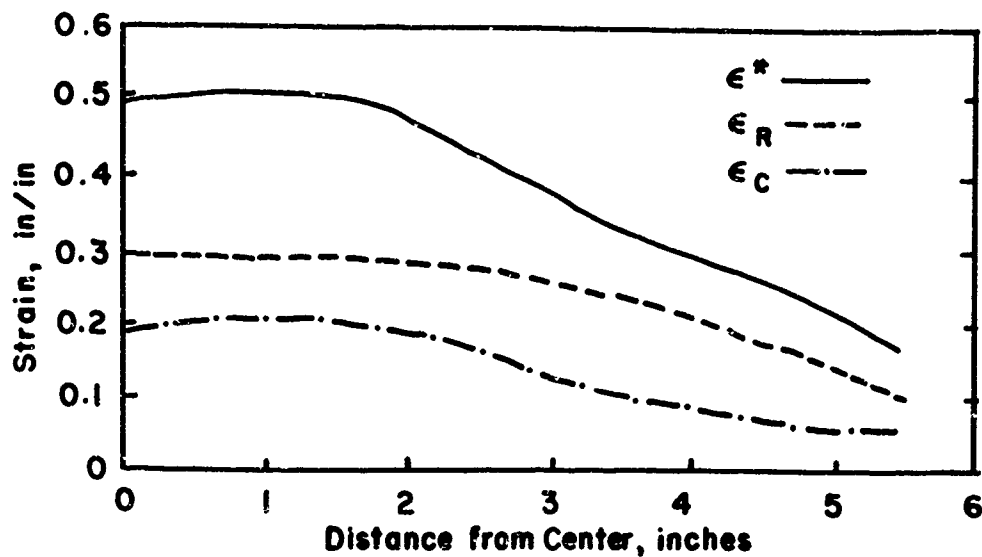


Figure 1. Typical Strain Distribution for Explosively Free Formed Domes

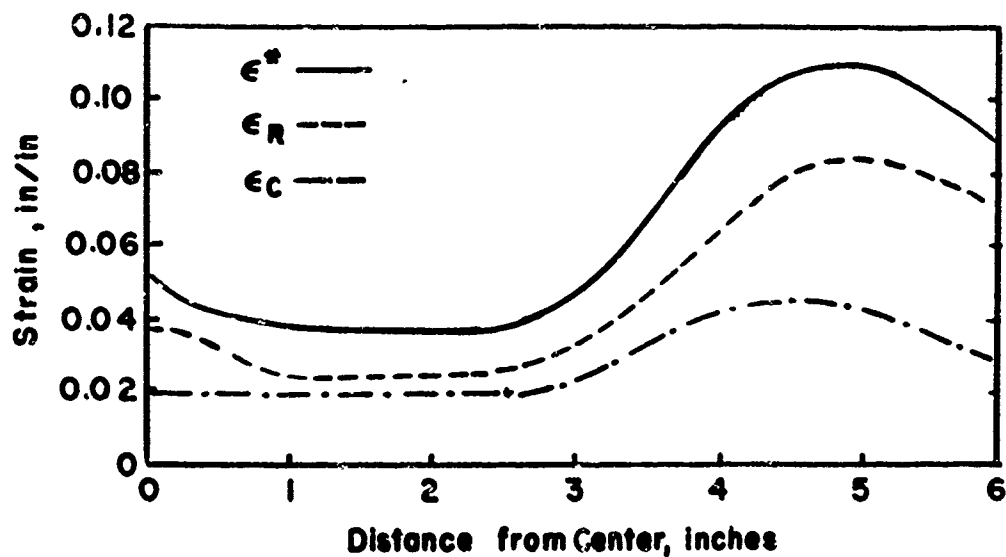


Figure 2. Typical Strain Distribution for Explosively Formed Flat Bottom Domes

Sub-size specimens were used since the thickness of the domes was not great enough to obtain a standard size Charpy specimen.

The A515 steel was tested both after forming and subsequent stress relief heat treatment. Tests on the A285 steel were made on formed and heat treated stock only. For both steels the heat treatment consisted of heating the steel at 650°C for 1 hr., then slowly cooling to 300°C. This is the standard^{12,13} heat treatment for these steels.

RESULTS AND DISCUSSION OF TESTS ON A285 STEEL

Tensile tests conducted on the stress relieved A285 steels were on specimens in which the orientation was longitudinal to the final rolling direction of the plate. Results of the tensile tests are presented in Table 2 and graphically shown in Figure 3. All of the test results fall within specifications¹² for the A285, Grade C steel. A comparison of the statically prestrained tests with the explosively formed tests does not show any dramatic differences in the strengths. The explosively free formed tests did show a decrease in ductility, but the ductility would be within specifications for this steel. There was no indication of any orientation effects in the tests.

The increase in yield strength noted for the strained specimens is matched by a corresponding drop in ductility. Statically prestraining the steel reduced the stress relieved ductility by 15%, while the decrease for the explosively formed steel was 19%. On the basis of reduction in area, essentially no difference exists in ductility. A trend is noted in that the ductility is greater in the transverse direction in all cases.

Table 2. Results of Tensile Tests Conducted on
Stress-Relieved A285, Grade C Steel

<u>Specimen Identification</u>	<u>Orientation</u>	<u>Yield Strength, psi</u>	<u>Tensile Strength, psi</u>	<u>Elongation, % in 1 inch</u>	<u>Reduction in Area, %</u>
As-received ⁽¹⁾	Longitudinal	38,000	61,000	40.7	54
	Transverse	38,500	61,000	44.8	60
Static Prestrain ⁽¹⁾	Longitudinal	44,000	61,500	35.1	52
	Transverse	45,000	61,500	38.7	60
Explosively Free Formed ⁽²⁾	Longitudinal	45,000	62,000	31.8	54
Explosively Die Formed ⁽²⁾	Transverse	45,000	61,000	35.4	61

(1) Average of three tests each orientation

(2) Average of four tests

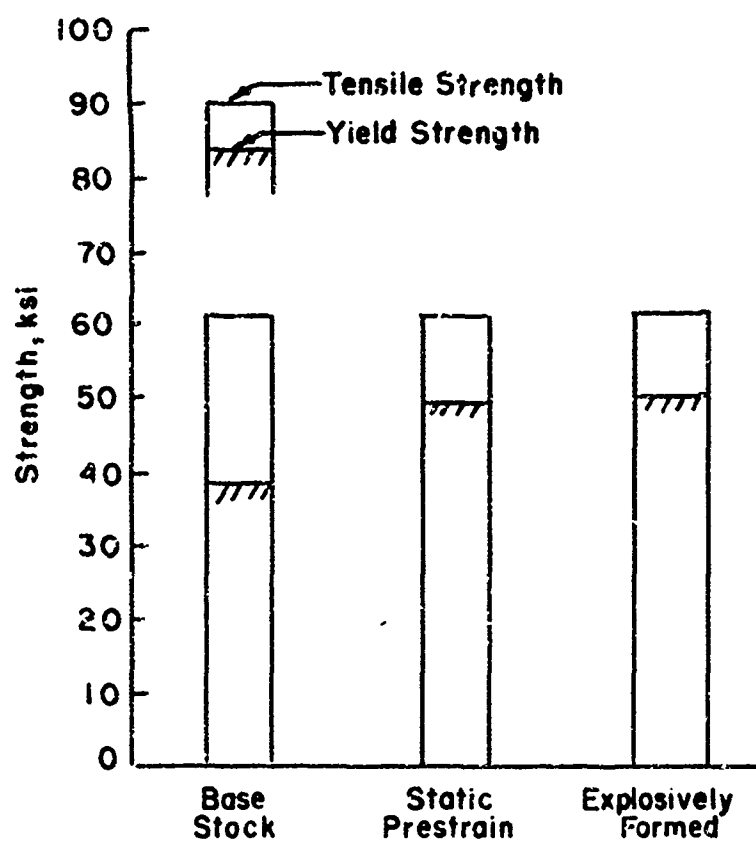


Figure 3. Results of Tensile Tests on Stress Relieved A285, Grade C Steel

Charpy tests were conducted on sub-size specimens of the A285 steel. All of the specimens were orientated with the notch normal to the final rolling direction with the exception of three specimens in the as-received condition.

Results of the impact tests are presented in Table 4 and Figure 4. The impact properties of the explosively formed materials are about the same regardless of whether they were free or die formed. Also, the non-stress relieved as-received specimens had impact properties about the same as those that had been heat treated. Explosively formed specimens had impact properties that were slightly better than the as-received stock in the longitudinal orientation, but about the same for the base stock in the transverse orientation. Static prestraining reduced the impact strength of the steel and increased the ductile to brittle transition temperature, as can be seen in Figure 4.

Metallographic studies of the A285 steel indicated no differences in the structure as a result of forming technique. There were a few shock twins in the explosively free formed stock, which might account for the lower ductility of this material. The material was isotropic with respect to the final rolling direction. The marked decrease in the impact resistance of the statically prestrained specimens could not be attributed to any difference in the microstructure as examined by light microscopy.

Since the A285 steel was tested in the stress relieved condition, no comparison can be made to prior work in which strengths of statically formed low carbon steel were greater than those of dynamically strained material. The heat treatment would tend to give more uniform results, especially at the low level of strain (0.053) used in these tests.

Table 4. Results of Charpy Impact Tests
on A285, Grade C Steel

<u>Condition</u>	<u>Temperature, °F</u>	<u>Impact Energy, ft.-lb.</u>
As-received, transverse	-25	2.0
	10	31.5
	85	40.0
As-received, longitudinal	-35	6.0
	5	12.5
	20	17.0
As-received, longitudinal, stress relieved	-90	2.0
	-35	6.0
	5	13.0
	20	17.5
	85	37.0
Explosively free formed, longitudinal, stress relieved	-310	0.5
	-190	1.0
	-90	1.5
	-40	6.0
	0	26.0
	5	25.0
	85	42.0
	85	43.0
Explosively die formed, longitudinal, stress relieved	-90	1.5
	-25	3.0
	0	23.0
	10	35.0
	55	41.0
	85	44.0
Statically prestrained, longitudinal, stress relieved	-275	1.0
	-90	1.5
	-30	2.0
	5	6.5
	25	11.0
	50	14.0
	85	16.5

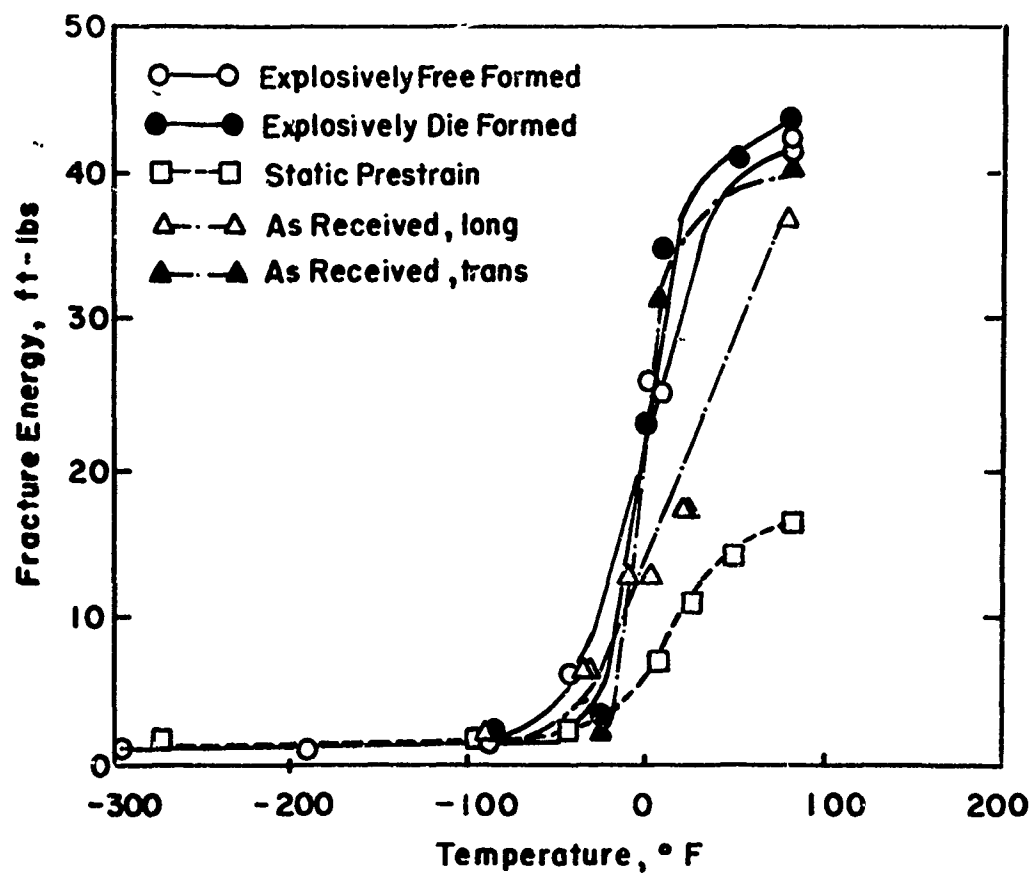


Figure 4. Results of Charpy Impact Tests
on A285, Grade C Steel

RESULTS AND DISCUSSION OF TESTS ON A515 STEEL

The A515 steel was tested both after forming and after subsequent heat treatment. Two levels of strain were used in the tests so strain effects could be distinguished as well as the effect of heat treatment. The results of the tensile tests on the as-received or base stock and the material after straining are presented in Table 5 and Figure 5. Results of tensile tests conducted on stress-relieved specimens are presented in Table 6 and are also included on a comparative basis in Figure 5.

Tests on the steel after straining indicated that at the lower strain level, a mixed result was present. The cold rolled 0.04 strain material had a higher yield strength but a lower tensile strength than the explosively formed material. The higher yield point of the cold rolled material would be consistent with results obtained in prior studies^{4,5,6} comparing static and dynamic strain conditions. The higher tensile strength of the explosively formed A515 steel would not be consistent with the earlier observations. At the high strain level, 0.35, both the yield and tensile strengths of the explosively formed material were higher, which does not agree with the earlier observations.

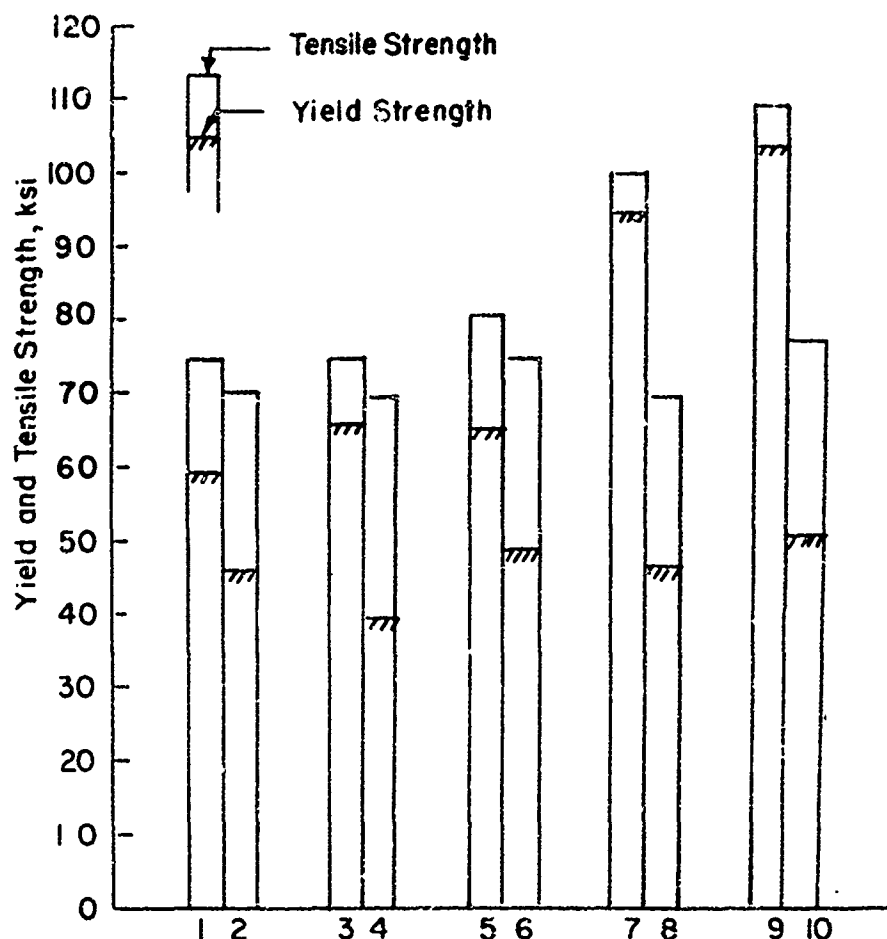
Strain hardening was evident as both the cold rolled and explosively formed material had higher yield strengths than the as-received material. At the higher level of strain (0.35) both the tensile and yield strengths were considerably higher than those of the as-received material. At the lower strain level (0.04) both the cold rolled and explosively formed stock would meet ASTM specifications without resorting to a stress relief heat treatment. At the higher strain level (0.35) the tensile strength would be too great and the ductility would not be great enough to meet specifications.

Table 5. Results of Tensile Tests Conducted
on A515, Grade 70 Steel⁽¹⁾

<u>Specimen Identification</u>	<u>Orientation</u>	<u>Yield Strength, psi</u>	<u>Tensile Strength, psi</u>	<u>Elongation, % in 1 in.</u>	<u>Reduction in Area, %</u>
As-received	Longitudinal	57,000	74,000	33.2	60.5
	Transverse	61,000	76,000	31.6	56.7
Cold Rolled, 0.04 Strain	Longitudinal	68,000	75,000	31.2	62.0
	Transverse	63,000	74,000	32.7	58.7
Explosive Die Formed, 0.04 Strain	Longitudinal	63,000	80,000	23.3	53.5
	Transverse	67,000	81,000	22.0	53.8
Cold Rolled, 0.35 Strain	Longitudinal	93,000	98,000	12.4	48.2
	Transverse	95,000	100,000	10.9	44.5
Explosive Free Formed, 0.35 Strain	Longitudinal	104,000	109,000	8.5 ⁽²⁾	34.2
	Transverse	103,000	109,000	8.8	36.4

(1) Average of three tests

(2) Average of two specimens



1. As Received
2. As Received, Stress Relieved
3. Cold Rolled $\epsilon^R=0.04$
4. Cold Rolled $\epsilon^R=0.04$, Stress Relieved
5. Explosively Formed $\epsilon^R=0.04$
6. Explosively Formed $\epsilon^R=0.04$, Stress Relieved
7. Cold Rolled $\epsilon^R=0.35$
8. Cold Rolled $\epsilon^R=0.35$, Stress Relieved
9. Explosively Formed $\epsilon^R=0.35$
10. Explosively Formed $\epsilon^R=0.35$, Stress Relieved

Figure 5. Results of Tensile Tests on A515, Grade 70 Steel

Table 6. Results of Tensile Tests Conducted on Stress Relieved A515, Grade 70 Steel⁽¹⁾

<u>Specimen Identification</u>	<u>Orientation</u>	<u>Yield Strength, psi</u>	<u>Tensile Strength, psi</u>	<u>Elongation, % in 1 in.</u>	<u>Reduction in Area, %</u>
As-received	Longitudinal	45,000	69,500	37.5	61.3
	Transverse	46,000	71,000	37.6	60.7
Cold Rolled, 0.04 Strain	Longitudinal	39,000	69,000	37.1	63.0
	Transverse	39,000	69,000	38.4	61.6
Explosive Die Formed, 0.04 Strain	Longitudinal	48,000	75,000	32.2	57.5
	Transverse	48,000	75,000	33.7	59.4
Cold Rolled, 0.35 Strain	Longitudinal	45,000	68,000	35.7	66.3
	Transverse	48,000	71,000	32.6	59.2
Explosive Free Formed, 0.35 Strain	Longitudinal	52,000	78,000	28.3	53.0
	Transverse	49,000	76,000	32.1 ⁽²⁾	58.5

(1) Average of three tests

(2) Average of two tests

Some orientation effects are present, but they are not consistent. The yield strength of the base stock in the transverse orientation to the final rolling direction is higher than the longitudinal. The same is true of the explosively formed material at a strain level of 0.04 and the cold rolled at the 0.35 strain level. The reverse situation is present for the cold rolled 0.04 strain and explosively formed 0.35 strain level specimens. The difference in properties as a result of orientation is not as marked at the high strain level.

The stress relief heat treatment had effects upon the A515 that would be anticipated with respect to recovery. However, the degree of decrease in yield and tensile strengths as a result of the type of strain mode was not as anticipated. In prior work with aluminum alloys, investigators^{15,16,17} had noted that heat treatments had to be adjusted to shorter times for explosively formed material. Using this analogy, the recovery of the explosively formed steel would have been greater than that of the cold rolled A515.

Stress relief heat treatment of the as-received stock resulted in a decrease in the tensile strength of about 6.6 percent (75,000 to 70,000 psi) and a decrease in the yield strength of about 23 percent (58,000 to 45,000 psi). At an effective strain level of 0.04 the corresponding decreases in the tensile and yield strengths were about 7.4 and 26 percent, respectively, for the explosively formed steel and 7.4 and 40 percent, respectively, for the cold rolled material. The results obtained by stress relieving the steel with 0.04 strain indicated that cold rolling had a dramatic effect upon the recovery process while explosive forming had about the same effect

as was noted in stress relieving the as-received or base stock. The recovery of the cold rolled A515 steel was so good that the tensile strength specification could no longer be met. This observation of a greater decrease in strength as a result of static straining conditions and an isochronal anneal was not consistent with the earlier observations of the effect of strain mode on heat treatment processes.

Explosive forming had a greater influence at the higher strain level, $\epsilon^* = 0.35$, on the tensile and yield strengths than cold rolling. Cold rolling increased the yield strength about 62% (58,000 to 94,000 psi) and the tensile strength about 32% (75,000 to 99,000 psi). Explosive forming increased the yield strength 67% (58,000 to 103,000 psi) and the tensile strength by about 45% (75,000 to 109,000 psi). Subsequent stress relief of the A515 steel strained to 0.35 effective strain reduced the yield strength of the cold rolled material by about 30 percent and that of the explosively formed material by about 29 percent. Decreases in tensile strengths were 52% and 51%, respectively, for the cold rolled and explosively formed material. At the higher strain levels the recovery was about the same on a percentage basis with a slightly greater effect being noted for the cold rolled material. On the basis of ductility the recovery of the explosively formed A515 was substantially greater than the cold rolled steel.

Stress relief annealing of the steel strained to 0.35 was required so the material would meet ASTM specifications. As with the steel cold rolled at 0.04 effective strain, the tensile strength of the cold rolled material strained to 0.35 effective strain was slightly below the 70,000 psi minimum. Again the heat treatment schedule would have to be altered for the cold rolled A515 so it could meet the minimum tensile strength requirement.

Charpy impact tests were conducted using standard size Charpy specimens for the as-received steel and the material strained to 0.045 effective strain. Results of the impact tests are given in Tables 7, 8, 9, 10, and 11 and are graphically presented in Figures 6, 7, 8, and 9. In Figure 6 a comparison is made of the results obtained with material strained to 0.04 effective strain and the as-received stock. Very little difference is present between the cold-rolled and explosively formed material, although the impact resistance of the cold-rolled material is slightly higher. The as-received material displays some orientation dependency with the longitudinal orientation having a lower ductile to brittle transition temperature and higher impact resistance. The orientation dependency is the same with the cold rolled material, but the reverse is true for the explosively formed stock. These results cannot be correlated with the tensile tests.

Stress relieving the A515 steel strained to 0.045 effective strain has an influence on the impact test results. A greater orientation effect is noted after stress relief for the explosively formed material. After forming, both orientations of the explosively formed steel were about the same with the transverse being slightly better. On stress relieving, the impact resistance of the transverse orientation was increased and the ductile to brittle transition temperature lowered. There was essentially no difference in the results obtained with the explosively formed longitudinal orientation.

Stress relieving the cold rolled specimens resulted in a slight decrease in the ductile to brittle transition temperature of the longitudinal orientation with very little difference being noted in the transverse orientation.

Table 7. Results of Impact Tests on Base Stock of
A515, Grade 70 Steel

<u>Condition</u>	<u>Orientation</u>	<u>Temperature, °F</u>	<u>Impact Energy, ft.-lb.</u>
As-received	Longitudinal	-238	2.0
		-148	2.0
		-58	3.5
		32	16.0
		75	65.0
		200	92.0
	Transverse	-234	2.0
		-145	3.0
		-58	3.0
		32	11.0
		75	32.0
		200	57.0
As-received, Stress Relieved	Longitudinal	-100	3.4
		0	5.0
		75	16.5
		200	83.0
		356	93.5
	Transverse	-100	3.5
		0	12.4
		75	42.0
		200	64.0
		356	66.5

Table 8. Results of Charpy Impact Tests on A515, Grade 70
Steel Cold Rolled to 0.04 Effective Strain

<u>Condition</u>	<u>Orientation</u>	<u>Temperature, °F</u>	<u>Impact Energy, ft.-lb.</u>
As-rolled	Longitudinal	-238	2.5
		-148	3.5
		-58	3.5
		32	4.0
		75	11.0
		75	13.0
		75	31.0
		136	44.0
		200	76.0
	Transverse	-148	2.0
		-58	3.3
		32	8.0
		75	18.5
		75	24.0
		75	18.0
		144	57.3
		200	56.9
Stress Relieved	Longitudinal	-148	3.0
		-58	3.0
		32	8.0
		32	9.0
		75	21.0
		75	36.5
		144	58.0
		200	79.2
		298	80.9
	Transverse	-148	2.3
		-58	2.3
		-58	7.5
		32	5.5
		74	19.5
		142	46.2
		200	59.5

Table 9. Results of Charpy Impact Tests on A515, Grade 70
Steel Explosively Formed, 0.04 Effective Strain

<u>Condition</u>	<u>Orientation</u>	<u>Temperature, °F</u>	<u>Impact Energy, ft.-lb.</u>
As-formed	Longitudinal	-238	3.5
		-148	3.5
		32	4.5
		75	27.5
		126	35.8
		200	52.5
		300	55.8
	Transverse	-148	3.5
		32	4.0
		50	5.5
		75	20.5
		126	46.0
		200	70.8
		305	53.2
Stress Relieved	Longitudinal	-148	3.8
		-58	3.3
		32	6.0
		32	14.0
		75	24.5
		126	36.0
		200	61.0
	Transverse	-148	2.0
		-58	3.0
		32	7.0
		75	49.0
		75	63.5
		126	61.5
		200	68.0
		306	89.0

Table 10. Results of Charpy Impact Tests⁽¹⁾ on A515, Grade 70
Steel Cold Rolled to 0.35 Effective Strain

<u>Condition</u>	<u>Orientation</u>	<u>Temperature, °F</u>	<u>Impact Energy, ft.-lb.</u>
As-rolled	Longitudinal	-100	1.5
		0	3.9
		75	8.0
		140	11.4
		200	13.7
		356	12.0
	Transverse	-100	1.2
		0	3.2
		75	5.5
		140	8.2
		200	10.2
		356	9.9
Stress Relieved	Longitudinal	-100	1.5
		-50	14.8
		0	17.2
		75	29.0
		200	34.0
		356	28.5
	Transverse	-100	1.4
		-50	4.9
		0	11.8
		75	21.0
		200	23.2
		356	22.5

(1) Sub-size specimens

Table 11. Results of Charpy Impact Tests ⁽¹⁾ on A515, Grade 70 Steel,
Explosively Formed, 0.35 Effective Strain

<u>Condition</u>	<u>Orientation</u>	<u>Temperature, °F</u>	<u>Impact Energy, ft.-lb.</u>
As-formed	Longitudinal	32	2.0
		75	4.0
		122	5.0
		167	6.0
		212	5.5
		302	7.0
	Transverse	32	2.0
		75	3.0
		122	7.0
		167	8.0
		212	8.0
		302	7.0
Stress Relieved	Longitudinal	-100	1.2
		-50	8.9
		0	10.5
		32	14.3
		75	18.3
		200	21.9
	Transverse	-100	1.2
		-50	8.9
		0	10.5
		32	10.5
		75	15.8
		200	20.5

(1) Sub-size specimens

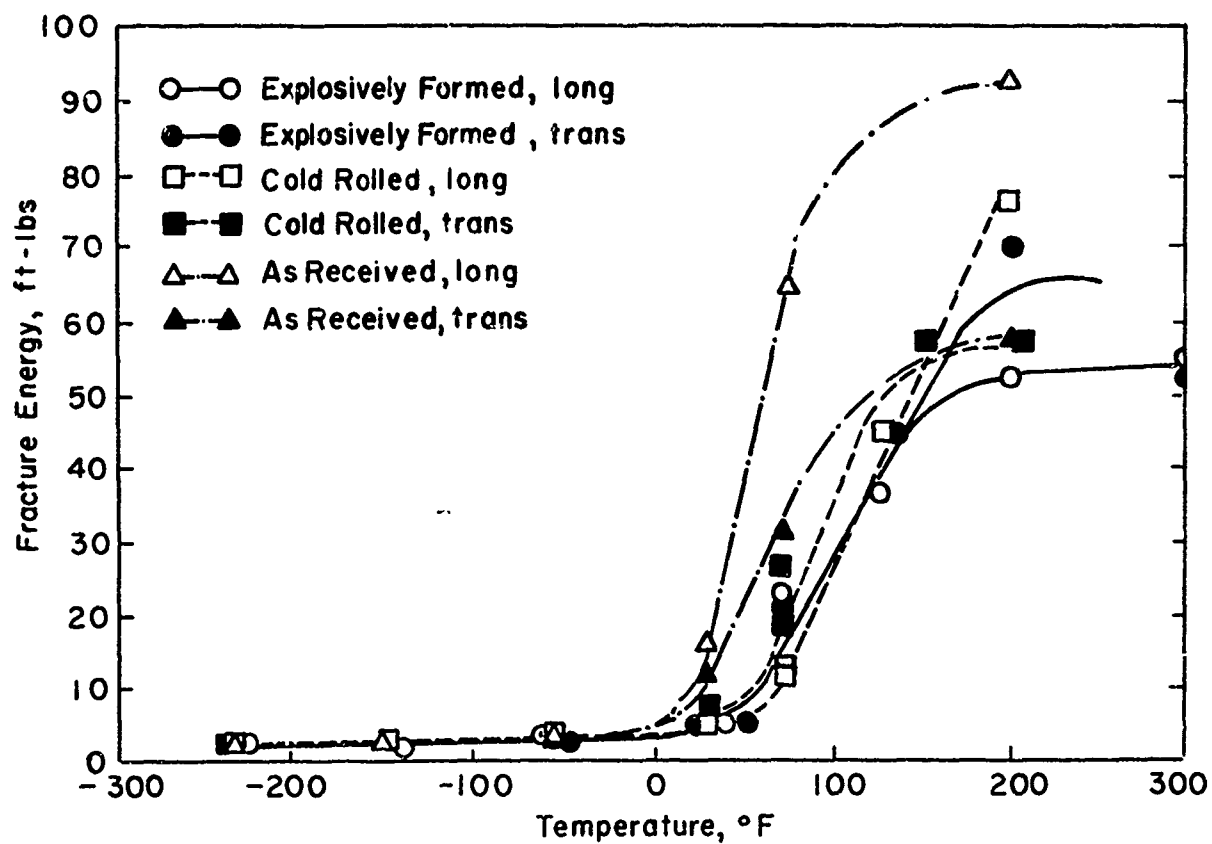


Figure 6. Results of Charpy Impact Tests on A515, Grade 70 Steel - As-Received; Cold Rolled and Explosively Formed, $\epsilon^* = 0.045$ Strain

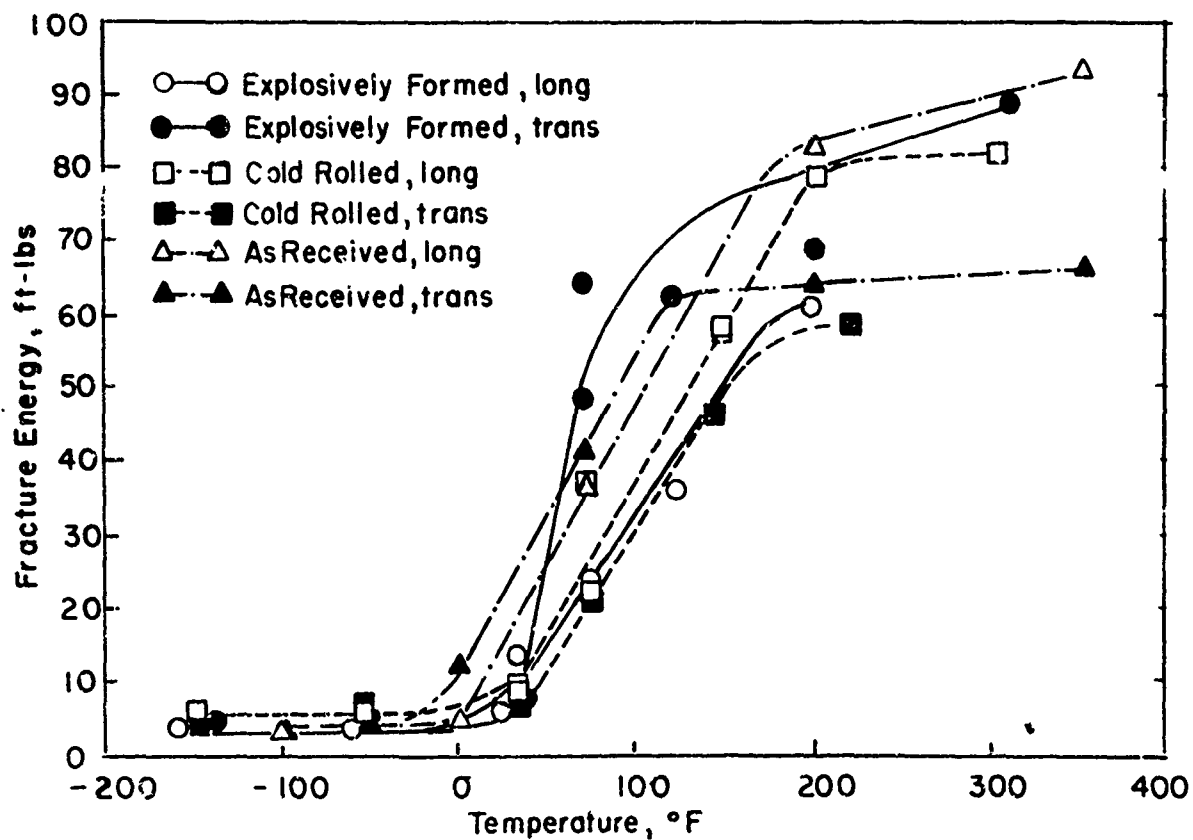


Figure 7. Results of Charpy Impact Tests on A515, Grade 70 Steel - As-Received; Cold Rolled and Explosively Formed, $\epsilon^* = 0.045$ Strain, Stress Relieved One Hour at 650°C

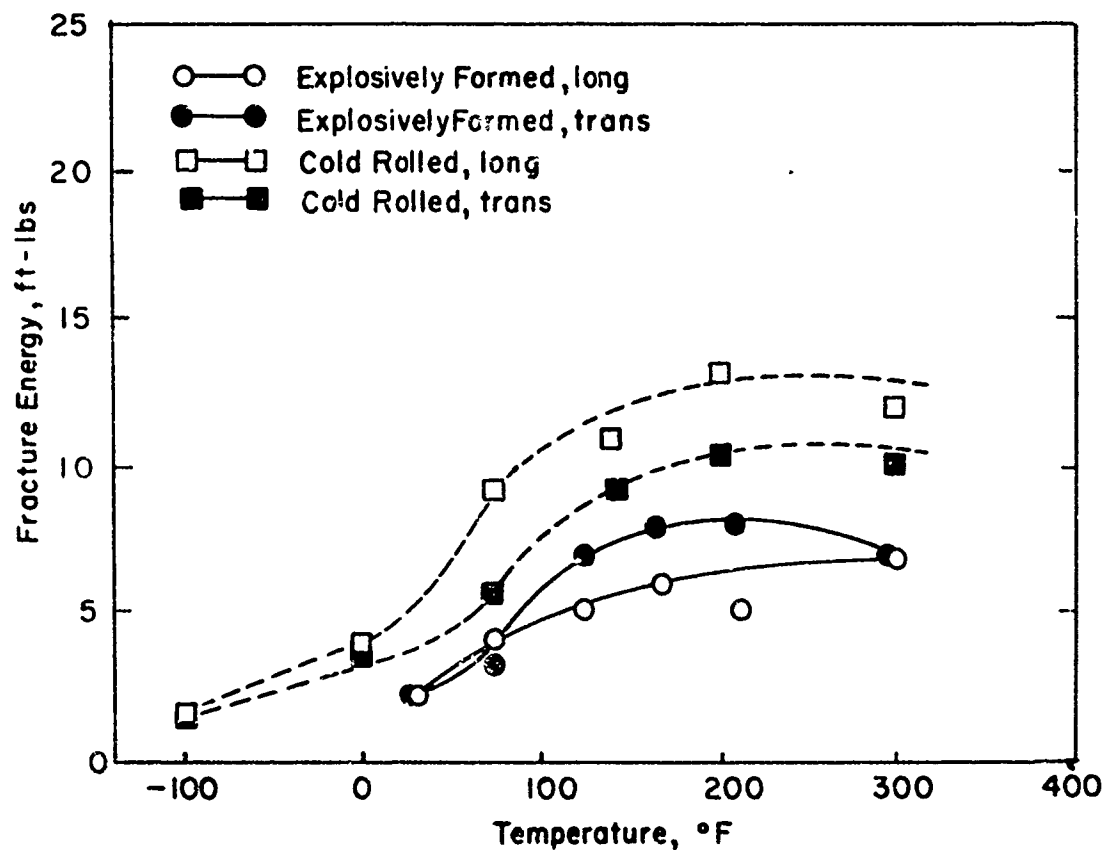


Figure 8. Results of Sub-Size Charpy Impact Tests on A515, Grade 70 Steel Cold Rolled and Explosively Formed to $\epsilon^* = 0.35$ Effective Strain

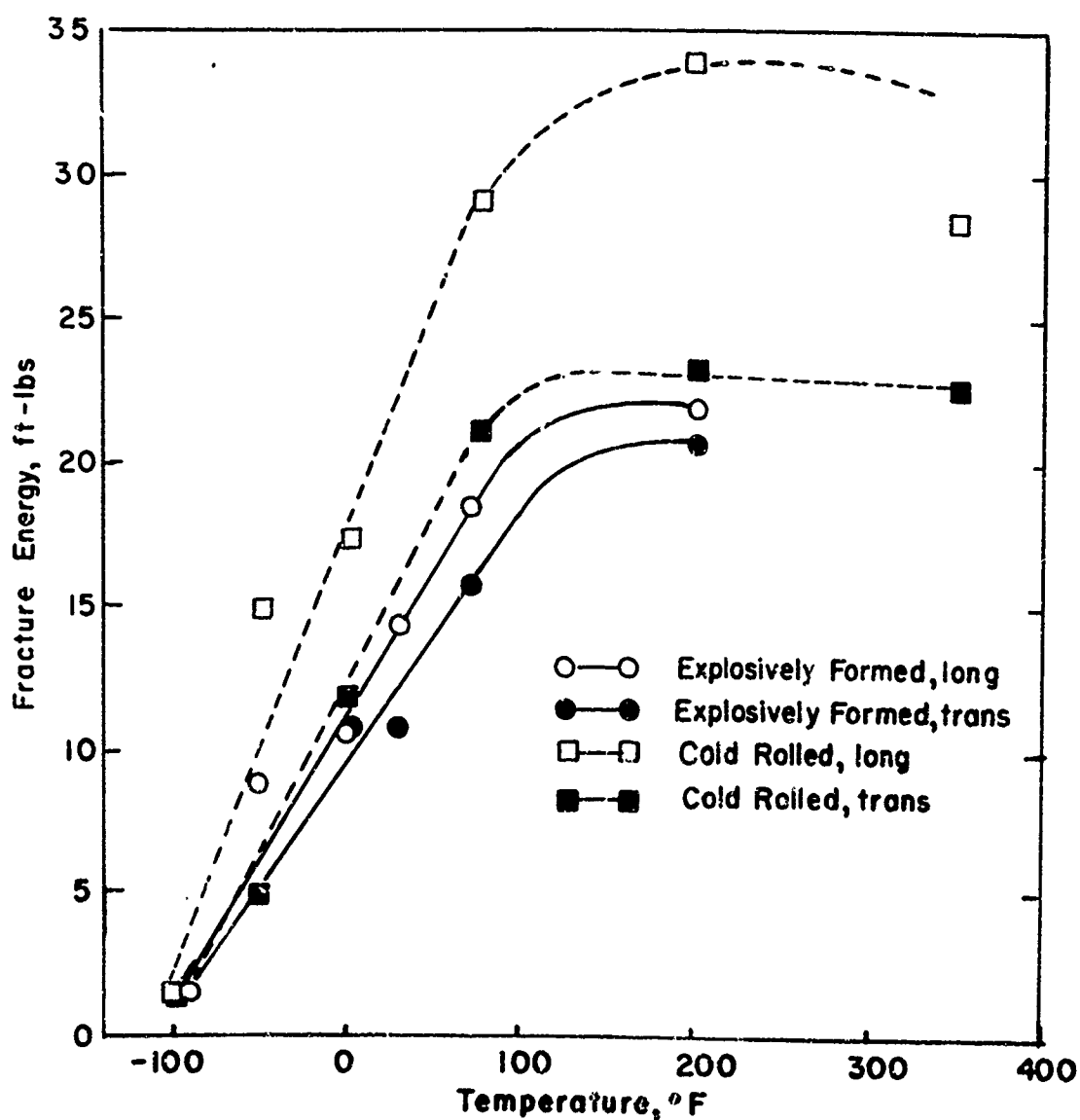


Figure 9. Results of Sub-Size Charpy Impact Tests on A515, Grade 70 Steel Cold Rolled and Explosively Formed to $\epsilon^* = 0.35$ Effective Strain and Stress Relieved at 650°C for One Hour

Table 12. Temperatures at Which an Impact Strength of 40 ft.-lb.
Is Obtained in A515, Grade 70 Steel -
As-Received, Cold Rolled and Explosively Formed
to 0.04 Strain, and Stress Relieved

<u>Straining Procedure</u>	<u>Orientation</u>	<u>Temperature for 40 ft.-lb., °F</u>	
		<u>Original Condition</u>	<u>After 650°C Stress Relief</u>
Cold Rolled	Longitudinal	125	100
Explosively Formed	Longitudinal	120	120
Explosively Formed	Transverse	120	70
Cold Rolled	Transverse	118	130
As-Received	Transverse	95	70
As-Received	Longitudinal	58	88
<u>Average of Both Orientations</u>			
As-Received		77	79
Cold Rolled		121	120
Explosively Formed		120	95

A marked increase was noted in the ductile to brittle transition temperature of the as-received longitudinal orientation specimens as a result of stress relief. In the transverse orientation a decrease in the ductile to brittle transition temperature was observed. Stress relief heat treatments generally increased the impact energy to fracture above the transition temperature for the materials strained to 0.045 effective strain.

A comparison of the impact results of the specimens strained at 0.045 effective strain is presented in Table 12. In this comparison the temperature at which an impact resistance of 40 ft.-lb is obtained is presented for each group of tests. After forming and before stress relief, the longitudinal orientation of the base stock has the lowest temperature and could be considered to have the greatest resistance to impact and the lowest DBT. On an average, the as-received stock is the best followed by the explosively formed and then the cold-rolled material. After stress relief the same average order is maintained.

Charpy impact tests conducted on the steel deformed to 0.35 effective strain indicated that cold rolling did not reduce the impact strengths as much as explosive forming (see Figure 9). This observation is consistent with the tensile tests in which the ductility of the cold rolled material was higher and the tensile strength lower than the explosively formed counterparts. Also, the longitudinal orientation of the Charpy tests gave the best results and in the tensile tests had the highest ductility within this group of specimens.

Stress relief annealing of the material strained to 0.35 effective strain markedly increased the impact energy to failure. The ductile to brittle transition temperature were reduced by stress relief heat treatment.

The cold rolled A515 steel had better resistance to impact than the explosively formed material after straining to 0.35 effective strain and stress relief. However, the tensile strength of the explosively formed stock was much higher and the ductility lower, which would explain the performance of this group of specimens.

A metallographic examination was conducted on the A515 steel corresponding to each condition tested. The base stock had a normalized isotopic structure which was not altered to any great extent by strains to 0.045 or subsequent stress relief heat treatment. At the higher strain levels (0.35 effective strain) grain elongation was apparent but was uniform in both orientations. Recrystallization of the ferrite grains occurred as a result of stress relief heat treatment at 650°C. Besides the recrystallization of the ferrite to give a smaller grain size, further spheroidization effects were noted in the pearlite grains. The recrystallization effects are consistent with other investigations¹⁸ in which increasing amounts of cold work reduce the temperature and time required for recrystallization.

CONCLUSIONS

The tests conducted on the A285, Grade C and A515 Grade 70 steels indicated that under the correct conditions of strain and heat treatment, these steels can be explosively formed and meet ASTM standards. At low strain levels up to 5%, stress relief annealing is not required to meet ASTM specifications for tensile properties but would be desirable for impact resistance.

The tests conducted on the A515, Grade 70 steel strained to 0.35 effective strain do indicate that regardless of how the strain is introduced,

stress relief heat treatments are required to restore the mechanical properties to meet specifications. Impact properties are enhanced as much as threefold by the stress relief heat treatment of the A515 strained to 0.35 effective strain.

The comparison of cold working methods indicates that very little difference can be anticipated in the tensile properties of the A285 steel at low strain levels. Impact strengths of the explosively formed and stress relieved A285 steels are comparable to non-strained stock subjected to the same heat treatment or not heat treated at all. Static straining plus heat treatment resulted in impact properties that were not as good as either the base stock or the explosively formed A285 steel.

Static straining of the A515 steel did not give tensile strengths that were as great as in explosively formed material. This is an anomaly when compared with existing data in which static strain rates as compared to dynamic generally result in harder and stronger low carbon steels. Stress relief annealing had a greater effect at both high and low increments of strains on reducing the tensile and yield strengths and on increasing the ductility. Again, if increase in strength were a function of stored energy and dislocation density, a greater effect on stress relief annealing would have been anticipated from the explosively formed steel than from the cold rolled. However, the situation was exactly the opposite, which again is another anomaly.

FUTURE WORK

In light of the anomalies found in this investigation, it would be beneficial to conduct electron microscope studies on the sub-structure and the effect of static and dynamic strain on recovery processes.

Bibliography

1. H. E. Otto and R. Mikesell, Proceedings 3rd Int'l. Conf. Center for High Energy Forming, Vail, Colorado, 1971, pp. 4.2.1-4.2.21.
2. K. R. Agricola et al., Advanced Explosive Forming Processes (HERF), AFML-TR-67-70, 1967.
3. T. Kvam and B. Augland, "High Energy Rate Working of Metals," Proc. NATO Advanced Study Institute, Central Institute for Industrial Research, Oslo, Norway, September 1964, pp. 264-77.
4. T. Williams, Sheet Metal Indust., Vol. 39, 1962, pp. 487-94.
5. J. D. Campbell and J. Duby, Proc. Roy. Soc. (London), Vol. A236, 1956, pp. 24-40.
6. J. D. Campbell and J. Duby, Proc. Conf. on Properties of Materials at High Rates of Strain, Inst. Mech. Eng. (London), 1957, pp. 214-20.
7. F. V. Warnock and J. A. Pope, Proc. Inst. Mech. Eng. (London), Vol. 157, 1947, pp. 33-44.
8. J. D. Campbell and C. J. Menden, J. Mech. Phys. Solids, Vol. 6, 1957, pp. 53-62.
9. R. N. Orava and H. E. Otto, J. Metals, Vol. 22, Feb. 1970, pp. 17-31.
10. C. A. Verbraak, Met. Progress, Vol. 83, January 1963, pp. 109-12.
11. R. N. Orava, R. M. Mikesell, G. S. Whiting, and H. E. Otto, Met. Trans. Vol. 2, June 1971.
12. Standard Specification for Low Carbon and Intermediate Tensile Strength Carbon Steel Plates for Pressure Vessels, ASTM Designation A-285-70a, 1972, Annual Book of ASTM Standards, ASTM, Philadelphia, 1972.
13. Standard Specification for Carbon Steel Plates for Pressure Vessels for Intermediate and Higher Temperature Service, ASTM Designation A515-71, ibid. Reference 12.
14. L. Alting, Proc. 3rd Int'l. Conf. Center for High Energy Forming, Vail, Colorado, 1971, pp. 6.1.1-6.1.17.
15. J. T. Snyder et al., "Explosive Forming of 2219 Aluminum," Martin Co., Report No. CR-65-41, 1965.
16. L. J. Van Torne and H. M. Otte, ASM Metals Eng. Quart., Vol. 6, February 1966, pp. 43-7.

17. B. Covell and D. Lovell, "Effect of Fabrication Processes on the Mechanical Properties of 0.375 Inch Thick 2219-T31 Aluminum Alloy," Boeing Co., Report No. D2-20910, 1962; AD 296 711.
18. W. C. Leslie, J. T. Michalak, and F. W. Aul, in Iron and Its Dilute Solid Solutions, edited by C. W. Spencer and F. E. Werner, Interscience, New York, 1963, pp. 119-212.

VII. EDGE PULL-IN IN EXPLOSIVELY FORMED DOMES

M. Kaplan

S. Kulkarni

SUMMARY

A simplified analysis for the prediction of edge pull-in of explosively formed domes is developed. The primary assumptions are that inertia effects are negligible and that the shape of the middle surface of the blank is known at all times in the forming process.

Markov's principle of minimum plastic work in conjunction with the Rayleigh-Ritz method is used. The results of the analysis are used to compare thickness strain both in static dome formation and bulge testing and to predict the initiation of necking in the dome. There is good agreement in all cases.

Predicted values of edge pull-in versus draw depth also agree well with explosive dome forming data. The analysis, however, does not accurately predict the strain field in the dome, particularly in the region of the apex. By an extension of Markov's principle, it is shown that the error in the prediction of strain is not a result of inertia effects, but rather is caused by differences in loading in the static and dynamic forming processes. The reduced thinout which occurs dynamically is a result, therefore, of the interaction between charge location, energy transfer medium, and the blank, and is not a property which is inherent in the explosive forming process itself.

INTRODUCTION

In the explosive forming of domes a thin circular metal blank supported by a suitable hold-down mechanism near its outer edge is subjected to a blast load when the explosive charge is detonated. The resulting pressure forces the central portion of the blank, i.e., the dome, into the die cavity. As the depth of the dome increases, the annular flange feeds material into the dome, thus preventing excessive thinout. The edge pull-in, i.e., the inward radial displacement at the edge of the blank, is appreciable for deep domes even with hold-down pressures sufficient to prevent flange wrinkling. With shallow domes, edge pull-in is insignificant.

The edge pull-in is an important parameter in determining the mechanical state of an explosively formed deep draw dome. Excessive pull-in can produce flange wrinkling, while insufficient pull-in can result in tearing of the blank. Also, since the flange is usually discarded after the dome is formed, prediction of pull-in is necessary for economic reasons.

In the present study, the edge pull-in as a function of draw depth will be predicted for a draw-formed hemispherical dome.

The deformation of clamped metal blanks subjected to blast or impulsive type loading has been considered by Hudson,⁽¹⁾ Wang,⁽²⁾ and Witmer, et al.^(3,4,5) Hudson used a moving plastic hinge concept to examine an unloaded blank with a specified initial velocity field. Wang considered only bending stresses in his rigid plastic analysis, and Witmer, et al. made a rigorous numerical analysis of a circular plate subjected to blast loading which gave good agreement with experimental results. Hill⁽⁶⁾ used

a quasi-static analysis to obtain an explicit solution for a clamped metal diaphragm which is bulged plastically by lateral pressure. These analyses do not include the flow of flange material into the die cavity and thus cannot be used to predict pull-in.

A simpler formulation of the dynamic problem led to the analysis by Thurston⁽⁷⁾ who extended the work of Boyd⁽⁸⁾ to include specified amounts of edge pull-in. This analysis, however, is restricted to shallow dish shapes.

DISCUSSION OF THE PROBLEM

A complete mathematical description of the process has not yet been achieved. A primary objective of this study is to provide a relatively simple analysis, based on realistic assumptions, that will yield reliable predictions of edge pull-in. Accordingly, two simplifying assumptions are made.

A_1 : The shape of the dome is always a segment of a sphere.

A_2 : The dome is formed at a sufficiently slow rate so that the flow process is quasi-static, i.e., the accelerations are negligible at all times.

Assumption A_1 is based on an investigation conducted by Ezra⁽⁹⁾ to determine optimal standoff distance with regard to uniformity of strain field, uniformity of draw, minimization of thin out and minimization of charge weight. He found that a standoff distance/die diameter ratio of 0.167 is most favorable. The domes which result from the use of this ratio are nearly spherical.

Assumption A_2 was based on the result of experiments conducted for the purpose of comparing the edge pull-in of statically and dynamically formed domes. The blank material was 2014-O aluminum. A die was used to assure the same final shape in both cases. Dynamic forming was achieved by forming the domes explosively in water. Static forming was accomplished by rubber pressing. A shaped rubber block, confined in a piston-cylinder arrangement, was pressed against a greased blank. The cylinder walls were

attached to the blank hold-down ring and pressure was applied to a steel piston on top of the rubber block.

Figure 1 shows the profiles of the statically and dynamically formed domes and Figures 2(a) and 2(b) show their circumferential and thickness strain distributions, respectively. The circumferential strains were determined from the change in length of the photographically etched circumferential grid lines. The thickness strains were calculated from the change in thickness.

These results show that even though the strain distribution is somewhat different in the two domes, the edge pull-ins are nearly identical. This implies that an analysis which proceeds from assumptions A_1 and A_2 should be suitable for predicting pull-in. It is clear from the experimental observations, however, that there will be some error in the predicted strain field, particularly in the neighborhood of the apex of the dome.

Based on experimental observations, we shall use the usual membrane assumptions that bending effects are negligible and the shear stresses and hence the shear strain rates vanish across the thickness. In view of A_1 it is appropriate to use spherical coordinates (R, ϕ, θ) for the dome. Cylindrical coordinates (r, θ, z) will be used for the flange. The longitudinal z axis is assumed to coincide with the axis of symmetry of the dome and the flange (Figure 3).

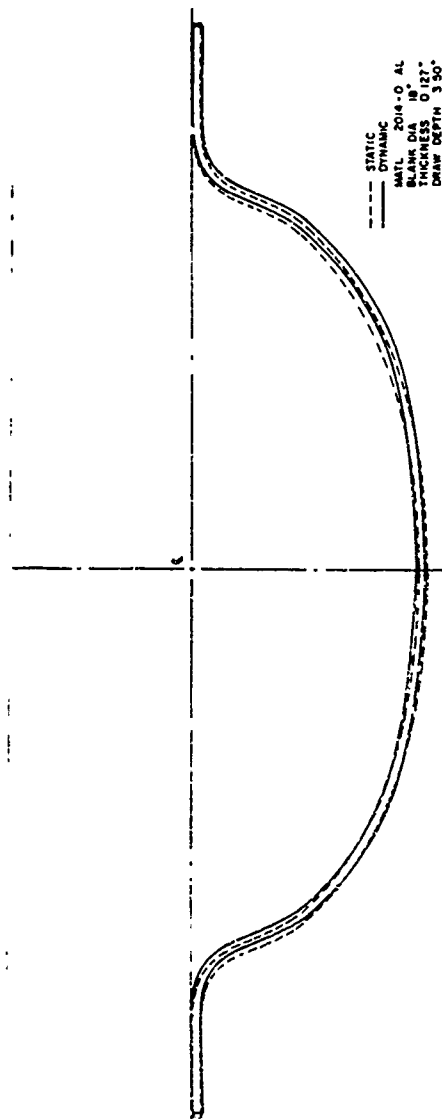


Figure 1. Profiles of Statically and Dynamically Die Formed 2014-O Aluminum Domes

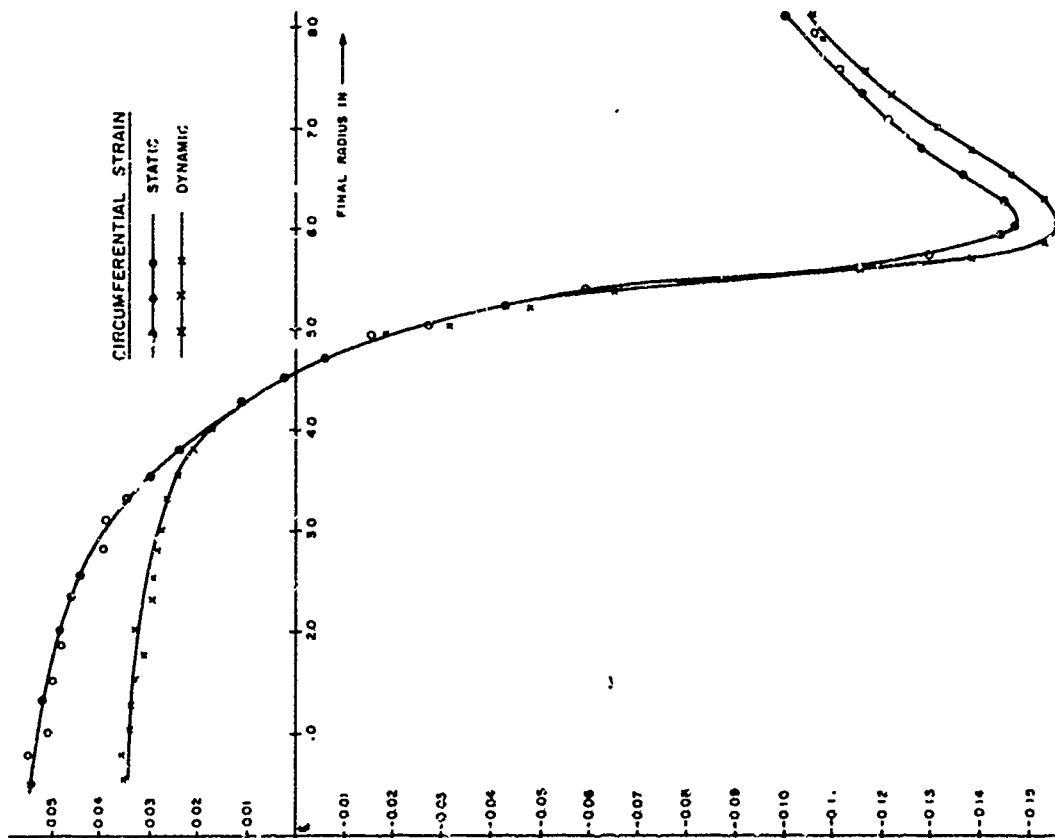


Figure 2(a). Circumferential Strain Distribution in Statically and Dynamically Die Formed 2014-0 Aluminum Domes

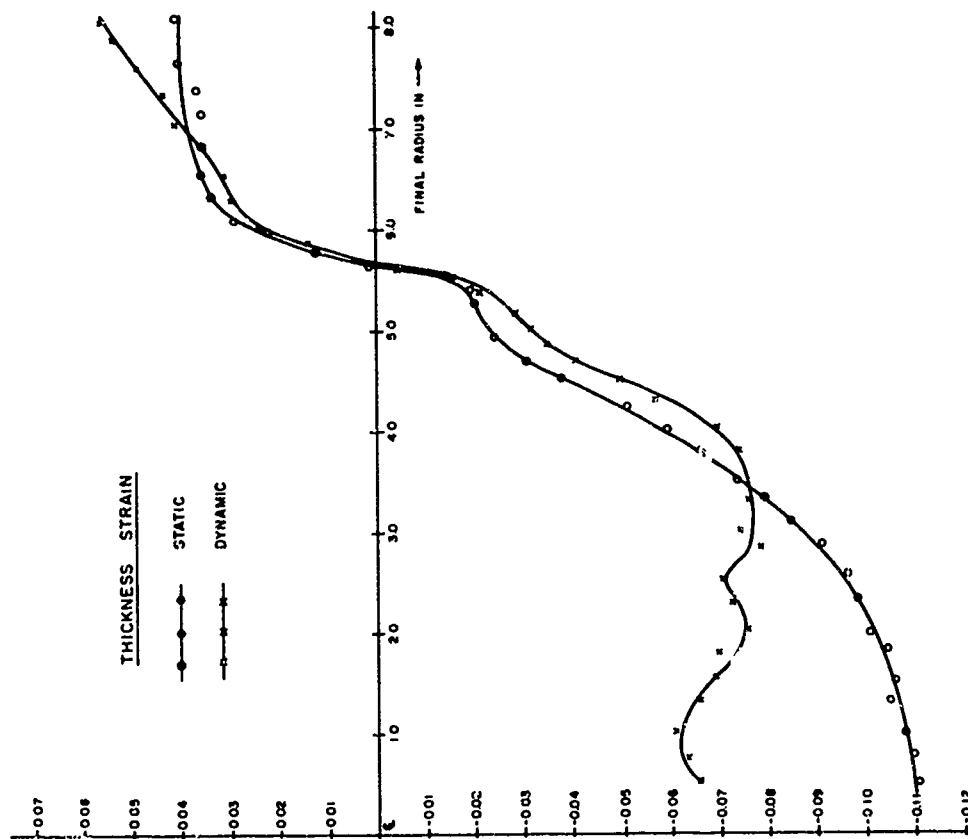


Figure 2(b). Thickness Strain Distribution in Statically and Dynamically Die Formed 2014-0 Aluminum Domes

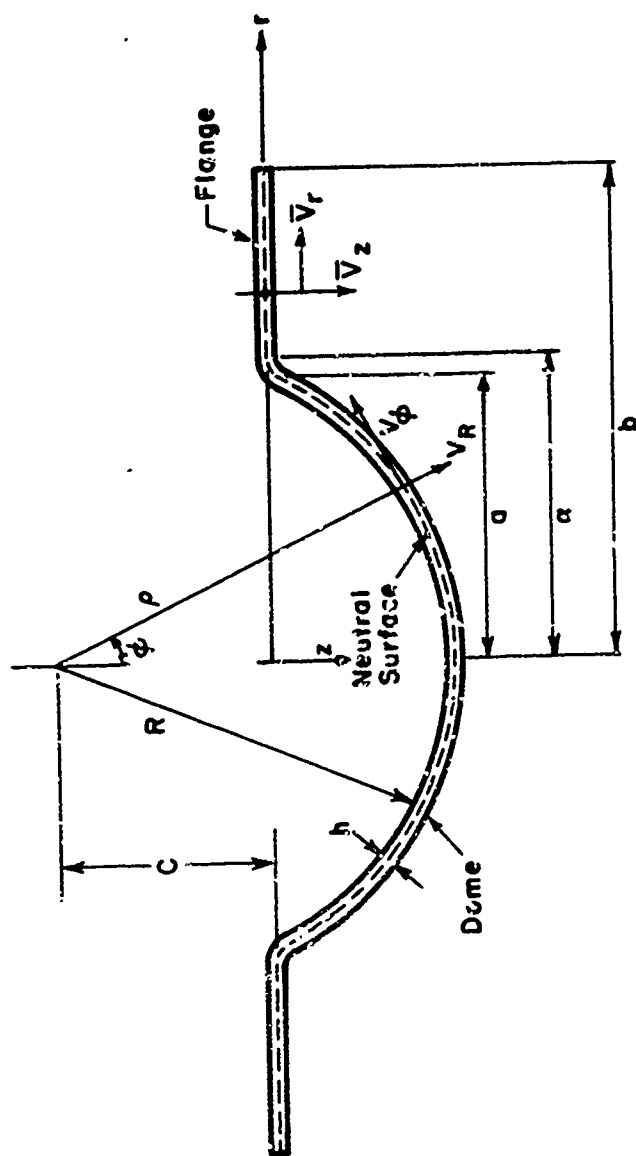


Figure 3. Nomenclature for Dome and Flange

MATHEMATICAL MODEL

The analytical approach will be to use the Rayleigh-Ritz method in conjunction with Markov's principle which states:

Among admissible solutions which satisfy the conditions of compatibility and incompressibility, as well as the geometrical boundary conditions, the actual solution renders the rate of work an absolute minimum.

The variational principle stated above has been developed for quasi-static problems in the flow theory of plasticity. Its use is restricted to rigid-plastic Prandtl-Reuss materials described by the equations

$$S_{ij} = \frac{\sqrt{2}}{\sqrt{3}} \frac{\sigma_o}{\sqrt{\dot{\epsilon}_{mn} \dot{\epsilon}_{mn}}} \dot{\epsilon}_{ij} \quad (1)$$

where S_{ij} and $\dot{\epsilon}_{ij}$ are the deviatoric stress and strain rates, respectively. σ_o is the yield stress in simple tension.

The work done per unit time on an elemental volume dV is given by

$$W = \frac{\sqrt{2}}{\sqrt{3}} \sigma_o \int_V \sqrt{\dot{\epsilon}_{ij} \dot{\epsilon}_{ij}} dV . \quad (2)$$

Equation (2) will be used to evaluate the rate of work for the dome and the flange.

Dome Analysis

The physical components of the normal strain rates in spherical coordinates, assuming axial symmetry, are

$$\begin{aligned}
\dot{\epsilon}_{RR} &= v_{R,R} \\
\dot{\epsilon}_{\phi\phi} &= \frac{v_R}{R} + \frac{1}{R} v_{\phi,\phi} \\
\dot{\epsilon}_{\theta\theta} &= \frac{v_R}{R} + \frac{v_{\phi}}{R} \cot \phi
\end{aligned}
\tag{3}$$

and $\dot{\epsilon}_{R\phi} = 0$ because of the membrane assumption. In equations (3) the v_i are the components of velocity. The comma is used to denote partial differentiation with respect to the spatial coordinates.

Assumption A_1 constrains the radial velocity field v_R at the neutral surface such that

$$v_R = \left(1 - \frac{a^2}{\sqrt{\rho^2 - a^2}} \cos \phi\right) \dot{\rho} \tag{4}$$

where ρ is the radius to the neutral surface and a is the radius of the die. Because of A_2 , the time can be replaced by any other parameter which varies monotonically with it and is characteristic of the deformation. In the following, therefore, we shall replace real time by the pseudo-time variable ρ . Noting that time differentiation with this procedure reduces to differentiation with respect to ρ , we have

$$\dot{\rho} = 1 \quad \text{and} \quad ()_{,t} = ()_{,\rho} . \tag{5}$$

Thus, the expression for the radial velocity at the neutral surface reduces to

$$v_R = \left(1 - \frac{\rho}{\sqrt{\rho^2 - a^2}} \cos \phi\right) . \quad (6)$$

The first of relations (3), physically, is the thickness strain rate. Using Alami's definition of finite strain,⁽¹⁰⁾ the average thickness strain is given by

$$\epsilon_{RR} = \frac{1}{2} \left(1 - \frac{h_0^2}{h^2}\right) \quad (7)$$

where h_0 and h are the original and current thickness respectively. For the velocity field associated with this problem, the material derivatives D/Dt of the principle strains are equal to the strain rates.* Therefore, the average thickness strain rate is given by

$$\dot{\epsilon}_{RR} = \frac{D\epsilon_{RR}}{Dt} = \frac{h_0^2}{h^3} (h_{,\rho} + \frac{v_\phi}{\rho} h_{,\phi}) . \quad (8)$$

The membrane assumption implies that the tangential strain rate $\dot{\epsilon}_{\phi\phi}$ and the hoop strain rate $\dot{\epsilon}_{\theta\theta}$ are constant across the thickness. Hence we can write the last two relations of (3), at the neutral surface, as

$$\dot{\epsilon}_{\phi\phi} = \frac{v_R}{\rho} + \frac{1}{\rho} v_{\phi,\phi} \quad (9)$$

$$\dot{\epsilon}_{\theta\theta} = \frac{v_R}{\rho} + \frac{v_\phi}{\rho} \cot \phi .$$

*For the derivation we refer readers to ref. (11).

Flange Analysis

A bar will be used to distinguish the flange displacement, velocity, strain rate and stress components from similar quantities in the dome. Neglecting friction, the equilibrium equations in the radial and axial directions are

$$\begin{aligned}\bar{\sigma}_{rr,r} + \frac{1}{r} (\bar{\sigma}_{rr} - \bar{\sigma}_{\theta\theta}) &= 0 \\ \bar{\sigma}_{zz,z} &= 0\end{aligned}\tag{10}$$

and the equation in the tangential direction is identically zero. The boundary conditions are (Figure 3)

$$\begin{aligned}\bar{\sigma}_{rr} &= 0 \quad \text{at} \quad r = b, \\ \bar{\sigma}_{zz} &= -P \quad \text{at} \quad z = \pm \frac{t}{2}\end{aligned}\tag{11}$$

where P is the clamping pressure.

The von Mises yield condition, which represents an ellipse in the $\bar{\sigma}_{rr}, \bar{\sigma}_{\theta\theta}$ plane, can be approximated by the straight line

$$\bar{\sigma}_{rr} - \bar{\sigma}_{\theta\theta} = \sigma_o\tag{12}$$

for the stress condition in the flange, i.e., $\bar{\sigma}_{rr} > 0$; $\bar{\sigma}_{\theta\theta} < 0$.

The problem is statically determinate. Using (12) in (10) together with (11), the stress field in the flange is

$$\begin{aligned}\bar{\sigma}_{rr} &= \sigma_o \ln \frac{b}{r} \\ \bar{\sigma}_{\theta\theta} &= \sigma_o \left(\ln \frac{b}{r} - 1 \right) \\ \bar{\sigma}_{zz} &= -P\end{aligned}\tag{13}$$

The stress-strain rate relations (1) will be used to determine the velocities and strain rates. The ratio of the radial and hoop strain rates is

$$\frac{\dot{\epsilon}_{rr}}{\dot{\epsilon}_{\theta\theta}} = \frac{2\bar{\sigma}_{rr} - \bar{\sigma}_{\theta\theta} - \bar{\sigma}_{zz}}{2\bar{\sigma}_{\theta\theta} - \bar{\sigma}_{rr} - \bar{\sigma}_{zz}} \quad (14)$$

Substituting the strain rate-velocity relations for the flange given by

$$\begin{aligned} \dot{\epsilon}_{rr} &= \bar{v}_{r,r} \\ \dot{\epsilon}_{\theta\theta} &= \frac{\bar{v}_r}{r} \\ \dot{\epsilon}_{zz} &= \bar{v}_{z,z} \end{aligned} \quad (15)$$

in (14) together with (13), gives

$$\bar{v}_r = \frac{\frac{db}{d\rho} r (-2\sigma_o + P)^3}{b[\sigma_o (\ln \frac{b}{r} - 2) + P]^3} \quad (16)$$

after satisfying the boundary condition that $\bar{v}_r = \frac{db}{d\rho}$ at $r = b$. It follows that the radial and hoop strain fields are

$$\dot{\epsilon}_{rr} = \bar{v}_{r,r} = \frac{\frac{db}{d\rho} (-2\sigma_o + P)^3 [\sigma_o (\ln \frac{b}{r} + 1) + P]}{b[\sigma_o (\ln \frac{b}{r} - 2) + P]^4} \quad (17)$$

and

$$\dot{\epsilon}_{\theta\theta} = \frac{\bar{v}_r}{r} = \frac{\frac{db}{d\rho} (-2\sigma_o + P)^3}{b[\sigma_o (\ln \frac{b}{r} - 2) + P]^3}$$

respectively. The axial strain rate $\dot{\epsilon}_{zz}$ is obtained from the incompressibility condition $\dot{\epsilon}_{rr} + \dot{\epsilon}_{\theta\theta} + \dot{\epsilon}_{zz} = 0$.

$$\dot{\epsilon}_{zz} = \frac{-\frac{db}{dp} (-2\sigma_o + p)^3 [\sigma_o (2 \ln \frac{b}{r} - 1) + 2p]}{b[\sigma_o (\ln \frac{b}{r} - 2) + p]^4} \quad (18)$$

Noting that $\dot{\epsilon}_{zz} = \bar{v}_{z,z}$, (18) can be integrated to give the axial velocity as

$$\bar{v}_z = \frac{-\frac{db}{dp} (-2\sigma_o + p)^3 [\sigma_o (2 \ln \frac{b}{r} - 1) + 2p]}{b[\sigma_o (\ln \frac{b}{r} - 2) + p]^4} z \quad (19)$$

after satisfying the boundary condition that $\bar{v}_z = 0$ at $z = 0$. The strain rate and velocity field for the flange have been found in terms of the outer radius b and its time rate of change.

Continuity Conditions at the Edge

The incompressibility of the blank material requires that the rate of mass flow at the inner edge of the flange be equal to that at the edge of the dome. Therefore,

$$\alpha (\bar{v}_r \bar{h})_{r=\alpha} = a (v_\phi h)_{\phi=\phi_e} \quad (20)$$

where the flange quantities are to be evaluated at $r = \alpha$ and the dome quantities at $\phi_e = \sin^{-1} \frac{a}{\rho}$ (Figure 3). Experimental observation indicates that the change in blank thickness over the edge is quite small (of the order of 0.2%). Equation (20) can then be simplified and expressed as two separate relations

$$\alpha (\bar{v}_r)_{r=\alpha} = a (v_\phi)_{\phi=\phi_e} \quad (21)$$

and

$$(\bar{h})_{r=\alpha} = (h)_{\phi=\phi_e} \quad (22)$$

Equations (21) and (22) provide two conditions for relating dome and flange quantities. In the preceding section, the flange velocities were found in terms of $b(\rho)$. Equation (21) is, therefore, a relationship between $b(\rho)$ and v_ϕ . Since both the radial and hoop velocities in the dome are known, the problem has been reduced to the determination of v_ϕ .

FORMULATION OF RATE OF WORK

The Rayleigh-Ritz method requires a representation of the velocity field in terms of arbitrary constants chosen such that the rate of work is minimized. A representation which satisfies the condition that the tangential velocity vanish in the entire blank when it is flat ($\rho=\infty$) and also vanish at the blank center for all values of ρ can be written as

$$v_{\phi} = b_0 \left(\frac{a}{\rho}\right) \sin \phi + b_1 \left(\frac{a}{\rho}\right)^2 \sin 2\phi + \dots \quad (23)$$

where b_0 , b_1 , etc. are arbitrary constants to be determined by the minimization procedure. The total rate of work is to be formulated and minimized with respect to these constants to determine the mechanical state in the deformed part.

The total rate of work is the sum of the rate of work in the dome, the rate of work in the flange and the rate of work at the lip of the die as the material flows over the edge and into the die. The rate of work at the lip of the die is very small in comparison to that in the dome and flange and will, therefore, be neglected.

Rate of Work in Dome

The rate of work (2) in the dome, as a function of the principal strain rates and the thickness h , is

$$W_D = \frac{\sqrt{2}}{\sqrt{3}} \sigma_0 \int_0^{\sin^{-1} \frac{a}{\rho}} \int_0^{2\pi} \sqrt{\dot{\epsilon}_{RR}^2 + \dot{\epsilon}_{\phi\phi}^2 + \dot{\epsilon}_{\theta\theta}^2} \rho^2 h \sin \phi \, d\phi \, d\theta \quad (24)$$

The use of equations (23) and (6) in the strain rate - velocity relations (3) yields the following expressions for the strain rates

$$\dot{\epsilon}_{RR} = \frac{h_0^2}{h^3} \left[h_{,\rho} + \frac{1}{\rho} \left\{ b_0 \left(\frac{a}{\rho} \right) \sin \phi + b_1 \left(\frac{a}{\rho} \right)^2 \sin 2\phi + \dots \right\} h_{,\phi} \right] \quad (25)$$

$$\dot{\epsilon}_{\phi\phi} = \frac{1}{\rho} \left(1 - \frac{\rho}{\sqrt{\rho^2 - a^2}} \cos \phi \right) + \frac{1}{\rho} \left\{ b_0 \left(\frac{a}{\rho} \right) \cos \phi + 2b_1 \left(\frac{a}{\rho} \right)^2 \cos 2\phi + \dots \right\}$$

$$\dot{\epsilon}_{\theta\theta} = \frac{1}{\rho} \left(1 - \frac{\rho}{\sqrt{\rho^2 - a^2}} \cos \phi \right) + \frac{1}{\rho} \left\{ b_0 \left(\frac{a}{\rho} \right) \cos \phi + 2b_1 \left(\frac{a}{\rho} \right)^2 \cos^2 \phi + \dots \right\}.$$

The dome thickness h in (24) and (25) is a function of the coefficients b_0, b_1, \dots . This follows from the recognition that h at any time depends on the previous history of deformation and that the specification of b_0, b_1, \dots determines the entire velocity field in the dome for all values of draw depth. The necessary functional relationship can be obtained by use of the incompressibility condition $\dot{\epsilon}_{RR} + \dot{\epsilon}_{\phi\phi} + \dot{\epsilon}_{\theta\theta} = 0$ and (25). The result is

$$\begin{aligned} & \frac{h_0^2}{h^3} \left[h_{,\rho} + \frac{1}{\rho} \left\{ b_0 \left(\frac{a}{\rho} \right) \sin \phi + b_1 \left(\frac{a}{\rho} \right)^2 \sin 2\phi + \dots \right\} h_{,\phi} \right] \\ &= -\frac{2}{\rho} \left(1 - \frac{\rho}{\sqrt{\rho^2 - a^2}} \cos \phi \right) - \frac{1}{\rho} \left[b_0 \left(\frac{a}{\rho} \right) \cos \phi + 2b_1 \left(\frac{a}{\rho} \right)^2 \cos 2\phi + \dots \right] \\ & \quad - \frac{1}{\rho} \left[b_0 \left(\frac{a}{\rho} \right) \cos \phi + 2b_1 \left(\frac{a}{\rho} \right)^2 \cos^2 \phi + \dots \right]. \end{aligned} \quad (26)$$

The relation (26) is a nonlinear partial differential equation for the current thickness h in the dome. It is clear from an examination of the rate of work integral that a substantial simplification in the numerical procedure

necessary for the determination of b_1 will result if a closed form solution for h in terms b_0, b_1 , etc. can be obtained. We note that an exact closed form solution for h can be determined at the center ($\phi = 0$) and edge of the dome ($\phi = \sin^{-1} \frac{a}{\rho}$). For the case where b_2, b_3, \dots are zero, these solutions are given by

$$\frac{h_o^2}{h_{edge}^2} = 1 - 4 \int_0^{\frac{1}{\rho}} \frac{b_0 a \sqrt{1-a^2 y^2} + b_1 a^2 y \sqrt{2-3a^2 y^2}}{1 - \{b_0 a y + 2b_1 a^2 y^2 \sqrt{1-a^2 y^2}\} (1-a^2 y^2)} dy \quad (27)$$

$$\frac{h_o^2}{h_{center}^2} = 0.5 - \ln 0.25 + 2 \ln \left(\frac{1}{1 + \sqrt{1 - \frac{a^2}{\rho^2}}} \right) - 2b_0 \left(\frac{a}{\rho} \right) - 2b_1 \left(\frac{a}{\rho} \right)^2 \quad (28)$$

An approximate solution for the entire dome is obtained by assuming a parabolic distribution for h between these two points.* This solution is

$$h = (h_{edge} - h_{center}) \frac{\phi^2}{(\sin^{-1} \frac{a}{\rho})^2} + h_{center} \quad (29)$$

The rate of work done in the dome can now be written as

$$W_D = \frac{4\pi\sigma_o}{\sqrt{3}} \int_0^{\sin^{-1} \frac{a}{\rho}} \sqrt{\dot{\epsilon}_{\phi\phi}^2 + \dot{\epsilon}_{\theta\theta}^2 + \dot{\epsilon}_{\phi\theta} \dot{\epsilon}_{\theta\phi}} \rho^2 h \sin \phi d\phi \quad (30)$$

after integrating (24) with respect to θ and using the incompressibility condition, where the strain rates $\dot{\epsilon}_{\phi\phi}$ and $\dot{\epsilon}_{\theta\theta}$ and thickness h are known functions of the arbitrary constants b_0, b_1, \dots

*Experimental values for h can be accurately fit by parabolic curves.

Rate of Work in Flange

Proceeding as in the case of the dome, the rate of work in the flange is

$$W_F = \frac{4\pi\sigma_o}{\sqrt{3}} \int_a^b \sqrt{\dot{\epsilon}_{rr}^2 + \dot{\epsilon}_{\theta\theta}^2 + \dot{\epsilon}_{rr}\dot{\epsilon}_{\theta\theta}} \bar{h} r dr \quad (31)$$

The current radius of the outer edge b is obtained as a function of ρ , b_o , b_1 , etc., from the continuity relationship (21). The result is

$$b = a \exp \left[\frac{2\sigma_o - P}{\sigma_o} - \frac{1}{\sigma_o} \sqrt{\frac{T}{b_o U + b_1 S + \dots - Q}} \right] \quad (32)$$

where

$$T = \frac{-\alpha(-2\sigma_o + P)^3}{2\sigma_o}$$

$$U = -\frac{a}{\alpha} \left(\frac{a^2}{\rho} \right)$$

$$S = \frac{a}{\alpha} \left[\frac{2}{3} a \left(1 - \frac{a^2}{\rho^2} \right) \sqrt{1 - \frac{a^2}{\rho^2}} - \frac{2}{3} a \right]$$

$$Q = \frac{\alpha(-2\sigma_o + P)^3}{2\sigma_o \left[\sigma_o \left\{ \ln \left(\frac{B}{\alpha} \right) - 2 \right\} + P \right]^2}$$

Equation (21) gives the flange thickness strain to be expressed in terms of b_o , b_1 , etc. However, an approximate solution for \bar{h} , determined in a manner similar to the procedure adopted for the dome, is not possible.

Therefore, an expression for \bar{h} derived by Boduroglu ⁽¹²⁾ will be used.

This expression is given by

$$\bar{h} = \frac{h_o \sigma_o r^2}{\sigma_o r^2 - b(b - B) \left(\sigma_o \ln \frac{b}{r} - \frac{\sigma_o}{2} + p \right)} \quad (33)$$

where h_o and B are the original thickness and original radius of the blank, respectively. Equation (33) has been found to agree closely with experimental results.

METHOD OF SOLUTION

With the results of the previous section, the total rate of work for the system can be written in the form

$$W_T = \int_0^{\sin^{-1} \frac{a}{\rho}} f(b_o, b_1) \rho^2 \sin \phi \, d\phi + \int_{\alpha}^{b(b_o, b_1)} g(b_o, b_1) r \, dr \quad (34)$$

where the integrals on the right hand side of (34) represent the rate of work in the dome (30) and flange (31), respectively. We are interested in the extremum of the function (34) under the subsidiary condition (22). This condition can be put in the framework of the minimization procedure by the introduction of a Lagrange multiplier λ . Thus, the rate of work is minimized at a stationary value of the function

$$I = \int_0^{\sin^{-1} \frac{a}{\rho}} f(b_o, b_1) \rho^2 \sin \phi \, d\phi + \int_{\alpha}^{b(b_o, b_1)} g(b_o, b_1) r \, dr + \lambda n(b_o, b_1). \quad (35)$$

The values of b_o , b_1 , and λ which render I stationary are found by solving the set

$$\frac{\partial I}{\partial b_o} = \int_0^{\sin^{-1} \frac{a}{\rho}} \frac{\partial f(b_o, b_1)}{\partial b_o} \rho^2 \sin \phi \, d\phi + \frac{\partial}{\partial b_o} \left[\int_{\alpha}^{b(b_o, b_1)} g(b_o, b_1) r \, dr \right] + \lambda \frac{\partial n(b_o, b_1)}{\partial b_o} = 0$$

$$\frac{\partial I}{\partial b_1} = \int_0^{\sin^{-1} \frac{a}{\rho}} \frac{\partial f(b_o, b_1)}{\partial b_1} \rho^2 \sin \phi \, d\phi + \frac{\partial}{\partial b_1} \left[\int_{\alpha}^{b(b_o, b_1)} g(b_o, b_1) r \, dr \right] + \lambda \frac{\partial n(b_o, b_1)}{\partial b_1} = 0$$

and

$$\frac{\partial I}{\partial \lambda} = n(b_o, b_1) = 0 \quad (36)$$

The Newton-Raphson numerical iterative procedure is used to solve these equations.

In the solution of the present problem, only two arbitrary constants were included in the series representation for the tangential velocity in the dome. The solution obtained appeared to be sufficiently accurate so that the inclusion of additional terms was not warranted.

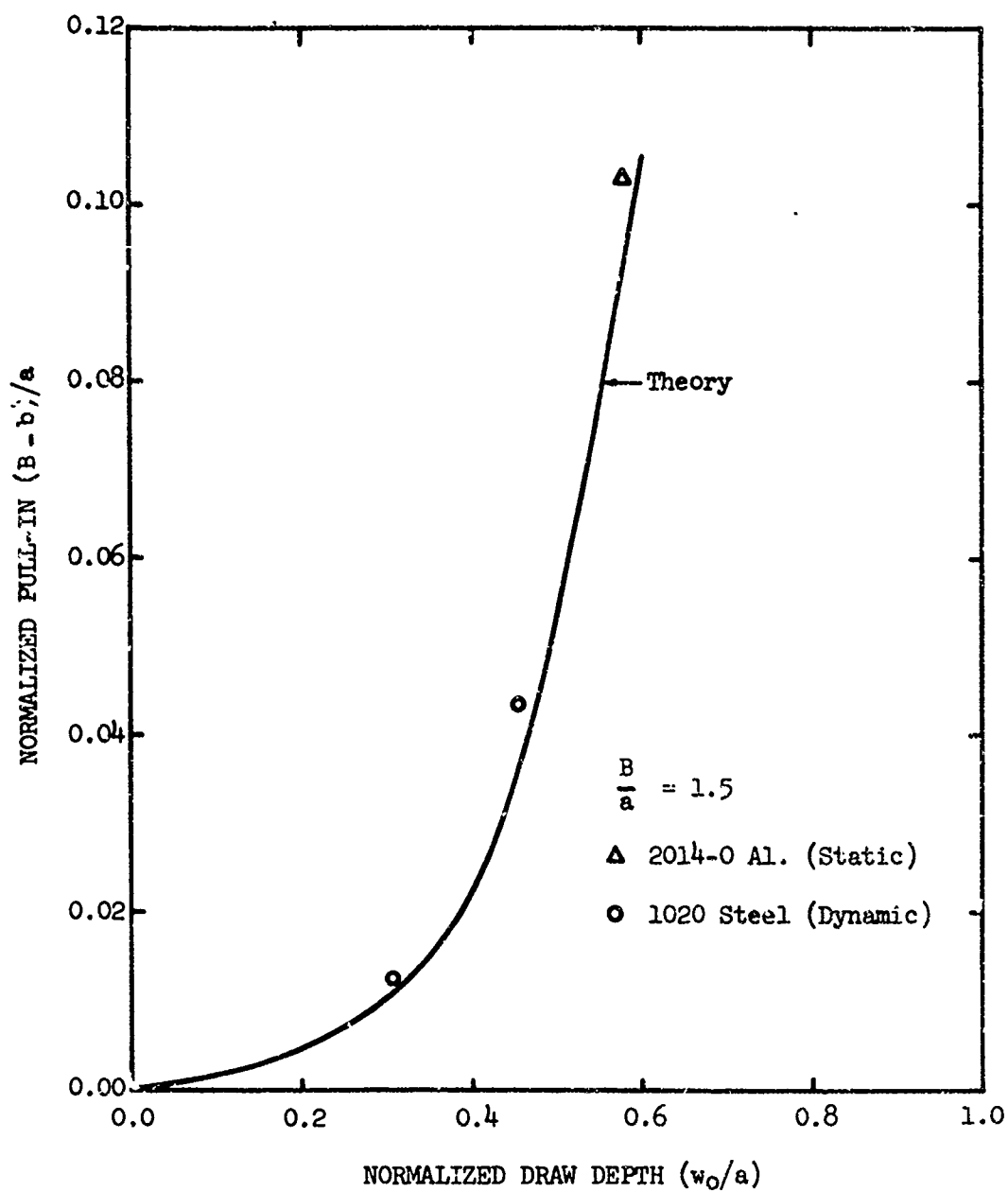


Figure 4. Blank Pull-In vs. Draw Depth - Comparison of Theory and Experiment

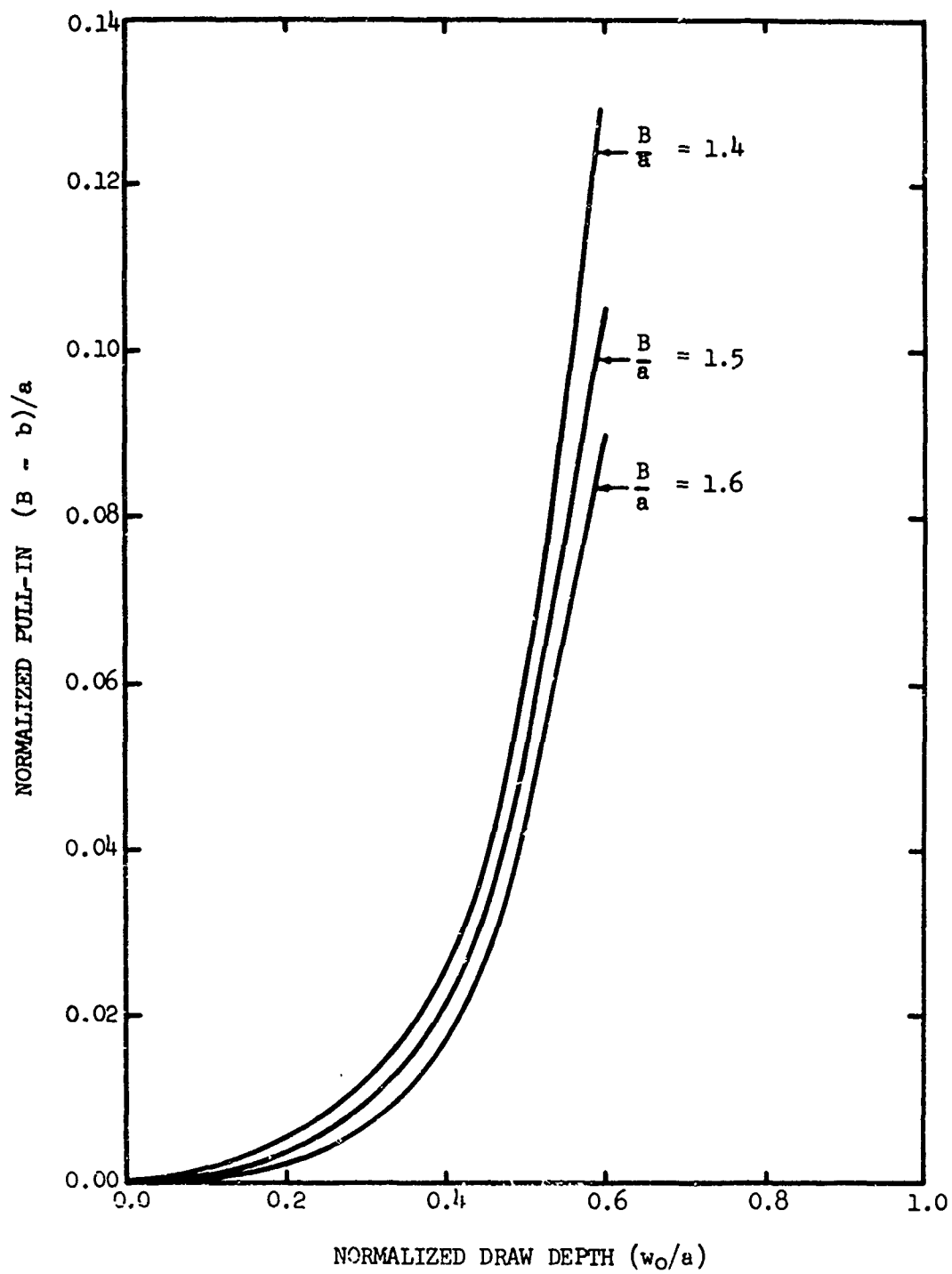


Figure 5. Parametric Curves for Blank Pull-In vs. Draw Depth

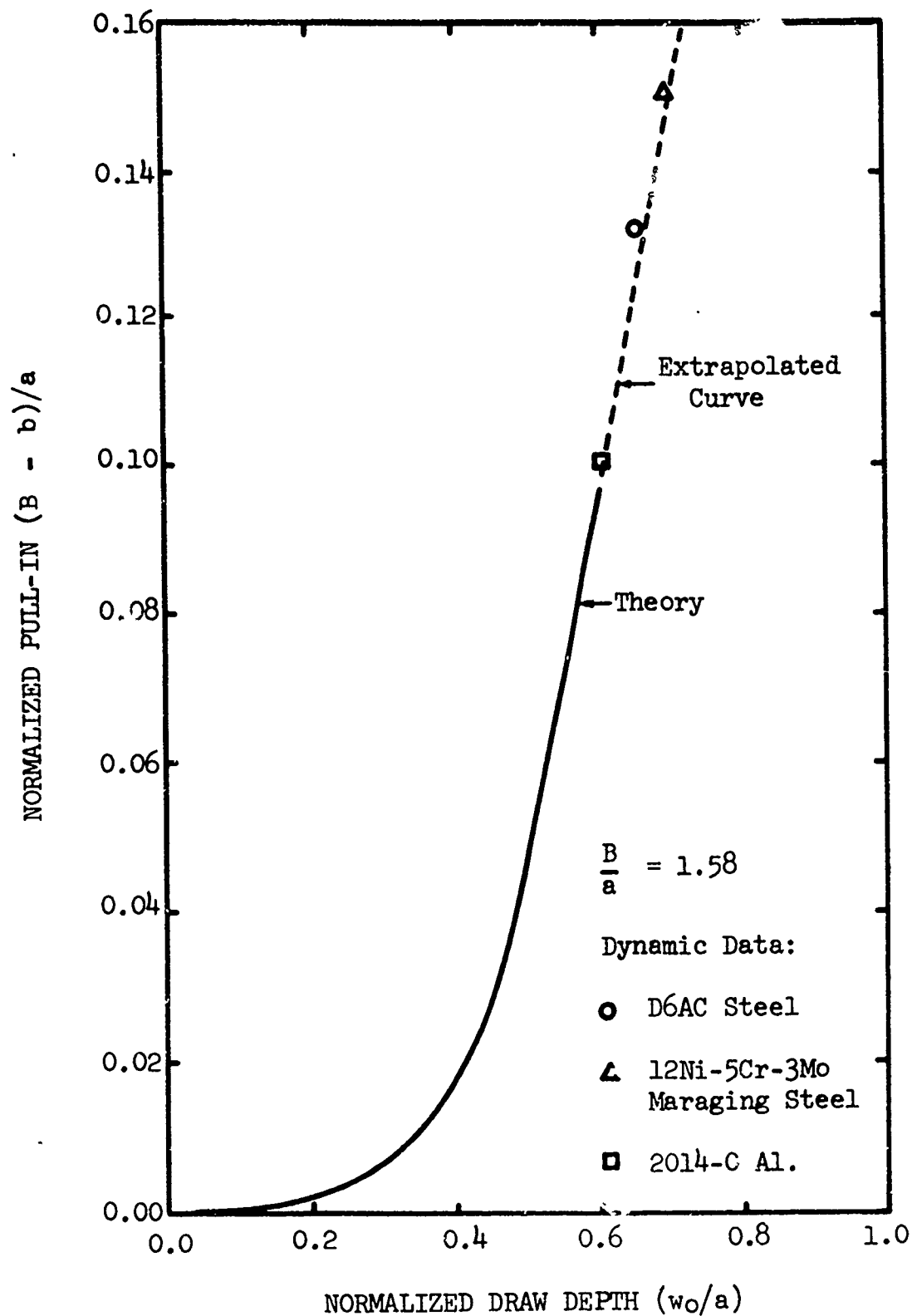


Figure 6. Comparison of Linearly Extrapolated Theory with Experimental Values of Pull-In

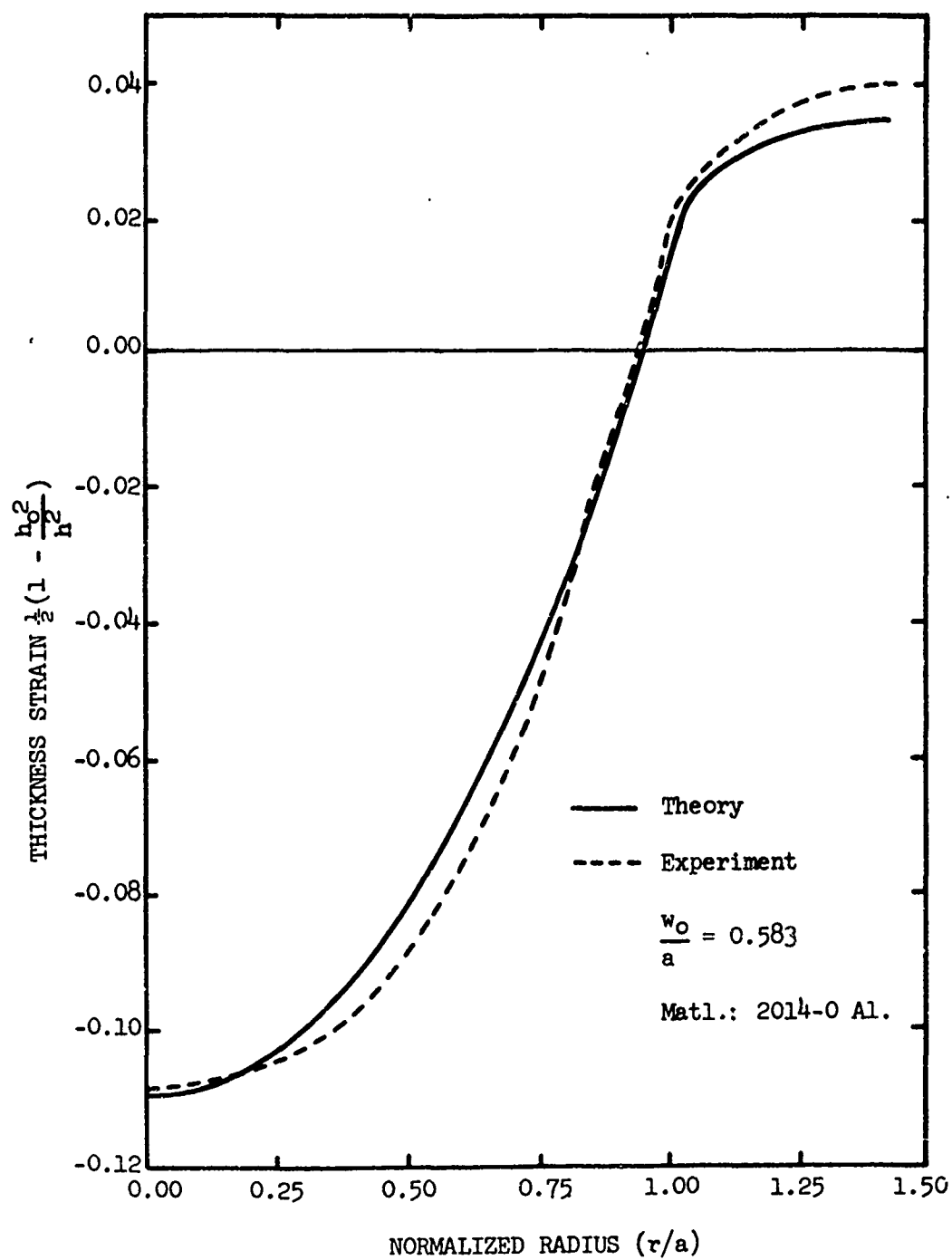


Figure 7. Comparison of Theory and Experiment for Thickness Strain Distribution - Static Forming

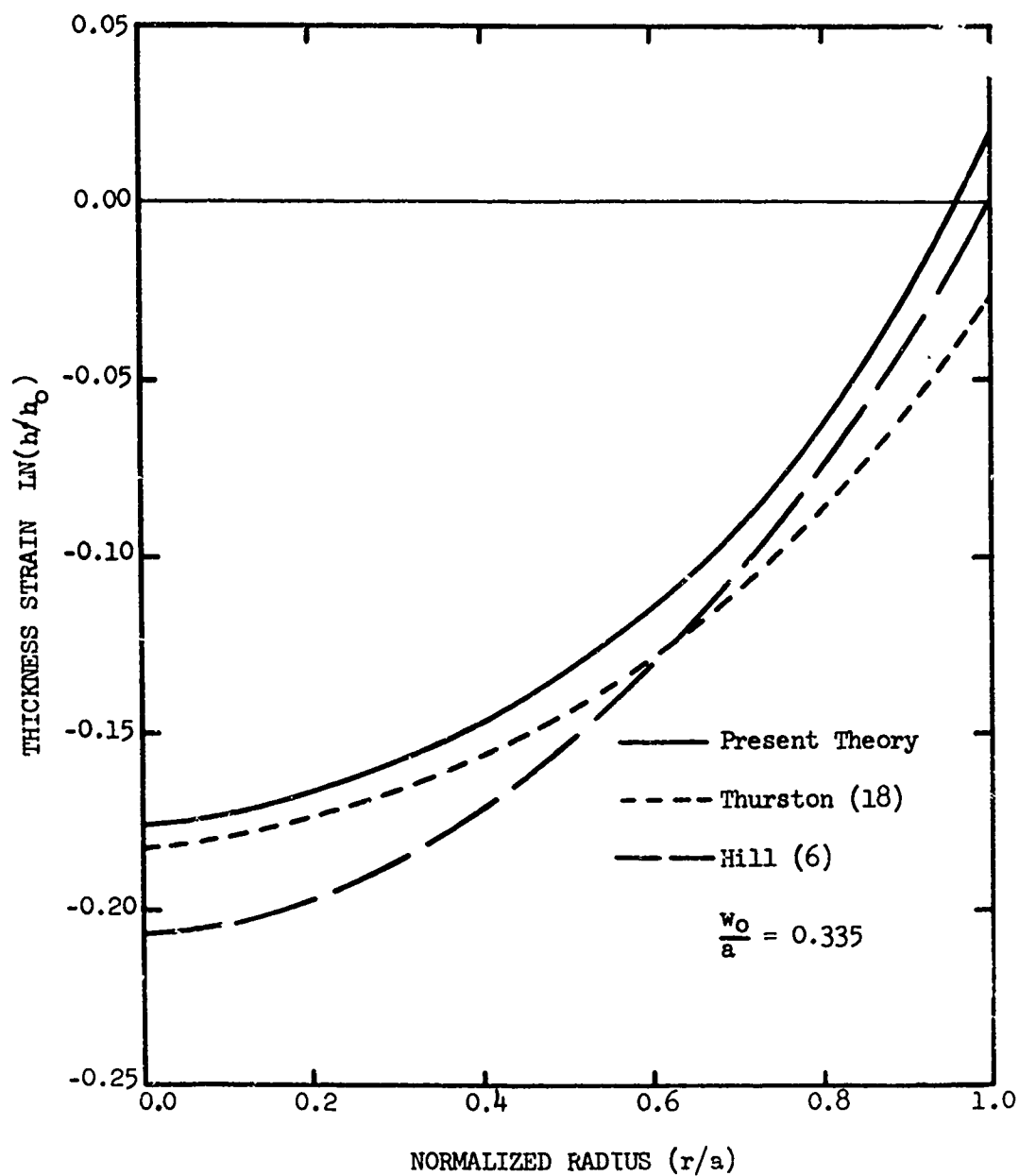


Figure 8. Comparison of Different Bulge Test Theories - Thickness Strain Distribution

DISCUSSION OF RESULTS

The primary objective of this study was to predict the edge pull-in. However, the analysis also enables the thickness strain distribution in the entire dome and flange to be determined. Because of assumption A₂ these strains will be compared with experimental results obtained by static forming only.

The pull-in at the outer edge of the blank is plotted as a function of the draw depth w_0 in Figure 4 for a B/a ratio (i.e., initial blank radius/die radius) of 1.5. The analytically determined pull-in is in close agreement with experimental values. The numerical results indicate that the yield stress has little effect on the pull-in. The magnitude of the force field necessary to produce the deformation depends intimately on the yield strength, however. Further, the assumption that the blank is a membrane excludes the effect of blank thickness on the pull-in.

Figure 5 shows a plot of the pull-in as a function of draw depth for different B/a ratios. It is evident that for a particular draw depth, the pull-in decreases as the ratio B/a increases. The explanation for this is simply that the surrounding annular flange restricts the flow of material into the die cavity. The larger the blank size, the greater the restriction. Figure 5 also shows that for a particular B/a ratio, the edge pull-in increases as the draw depth is increased. The curves have not been drawn beyond $w_0/a = 0.6$ due to instability at the apex of the dome. At this point the apex begins to neck (or thin rapidly). However, the pull-in for very deep draw depths can be obtained by linear extrapolation.

This is demonstrated in Figure 6 for a B/a ratio of 1.58, where the experimental points fall in the close neighborhood of the extended curve. The experimental data for Figure 6 has been obtained from the Martin-Marietta Corporation. (13)

The analytically determined thickness strain field is in good agreement with thickness strain measurements obtained from a statically formed 2014-0 aluminum dome. This comparison is shown in Figure 7. Additional verification of the formulation is provided by the prediction of flange instability and modeling of the bulge test.

The initiation of instability is assumed to be the point at which the flange becomes rigid so that further increase of draw depth does not result in an increase in pull-in. The predicted value of the apex thickness strain at the onset of necking for a 2014-0 aluminum dome is compared with experiment and Hill's analysis in Table 1. The three values are within 3% of each other.

TABLE 1. COMPARISON OF INSTABILITY STRAINS

	<u>Experiments</u>	<u>Present Analysis</u>	<u>Hill's Analysis</u>
$\bar{\epsilon} = \ln \frac{h_0}{h}$	0.357	0.352	0.364

In the bulge test, hydrostatic pressure is applied to a thin circular diaphragm clamped at the edge. The clamping effect is introduced in the present analysis by making the flange radius large in comparison to the die radius. Figure 8 shows that Thurston's⁽¹⁴⁾ and Hill's⁽⁶⁾ results are in the same range as the current numerical results.

Extension of Markov's Principle to Include Inertia Effects

The solution to the present problem was obtained under the assumption that the flow process is quasi-static. Inertia effects can be estimated by extending Markov's principle to include acceleration terms. The modified Markov's principle, proven in the Appendix for the case where the boundary conditions are entirely geometrical, is

$$\int_V \left(\frac{\sqrt{2}}{\sqrt{3}} \sigma_0 \sqrt{\dot{\epsilon}_{ij}^* \dot{\epsilon}_{ij}^*} - \rho_0 a_i v_i^* \right) dv \geq \int_V \left(\frac{\sqrt{2}}{\sqrt{3}} \sigma_0 \sqrt{\dot{\epsilon}_{ij} \dot{\epsilon}_{ij}} - \rho_0 a_i v_i \right) dv \quad (37)$$

where $\dot{\epsilon}_{ij}^*$ and v_i^* are arbitrary admissible quantities and the unstarred terms represent the correct solution to the problem. Therefore, a_i on the left hand side of (37) cannot be assumed in terms of arbitrary constants.

The expansion of the inertia term in (37) yields

$$\int_{V_{\text{dome}}} -\rho_0 (a_R v_R^* + a_\phi v_\phi^*) dv + \int_{V_{\text{flange}}} -\rho_0 (\bar{a}_r \bar{v}_r^* + \bar{a}_z \bar{v}_z^*) dv \quad (38)$$

where the first integral is for the dome and the second for the flange.

Because of the nature of the explosive forming process all but the $a_R v_R^*$ term in (38) is negligible compared to the term containing the strain rates in (37). This can be confirmed experimentally. Therefore, (38) reduces to

$$\int -\rho_0 a_R v_R^* dR \quad (39)$$

and (37) becomes

$$\int_V \left(\frac{\sqrt{2}}{\sqrt{3}} \sigma_0 \sqrt{\dot{\epsilon}_{ij}^* \dot{\epsilon}_{ij}^*} - \rho_0 a_R v_R^* \right) dv \geq \int_V \left(\frac{\sqrt{2}}{\sqrt{3}} \sigma_0 \sqrt{\dot{\epsilon}_{ij} \dot{\epsilon}_{ij}} - \rho_0 a_R v_R \right) dv \quad (40)$$

for the entire dome and flange. The method of solution is to prescribe $a_R = a_R(\rho, \phi, t)$ and minimize (40) at any instant of time (note that $D\rho/Dt \neq 1$ in this case). However, since v_P has been obtained in closed form (6) independently of the arbitrary constants b_0, b_1 , etc., minimization of (40) with respect to these constants will not result in any contribution by the acceleration term to the present formulation of the problem. Therefore, we can conclude that inertia has no effect on the explosive forming of domes. This appears to be in contradiction to the experimental results which showed significant differences between static and dynamically formed domes in the region of the apex of the dome. The reason for this contradiction is the assumption that the shape of the dome is a segment of a sphere at all times in the forming process.

This is not the case in the actual process, since the blank in the vicinity of the apex is nearly flat during a considerable portion of the forming operation. The favorable strain distribution produced dynamically is, therefore, due primarily to geometric rather than inertia effects.

CONCLUSIONS

The present study is part of a continuing investigation of the complex explosive forming process. With the present state of knowledge, there is not enough information to predict all the required process parameters. Such prediction is necessary in order to derive maximum economic benefits which lie in the limited production of very large parts.

In this study we have obtained satisfactory analytical results for predicting the edge pull-in of a flat circular blank, formed into an axisymmetric dome. These can be used by designers to aid in the determination of initial blank size, given the final dimensions of the dome. The analysis also provides a rough estimate of blank thin out.

In view of the resulting simplicity of the formulation as compared with other methods for handling finite deformation plasticity problems, the use of this approach appears to be suitable in all metal forming membrane problems in which the shape of the middle surface is specified during the forming process. Whether the forming were done statically or dynamically would, as indicated by the extended Markov's principle, have little effect on the final strain field although it would affect the forces necessary to form the part. Examples of problems of this type are the bulging and sizing of tubing (used in the plumbing systems of space vehicles to carry fuel and oxygen to the engines), recessing of panels (used in heat exchangers) and the forming of other rotationally symmetrical shapes (conical, ellipsoidal, paraboloidal, etc.).

APPENDIX

Let the stresses, strain rates and velocities of the exact solution be denoted by σ_{ij} , $\dot{\epsilon}_{ij}$ and v_i , and the velocities and resulting strain rates of an admissible solution by v_i^* and $\dot{\epsilon}_{ij}^*$. An admissible solution is one which satisfies the conditions of incompressibility, compatibility and the geometric boundary conditions. By Schwarz's inequality,

$$s_{ij} \dot{\epsilon}_{ij}^* \leq \sqrt{s_{ij} s_{ij}} \sqrt{\dot{\epsilon}_{ij}^* \dot{\epsilon}_{ij}^*} \quad (41)$$

Using the incompressibility condition $\dot{\epsilon}_{ii} = 0$ in

$$s_{ij} = \sigma_{ij} - \frac{1}{3} \sigma_{kk} \delta_{ij} \text{ gives} \quad (42)$$

$$s_{ij} \dot{\epsilon}_{ij}^* = \sigma_{ij} \dot{\epsilon}_{ij}^* .$$

Substituting (42) and the yield condition $s_{ij} s_{ij} = \frac{2}{3} \sigma_0^2$ into (41), the relation

$$\sigma_{ij} \dot{\epsilon}_{ij}^* \leq \frac{\sqrt{2}}{\sqrt{3}} \sigma_0 \sqrt{\dot{\epsilon}_{ij}^* \dot{\epsilon}_{ij}^*} \quad (43)$$

is obtained. Combining the flow equations (1) into the incompressibility condition, we get

$$s_{ij} \dot{\epsilon}_{ij} = \sigma_{ij} \dot{\epsilon}_{ij} = \frac{\sqrt{2}}{\sqrt{3}} \sigma_0 \sqrt{\dot{\epsilon}_{ij} \dot{\epsilon}_{ij}} . \quad (44)$$

The subtraction of (44) from (43) yields

$$\frac{\sqrt{2}}{\sqrt{3}} \sigma_0 [\sqrt{\dot{\epsilon}_{ij}^* \dot{\epsilon}_{ij}^*} - \sqrt{\dot{\epsilon}_{ij} \dot{\epsilon}_{ij}}] \geq \sigma_{ij} (\dot{\epsilon}_{ij}^* - \dot{\epsilon}_{ij}) . \quad (45)$$

Now integrate both sides of (45) through the entire body. The integration of the right-hand side of (45) gives

$$\int_V \frac{1}{2} \sigma_{ij} [(v_{i,j}^* + v_{j,i}^*) - (v_{i,j} + v_{j,i})] dv \quad (46)$$

when the strain rate-velocity relation $2\dot{\epsilon}_{ij} = v_{i,j} + v_{j,i}$ is considered.

Since σ_{ij} is symmetric, we can write (46) as

$$\int_V \sigma_{ij} (v_{i,j}^* - v_{i,j}) dv \quad (47)$$

or as

$$\int_V [\{(\sigma_{ij} v_i^*),_{,j} - \sigma_{ij} v_{i,j}^*\} - \{(\sigma_{ij} v_i)_{,j} - \sigma_{ij,j} v_i\}] dv \quad (48)$$

Noting that $\sigma_{ij,j} = \rho_0 a_i$ where a_i is the acceleration and ρ_0 is the density of the continuum, the use of Green's theorem in (48) yields

$$\int_S \sigma_{ij} v_j v_i^* ds - \int_S \sigma_{ij} v_j v_i ds + \int_V \rho_0 a_i v_i^* dv - \int_V \rho_0 a_i v_i dv \quad (49)$$

When only velocity boundary conditions are prescribed on the entire surface,

$v_i = v_i^*$ on S , and (49) reduces to

$$\int_V \rho_0 a_i v_i^* dv - \int_V \rho_0 a_i v_i dv \quad (50)$$

The integration of the left-hand side of (50) through the entire body gives

$$\int_V \frac{\sqrt{2}}{\sqrt{3}} \sigma_0 [\sqrt{\dot{\epsilon}_{ij}^* \dot{\epsilon}_{ij}} - \sqrt{\dot{\epsilon}_{ij} \dot{\epsilon}_{ij}}] dv \quad (51)$$

Combining (50) and (51) and rearranging terms, we obtain

$$\int_V \left(\frac{\sqrt{2}}{\sqrt{3}} \sigma_0 \sqrt{\dot{\epsilon}_{ij}^* \dot{\epsilon}_{ij}} - \rho_0 a_i v_i^* \right) dv > \int_V \left(\frac{\sqrt{2}}{\sqrt{3}} \sigma_0 \sqrt{\dot{\epsilon}_{ij} \dot{\epsilon}_{ij}} - \rho_0 a_i v_i \right) dv \quad (52)$$

In equation (52) the right-hand side consists of terms which involve actual quantities, i.e., quantities which would be obtained by the correct solution of the problem. The left-hand side contains arbitrary admissible quantities (except for the a_i which are true acceleration components). The proof of the modified Markov's principle is completed if the a_i are prescribed because the actual quantities are then separated entirely from the admissible quantities in equation (52).

REFERENCES

1. Hudson, G. E., "Theory of the Dynamic Plastic Deformation of a Thin Diaphragm," Journal of Applied Physics, Vol. 22, No. 1, pp. 1-11, January 1951.
2. Wang, A. J., "Permanent Deflection of a Plastic Plate Under Blast Loading," Journal of Applied Mechanics, Vol. 22, pp. 376, 1955.
3. Witmer, E. A., H. A. Balmer, J. W. Leech, and T. H. H. Pian, "Large Dynamic Deformations of Beams, Rings, Plates and Shells," A.I.A.A. Journal, Vol. 1, No. 8, pp. 1848-1857, 1963.
4. Witmer, E. A., H. A. Balmer, and E. N. Clark, "Experimental and Theoretical Studies of Explosive-Induced Large Dynamic and Permanent Deformations of Simple Structures," Presented at the S.E.S.A. Spring Meeting, Denver, Colorado, May 5-7, 1965.
5. Witmer, E. A., J. W. Leech, and L. Morino, "PETROS 2: A New Finite Difference Method and Program for the Calculation of Large Elastic-Plastic Dynamically-Induced Deformations of General Thin Shells," Prepared for Ballistic Research Laboratories, U. S. Army Aberdeen Research and Development Center, Aberdeen Proving Ground, Maryland, Report No. ASRL TR 152-1, BRL Contract Report No. 12-Appendix D, December 1969.
6. Hill, R., "A Theory of the Plastic Bulging of a Metal Diaphragm by Lateral Pressure," Phil. Mag., Vol. 41, No. 1133, pp. 1133-1142, 1950.
7. Thurston, G. A., "On the Effects of Edge Pull-In on the Explosive Forming of Domes," Proceedings of the Seventh International Machine Tool Design and Research Conference, Sept. 12-16, 1966, Pergamon Press.
8. Boyd, D., "Dynamic Deformation of Circular Membranes," Journal of the Engineering Mechanics Division, Proceedings of the A.S.C.E., Vol. 92, No. EM3, June 1966.
9. Ezra, A. A. and M. A. Malcolm, "An Investigation of the Effect of Explosive Stand-Off Distance on the Forming of Metal Blanks," First International Conference of the Center for High Energy Forming, Estes Park, Colorado, Vol. 2, pp. 6.4.1-6.4.20, June 19-23, 1967.
10. Fung, Y. C., Foundations of Solid Mechanics, Prentice-Hall, Inc., New Jersey, 1965.

11. Kulkarni, S. B., "The Prediction of Edge Pull-In in Explosively Formed Domes", Doctoral Dissertation, University of Denver, 1971.
12. Kaplan, M. A. and H. M. Boduroglu, "Flange Buckling of Explosively Formed Domes," Fifth Annual Report of the Center for High Energy Forming, U. S. Army Materials and Mechanics Research Center, Watertown, Massachusetts, Report No. AMRA CR-66-05/25, pp. 40-65, September 1970.
13. Agricola, K. R., J. T. Snyder, J. B. Patton, et al., "Explosive Forming Processes," Technical Report No. AFML-TR-67-70, Martin Marietta Corporation, May 1967.
14. Thurston, G. A., and R. J. Harris, "Plastic Deformation of a Circular Membrane Under Pressure," Developments in Mechanics, Proceedings of the 11th Midwestern Mechanics Conference, Vol. 5, pp. 669-689, 1969.

FIGURE CAPTIONS

- Figure 1. Profiles of Statically and Dynamically Die Formed 2014-O Aluminum Domes.
- Figure 2(a). Circumferential Strain Distribution in Statically and Dynamically Die Formed 2014-O Aluminum Domes.
- Figure 2(b). Thickness Strain Distribution in Statically and Dynamically Die Formed 2014-O Aluminum Dies.
- Figure 3. Nomenclature for Dome and Flange.
- Figure 4. Blank Pull-in vs. Draw Depth - Comparison of Theory and Experiment.
- Figure 5. Parametric Curves for Blank Pull-in vs. Draw Depth.
- Figure 6. Comparison of Linearly Extrapolated Theory with Experimental Values of Pull-in.
- Figure 7. Comparison of Theory and Experiment for Thickness Strain Distribution - Static Forming.
- Figure 8. Comparison of Different Bulge Test Theories - Thickness Strain Distribution.

VIII. THE DESIGN AND ANALYSIS OF
EXPLOSIVE FORMING THIN SHELL DIES

S. B. Kulkarni

A. A. Ezra

SUMMARY

Thin shell dies backed up by water have been found to be a very economic solution for the explosive forming of metal domes. A method of analysis is presented here that will permit the rational design of such dies. Experimental observations of strain in the die are shown to agree very well with the theoretical predictions.

Based on these results, it is possible to analyze and design thin shell dies with complete confidence for the explosive forming of domes.

NOMENCLATURE

$\tau_\theta, \tau_\phi, \tau$ = Normal stress, lb/in²

w = radial displacement, in.

h = shell thickness, in.

R = shell radius, in.

ρ = mass density of shell material, lb-sec²/in⁴

m = mass per unit area of shell wall = ρh , lb-sec²/in³

E = Young's Modulus, lb/in²

ν = Poisson's ratio

F_1 = Pressure force on the internal surface of shell, lb-sec/in³

F_2 = Reactive pressure force on the external surface of shell, lb-sec/in³

ρ_w = mass density of water, lb-sec²/in⁴

C_w = sonic velocity of water, in/sec

ρ_R = mass density of die back-up media, lb-sec²/in⁴

C_R = wave velocity in back-up media, in/sec

t = time, sec

v = velocity of shell = $\frac{dw}{dt}$, in/sec

ϵ = Hoop strain, in/in

e = Specific energy of explosive, in-lbs/lb

τ = time to maximum radial displacement of die wall

ξ = $\rho C_w / m \omega$. The damping factor of the die wall

ω = fundamental frequency of oscillation of die wall

INTRODUCTION

The present study is part of a continuing investigation of the explosive forming process. In this paper we shall investigate the design of one of the largest single items of cost in the process, namely, the die.

Large dies result in significant expenditures and, therefore, various die materials and designs have been used in minimizing this expense. Because of the large pressures involved in explosive forming, a reliable way must be found to reduce the resulting stresses in the die and the die material required. The use of a thin shell die backed by water has been found to be very effective. The purpose of this paper is to provide the analytical capability for designing such dies. The concept of supporting the die with water was first introduced by Beyer⁽¹⁾. The double die configuration wherein two lightweight shell dies are placed face-to-face would also alleviate this problem because of opposite reacting forces during forming.

The critical shots in explosive forming are the initial and final sizing shots. A large part of the energy of the initial shot is absorbed by the plastic deformation of the blank into the die. Therefore, it is in the final sizing shot that the die has to withstand almost directly the incident explosive pressures. While it is better to avoid the necessity of a final sizing shot, the die should be designed with this eventuality in mind.

Die stresses have been investigated theoretically by Reismann and Jurney⁽²⁾. They have shown that the stresses may be substantially reduced

by water immersion. In preparation for an experimental investigation of this case, theoretical calculations similar to Reismann's have been carried out and stresses in thin shell dies subjected to internal blast loads have been measured. The comparison of theoretical and experimental results is summarized herein.

THEORY

The physical limitation on the die under repeated final sizing shots is that it should remain elastic. In this section we will develop the theory to predict the response of a thin spherical shell subjected to pressures from underwater explosions. This pressure will be assumed to act uniformly over the internal surface of the shell.

a. Underwater Explosion Assumptions

Some well known underwater explosion formulae will be stated. The pressure history of the major portion of the shock wave can be approximated by

$$P(t) = P_m e^{-t/\theta} \quad (1)$$

where P_m is the peak pressure from an underwater explosion and θ is known as the exponential decay constant. The peak pressure and the decay constant can be represented by the empirical equations

$$P_m = B \left(\frac{W^{1/3}}{R} \right)^\alpha$$

$$\theta = C W^{1/3} \left(W^{1/3}/R \right)^\beta \quad (2)$$

where W = weight of the explosive in pounds,

R = distance from the explosive in feet.

The values of the empirical constants B , C , α and β have been experimental;

determine for each explosive and are given in the table below.

Explosive	Peak Pressure (psi)		Decay Constant (millisec.)	
	B	α	C	β
PETN	23,100	1.13	0.06	-0.18
Pentolite	22,500	1.13	0.06	-0.18
Comp C4	22,500	1.13	0.06	-0.18
Comp A3	23,500	1.13	0.06	-0.18
HBX-1	28,400	1.15	0.049	-0.29
HBX-3	20,900	1.14	0.06	-0.218

b. Shell Response

For a thin shell die the die radius is normally very large in comparison to the die thickness. Therefore, membrane theory can be used to analyze the die stresses. Further, because of spherical symmetry, the die is in a biaxial state of stress with $\sigma_{\theta} = \sigma_{\phi} = \sigma$ (Figure 1).

The hoop strain ϵ is given by

$$\epsilon = \frac{w}{R} = \frac{\sigma}{E} (1-\nu) \quad (3)$$

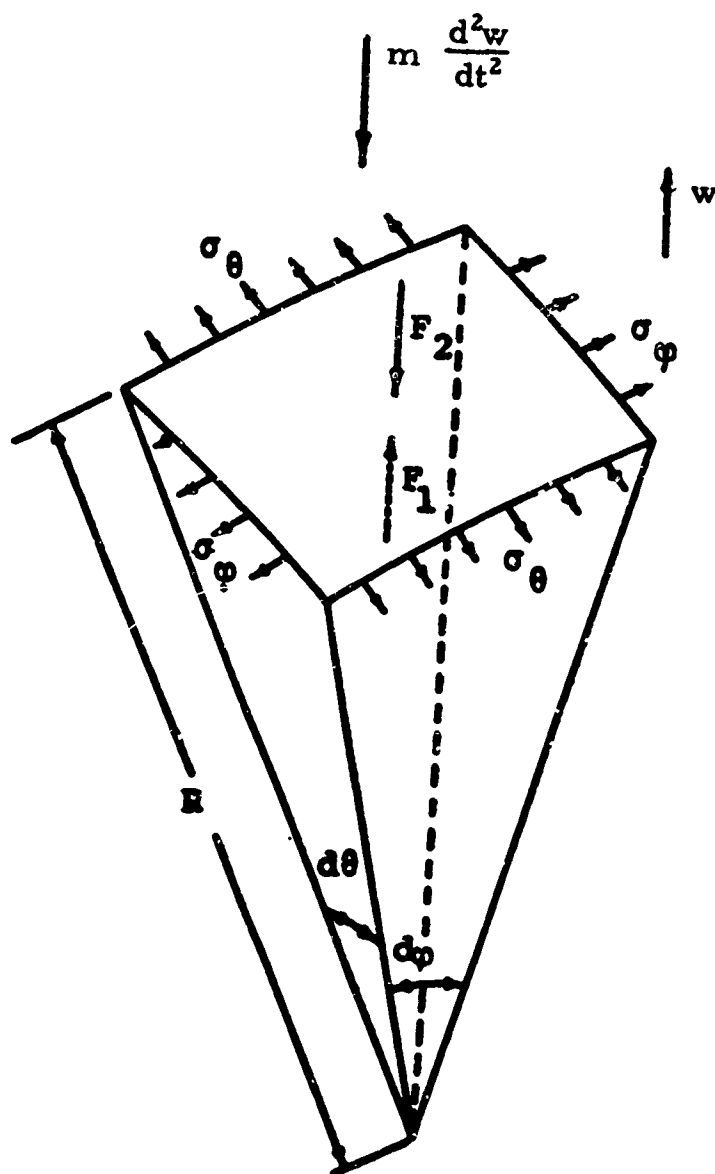
where E is Young's modulus and ν is Poisson's ratio. The radial equation of motion can be written as

$$m \frac{d^2 w}{dt^2} = \frac{2\sigma h}{R} + F_1 - F_2 \quad (4)$$

where F_1 is the pressure force on the internal surface of the shell and F_2 is the reactive pressure force exerted by the water. If a dome is being formed in the final sizing shot, then the mass m per unit area should include the blank.

In equation (1) the pressure P is doubled due to the reflection of the pressure wave from the die wall. Therefore, we can write

$$F_1 = 2 P_m e^{-t/\theta} \quad (5)$$



$$F_1 = 2P_m e^{-t/\theta}$$

$$F_2 = 2\rho_w C_w \frac{dw}{dt}$$

Figure 1. Spherical Shell Element

The rarefaction wave due to the outward motion of the die wall causes a suction pressure acting radially inward given by

$$F_2' = \rho_w C_w V \quad (6)$$

where ρ_w is the density of water, C_w is the sonic velocity of water and V is the velocity of the die wall ($\frac{dw}{dt}$). The pressure force resisting the die wall movement has the same form as equation (6). This resisting pressure force and the effect of the rarefaction wave (6) can be combined to give the total reactive pressure force F_2 as

$$F_2 = \left(\rho_R C_R + \rho_w C_w \right) V. \quad (7)$$

If the die were backed by water, then $\rho_R = \rho_w$ and $C_R = C_w$, respectively, so that

$$F_2 = 2\rho_w C_w \frac{dw}{dt} \quad (8)$$

Substituting equations (8), (5) and (3) in (4), we have

$$m \frac{d^2 w}{dt^2} + 2 \left(\rho_w C_w \right) \frac{dw}{dt} + \frac{2hE}{R^2(1-\nu)} w = 2 P_m e^{-t/\theta} \quad (9)$$

Equation (9) is easily recognized to be the differential equation of a mass-spring model with damping and a disturbing force present. Written in the standard form, it is

$$\frac{d^2 w}{dt^2} + 2 \xi \omega \frac{dw}{dt} + \omega^2 w = \frac{2 P_m e^{-t/\theta}}{m} \quad (10)$$

$$\text{where } \omega^2 = \frac{2 h E}{m R^2 (1-\nu)}$$

$$\text{and } \xi = \frac{\rho_w C_w}{m \omega} = \rho_w C_w R \sqrt{\frac{(1-\nu)}{2 m E h}}$$

For $\xi > 1$, the solution of (10) is

$$\begin{aligned} \frac{w}{\psi} = e^{-t/\theta} - e^{-\xi \omega t} & \left[\cosh \left(\sqrt{\xi^2 - 1} \omega t \right) \right. \\ & \left. + \frac{1}{\omega \theta} \frac{(\xi \omega \theta - 1)}{\sqrt{\xi^2 - 1}} \sinh \left(\sqrt{\xi^2 - 1} \omega t \right) \right] \end{aligned} \quad (11)$$

If $\xi < 1$, the solution is

$$\begin{aligned} \frac{w}{\psi} = e^{-t/\theta} - e^{-\xi \omega t} & \left[\cos \left(\sqrt{1 - \xi^2} \omega t \right) \right. \\ & \left. - \frac{1}{\omega \theta} \frac{(1 - \xi \omega \theta)}{\sqrt{1 - \xi^2}} \sin \left(\sqrt{1 - \xi^2} \omega t \right) \right] \end{aligned} \quad (12)$$

If $\xi = 1$

$$\frac{w}{\psi} = e^{-t/\theta} - e^{-\omega t} \left(1 - \frac{t}{\theta} + \omega t \right) \quad (13)$$

In equations (11) through (13)

$$\psi = \frac{2 P_m \theta^2}{m [1 - 2 \xi \omega \theta + \omega^2 \theta^2]}$$

The time τ to reach the maximum deflection is given by the lowest non-zero roots of the following three equations:

For $\xi > 1$

$$-e^{-\tau/\theta} + e^{-\xi\omega t} \left[\cosh \left(\sqrt{\xi^2 - 1} \omega\tau \right) + \frac{(\omega\theta - \xi)}{\sqrt{\xi^2 - 1}} \sinh \left(\sqrt{\xi^2 - 1} \omega\tau \right) \right] = 0 \quad (14)$$

For $\xi < 1$

$$-e^{-\tau/\theta} + e^{-\xi\omega t} \left[\cos \left(\sqrt{1 - \xi^2} \omega\tau \right) + \frac{(\omega\theta - \xi)}{\sqrt{1 - \xi^2}} \sin \left(\sqrt{1 - \xi^2} \omega\tau \right) \right] = 0 \quad (15)$$

For $\xi = 1$

$$-e^{-\tau/\theta} + e^{-\omega t} \left[1 - \omega\theta (1 - \omega\theta) \frac{\tau}{\theta} \right] = 0 \quad (16)$$

Computations have been made for various values of ξ for τ/θ versus $\xi\omega\theta$. These are shown in Figure 2. The curves represent the solutions of the transcendental equations (14) through (16).

COMPARISON WITH EXPERIMENTS

A series of tests were conducted to compare the theoretical response with strains actually measured on shell dies subjected to explosive loading on the inside. The die shells were segments of spheres fabricated from sheet metal by explosive forming. Two Bean-type BAE-06-187BB-350TE strain gages were mounted in the conventional manner using an epoxy cement. The gages were waterproofed with No. 5 Gagekote rubber and excited by constant current DC sources. A Tektronix Model 555 Oscilloscope was used for readout. Figure 3a shows the location of the gages and Figure 3b the installation. A schematic of the electronics is shown in Figure 4.

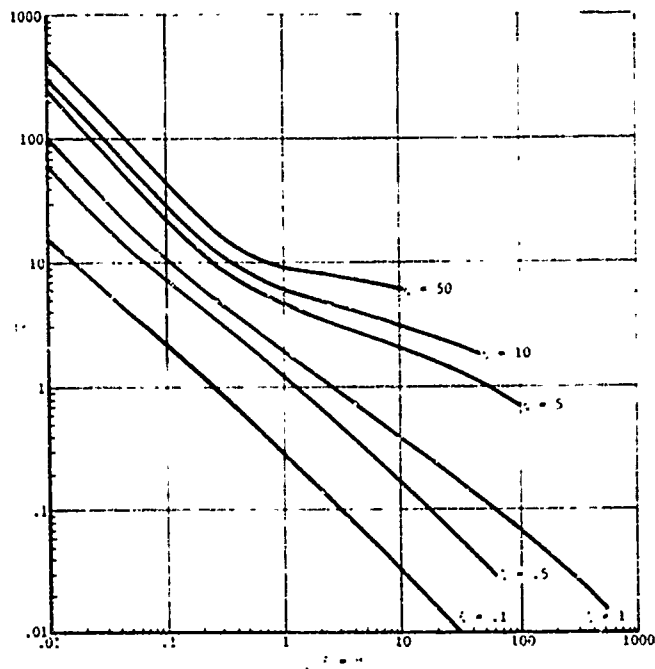


Figure 2 Lowest Non-Zero Roots of Transcendental Equation for Calculating Maximum Radial Well Deflection

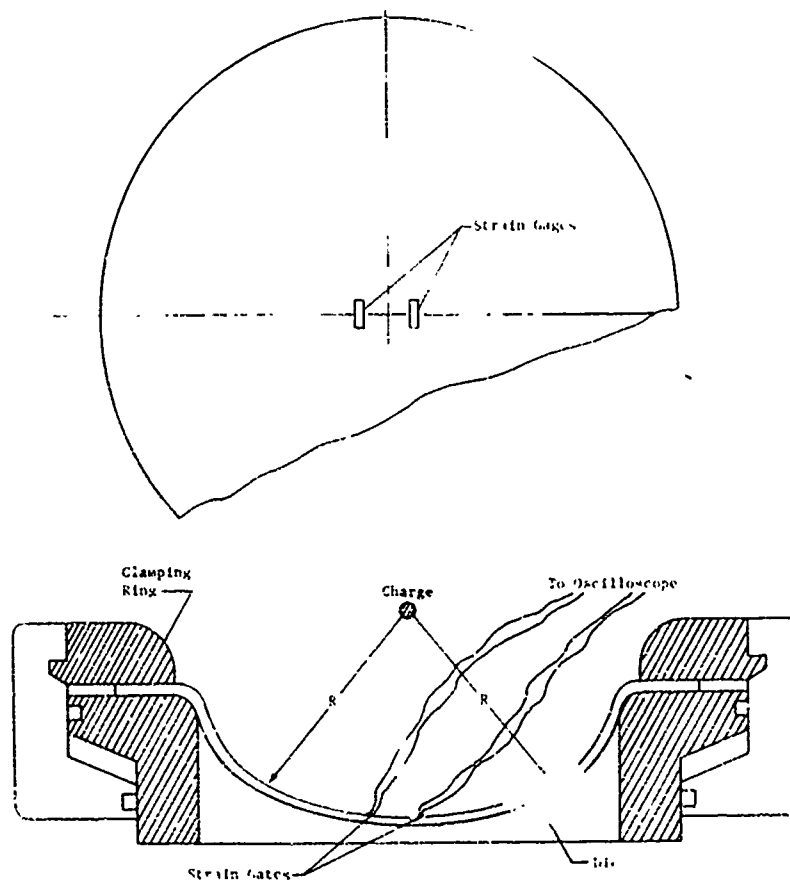


Figure 3a Schematic Representation of Test Set-Up

Explosive charges of composition C-4, pentolite, and PETN varying in weight from 0.3 gm to 6.0 gms were detonated by Dupont No. 6 blasting caps. The charges were placed at the center of the die shell (Figure 3a). The die was backed by water for all experiments.

Acceptable results were obtained from the gages during the tests. Figure 5 shows the actual recorded data from one of the tests. The maximum deflection of the die is given by the first peak on the trace.

The die strains were calculated from the maximum deflection w of the die wall. These strains are tabulated along with theoretical predictions in Table 1 and plotted as a function of charge size in Figure 6.

Table I

Die Material	Explosive	Wt. of Charge-gms	R/h	Max. wall strain		Ratio Obs./Predicted
				Predicted	Observed	
A1	Cap (PETN)	0.316	59.0	4.43×10^{-4}	4.21×10^{-4}	0.95
A1	C4	1.0	59.0	0.896×10^{-3}	0.878×10^{-3}	0.98
A1	C4	2.0	59.0	1.41×10^{-3}	1.344×10^{-3}	0.954
MS	Cap (PETN)	0.316	54.0	4.54×10^{-4}	4.21×10^{-4}	0.93
MS	PETN	1.08	54.0	0.986×10^{-3}	0.98×10^{-3}	0.99
MS	PETN	2.16	54.0	1.485×10^{-3}	1.29×10^{-3}	0.87
MS	PETN	4.33	54.0	2.187×10^{-3}	1.779×10^{-3}	0.81
MS	C4	6.0	50.0	2.523×10^{-3}	2.24×10^{-3}	0.89

The die material properties used in the numerical computations are shown in Table 2.

Table 2

Material	E (lb/in ²)	ρ (lb-sec ² /in ⁴)	Poisson's Ratio
Aluminum	10×10^6	2.59×10^{-4}	0.25
Mild Steel	30×10^6	7.25×10^{-4}	0.25

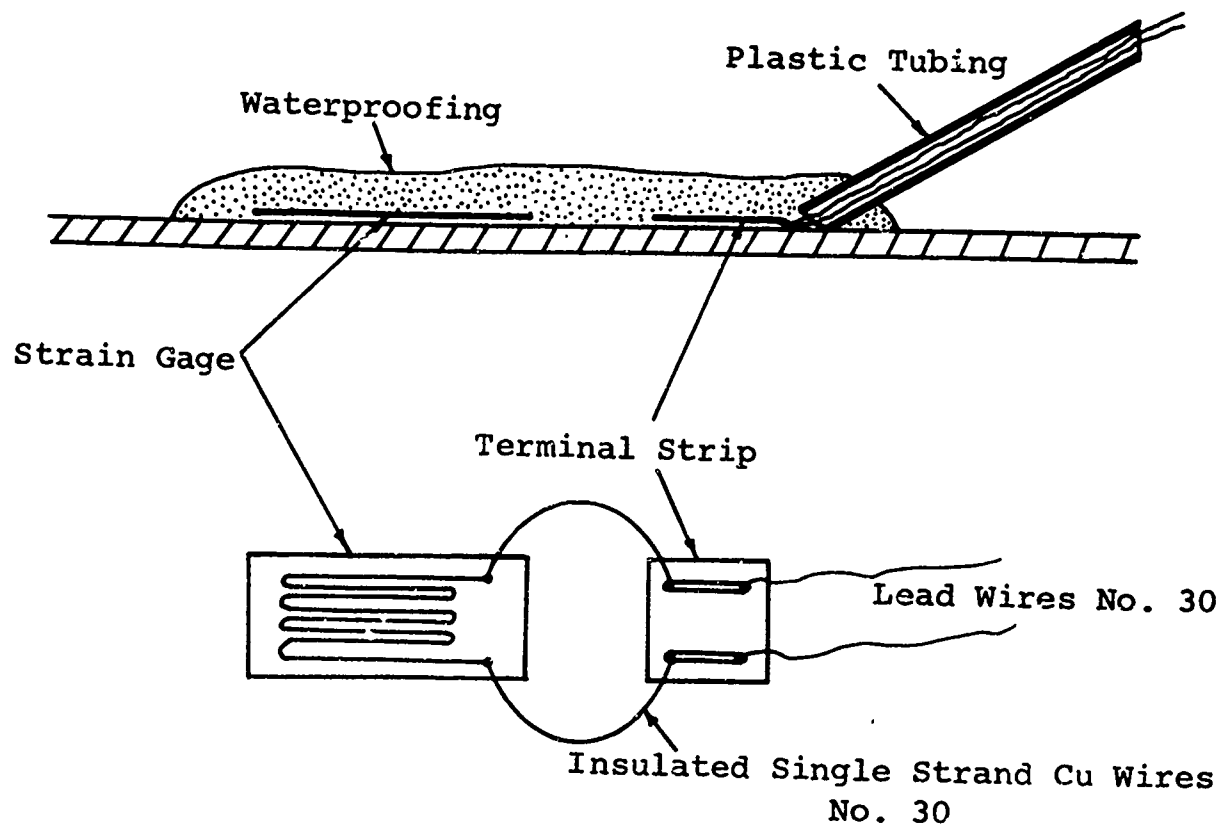


Figure 3(b). Strain Gage Installation

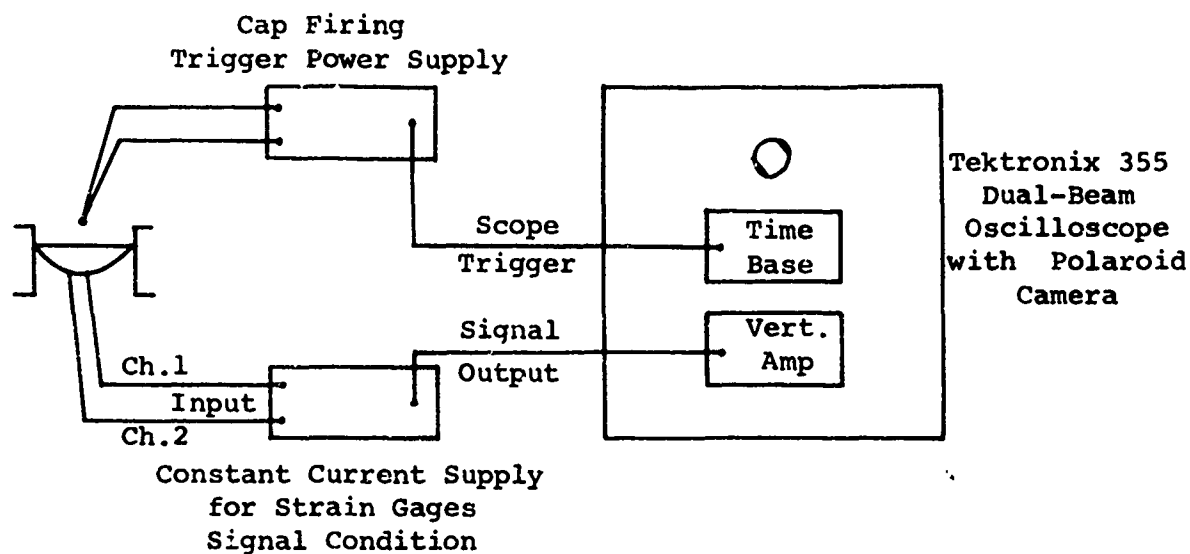
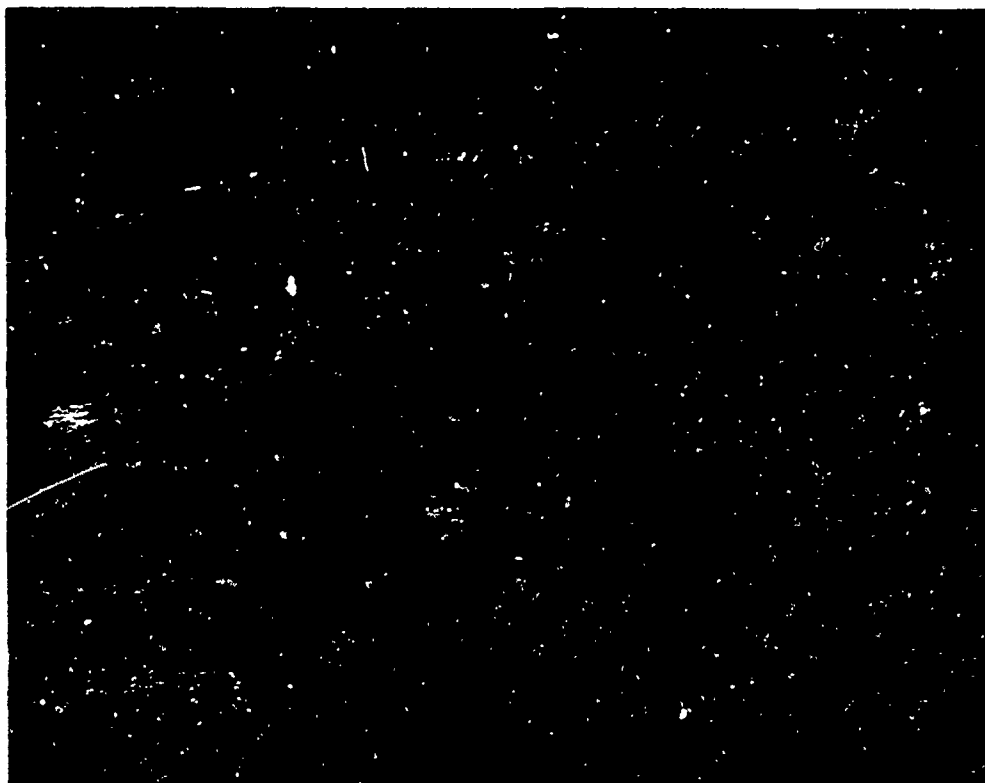


Figure 4. Schematic of Electronics

50 mv/cm



Sweep Rate 0.2 msec/cm.

Figure 5. Oscilloscope Trace of Output from Strain Gage on Aluminum Die

The water surrounding the die has properties $\rho_w = 9.362 \times 10^5 \text{ lb-sec}^2/\text{in}^4$ and $C_w = 6.0 \times 10^4 \text{ in/sec}$.

It is clear that since deep draw domes were used to compare results with the spherical shell analysis, there will be some error in the experimental maximum strains due to the existence of a clamping effect at the edge of the die. From the results of Table I, the good agreement between analytically and experimentally determined peak strain rates shows that the magnitude of this error is small. Further, the empirical formula for pressure given by equation (1) does not include the energy delivered in the reloading phase of the explosion. Because of the shallow depth of submergence used in the experiments to avoid the occurrence of this effect, it is not surprising, therefore, that the discrepancy between the experimental and analytical results is not significant.

Figures 7a and 7b show dimensionless plots, for steel and aluminum respectively, of the peak strain as a function of the explosive energy for different die radius/thickness ratios. A value of $19.7 \times 10^6 \text{ in. lb/lb}$ for the specific energy of C4 has been used in these plots. Alternative explosives and die materials could be chosen resulting in obvious modifications to these parametric curves.

Of useful interest is the reduction in die stresses due to water immersion. If we define percentage alleviation as

$$\text{Percentage Alleviation} = \frac{\text{max. disp. in air} - \text{max. disp. in water}}{\text{max. disp. in air}} \times 100,$$

then Figure 8 shows a plot of the percentage alleviation versus radius to thickness ratios, R/h , for mild steel and aluminum. An inspection of this figure indicates that for a R/h ratio of 80 alleviation of up to 46

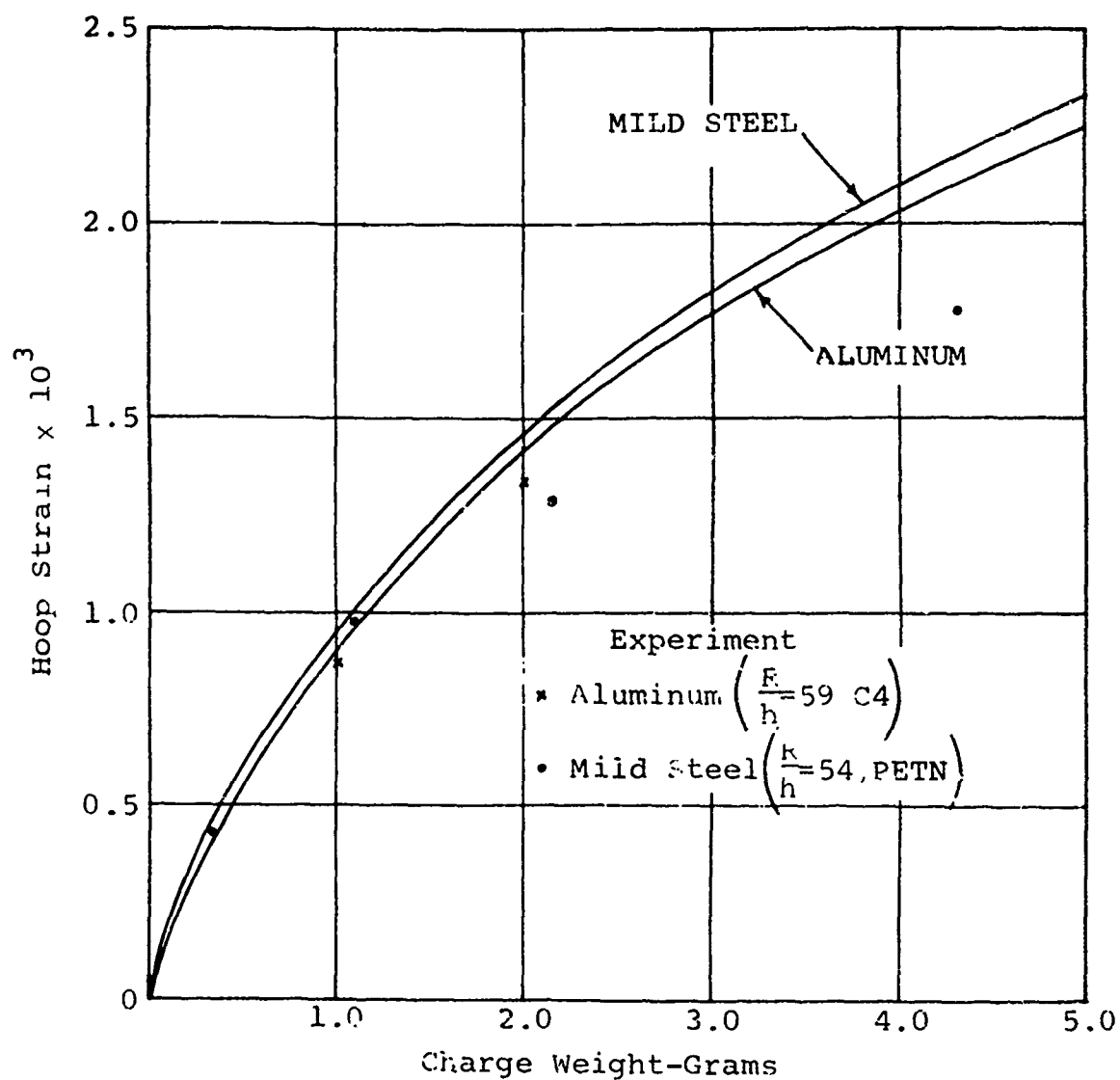


Figure 6. Maximum Hoop Strain Versus Charge Weight-Comparison of Theory and Experiment

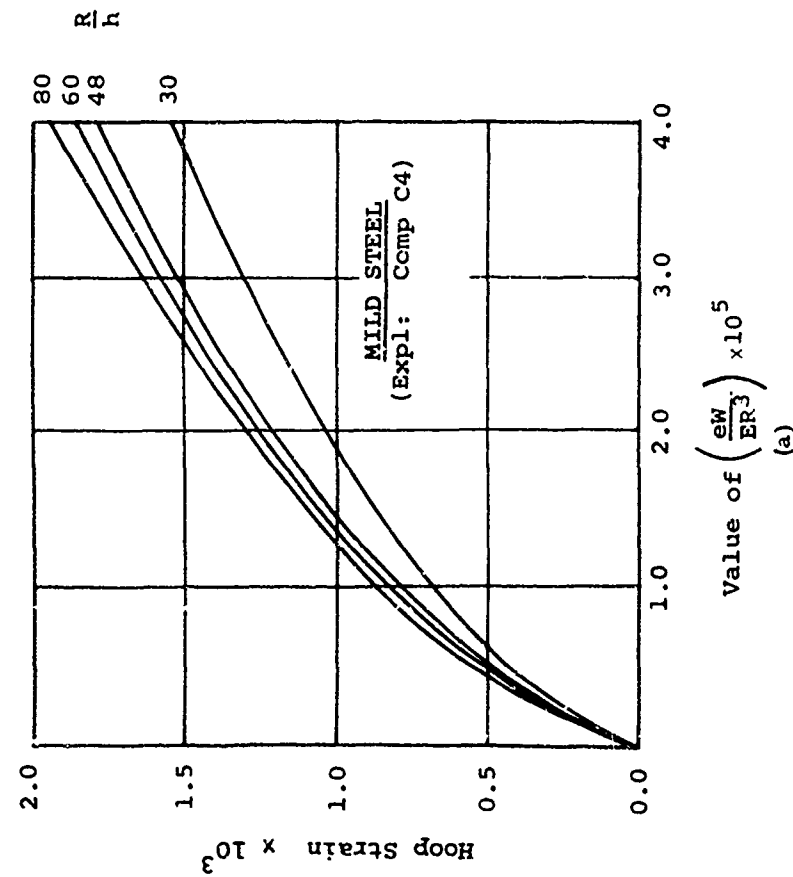


Figure 7(a). Parametric Curves for Die Strains vs. Explosive Energy - Mild Steel

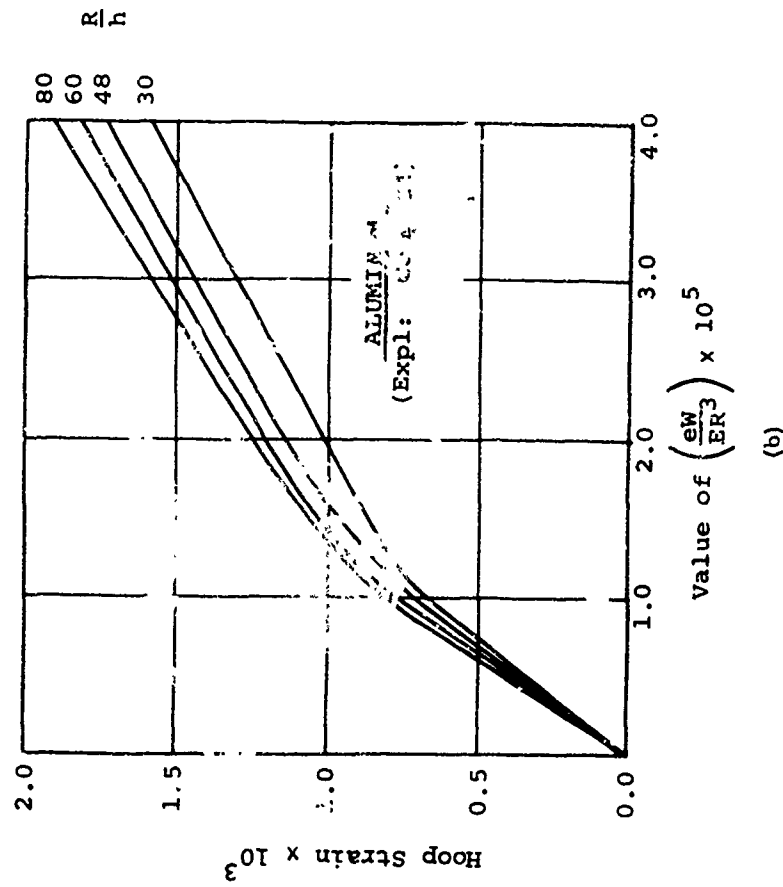


Figure 7(b). Parametric Curves for Die Strains vs. Explosive Energy - Aluminum

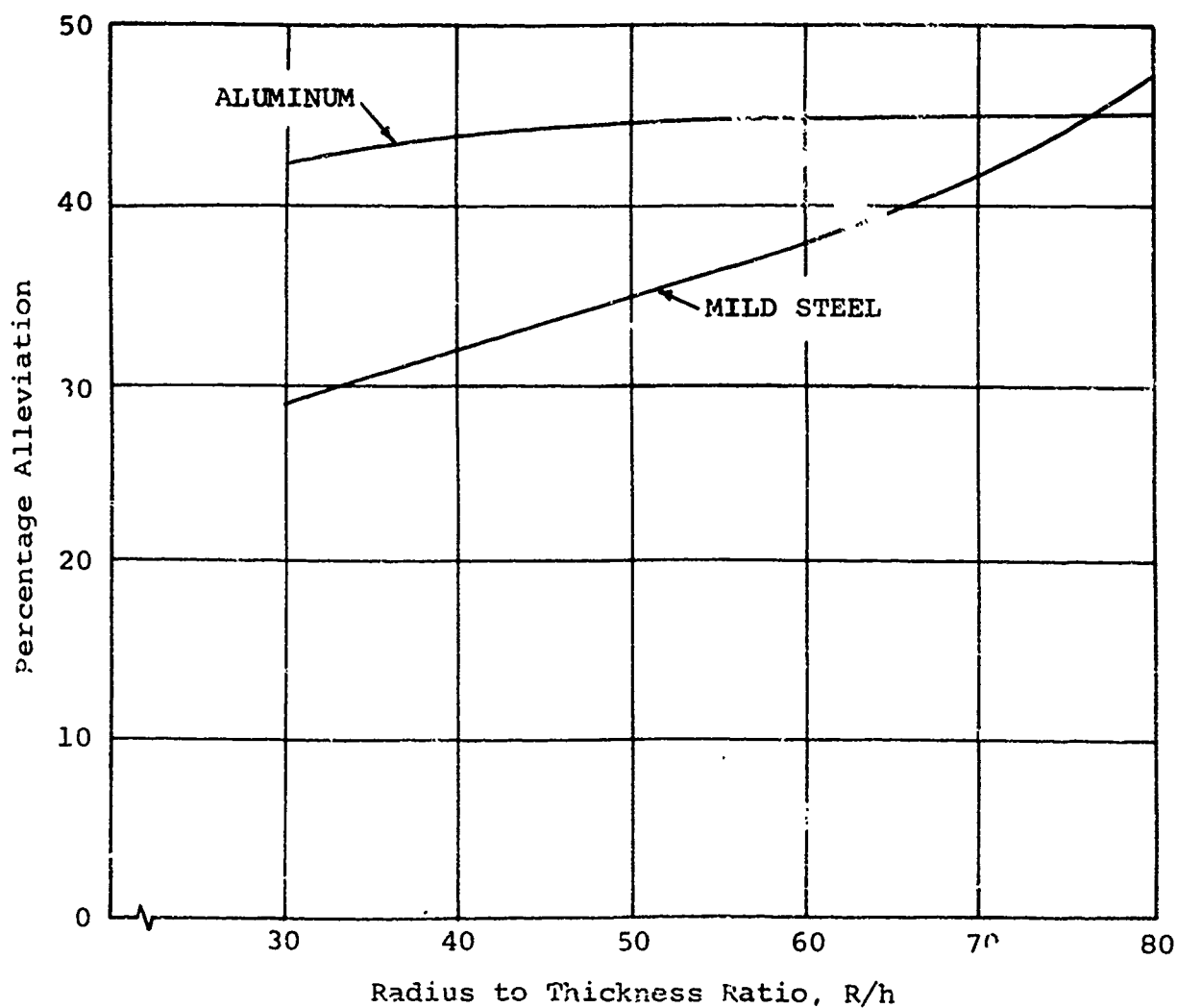


Figure 8. Percentage Alleviation versus Radius to Thickness Ratios

percent for mild steel and 44 percent for aluminum is obtained. Therefore, a significant reduction in die stress is provided by the surrounding water.

Figure 8 also shows that alleviation increases with R/h . The explanation for this is simply that for the same amount of explosive charge, the velocity of the die wall increases as the ratio R/h is increased. Consequently, the damping force resisting the wall motion also increases. The alleviation increase, however, is greater for mild steel than for aluminum.

CONCLUSIONS

In this paper, the authors have presented a simple analysis to predict the peak strain (and hence peak stress) in a thin die subjected to known explosive pressures. These predictions, confirmed by experimental measurements, are necessary to prevent die failures in the explosive forming process.

The analysis has also been used to determine the effect of water immersion on the die stresses and shows that they are substantially reduced. It is interesting to note that the dynamic response of the die can be used to mobilize the resistance of the surrounding water and reduce the stress in the die walls. This important result can be effectively used to design, in a rational manner, thin shell dies for use in explosive forming thereby substantially reducing the die cost.

ACKNOWLEDGMENTS

The authors wish to acknowledge the able assistance of Mr. L. Brown and Mr. R. P. Marchese in performing the experiments.

REFERENCES

1. Beyer, W. K., "The Pool is the Tool," Paper No. SP 64-124, Creative Manufacturing Seminar, American Society for Tool and Manufacturing Engineers, May 1964.
2. Reismann, H., and W. H. Journey, "Effect of Water Immersion on Reduction of Die Stresses in Explosive Forming," Journal of Engineering for Industry, pp. 111-116, February 1966.

IX. THE MECHANICS OF ENERGY TRANSFER
FROM UNDERWATER EXPLOSIONS

V. D'Souza

G. A. Thurston

INTRODUCTION

A large cost item in explosive forming of large domes is the female die. If the parameters of weight of explosive, shape of charge, standoff distance and edge pull-in can be adjusted correctly, the impact forces on the die can be reduced and the weight of die minimized. This is a progress report on a thesis whose topic will be the analytical study of the forming process. Prior studies at the Center have been concerned with mechanics of blank deformation. This analysis will primarily deal with blank and water interaction during the reloading phase after the initial shock loading.

The configuration is shown in Figure 1. The thin uniform thickness blank is held between frictionless annular rings. The set-up is immersed in sufficient depth of water. The charge in the shape of a sphere is placed at the appropriate standoff distance and set off. The resulting motion of the deforming blank is studied analytically and the final strains and shape of the dome that is formed is computed.

The problem can be considered as consisting of two parts--first to determine the pressure loading on the blank as a function of time and secondly to use this pressure in computing the dynamic response of the blank during the large plastic deformations that occur. Both these aspects of the problem are coupled and hence a numerical solution by means of a digital computer will be sought. The problem is complex because of the various interactions; but by means of suitable approximations that represent the physical phenomenon, a realistic model that provides good correlation with experiments is expected.

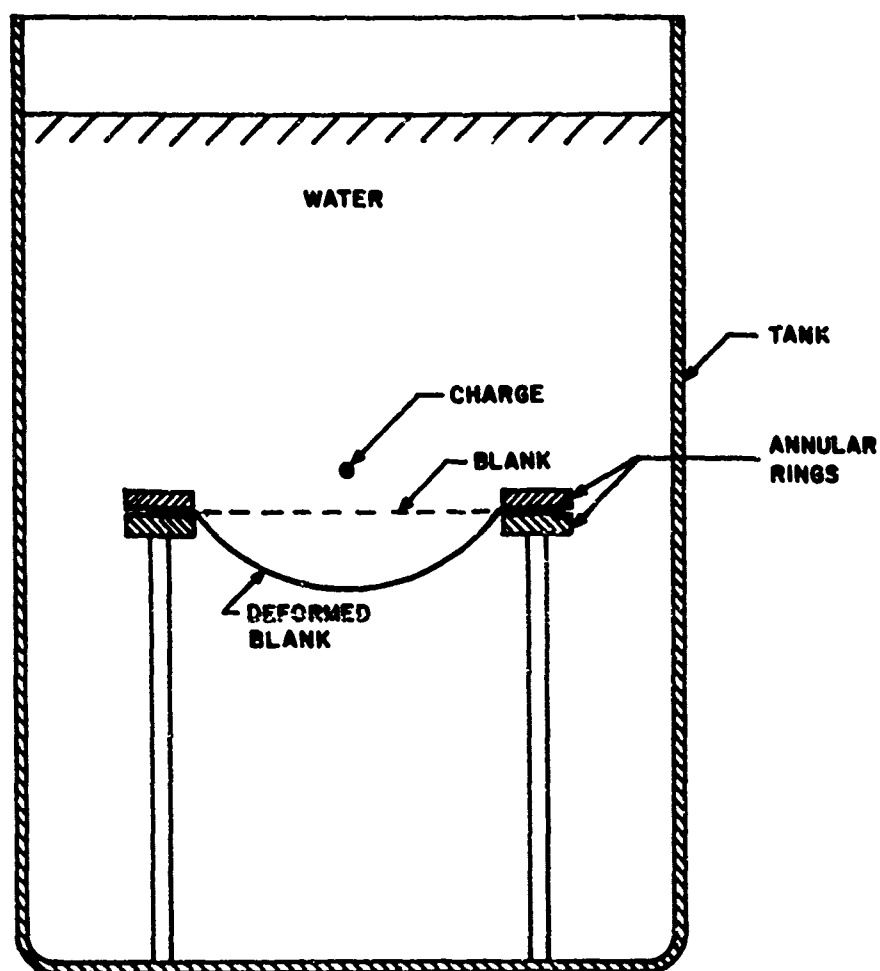


FIG. 1 SCHEMATIC OF SET UP

BACKGROUND

Some of the early work relevant to this problem arose out of the military objective of determining the damage to structures by underwater explosions. The work of Kirkwood (Ref. 1) and Taylor (Ref. 2) fall into this type. They both used the plane shock wave pressure-time history to determine the deformation of a circular clamped plate, neglecting the effect of the gas bubble. In view of the fact that in explosive forming of domes, the charge is placed close to the plate, Thurston et al (Ref. 3) improved the solution by considering a spherical shock wave. Following this improvement, Thurston (Ref. 4) was able to find reasonable agreement with the experimentally observed initial deformations. However, the energy in domes due to the shock wave loading was a fraction of the energy of the observed total deformation of the domes. Attempts to explain this extra energy by considering the large amount of energy still remaining in the gas bubble after the release of the shock wave was first made by Schauer (Ref. 5). His model for the reloading phenomenon assumed that a portion of the kinetic energy of the gas bubble flow was absorbed by the plate, an approach that we shall also use in this study.

The dynamic response of a circular clamped plate to an impulse has been treated by Witmer et al (Ref. 6) using an extensive computer program. A simplified approach using Hamilton's Principle has been developed by Boyd (Ref. 7) which uses much less computer time than in Ref. 6 while still giving reasonable results. In neither of the above two studies has the pull-in of the flange, as occurring in explosive dome forming, been considered. The

flow of the flange material into the dome affects the final strains in the dome. This effect, which Thurston (Ref. 8) considered, will be included in this study.

SCOPE OF WORK

Dynamic Response of the Blank

The equations describing the dynamic response of the blank to an arbitrary pressure load are determined by using Hamilton's Principle and the corresponding Euler-Lagrange variational equations (Ref. 9, 10).

The following assumptions are made:

- (1) Deformation theory of plasticity is assumed adequate.
- (2) Bending is neglected.
- (3) Radial and rotatory inertias are neglected.

Also, the power-law representation of the stress-strain law ($\sigma = \alpha \epsilon^n$) for the material of the blank is used leading to the neglect of elastic strains and elastic springback, which are both assumed to be small compared to the plastic strains of the deformed blank.

The amount of work done during loading which is independent of the deformation history of the body as long as unloading does not occur, resulting from assumption (1), allows the use of Hamilton's Principle to this nonconservative system, as w_i is then a time-dependent potential energy function.

Hamilton's Principle may be expressed mathematically as $\delta A = 0$ where A , the Action integral is given by

$$A = \int_{t_1}^{t_2} (T + w_e + w_i) dt$$

with T = total kinetic energy of the system

w_e = work of external forces acting on the surface

w_i = work of internal forces acting within the membrane

t_1, t_2 = two arbitrary times

Pressure-Time History

The pressure loading on the blank during the explosive forming appears in the equations of motions derived from the action integral.

It is convenient to treat the pressure acting on the blank as arising from two distinct phenomena--the shock wave and the gas bubble motion.

1. Shock Wave Loading. The detonation of the charge at its center results in a detonation wave in the explosive, converting it into certain decomposition products. When the front of the detonation wave arrives at the boundary of the charge, a shock wave advances in the water and a reflected wave travels into the gas sphere, composed of the products of the explosion. The shock wave with a profile consisting of almost zero time to rise, and a tail of diminishing intensity produces the initial pressure pulse in the environment of the explosive.

The hydrodynamic analysis of the initial pressure pulse has been treated by Kirkwood and Bethe (Ref. 11). This theory will be used to give the pressure-time history at a point in water. The presence of a moving plate near the explosive, however, changes the pressure that is felt on the plate. An acoustic theory for the resulting pressure treated in Ref. 3 will be used. The model used is that of a spherical wave traveling at a constant velocity striking the plate at an angle of incidence of ψ and reflecting at the same angle. The boundary condition at the plate that is used is that the normal component of the fluid flow velocity is equal to the normal velocity of the moving blank. This leads to the equation

for the effective pressure on the moving plate given by

$$P = 2P_1 \cos\psi - \rho_o C_o \frac{\partial w}{\partial t}$$

where P = effective pressure on the plate

P_1 = pressure at the position in the absence of the plate

ψ = angle between the normal of the plate and the path
of the wave

ρ_o = density of water

C_o = velocity of sound in water

$\frac{\partial w}{\partial t}$ = velocity of the plate

The impact of the shock wave accelerates the thin plate to a high velocity. This takes place in a short time. The pressure in the water subsequently decreases rapidly with time and cavitation results near the plate.

2. Gas Bubble Motion. After emission of the shock wave, the gaseous products of explosion continue to expand radially outwards at a gradually decreasing rate. There is thus considerable displacement of water, though the changes in velocity take place at a much slower rate than in the initial phases of the motion immediately following detonation. An incompressible approximation is thus suitable for the study of the gas bubble motion.

To explain the reloading phenomenon, the motion of the gas bubble must be considered especially as, after the release of the initial shock wave, about 50 percent of the initial chemical energy remains

in the explosion products. The model to be used to calculate the energy given to the plate is calculated thus--the flow due to the expanding bubble closes the cavitation region in the shock wave loaded plate resulting in an impact on the plate at the time of closure. An approximate way to treat this part of the problem is to determine the kinetic energy of the bubble motion which can be absorbed by the plate and assume that a portion is absorbed. The empirical constant used is to take care of turbulence in the flow, the partial elastic impact of water on the plate, etc. The plate will thus be assumed to get a jump in its velocity distribution when the cavitation front is closed. The pressure during this time, it is assumed, will be zero.

To obtain this kinetic energy, the model of an expanding high pressure gas bubble in water is considered (fig. 3) assuming:

1. water is inviscid and incompressible,
2. explosion gas is inviscid and its expansion adiabatic, and
3. gas-water interface remains a sphere.

The governing equation for the flow of water outside the sphere is $\nabla^2 \phi (r, \theta, t) = 0$, where ϕ is the velocity potential. A variable separable solution for this Laplacian is determined by using the assumptions that the solution is axisymmetric, the inner boundary remains a sphere and the appropriate boundary conditions at infinity of zero perturbations in velocity and pressure. The pressure on the fluid boundary is then equated to the pressure inside the gas resulting in the following first order nonlinear

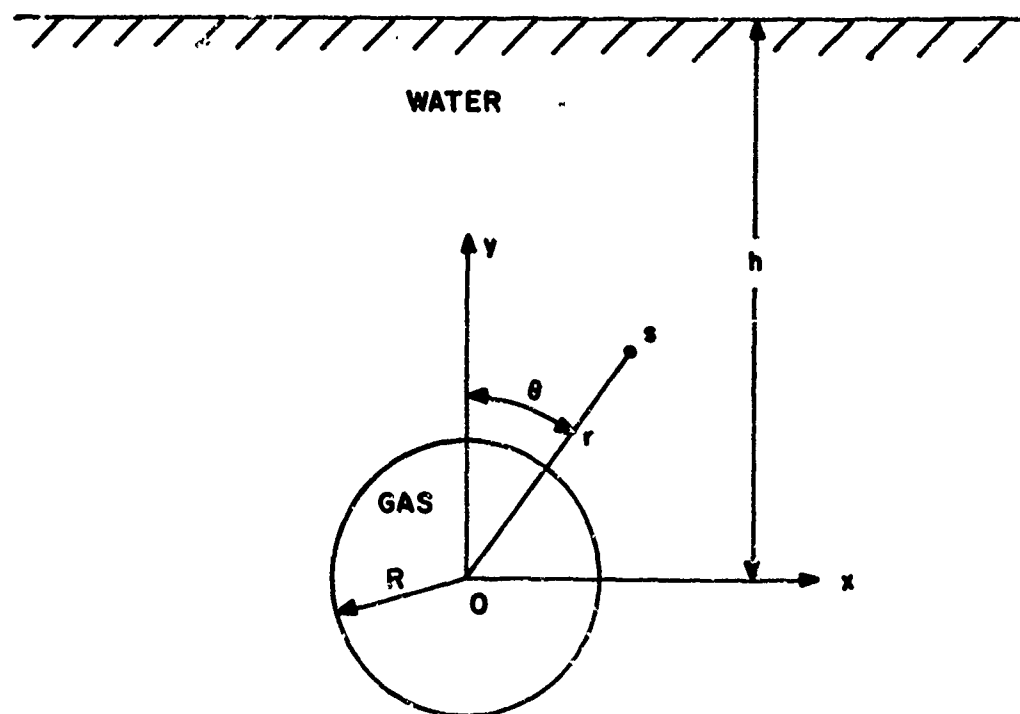


FIG. 3 COORDINATE SYSTEM FOR THE EXPANDING GAS SPHERE

differential equation

$$\dot{R}^2 = \frac{2gh}{3} \left\{ \left(\frac{R_i}{R} \right)^3 \left[\frac{P_i}{P_o(\gamma-1)} + 1 \right] - \frac{P_i}{P_o(\gamma-1)} \left(\frac{R_i}{R} \right)^{3\gamma} - 1 + \left[R - R_i \left(\frac{R_i}{R} \right)^3 \right] \frac{\cos \theta}{4h} \right\}$$

with the initial condition $R(0) = R_i$.

Here R = radius of the bubble

R_i = initial radius of the bubble

$R = \frac{dR}{dt}$

P_o = hydrostatic pressure at center of the bubble

P_i = initial gas pressure

γ = specific heat ratio for the gas

h = depth of the bubble center from surface

θ = angular position of a point in the water measured from the vertical

g = acceleration due to gravity

The analysis to determine the kinetic energy of the flow is incomplete.

The final set of equations will be solved numerically. Results will be compared with experiments to determine the efficiency factor for the energy transfer from the gas bubble expansion to the blank.

REFERENCES

1. J. G. Kirkwood, "Memorandum on the Plastic Deformation of Marine Structures by an Underwater Explosion," OSRD-788.
2. G. I. Taylor, "The Pressure and Impulse of Submarine Explosion Waves on Plates", "Underwater Explosions Research," A Compendium of British and American Reports, Vol. I, Office of Naval Research (1950), pp. 1155-1173.
3. G. A. Thurston, R. J. Harris and D. D. Bouma, "Explosive Forming of Domes from Flat Circular Blanks," The Third Annual Report of the Center for High Energy Forming, August 1968.
4. G. A. Thurston, unpublished paper.
5. H. M. Schauer, "The Afterflow Theory of the Reloading of Airbacked Plates at Underwater Explosions," Proceedings of the First U. S. National Congress of Applied Mechanics, ASME, Ed. E. Sternberg et al. (1952), pp. 887-892.
6. E. A. Witmer, H. A. Balmer, J. W. Leech, and T. H. H. Pian, "Large Dynamic Deformations of Beams, Rings, Plates and Shells," A.I.A.A. Journal, Vol. 1, No. 8, August 1963, pp. 1848-1857.
7. D. E. Boyd, "Dynamic Deformations of Circular Membranes," J. Engineering Mechanics Division, ASCE, Vol. 92, June 1966, pp. 1-16.
8. G. A. Thurston, "On the Effect of Edge Pull-In on the Explosive Forming of Domes," Advances in Machine Tool Design and Research, Proceedings of the 7th International MTDR Conference, University of Birmingham, England, Sept. 1966, pp. 129-143.
9. H. Goldstein, Classical Mechanics, Addison-Wesley Publishing Co. Inc., 1950.
10. H. L. Langhaar, Energy Methods in Applied Mechanics, John Wiley and Sons Inc., 1962.
11. J. G. Kirkwood and H. A. Bethe, "The Pressure Wave Produced by an Underwater Explosion I," OSRD-588.
12. G. A. Thurston, "Newton's Method Applied to Problems in Nonlinear Mechanics," Journal of Applied Mechanics, June 1965, pp. 383-388.

X. THE RADIAL PISTON APPROACH TO THE DYNAMIC AUTOFRETTAGE
OF THICK WALLED FORGING DIES

M. Kaplan

H. Glick

R. E. Knight

V. D'Souza

and

W. Howell

SUMMARY

A new process for obtaining residual compressive hoop stresses at the bore of thick-walled forging dies is presented. The process uses explosive energy in a controlled manner to produce plastic flow in the die. High residual stresses are generated as the applied pressures decay. A theoretical model of the process is developed which predicts residual stress and deformation as a function of the material properties and geometry of the system and the characteristics of the explosive. Experimental data are presented and compared with analytical results. The experiments demonstrate the validity of the analysis and the process itself. An alternate method of dynamic autofrettage, in which the piston is eliminated, is also discussed. The application of explosive autofrettage to a specific production forging die is described. The process is compared with existing methods for producing residual stresses in thick-walled cylinders.

NOMENCLATURE

ρ, ρ_w, ρ^p	Mass densities of the outer cylinder, water, and radial piston
ρ_o	Initial mass density of the water
p_g, p_w	Gas and water pressures
p_o	Initial explosion pressure
a, b, d	Inner radii of the liner, radial piston, and outer cylinder
a_o, b_o	Initial inner radii of the liner and radial piston
c, e	Outer radii of the radial piston and outer cylinder
k^p, K	Radial displacement functions for the radial piston and outer cylinder
e_{ij}	Strain tensor
\dot{e}_{ij}	Strain rate tensor
S_{ij}	Deviatoric stress tensor
$\sigma_r, \sigma_\theta, \sigma_z$	Radial, tangential, and axial stress components
$\sigma_{rj}, \sigma_{\theta j}$	Radial and tangential stress components at time t_j
$\sigma_{r\infty}, \sigma_{\theta\infty}$	Residual radial and tangential stresses
k^L, k^p, k	$2/\sqrt{3}$ times the tensile yield strength of the liner, piston, and outer cylinder
γ	Specific heat ratio
E	Specific energy of the explosive
η	Radial position of the elastic-plastic interface
μ	Positive scalar function

INTRODUCTION

There are many applications in which thick walled cylindrical structures are subjected to large transient internal pressures. Failure, in these situations, generally occurs by the propagation of radial cracks from the inner radius of the cylinder. Structural life can often be extended by introducing residual compressive hoop stresses into the cylinder. These stresses prevent premature failure by retarding radial crack growth.

Residual compressive hoop stress can be developed in a variety of ways. In the case of cannon barrels, it was empirically found many years ago that a single firing with a double charge of powder substantially increased the life of the cannon. More recently, cannon barrels have been strengthened by either hydraulic or mechanical autofrettage. In the hydraulic autofrettage process a fluid is pumped into the cavity at high pressure and then released. Mechanical autofrettage involves forcing an oversized mandrel through the length of the bore. Both methods cause the cylinder wall to become partially or totally plastic during the loading phase. The resulting residual stress distribution is caused by the differences between the plastic loading stresses and the elastic stresses developed during unloading. Large and expensive facilities are required for either method, even for medium sized cannon barrels.

In the case of cylindrical forging dies, a shrink ring on the outside diameter of the die produces compressive hoop stress at the inner radius. The method is not very satisfactory since only relatively small stresses can be achieved in practical applications. Mechanical autofrettage cannot

be used on cylindrical forging dies because of die geometry and the unit cost of hydraulic autofrettage appears to be too high to be practical.

The purpose of this paper is to describe a new method for producing large residual compressive hoop stresses in thick walled cylinders. It is called the radial piston method of explosive autofrettage and appears to be completely feasible for use on cylindrical forging dies.

RADIAL PISTON METHOD

Initial experiments in explosive autofrettage⁽¹⁾ used a line charge of explosive placed along the axis of a thick walled tube immersed in water. Following detonation of the explosive, the inner wall of the tube was subjected to an intense pressure wave which decayed rapidly. Although the method produced substantial plastic flow in the wall, the residual hoop stresses were only about 30 percent as large as comparable stresses obtained with hydraulic autofrettage. It was demonstrated in Reference 1 that the loss of residual stress was due primarily to plastic flow during unloading of the tube, and that the development of full residual stress required some control of the magnitude and decay rate of the applied pressure.

These considerations led to the radial-piston concept in which a ductile tube, called the radial piston, is placed co-axially with the thick walled tube to be autofrettaged (Figure 1). The radial piston is separated from the outer cylinder by water and is filled with explosive powder. The powder is ignited by a thin rod of high detonation velocity explosive so that the motion of the piston is essentially radial. A restraining end fixture is used to position the radial piston and outer tube and to prevent leakage of the water and gaseous products of the explosion.

The piston acts primarily as an attenuator of the rate of energy transfer. The explosive energy released at detonation is not transferred to the outer tube as a series of shock waves; rather, it is used to accelerate the piston, which in turn compresses the water sufficiently to produce

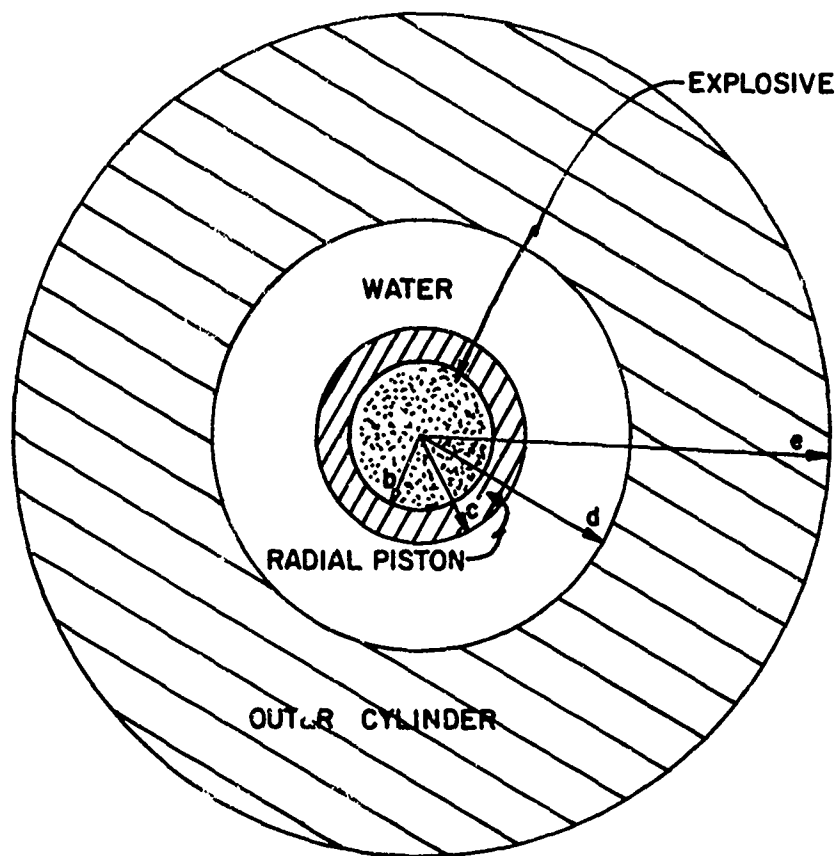


Figure 1. Radial Piston Autofrettage Configuration.

plastic flow in the outer tube. A high rate of pressure decay is possible only if the piston is rapidly driven radially inward. This is prevented by the piston's inertia and yield strength and the internal gas pressure in the piston. The gas pressure is maintained at relatively high values because the piston separates it from the surrounding water, thus preventing the sudden decrease in pressure produced by quenching.

MATHEMATICAL MODEL OF THE RADIAL PISTON CONFIGURATION

The purpose of the mathematical model is to predict residual stress and deformation as a function of system geometry and initial explosion pressure. Although explosive detonation generally produces significant wave effects, there is strong motivation for neglecting wave motion in this instance. The radial piston configuration is designed to smooth the pressure pulse produced by detonation. Because of the impedance mismatch between steel and water, only a small percentage of the initial detonation wave is transmitted to the water, and an even smaller percentage to the outer thick walled tube. Although wave motion in the radial piston is probably significant during its initial outward motion, a highly accurate description of piston motion is not necessary. The water gap acts as a weak non-linear spring and moderate changes in piston position are reflected as small changes in the water pressure. Similarly, some error in the water pressure can be tolerated. The residual stress and deformation are functions of the integral of the pressure time history—not of the instantaneous pressure. Rapid time variations in the piston's internal gas pressure, for the same reasons, need not be modeled exactly. For these physical reasons, as well as for the substantial simplification produced in the mathematics, wave motions will not be considered.

The specific models used for the gas, radial piston, water, and outer cylinder are described below.

1. Outer Cylinder

Typically, forging dies are composed of high yield strength steels. Such materials exhibit little work hardening and low strain rate

sensitivity. Therefore, the die will be treated as an elastic-perfectly plastic strain rate insensitive body. Also, elastic incompressibility will be assumed. This produces a completely incompressible body and eliminates the possibility of wave solutions.

Under these conditions, the elasticity equations are written

$$\Delta S_{ij} = 2G \Delta e_{ij} \quad (1)$$

where the Δ 's are used to represent the changes in deviatoric stress and strain from an initial stress state. The Prandtl-Reuss equations

$$\dot{e}_{ij} = \mu S_{ij} + \dot{S}_{ij}/2G \quad (2)$$

will be used to describe plastic flow, where μ is a positive scalar function, and \dot{e}_{ij} is the strain rate tensor. \dot{S}_{ij} is, for this particular problem, the material time derivative of S_{ij} . The Von-Mises yield condition

$$S_{ij}^i S_{ij}^j = \frac{1}{2} k^2 \quad (3)$$

is used as the condition for plastic flow. The constant k is equal to $2/\sqrt{3}$ times the yield strength in tension.

2. Water Gap

The water between the radial piston and the outer cylinder is treated as a compressible fluid. Since the dynamic portion of the autofrettage process is generally completed in a time scale of the order of microseconds, the compression and expansion of the water are assumed to be adiabatic. The pressure-specific volume adiabat for

$p = 15$ psia, $T = 80^\circ\text{F}$, and $s = 0.0932$ Btu/lbm- $^\circ\text{R}$ was obtained from Reference 2. This curve is closely approximated by the following equations.

$$\begin{aligned} p_w &= 31.62Q ; 0 < Q \leq 0.079 \\ p_w &= -0.134 + 29.2Q + 82.1Q^2 + 104.9Q^3 ; 0.079 < Q < 1.5 \end{aligned} \quad (4)$$

where p_w is in kilobars and Q is a function of the ratio of the final and initial densities, i.e.,

$$Q = \frac{\rho_w}{\rho_o} - 1 \quad (5)$$

3. Radial Piston

The piston is treated as a rigid-perfectly plastic material.

Its constitutive equation is

$$\dot{\epsilon}_{ij} = \mu s_{ij} \quad (6)$$

when the yield condition (3) is satisfied.

4. Gas Pressure

The gas pressure in the piston is computed from the isentropic expansion relations for a perfect gas. Thus,

$$p_g = p_o (b/b_o)^{2\gamma} \quad (7)$$

with p_o the initial explosion pressure, γ the specific heat ratio, and b_o the initial radius of the piston. The value of γ is obtained

from the ideal gas relation

$$p_0 = (\gamma - 1)E \quad (8)$$

where E is the specific energy of the explosive. The initial explosion pressure cannot be accurately computed from existing theory. It is estimated by correlating analytical predictions of residual deformation with experimental results. This is normally done only once for a given explosive.

Experimental evidence indicates that the flow process is essentially radial. Therefore, the axial and tangential velocities and displacements are zero, and the partial derivatives of all quantities with respect to these directions vanish, i.e., a state of axial symmetry and plane strain exists. Under these conditions, the incompressibility equation in terms of velocities can be integrated to give the radial velocity v as

$$v = \dot{K}(t)/r \quad (9)$$

where \dot{K} is an unknown time function and r is the radial position. Equation (9) is valid for a tube undergoing elastic, constrained plastic or total plastic flow. The radial acceleration, taking the material derivative of (9), is

$$a = \ddot{K}/r - \dot{K}^2/r \quad (10)$$

In the case of elastic or constrained plastic flow (when the tube is

partially elastic and partially plastic), the convective term in the material derivative can be neglected. In this case, the radial displacement, velocity, and acceleration in terms of K are simply

$$u = K/r \quad ; \quad v = \dot{K}/r \quad ; \quad a = \ddot{K}/r \quad . \quad (11)$$

The governing equations for the radial piston and outer cylinder are obtained when (1) through (11) are used with the radial equation of motion. With no body forces, this equation is

$$\frac{\partial \sigma_r}{\partial r} + (\sigma_r - \sigma_\theta)r = \rho a \quad (12)$$

with ρ the mass density and σ_r and σ_θ the radial and tangential components of stress respectively.

GOVERNING EQUATIONS FOR THE RADIAL PISTON

In order to avoid confusion between the piston and outer cylinder, all quantities associated with the piston will be superscripted with a p . The use of (9) in the strain rate-velocity relations $\dot{e}_{ij} = \frac{1}{2}(v_{i;j} + v_{j;i})$ gives two non-vanishing components. These are

$$\dot{e}_r^p = -\dot{e}_\theta^p = -\dot{K}^p/r^2 \quad (13)$$

Then, from (6), (3), and (13), it is found that

$$\sigma_\theta^p - \sigma_r^p = \pm k^p \quad (14)$$

and the axial stress is

$$\sigma_z^p = \frac{1}{2} (\sigma_r^p + \sigma_\theta^p) \quad (15)$$

The choice of sign in (14) is determined by the direction of the radial velocity. The sign is positive when the piston is moving outward; i.e., when $\dot{K}^p > 0$.

The radial stress is found in terms of K^p by integration of the equation of motion using (14) and (10). The result is

$$\sigma_r = \rho^p (\ddot{K}^p \log r + (\dot{K}^p)^2 / 2r^2) - (\pm k^p \log r) \quad (16)$$

Application of the boundary conditions $\sigma_r = -p_g$ at $r = b$ and $-p_w$ at $r = c$ yields the Riccati equation in \dot{K} ,

$$-\ddot{K}^p = \frac{1}{2} \left(\frac{1}{b^2} - \frac{1}{c^2} \right) \frac{(\dot{K}^p)^2}{\log b/c} + \frac{1}{\rho^p} \left(\pm k^p + \frac{p_g - p_w}{\log b/c} \right) \quad (17)$$

The radii b and c and pressures p_w and p_g are functions of time in (17). The piston begins flowing outward plastically when

$$p_g - p_w > k^P \log c/b \quad (18)$$

When (18) is not satisfied, the solution to (17) violates the yield condition. The condition for plastic flow in the reverse direction is obtained by replacing the left-hand side of (18) by $p_w - p_g$. The inequalities are applied only when the piston's velocity is zero. If the piston is moving, it continues flowing plastically until brought to rest by changes in the gas and water pressure.

When the wall thickness of the outer cylinder is not constant (e.g., tapered die), a uniform charge in the radial piston produces non-uniform expansion of the cylinder. One method of correction is the use of a stepped or tapered plastic liner in the piston. This allows the explosive energy per unit length of piston to be easily varied. Assuming the liner to be an incompressible material with yield stress k^L and density ρ^L , the governing equation for K^P becomes

$$-\ddot{K}^P = \frac{-\rho^L \left(\frac{1}{b^2} - \frac{1}{a^2} \right) + \rho^P \left(\frac{1}{b^2} - \frac{1}{c^2} \right)}{2(\rho^P \log b/c - \rho^L \log b/a)} (\dot{K}^P)^2 + \frac{+(k^P \log b/c - k^L \log b/a) + p_g - p_w}{\rho^P \log b/c - \rho^L \log b/a} \quad (19)$$

where a is the inner radius of the liner. The use of a liner also requires that b/b_0 in (7) be replaced by a/a_0 .

GOVERNING EQUATIONS FOR THE OUTER CYLINDER

As the water pressure increases, the outer cylinder first deforms elastically, then begins to yield at the inner surface $r = d$. With further increases in pressure, the extent of the plastic region grows until, at sufficiently high pressures, the tube is totally plastic. The plastic unloading phase of the process may, in some instances, be interrupted by additional plastic flow (reyielding). The governing equations for each of these conditions are given below. These equations were developed by following the same procedure used in obtaining the radial piston equations, the only differences being the use of (1) and (2) in place of (6), and (11) rather than (10) for elastic and constrained plastic flow.

1. Elastic Deformation

The equations are written for the time $t \geq t_j$ when the tube becomes completely elastic. The hoop and radial stresses at t_j are $\sigma_{\theta j}(r)$ and $\sigma_{rj}(r)$ respectively. Similarly, K at t_j is denoted by K_j . With the boundary conditions $\sigma_r = -p_w$ at $r = d$ and zero at $r = e$,

$$\sigma_r = \rho \ddot{K} \log r/e - 2G(K - K_j) \left(\frac{1}{r^2} - \frac{1}{e^2} \right) - \int_r^e \frac{1}{\lambda} (\sigma_{\theta j} - \sigma_{rj}) d\lambda \quad (20)$$

$$\sigma_r - \sigma_{\theta} = \sigma_{rj} - \sigma_{\theta j} - 4G(K - K_j)/r^2 \quad (21)$$

$$\rho \ddot{K} \log e/d + 2G(K - K_j) \left(\frac{1}{d^2} - \frac{1}{e^2} \right) = p_w - \int_d^e \frac{1}{\lambda} (\sigma_{\theta j} - \sigma_{rj}) d\lambda \quad (22)$$

The stress field, (20) and (21), is determined from the solution to (22). The solution is valid until plastic flow begins; i.e., until

$$|\sigma_{\theta} - \sigma_r| = k.$$

2. Elastic - Plastic Deformation

The tube is elastic in the region $\eta \leq r \leq e$ and plastic for $d \leq r \leq \eta$. The position of the elastic-plastic interface $r = \eta$ is a function of time. In addition to satisfying the boundary conditions, the stresses must also be continuous across $r = \eta$. The equations are written for time $t \geq t_j$ at which yielding begins, assuming a positive radial velocity.

In the plastic region,

$$\sigma_{\theta} - \sigma_r = k \quad (23)$$

$$\sigma_r = \rho \ddot{K} \log r/d + k \log r/d - p_w \quad (24)$$

In the elastic region, the equations for σ_r and $\sigma_r - \sigma_{\theta}$ are the same as (20) and (21). The equations for determining η and K come from application of the stress continuity condition. The result is

$$K - K_j = (\eta^2/4G) (\sigma_{rj}(\eta) - \sigma_{\theta j}(\eta) + k) \quad (25)$$

$$\rho \ddot{K} \log e/d + 2G \left(\frac{1}{\eta^2} - \frac{1}{e^2} \right) (K - K_j) = k \log d/\eta + p_w - \int_{\eta}^e \frac{1}{\lambda} (\sigma_{\theta j} - \sigma_{rj}) d\lambda \quad (26)$$

For negative radial velocities, the sign of k is changed in the above equations. Plastic flow, once begun, continues until the radial velocity vanishes. The solutions for K and η are, therefore, valid until $\dot{K} = 0$ or the tube becomes totally plastic ($\eta = e$).

3. Total Plastic Flow

Since the deformations are potentially large in this case, (10) is used. The final equations, for positive velocities, are

$$\sigma_{\theta} - \sigma_r = k \quad (27)$$

$$\sigma_r = \rho \ddot{K} \log r/e + k \log r/e + \frac{1}{2} \rho \dot{K}^2 \left(\frac{1}{r^2} - \frac{1}{e^2} \right) \quad (28)$$

$$\rho \log \ddot{K} \log e/d = p_w - k \log e/d + \frac{1}{2} \rho \dot{K}^2 \left(\frac{1}{d^2} - \frac{1}{e^2} \right) \quad (29)$$

Again, negative velocity, requires a sign change in k . The equations represent the material's behavior until \dot{K} is zero.

The solution to the governing equations (14) through (29) is obtained by numerical integration with the initial values $p_w = K = \dot{K} = K^p = \dot{K}^p = 0$ and the initial gas pressure p_0 . Typical results are given in the next section.

A similitude analysis can be conducted with the governing equations of the system. The results show that both model and prototype have the same residual stress and percent residual deformation at the inner radius when they are geometrically similar and when the parameters γ ,

k^P/p_0 , k/p_0 , G/p_0 , and ρ^P/ρ remain constant. This can be accomplished by using the same piston and cylinder material and the same explosive, packed at the same powder density, in both the model and prototype.

NUMERICAL RESULTS

As an example of the dynamic response of the system following detonation, the time variations of cylinder velocity, piston velocity, water pressure, and gas pressure are shown in Figure 2 for a configuration used in the experimental program. The geometry, material properties, and initial explosion pressure for this configuration are given in Table 1.

Table 1

Radial Piston: I.D. = 0.620", O.D. = 0.750", Yield Strength = 69 KSI

Outer Cylinder: I.D. = 1.130", O.D. = 1.984", Yield Strength = 160 KSI

Initial Explosion Pressure = 62 KSI

The results show the oscillatory nature of the process. Following detonation, the piston's velocity rapidly increases. As the piston moves outward, volume changes produce an increase in the water pressure and a decrease in the gas pressure. When the water pressure exceeds the gas pressure, the piston begins slowing down. The point of zero velocity, i.e., the point of maximum piston expansion, approximately corresponds to the initial pressure peak in the water. Because of the energy dissipated through plastic flow and the increase in the water gap produced by expansion of the outer cylinder, the oscillatory motion of the piston is highly damped. The piston and gas pressure become nearly stationary after a relatively short period of time. The outer cylinder, after deforming elastically, begins to yield slightly prior to the initial pressure peak. Plastic flow, extending through 70 percent of the tube wall in this instance, ceases when the radial velocity vanishes. The tube then oscillates elastically in its fundamental breathing mode, producing an undamped oscillation of the water pressure.

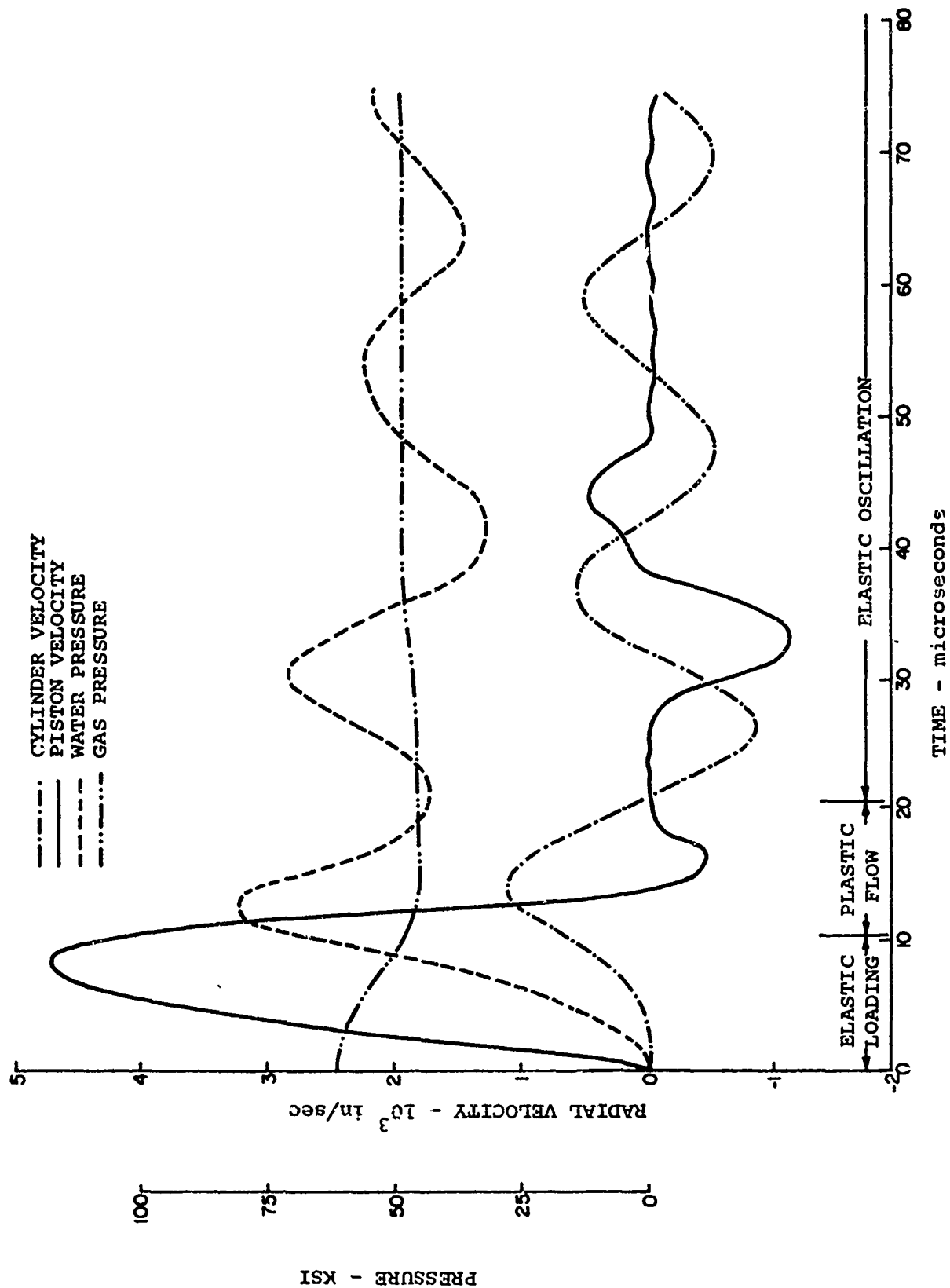


Figure 2. Predicted System Response Following Detonation.

Physically, end leakage gradually reduces the gas and water pressure to zero and internal dissipative mechanisms bring the outer cylinder to rest. The residual stresses are computed by assuming elastic unloading from time t_n to a rest state at $t = \infty$. The time t_n is any time beyond the cessation of all plastic flow. Thus, the final value of K is found by setting \ddot{K} and p_w to zero in (22) and replacing j by n . Using this result in (20) and (21), the residual stresses $\sigma_{r\infty}$ and $\sigma_{\theta\infty}$ are

$$\sigma_{r\infty} = \int_d^r \frac{1}{\lambda} (\sigma_{\theta n} - \sigma_{rn}) d\lambda - \frac{(1/e^2 - 1/r^2)}{(1/d^2 - 1/e^2)} \int_d^e \frac{1}{\lambda} (\sigma_{\theta n} - \sigma_{rn}) d\lambda \quad (30)$$

$$\sigma_{\theta\infty} = \sigma_{r\infty} + \sigma_{\theta n} - \sigma_{rn} - \frac{2/r^2}{(1/d^2 - 1/e^2)} \int_d^e \frac{1}{\lambda} (\sigma_{\theta n} - \sigma_{rn}) d\lambda \quad (31)$$

The residual radial and hoop stress distributions for the previous example are exactly those obtained by hydraulic autofrettage under conditions producing the same degree of plastic flow. This result is typical of situations in which reyielding does not occur (reyielding is defined as plastic flow during contraction of the cylinder). Thus, with no reyielding, explosive and hydraulic autofrettage produce the same residual stress states. When reyielding does occur, it reduces the size of the residual hoop stress at the inner radius ⁽¹⁾. Relyielding is caused by excessive radial contraction following initial plastic flow, a situation produced by rapid changes in the equilibrium position of the cylinder. With the radial piston method reyielding can generally be avoided with reasonable choices for the radial piston and initial explosion pressure. The system substantially reduces

the possibility of reyielding by reducing the rate of pressure decay. Also, the increase in water pressure during contraction of the outer cylinder limits the cylinder's radial displacement (see Figure 2).

The effects of the variation of initial explosion pressure, piston material, and piston geometry were studied with the analysis, and are discussed below. The basic configuration used for the study is given in Table 1.

1. Initial Explosion Pressure

The residual radial deformation at the inner diameter is shown in Figure 3 as a function of initial explosion pressure. The residual stresses can be obtained from the solid curve in Figure 7. The cylinder begins yielding at an initial gas pressure of 46 KSI, and total plastic flow is not developed until $p_o = 74$ KSI. This "working range" is large enough so that, in practice, substantial residual stress can be developed without the danger of the cylinder fracturing from excessive deformation. One of the advantages of explosive autofrettage, is that the rapid decay of pressure (as compared to the hydraulic process) limits the amount of cylinder expansion without the use of constraining dies. Thus, total plastic flow at 74 KSI produces only a one percent expansion of the inner diameter. Even with a 25 percent overpressure of 92 KSI, the permanent deformation is only about two percent.

2. Piston Geometry

The effect of varying the piston wall thickness, while keeping the outer diameter and initial explosion pressure constant, is shown

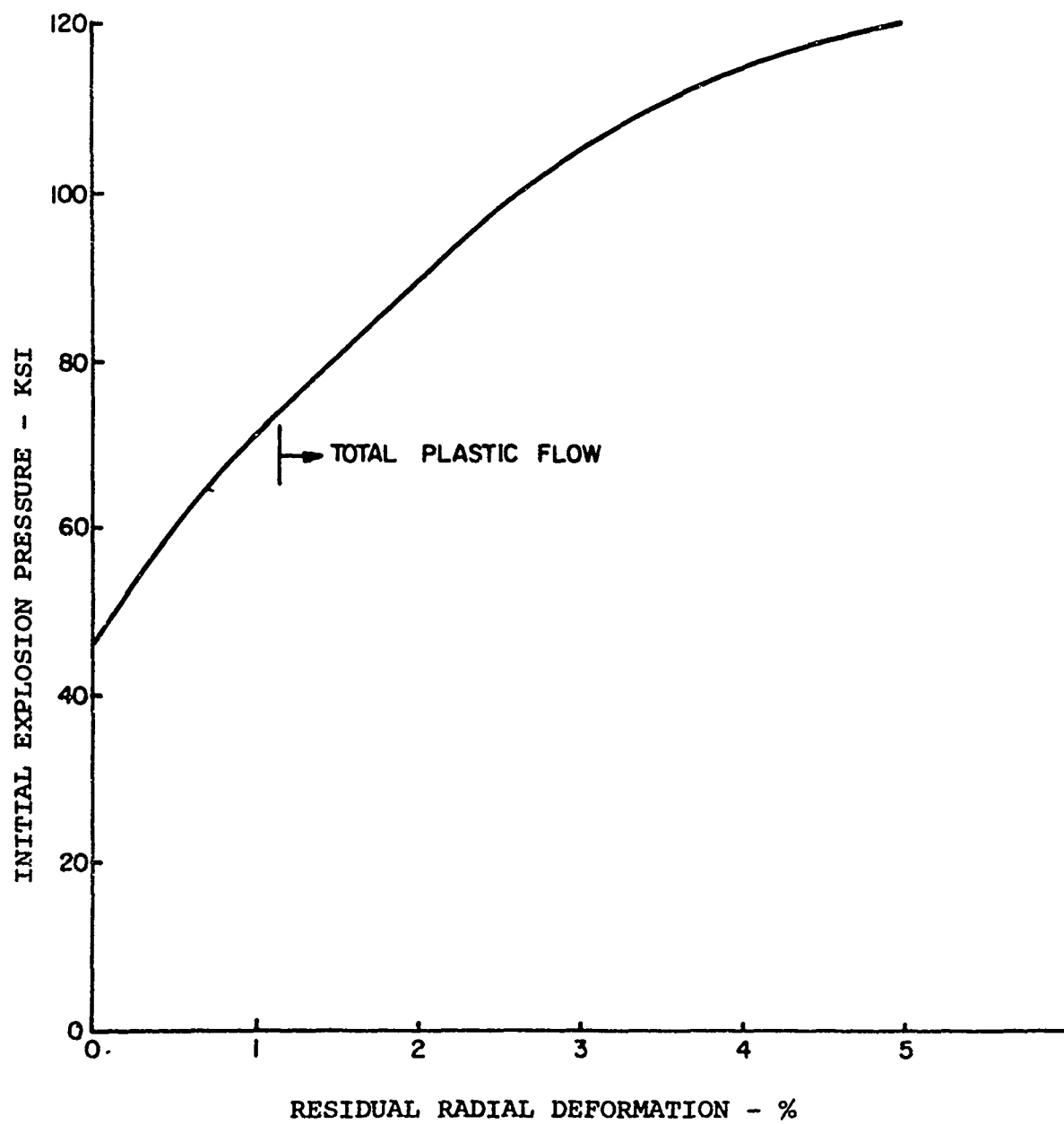


Figure 3. Effect of Varying the Initial Explosion Pressure.

in Figure 4. The increase in stiffness produced by thickening the wall reduces the piston's response to internal pressure. The resulting lowering of the water pressure is reflected as a decrease in the residual stress and deformation in the outer cylinder. Extensive thinning of the wall increases the piston's response frequency. Although higher peak water pressures are developed, their application time is sufficiently reduced as to produce a decrease in plastic flow in the cylinder; thus, the resulting decrease in residual stress and deformation.

A similar effect occurs when the size of the water gap is varied by keeping the piston's wall thickness constant and changing its outer diameter. Figure 5 shows that there is an optimal piston size for a given wall thickness. This is primarily due to changes in the stiffness of the non-linear water spring. When the water acts as a relatively soft spring (small piston), the piston expansion is not sufficient to produce high pressures. With small water gaps, the resulting high frequency system response reduces the time available for developing plastic flow.

3. Material Properties

The residual hoop stress was determined as a function of initial explosion pressure for four materials—304 stainless, mild steel, 5056-O aluminum, and 1100-O*aluminum. These materials were chosen because of their high ductility. The piston, as shown in Figure 6, is typically required to expand 10 to 20 percent without fracture.

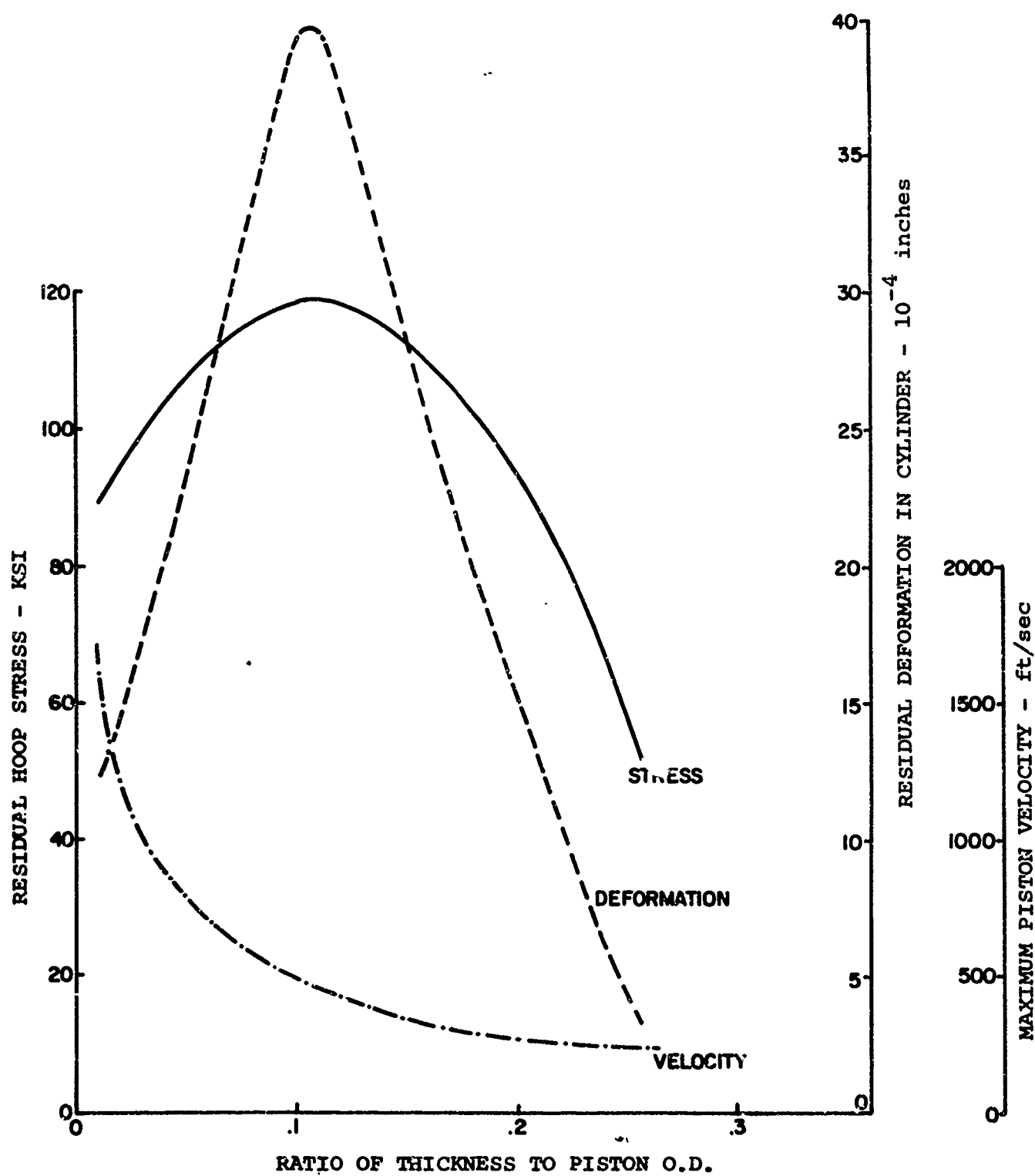


Figure 4. Effect of Varying the Piston's Wall Thickness.

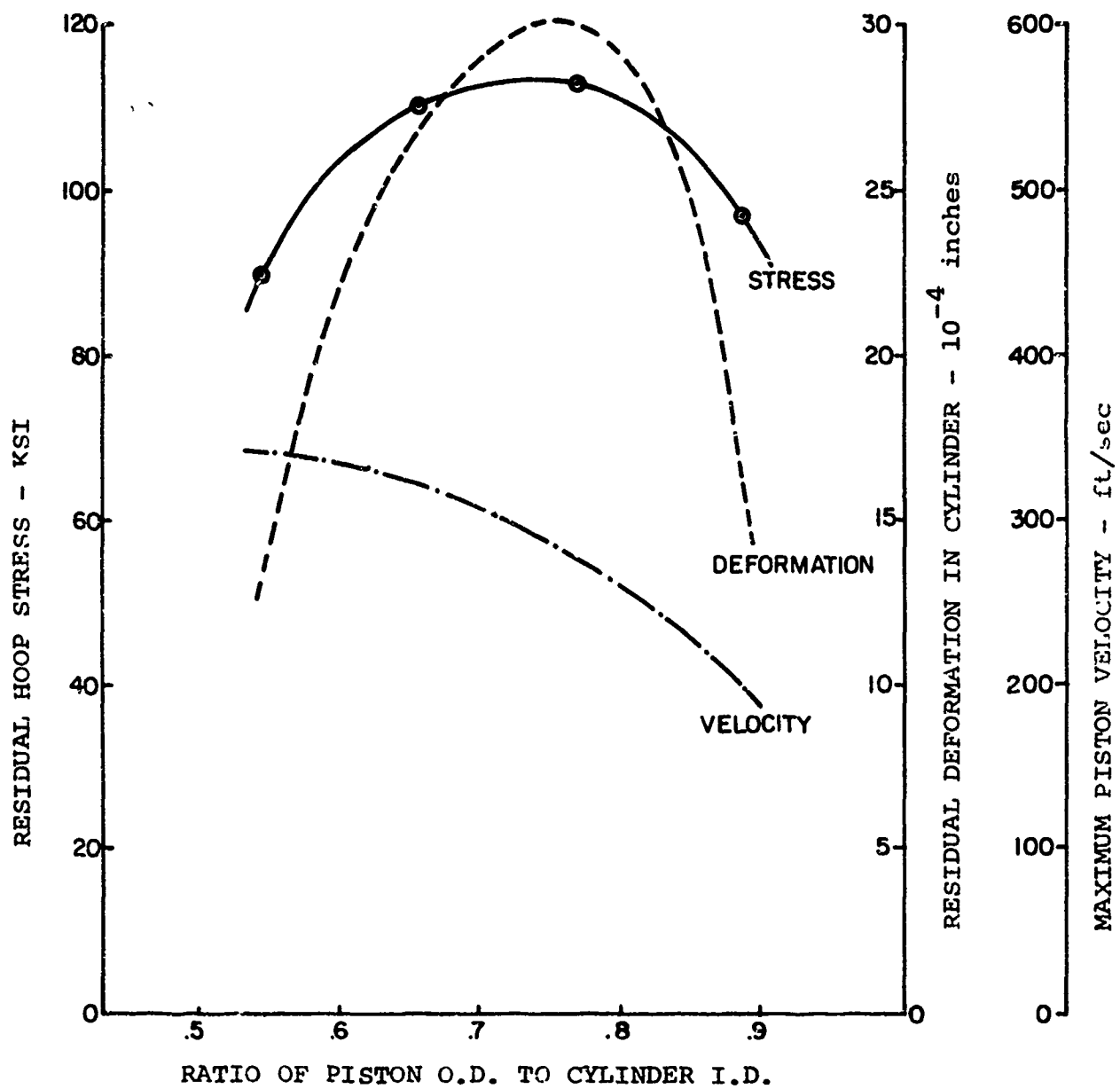


Figure 5. Effect of Varying the Size of the Piston.

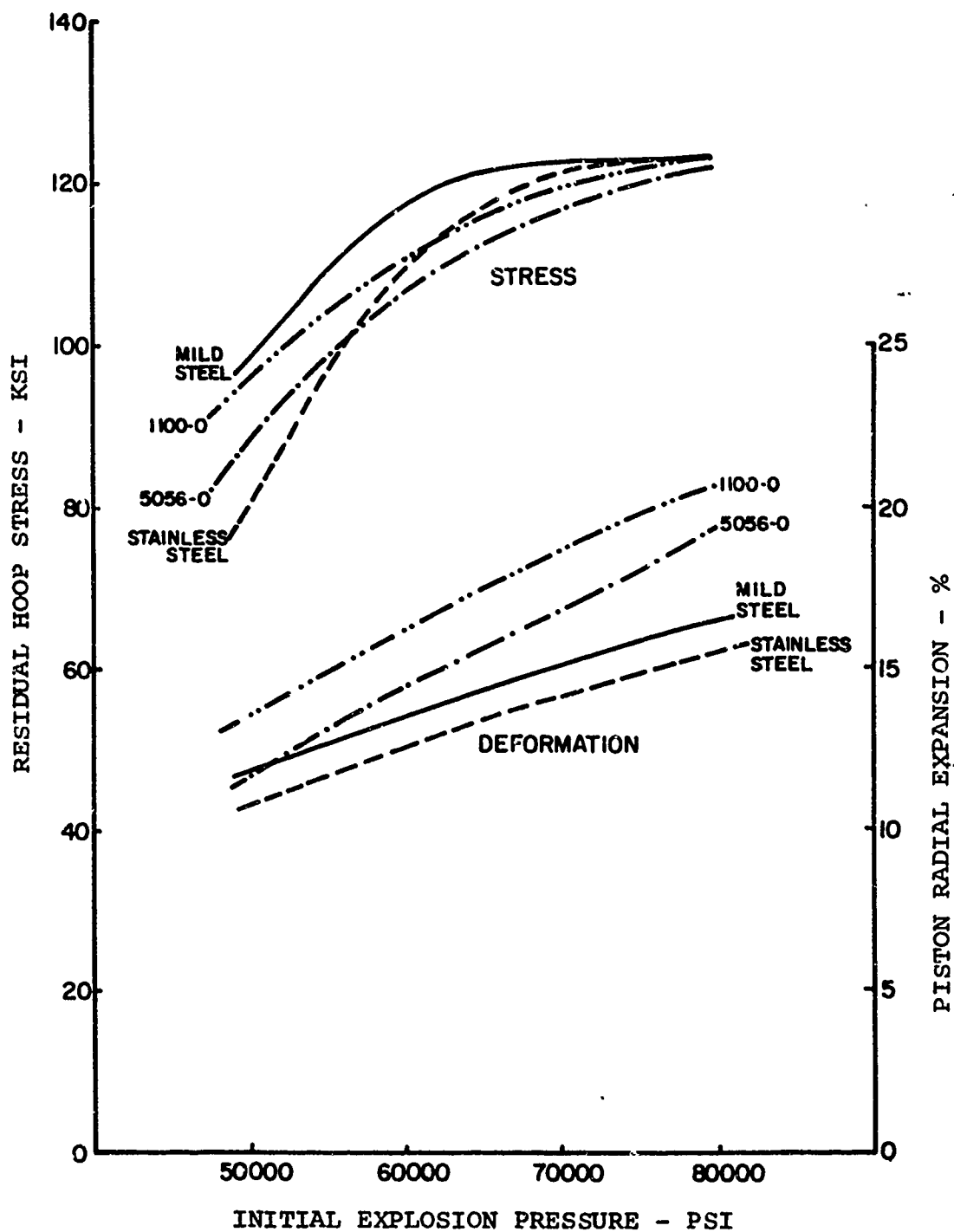


Figure 6. Effect of Varying the Piston Material.

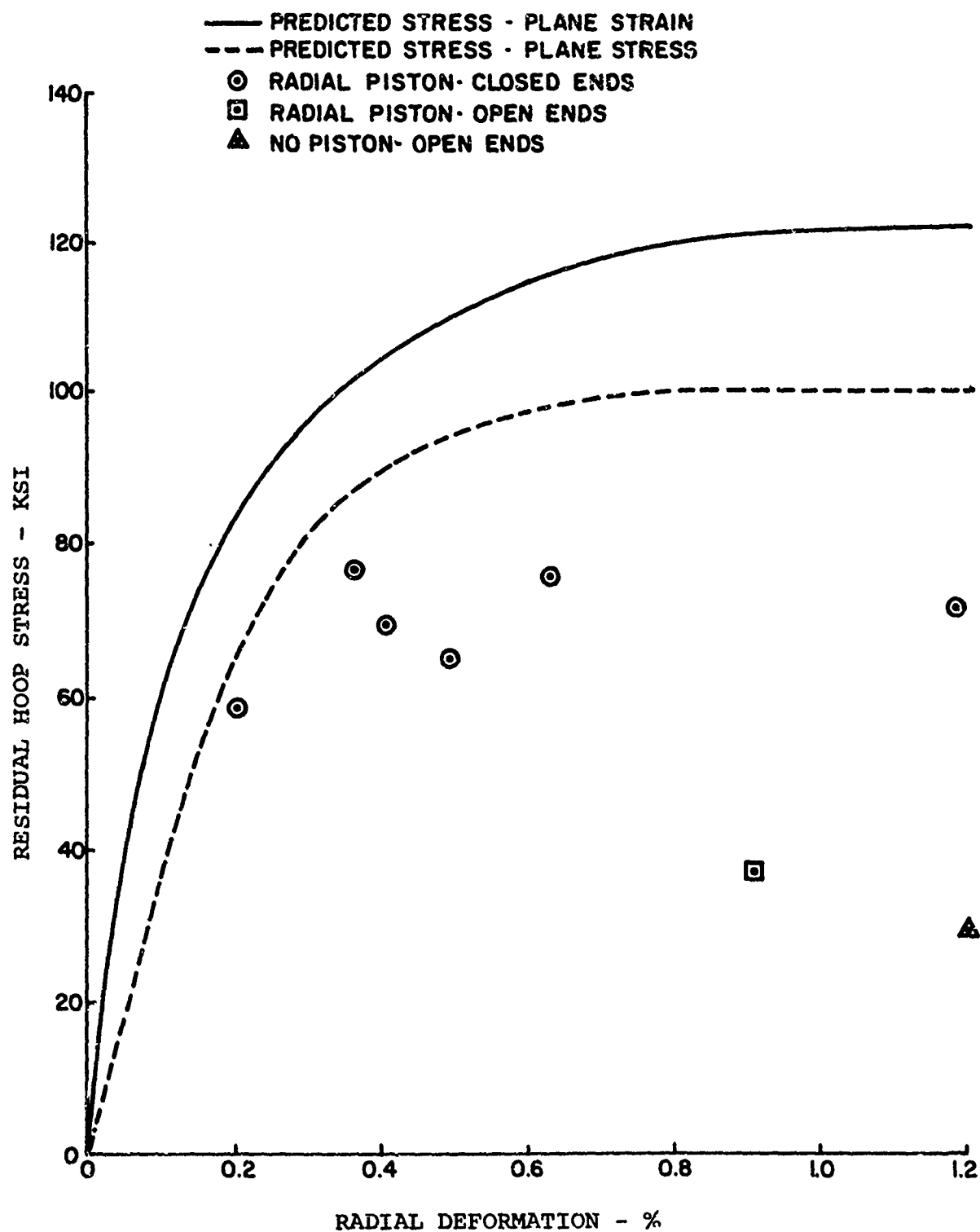


Figure 7. Comparison of Experimental and Predicted Values of Residual Hoop Stress.

The effect of increased yield strength in both aluminum and steel is to lower the residual stress in the outer cylinder. This result, as in the case of increased wall thickness, is caused by the change in the stiffness of the piston. The effect of material density can be seen from the mild steel and 5056-0 curves. Mild steel has a somewhat higher yield stress, but it produces larger residual stresses than 5056-0 at equivalent initial explosion pressures. Although the results show mild steel to be the best of the four materials, the differences between them are small and all would be suitable in practice.

EXPERIMENTAL PROGRAM

The experimental program with the radial piston configuration was conducted using 4340 steel tubes, heat treated to produce tensile yield strengths of approximately 160,000 psi. The radial piston was standard 304 stainless steel seamless tubing. Measurements were taken of residual deformation as a function of axial and tangential position. Many of the tubes were bored out to produce the data necessary for residual stress determination by the Sach's method. The aim of the test program was to demonstrate that explosive autofrettage would produce large residual hoop stresses. There was no attempt at optimization and, therefore, the tests were conducted with only minor variations in the basic parameters.

The basic test sequence used a 1.98" O.D. tube with a 0.425" wall and a 3/4" O.D. piston whose wall thickness was 1/16". Several tests were run using 34.9 grams of an ammonium nitrate explosive with aluminum additive. The specific energy of the explosive is 1.9×10^6 ft-lb/lb. A single axial strand of a 25 grain/ft detonating fuse with PETN explosive as the core was used for detonation.

The residual stresses were experimentally determined by the Sach's method⁽³⁾ in which concentric rings are bored from the tube. Each cut relieves residual stresses at the inner diameter. The resulting change in strain is measured by a hoop gauge placed on the outside of the tube. The residual stresses are determined by relating the strain readings to the initial stress state through the standard elasticity equations. Because the technique is applied to short, open ended tube sections cut from the complete tube, the appropriate end condition is the vanishing of the axial

stress (plane stress). The resulting residual hoop stress at the inner diameter, is

$$\sigma_{\theta\infty} \Big|_{r=a} = (e^2 - d^2) Y \epsilon_{\theta 1} / (d_1^2 - d^2) \quad (32)$$

where Y is Young's Modulus, and d_1 and $\epsilon_{\theta 1}$ are respectively the inner radius of the cylinder and the measured hoop strain after the first cut.

The residual hoop stresses at the inner diameter for the basic test series are shown as the circular points in Figure 7, plotted as a function of the percent deformation of the inner radius. The solid curve is the residual stress predicted from the analysis (with no reyielding), and the dashed curve is the residual stress that would be predicted if the end conditions were changed from plane strain to open ended* (plane stress). Although the analysis used the plane strain end condition for simplicity, in actual practice the end condition is closer to being open ended, since there is no restraint on the axial contraction of the cylinder. The expected residual stresses are, therefore, those given by the lower curve in Figure 7. The experimental values of residual stress, typically about 70,000 psi, are considerably less than the predicted values. This phenomena occurs in the hydraulic autofrettage process also and is generally attributed to reyielding produced by the Bauschinger effect (6). Experimental results

*In computing this curve, the material was assumed to be elastically compressible. Initial plastic flow was governed by the Tresca rather than the Von-Mises yield condition. The change in yield condition does not significantly effect the results. (4)

with a high strength 4330 steel show that the compressive yield strength is reduced by as much as 50 percent following plastic flow in tension (5). This also explains why the experimental value of residual stress at 1.2 percent deformation in Figure 7 is no higher than at 0.4 percent deformation.

A check on the scaling law was made by doubling the size of the piston and outer cylinder and using four times as much explosive. The residual hoop strains were essentially unchanged. The residual hoop stress was about 10 percent lower than was obtained with the original configuration. This could have been the result of a lower yield strength in the larger cylinder; its hardness was 37 Rockwell C, while the smaller cylinder had a hardness of 43 Rockwell C.

One test was run using a radial piston with no end fixture. The explosive used was a type of detonating fuse with PETN core that is unaffected by water. With no way of preventing the water from leaking out the ends, there was an increase in the rate of pressure decay. This apparently produced reyielding. The residual hoop stress was only 38 KSI, despite the cylinder's nearly one percent residual deformation. In another test with no radial piston and open ends the residual hoop stress was even lower—about 30 KSI. These results are shown in Figure 7.

The results of the experimental program show that the radial piston method of dynamic autofrettage produces residual hoop stresses which are of the same order of magnitude as those developed in the static processes. It also demonstrates that the analysis can be used to accurately predict residual deformations and to provide reasonable estimates of residual stress.

The cost of the radial piston is a significant part of the total expense of the process. Therefore, an experimental program was conducted in an attempt to find a ductile piston material which is relatively inexpensive. The materials considered were 1010, 1020, 1045, 4130, and 4340 seamless steel tubing and 6061-0, 6061-T6, and 5052-0 aluminum tubing. Although most of these materials have adequate static ductility, testing was required to determine their ductility while deforming radially at high strain rates.

The test conditions with each piston material were similar to the basic test involving a stainless-steel piston. The results of the tests indicated that none of the above materials is suitable. In all of the tests, one or more longitudinal cracks developed in the piston. The thick walled outer tube in these tests suffered no significant permanent deformation and thus could not have been autofrettaged.

EXPLOSIVE AUTOFRETTAGE - NO PISTON

In an attempt to minimize the cost of explosive autofrettage, a second process was investigated in which the piston was eliminated. In this process, Figure 9, a slow burning gunpowder is placed in a cardboard or paper cylinder which fits snugly into the thick-walled tube. The ends of the tube are sealed, as before, to prevent rapid pressure decay. Detonation, in this case, is achieved by electrically heating a copper wire passing through the center of the gunpowder. The resulting deformation is as uniform as that produced with a radial piston, as can be seen in Figure 10. The residual stress has been measured in only one tube. The resulting value of 77,000 psi at the inner diameter is comparable with the residual stresses obtained with the radial piston method.

When the gunpowder is replaced by SWP-6 explosive, the residual stress at the bore is reduced to 21,000 psi, indicating that extensive reyielding occurs. The method, therefore, appears suitable only with an extremely slow burning material.

The advantages of the method are:

1. Elimination of the relatively expensive stainless-steel piston.
2. Elimination of the storage problems associated with explosives (gunpowder is not classified as an explosive).
3. Elimination of a potential safety hazard, the electric blasting cap.
4. Reduction in set-up time, since no water is used.

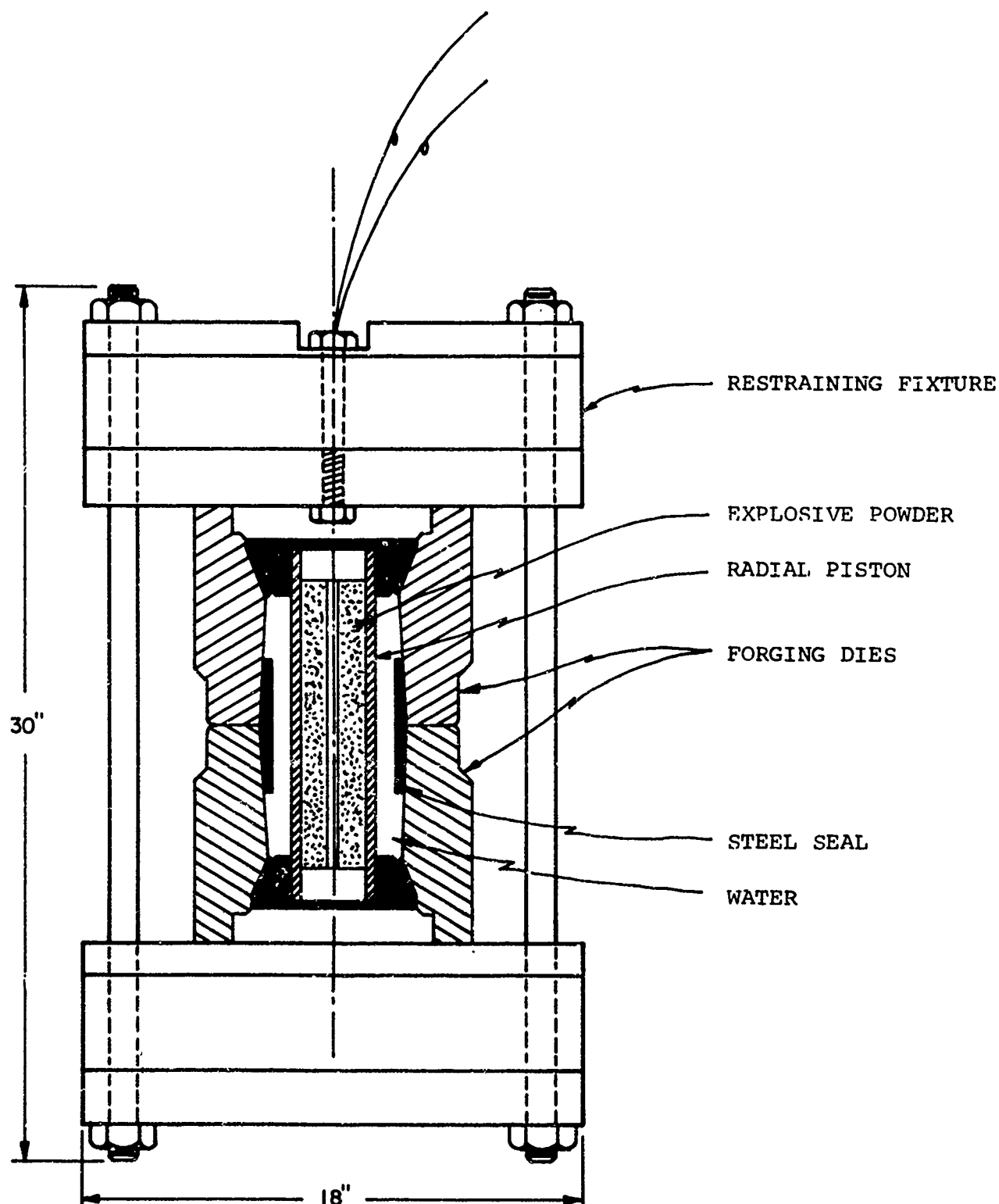


Figure 8. Autofrettage Configuration -
Production Forging Dies.

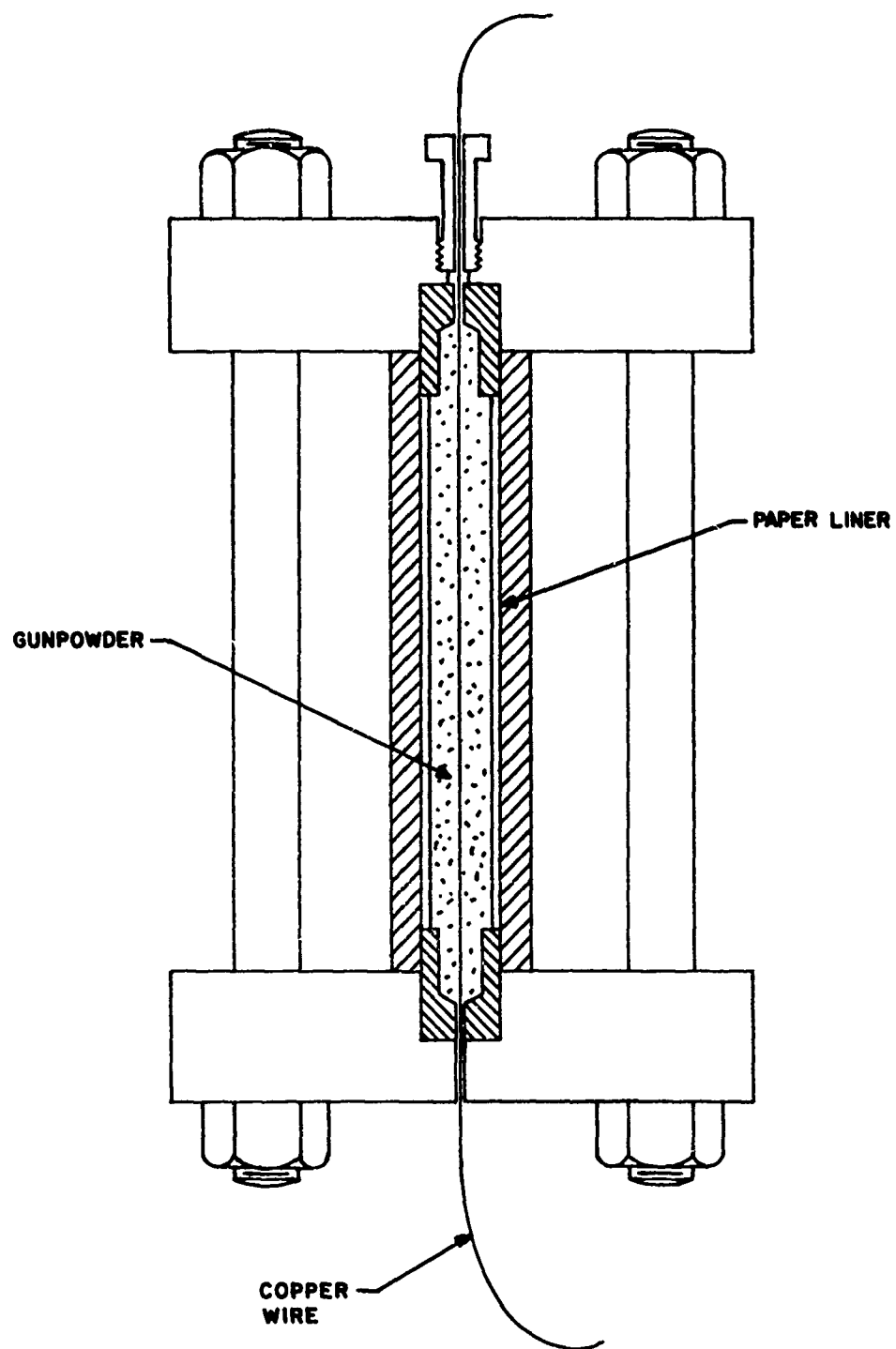


Figure 9. Autofrettage Configuration -
No Radial Piston.

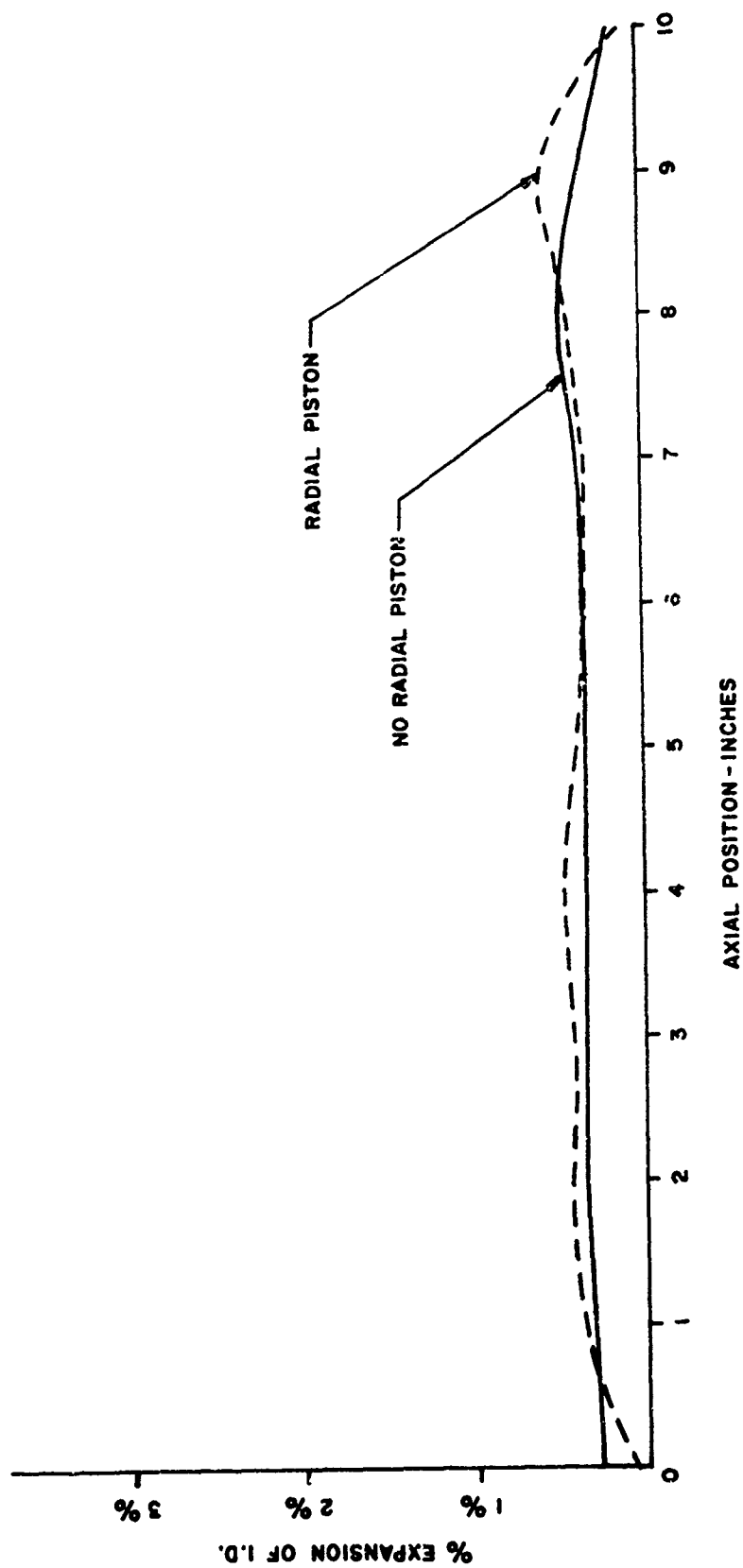


Figure 10. Radial Expansion at the Inner Diameter

The method requires further development before it can be applied with confidence. Also, an analytical model which predicts, at the minimum, residual deformation versus charge size needs to be developed.

THE AUTOFRETTAGE OF A PRODUCTION FORGING DIE

Two production forging dies, obtained from a manufacturing company, were autofrettagged explosively. The die material was H-13 steel hardened to 44-48 Rockwell C. The average diameter of the die cavity was 4.88" and its minimum wall thickness was 2.17". The autofrettage configuration, shown in Figure 8, enabled both dies to be autofrettagged simultaneously. This eliminated end effects and reduced the time for the process. A steel seal was used to prevent leakage at the center, where the two dies were in contact.

The residual deformation at the inner radius of the dies, following autofrettage, was 0.20 percent in one die and 0.07 percent in the other. The theoretical residual stresses were 90 KSI and 70 KSI, respectively. The actual residual stresses were probably somewhat lower, but an accurate determination could not be made because the magnitude of the Bauschinger effect for the die material is not known. The Sach's method cannot, of course, be used on production dies.

The two dies were returned to the manufacturer and were used in production. With no shrink ring, they failed by wear after producing an average of 3500 parts. This is about the same life and failure mode of non-autofrettagged dies when massive shrink rings are used.

CONCLUSIONS

It has been demonstrated that the radial piston method of explosive autofrettage produces large residual hoop stresses at the inner diameter of thick walled, high strength cylinders. The primary advantage of the method over the conventional mechanical and hydraulic autofrettage processes is that it requires little in the way of capital investment. Pumping equipment, external dies, and hydraulic presses are eliminated. End sealing is not as critical as in hydraulic autofrettage because high pressures are maintained for extremely short times. Furthermore, the method can be readily applied to cylindrical forging dies. The hole size in these dies is not generally uniform, so that the use of mechanical autofrettage would be difficult or impossible. As already noted, the unit cost of hydraulic autofrettage is probably excessive.

The alternate method of dynamic autofrettage, in which the piston is eliminated, would reduce the cost substantially. However, in applications, where the die wall is stepped or tapered, the piston method would probably be preferable, since it is easily adapted to this type of configuration.

The life of a forging die is generally maximized by using the hardest material that will fail by wear rather than cracking. Increasing the residual hoop stress reduces the possibility of fracture and permits the use of harder materials. For example, the H-13 production die described in the last section breaks after producing one part when it is used without a shrink ring. With a shrink ring, the die has a maximum compressive hoop stress of 7 KSI and fails by wear after 3 - 4,000 parts. The generation

of higher residual stresses does not significantly effect wear. The autofrettaged dies, therefore, produced only 10 percent more parts, on the average, than a typical die with a shrink ring. We believe, however, that major increases in die life are possible with autofrettage, since it allows the use of harder die materials than are feasible with shrink rings.

REFERENCES

1. J. MOTE, L. CHING, R. KNIGHT, R. FAY, and M. KAPLAN, "Explosive Autofrettage of Cannon Barrels", Army Materials and Research Center Report - AMMRC CR 70-25, February 1971.
2. 1967 ASME Steam Tables, ASME, New York, 1967.
3. G. SACHS and G. ESPEY, "A New Method for Determination of Stress Distribution in Thin-Walled Tubing", Metals Tech., 1384, (1941).
4. T. DAVIDSON, D. KENDALL, and A. REINER, "Residual Stresses in Thick-Walled Cylinders Resulting from Mechanically Induced Overstrain", Exp. Mech. 3, (1963), p. 253.
5. R. MILLIGAN, W. KOO, and T. DAVIDSON, "The Bauschinger Effect in a High Strength Steel", Journal of Basic Engineering, 88 (1966), p. 480.
6. T. DAVIDSON and D. KENDALL, "The Design of Pressure Vessels for Very High Pressure Operation", Watervliet Arsenal Technical Report WVT - 6917, May 1969.

XI. PRELIMINARY ANALYSIS OF THE
MARKET FOR CUSTOM METAL HEADS

E. Jaeckel

J. Byrden

M. Robbins

INTRODUCTION

Purpose

This report presents the findings of a market survey conducted during April - May 1972 for the Mechanical Sciences and Environmental Engineering Division of the Denver Research Institute, for presentation in the 1972 Annual Report of the Center for High Energy Forming.

The purpose of the project was to determine, to the extent possible, the market potential for custom metal heads in the United States, and to examine related marketing influences.

For this report, a metal head is considered an end closure for a cylindrical metal shell. Generally, a metal fabricator will form a cylindrical shell by rolling or hydraulic pressing. The joints are then welded together, and the metal heads are welded to each end of the shell to form a vessel.

Procedure

In particular, the major concern was developing a preliminary estimate of the size of the market for custom metal heads, the distribution of the product mix, and major influences operating in the marketplace. The study was restricted to metal heads having an outside diameter of over 60 inches and a rolled thickness of over 5/16 inches.

Data for the project were collected from both personal and telephone interviews and a mail questionnaire. Telephone interviews were conducted with research, engineering, and sales personnel in companies producing metal heads; and with the chief vessel design engineers in engineering design

firms responsible for metal head specifications and for selection of the vessel fabricator, (see Appendices A, B, and C). In addition, personal interviews were conducted in Colorado with persons knowledgeable in the metal head market (see Appendix C).

Additional information was obtained from data published by the U. S. Department of Commerce, trade associations, catalogues of producer product lines, and various articles and brochures related to the market (see Appendix D).

The telephone survey to producers provided data on the size of the total market in net tonnage. The mail survey to fabricators provided data on selected head characteristics. Information generated in the mail survey and supplemented from product catalogues was applied to the data in the telephone surveys to arrive at a total annual market size expressed in dollars.

Data on the future potential for metal heads was gathered from telephone interviews to engineering design firms who concentrate on the design and construction of plant facilities incorporating metal heads as components of metal structures.

Limitations

The work was performed on a best-efforts basis. The brief period of time for work performance imposed limitations upon the depth and breadth of the research. Consequently, a certain degree of professional judgement was involved in arriving at market figures.

SUMMARY

Based upon a preliminary analysis of the market for large, custom manufactured metal heads (over 60 inches in outside diameter and over 5/16 inches in rolled thickness), the major findings are:

- o Total annual sales volume by weight for all types of metal heads in the United States approximates 200,000 net tons.
- o The custom manufactured metal head market amounts to 70,000 - 80,000 tons annually or 35 percent to 40 percent of the total head market by weight. Approximately 60 percent of the custom manufactured head market by weight, or 42,000 to 48,000 tons are large size: over 60 inches in outside diameter and with a rolled thickness over 5/16 inches.
- o Average sales value for the forming and the metal of large, custom manufactured heads is \$0.34 per pound (\$0.14 per pound for forming and \$0.20 per pound for the metal).
- o Total annual sales dollar value for large, custom manufactured heads ranges between \$28.6 million to \$32.6 million, an average of \$30 million.
- o Average annual growth rate of the market is projected at approximately 6 percent per year, based upon historical and future trends for large, custom manufactured heads.
- o The market for large, custom manufactured heads geographically is concentrated in two regions: East North Central with 28 percent of shipments and West South Central with 26 percent of shipments.

- o The analysis of product mix reveals that the most frequently occurring characteristics of large, custom manufactured heads are as follows: 43 percent have an outside diameter from 60 to 90 inches; 26 percent have a rolled thickness of 5/16 - 7/16 inches; 47 percent are flanged and dished, ASME Code; and 33 percent utilize ASTM-A-515 or an equivalent metal.

SECTION I

OVERVIEW OF THE MARKET

This section will provide a general description of some of the characteristics affecting the market for custom metal heads. Included will be the following; an overview of participants in marketplace concentrating on head manufacturers, engineering design firms, metal fabricators, end user industries, demand criteria, and types of structures using heads.

Overview of Participants

The initiation of an order for a large, custom manufactured head starts with the end-user of a vessel such as a chemical or petroleum company wanting to build a new plant or to expand and/or modify an existing facility. The engineering department of the end-user company initially prepares a bid package identifying the basic needs. Typically, the bid package is issued to about five engineering design firms for competitive bidding, with one of the design firms selected for the job.

The engineering firm is responsible for preparing final drawings and specifications, and for coordinating the construction of the plant and equipment. Upon completion of the final equipment plans, the design firm releases bid packages to approximately 5 fabricators for the construction of vessels incorporating large, custom manufactured heads. The design firm then selects a fabricator based upon competitive bidding.

The fabricator is responsible for constructing the vessel or the structure. If a metal head is required, the fabricator either purchases the head from a custom specialty manufacturer, or the fabricator

produces the head himself at his plant or in the field at the construction site depending upon size and specifications. If a purchase is necessary, the fabricator generally obtains a minimum of three bids from head producers.

Segmentation of Head Industry

Based upon telephone interviews to producers of metal heads (see Appendix C), the total market for heads expressed in annual production figures ranges from 175,000 to 225,000 tons for an average of 200,000 tons. The industry can be divided into four segments.

1. Standard Mass Producers. This segment represents about 50 percent of the total head market, or 100,000 tons per year. These heads are produced by 85 to 100 nonintegrated firms (do not produce plate) who purchase flat plate from steel mills, and who manufacture heads and/or tanks both for pressure and nonpressure applications. Primary production technique is cold formation using bumping and hydraulic equipment. In general, these manufacturers concentrate on heads under 48 inches outside diameter for use in propane vessels.
2. Custom, Specialty Producers. This segment accounts for about 70,000 to 80,000 tons per year, or 35 to 40 percent of the total head market. The producers consist of about ten to fifteen firms, of which three are dominant: Lukens Steel Company, Coatesville, Pennsylvania; Bethlehem Steel Company, Bethlehem, Pennsylvania; and Phoenix Steel Company, Claymont, Delaware. These three firms are vertically integrated since they produce

their own steel plate. The normal production process is spinning, both hot and cold. Typical applications for custom metal heads are pressure and process vessels, containment vessels, cryogenic vessels, and other specialty vessels.

3. Fabricators with Excess Capacity. These are large vessel and tank fabricators who produce about 15,000 tons annually, for a 7.5 percent market share of the head market. There are about ten to twenty producers who are essentially vessel and tank fabricators with the ability to produce their own heads on large hydraulic presses. Their principal activity is the fabrication of railroad tank cars and steam boilers, and subcontract work for other fabricators who require heads.
4. Other Integrated Steel Producers. This segment generates about 5,000 tons annually or 2.5 percent of the head market, and is composed of three integrated steel companies: Armco Steel Company, Inland Steel Company, and Kaiser Steel Company. These firms manufacture heads as a convenience to their customers in order to provide a full product line of steel products.

Custom Specialty Producers

Of the ten to fifteen custom manufacturers, the following companies account for the majority of the 70,000 to 80,000 tons per year annual volume:

Lukens Steel Company, Coatesville, Pennsylvania
Bethlehem Steel Company, Bethlehem, Pennsylvania
Phoenix Steel Company, Claymont, Delaware
Brighton Corporation, Cincinnati, Ohio
Paul Mueller Company, Springfield, Missouri

Universal Lockport Corporation, Joliet, Illinois
Hackney Iron and Steel, Dallas, Texas
Trinity Steel Company, Dallas, Texas
Gorbett Brothers Steel Company, Ft. Worth, Texas

Three of the above companies account for the major proportion of custom metal head production: Lukens, Bethlehem, and Phoenix.

All of these companies provide heads for the construction of custom vessels and tanks to metal fabricators performing job shop operations, and secondarily, for custom vessels and tanks that are fabricated and field-erected. Field-erected vessels generally use heads made from sectional components rather than one-piece heads.

The demand for specialty heads is based on the needs of end-user companies, and mass production techniques cannot be employed due to the requirements for a large variety of outside diameters, rolled thicknesses, shapes, and types of metal.

Some of the head producers are located on or nearby a source of navigable water to capitalize on this low-cost method of transportation.

Specialization by type of metal appears to occur in the market, that is, Lukens specializes in clad steels; Bethlehem and Phoenix's strength is in carbon steels; Mueller specializes in stainless steel; and Brighton concentrates on alloys.

Engineering Design Firms

There are about 400 engineering design firms nationally, of which approximately 200 can be classified as designers and builders of process plants requiring vessels equipped with metal heads.¹ Two of the largest

¹"The ENR 400", Engineering News Record (April, 1971), pp. 48-58.

firms are the Bechtel Corporation, San Francisco, California; and Brown and Root, Inc., Houston, Texas.

The majority of projects conducted by the design firms tend to be located in the Great Lakes region and the Texas/Oklahoma area.

Fabricators of Metal Vessels and Tanks

Nationally there are over 350 firms fabricating vessels and tanks; however, only 159 firms are listed as having assets over \$1 million.²

The Steel Plate Fabrication Trade Association lists 31 major firms involved in fabricating pressure vessels.³

Demand Criteria

Fabricators are the principal purchasers of metal heads; however, some end-user companies having construction capabilities may purchase heads directly from the manufacturer and then fabricate the heads to vessels.

Heads are generally purchased on competitive bidding with a fabricator requesting bids from a minimum of three head producers.

The major criteria used by a fabricator in the selection of a supplier of heads are as follows in order of decreasing importance:

- o Delivery time
- o Price
- o Quality
- o Past experience (judgment)

²"Vessels, Pressure", Thomas Register of American Manufacturers, Vol. VI, (New York: Thomas Publishing Company, 1972), pp. 9089-9094.

³Directory of Metal Plate Fabricators. Hinsdale, Illinois: Steel Plate Fab. Asso., 1971.

End-User Industries

Prime users of vessels and tanks incorporating metal heads include the following:

- Chemical process
- Food processing
- Marine
- Petrochemical
- Petroleum refining
- Power utilities

Types of Fabricated Structures

Major types of fabricated structures utilizing custom metal heads are as follows:

- Cryogenic vessels (large capacity, over 3,000 gallons)
- Heavy wall pressure vessels (ASME, Sec. 8, Div. 2)
- Nuclear reactor containment vessels
- Pressure vessels
- Process vessels
- Storage vessels

SECTION II

SIZE OF MARKET

The size of the market for large, custom manufactured metal heads (over 60 inches in outside diameter and over 5/16 inches rolled thickness) was derived from an analysis of telephone interviews to head producers, mail surveys to fabricators, and data from product catalogues of head producers. There is no published information on the size of the market.

Custom Manufactured Heads

The average annual volume of all custom manufactured heads is between 70,000 to 80,000 tons. About 60 percent of the volume by weight are heads with an outside diameter over 60 inches and with a rolled thickness over 5/16 inches or 42,000 to 48,000 tons.⁴

A mail survey was sent to fabricators (see Appendix A) to obtain a percentage breakdown on four key characteristics of heads: outside diameter dimensions; rolled thickness dimensions; types of metal used; and types of shapes. The survey was sent to 69 large fabricators accounting for a large proportion of national head purchases, and a 40 percent response level was achieved.

For each shape of head in the survey, a weighted average technique was employed to derive an average outside diameter and rolled thickness dimension. Using the average outside diameter and rolled thickness, the average weight and average forming price for each shape was calculated by

⁴Derived from telephone interviews to head producers, Appendix C.

using the product catalogues of major producers.⁵ Average forming price per pound was then calculated for each shape of head.

Since a percentage distribution of sales by shape of head was also obtained from the mail survey, the percent of volume represented by each shape was applied to the average forming price per pound for that shape to arrive at a weighted average forming price per pound for all large, custom manufactured heads, which amounted to \$0.11 per pound.

The forming cost per pound was then adjusted to account for differences in forming cost due to type of metal. The forming prices for different metals ranged from a list base to a list base plus 100 percent depending upon the complexity of the metallurgy. This adjustment yielded an average forming price per pound of \$0.14.

To determine the average metal price per pound, a weighted average technique was employed using the percentage by metal type derived from the survey, and the average price per pound for each metal type derived from catalogues and secondary data. This analysis yielded an average metal price per pound of \$0.20.

The forming and metal price per pound were added together to yield an average cost for large heads of \$0.34 per pound. This figure was then applied to the total range of annual poundage to arrive at a dollar market sales value, F. O. B., of \$28.6 million to \$32.6 million, for an average of \$30 million market.

⁵See bibliography for list of product catalogues.

	<u>Low</u>	<u>High</u>
All heads, weight in tons	70,000	80,000
Large Heads, weight in tons	42,000	48,000
Average forming cost per pound	\$ 0.14	\$ 0.14
Average metal cost per cost per pound	<u>0.20</u>	<u>0.20</u>
Total average cost per pound	\$ 0.36	\$ 0.36
Forming cost, millions of dollars	\$11.76	\$13.44
Metal cost, millions of dollars	<u>16.80</u>	<u>19.20</u>
Total cost, millions of dollars	\$28.56	\$32.64

The forming cost per pound does not include the following types of special charges which tend to vary by each job: cost of annealing, descaling, pickling, machining, flame cutting, cost of internals or externals, cost of cladding.

Vessels and Metal Tanks, Custom Fabricated at Factory

The major potential market for custom metal heads exists within the fabricated steel plate products industry designated Standard Industrial Code #3443. Within this industry, there is one major segment that accounts for the majority of head purchases:

S. I. C. 34438: Vessels and Metal Tanks, Custom Fabricated at the Factory

The total value in constant dollar shipments from this industry to end-user industries is shown in Table I as one of the market parameters for custom metal heads. Due to the variability in length and outside diameter of each vessel, it is not possible to derive an accurate dollar value for the head portion of the total vessel value. The data also includes metal tanks which have been excluded in this research project.

The information indicates that the market showed positive increases from 1963 to 1967, a downturn in 1968, and stabilization of shipments from 1969 to 1970.

TABLE I
VALUE OF SHIPMENTS OF VESSELS AND
METAL TANKS, CUSTOM FABRICATED AT FACTORY^{6,7}
IN CONSTANT DOLLARS (1957-1959=100)

<u>Year</u>	<u>63</u>	<u>64</u>	<u>65</u>	<u>66</u>	<u>67</u>	<u>68</u>	<u>69</u>	<u>70</u>
Value of shipments (millions of dollars)	195.7	228.4	314.1	394.6	435.5	397.7	387.3	380.6
Percent annual change		16.7	31.5	25.6	10.4	(8.7)	(2.7)	(1.8)

⁶1963, 1967 Census of Manufacturers, U. S. Department of Commerce, Washington, D. C.;
1968-1970 data from telephone interview to U. S. Department of Commerce, Washington, D. C.

⁷Value of shipments have been adjusted by Industrial Commodities Wholesale Price Index,
Department of Labor, Bureau of Labor Statistics.

SECTION III

DISTRIBUTION OF PRODUCT MIX

The mail questionnaire to fabricators of metal vessels incorporating metal heads provided percentage of distribution on the following characteristics: outside diameter, rolled thickness, shape, and metal type.

Data on prices of metal was obtained from catalogues and secondary sources.

The distributions apply only to large metal heads with outside diameters over 60 inches and rolled thicknesses over 5/16 inches used in pressure and process vessels, cryogenic vessels (over 3,000 gallon capacity), nuclear containment vessels, and storage process vessels.

Outside Diameter

The largest category of heads occurred in the 60" - 90" range with almost 43 percent of the total volume. As the outside diameter dimension increased, the number of heads in each category decreased. Almost 80 percent of total units fall between 60" to 120" outside diameter.

<u>Outside Diameter</u> <u>Inches</u>	<u>Percent of Total Volume</u>
60 - 90	42.9
90 - 120	36.5
120 - 180	18.2
180 - 240	..
over 240	5.4
	<u>100.0</u>

Rolled Thickness

About 26 percent of the total units manufactured are between 5/16 to 7/16 inches in thickness with almost 50 percent of all heads between 5/16

and 5/8 inches. Slightly over one fifth of all units are over 1 inch in rolled thickness.

<u>Rolled Thickness</u> <u>Inches</u>	<u>Percent of Total Unit Volume</u>
5/16 - 7/16	25.8
7/16 - 5/8	23.0
5/8 - 7/8	17.6
7/8 - 1	12.4
over 1	<u>21.2</u>
	100.0

Shape

Three major shapes are purchased by fabricators: flanged and dished, ASME Code; elliptical (2:1 ratio); and hemispherical. Flanged and dished, ASME represents almost 50 percent of all units while elliptical represented slightly over one third of all units.

<u>Shape</u>	<u>Percent of Total Unit Volume</u>
Flanged & dished, ASME	47.4
Elliptical (2:1 ratio)	34.1
Hemispherical	9.7
Flanged & dished, standard	4.5
All others	<u>4.3</u>
	100.0

Type Metal

Almost one third of the metal used in large heads was represented by ASTM-A-515 or its equivalent, and total carbon steels represented 71.1 percent. Stainless steel accounted for 14.3 percent of all heads produced.

<u>Type Metal</u>	<u>Percent of Total Unit Volume</u>
ASTM-A-515	32.7
ASTM-A-285	27.6
Stainless steel	14.3
Other carbon	10.8
Clad	4.0
Aluminum	0.9
Nickel	0.9
Monel	0.9
Other (alloys)	0.9
	<u>100.0</u>

Metal Plate Prices

From secondary sources and catalogues of producers, metal plate prices per pound were derived. The following shows the average plate prices that were obtained.

<u>Metal</u>	<u>Dollars/Pound</u>
ASTM-A-515	0.13
ASTM-A-285	0.12
Stainless steel	0.50
Other carbon	0.14
Clad steel	0.20
Aluminum	0.26
All others (alloys)	0.25

Metal Forming Price Groups

Since forming prices vary by type of metal used, it was necessary to determine the percentage of total volume represented by metals formed at the base list price, and metals formed at the base price plus premium of 50 and 100 percent over base. Almost three-quarters of all heads were priced at the minimum base; however, almost one-quarter were priced at the base plus a premium of 100 percent.

<u>Price Category</u>	<u>Percent of Total Unit Volume</u>	<u>Type of Metal</u>
Base of list	71.1	515, 285, other carbon
Base and 50 percent	4.9	Clad, nickel
Base and 100 percent	<u>24.0</u>	Stainless, aluminum,
	100.0	monel, all others (alloys)

SECTION IV

GEOGRAPHIC CONCENTRATION OF MARKET

The location of head producers and principal vessel fabricators, and the value of shipments of vessels and tanks tends to be concentrated in defined geographic areas.

Producers

Three distinct regional areas account for the location of the majority of producers: Philadelphia, Dallas, and the Great Lakes area. Three companies are located within a radius of 60 miles of Philadelphia: Lukens, Bethlehem, and Phoenix Steel. In the Dallas - Ft. Worth area, there are three producers: Hackney, Trinity, and Gorbett. In the Great Lakes area, there are three producers: Brighton in Cincinnati; Universal in Joliet; and Mueller in Missouri.

Fabricators

Fabricators that are members of the Steel Plate Fabricators Trade Association are concentrated in four areas: Pennsylvania/Maryland; Great Lakes perimeter; Dallas/Houston area; and Los Angeles/San Francisco area (see Figure 1).

Value of Shipments

Shipments of vessels and metal tanks, custom fabricated at factory are concentrated in the Great Lakes and Texas/Oklahoma region. These two regions accounted for 54 percent of total shipments (see Table II).

The largest volume area was East North Central accounting for 29 percent of volume. This area consists of the five major industrial states of Ohio, Indiana, Illinois, Michigan, and Wisconsin.

The West South Central is the second largest volume area accounting for 26 percent of volume. This region is comprised of Texas and Oklahoma, active in chemical process, petrochemical, and oil.

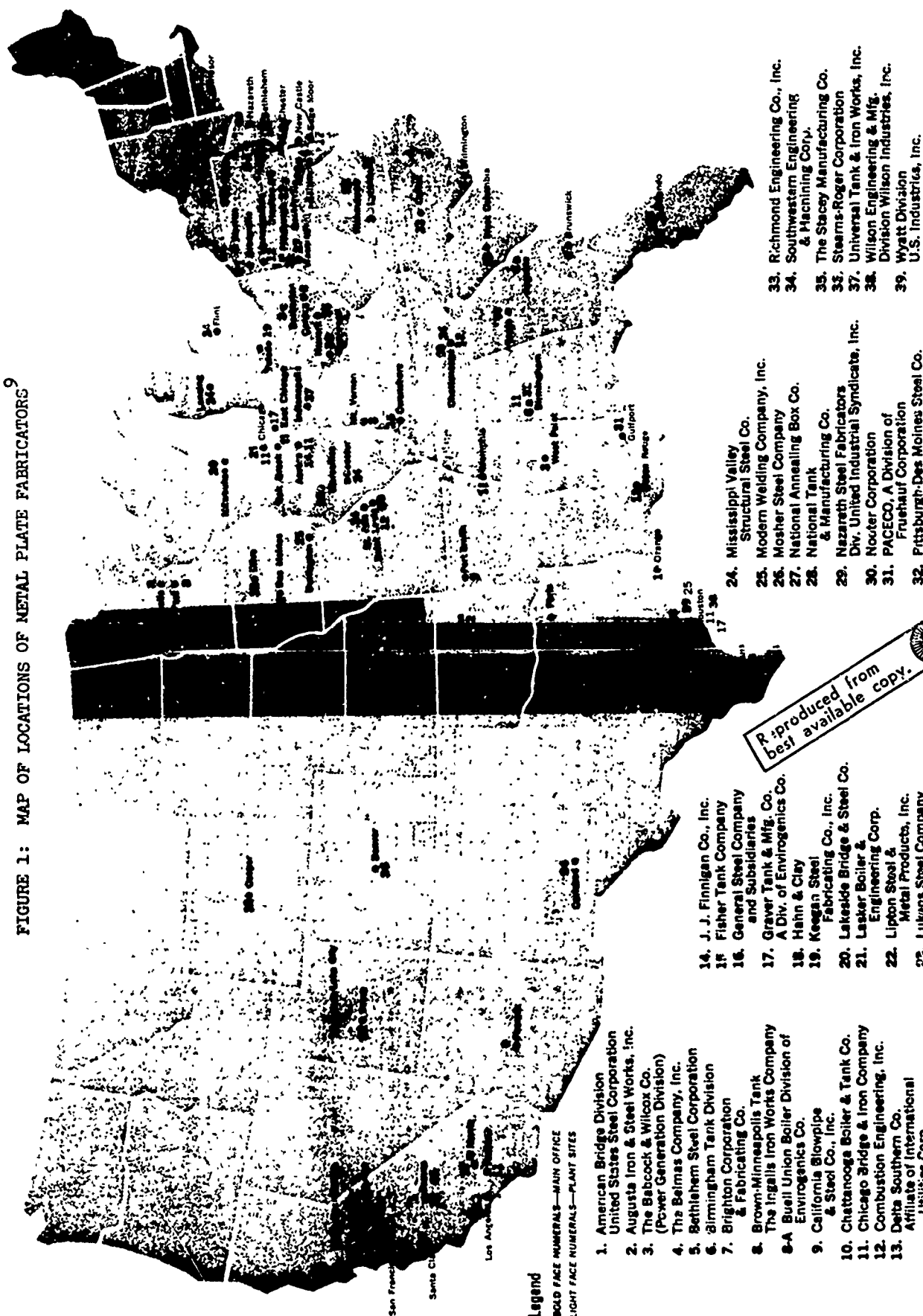
TABLE II

VALUE OF SHIPMENTS OF GEOGRAPHIC AREA⁸
 METAL TANKS AND VESSELS, CUSTOM FABRICATED AT FACTORY

<u>Area</u>	<u>Value of Shipments (Millions of Dollars)</u>	<u>Percent of Total Shipments</u>
New England	7.7	1.5
Middle Atlantic	<u>66.5</u>	<u>14.3</u>
Northeast	74.2	15.8
East N. Central	134.4	28.8
West N. Central	<u>14.3</u>	<u>3.0</u>
North Central	148.7	31.8
South Atlantic	23.9	5.1
East S. Central	51.9	11.6
West S. Central	<u>121.2</u>	<u>26.0</u>
South Region	197.0	42.7
Mountain	10.1	2.2
Pacific	<u>34.7</u>	<u>7.5</u>
West Region	<u>44.8</u>	<u>9.7</u>
Total U. S.	464.7	100.0

⁸
1967 Census of Manufacturers, U. S. Department of Commerce, Washington, D. C.

FIGURE 1: MAP OF LOCATIONS OF METAL PLATE FABRICATORS⁹



SECTION V

KEY MARKET CONSIDERATIONS

Through personal and telephone interviews, several key market considerations were identified that affect the production and distribution of custom metal heads. These considerations tend to act as limitations on existing producers or to act as inhibitors of growth; however, some of the factors have a positive influence on the future market. A brief analysis will be made of the following factors: transportation, steel plate size, custom production, seasonality, capital investment, derived demand, competition, imported steel plate, and environmental demands.

Transportation

Due to a combination of high freight rates for heavy steel products and maximum shipping clearances, the market for metal heads tends to be concentrated with plate producers, head producers, vessel fabricators, and end-user industries grouped together in defined geographic areas, often in close proximity to water transportation.

Close access to a form of water transportation tends to offset the constraints imposed by the truck and rail carriers. Use of rail or truck carriers requires careful analysis of width, length, height, and weight limitations of the carrier route as compared to the same characteristics of the metal head or vessel that is to be transported.

In general, the following considerations apply to rail transportation: the type of railcar will be a flatbed; the load will be tilted for larger heads; and special routing might be required. The minimum economical shipping

weight is 80,000 pounds since the rates below this level tend to be disproportionately high.

Every carrier has their own clearance charts so each job has to be analyzed individually; however, the following clearances are a good indication of the average situation.

<u>Inside Width (in.)</u>	<u>Inside Length (in.)</u>	<u>Height (top of rail to top of load - inches)</u>	<u>Minimum Economical Weight (pounds)</u>
156 - 166	648 - 1068	240	80,000

For truck transportation, a flatbed unit is used. For the larger diameter heads, special clearance is required, and minimum economical weight is 40,000 pounds per truck.

<u>Width (in.)</u>	<u>Length (in.)</u>	<u>Height (in.)</u>	<u>Minimum Economical Weight (pounds)</u>
96	480	96 - 120	40,000

The head producer has two alternatives to pursue if the outside diameter of the head cannot meet the above clearances: (1) use of water transportation to convey the unit to the vessel fabricator; or (2) manufacturing the head in segments for field erection.

Steel Plate Size

The production of a one-piece head is also limited by the width of rolled plate used for construction. The maximum width possibility appears to be in the 200 inch range, although one producer appears to have the capability of going to 240 to 276 inches. The need for an integrated steel operation or close access to water transportation becomes apparent here since railroads can only accomodate a 166-inch wide plate.

Ideally, the construction of a one-piece head is preferred, since segmental construction tends to increase the labor cost due to additional welding, handling, and inspection. A nonintegrated head producer should be located close to a source of plate to reduce the possibility of requiring segmental construction.

Custom Production

Our analysis shows that the fabrication of vessels is characterized by job shop operations, rather than by mass production techniques. The needs for a specific head size tend to vary for each construction job since there are different requirements for outside diameter, thicknesses, shapes, and types of metal.

With the existing production techniques of pressing, spinning, and forging a large variety of costly metal dies are required to accommodate the many variations of head specifications.

Seasonality

The market for metal heads exhibits some degree of seasonality in the Northeast and North Central Regions due to the fact that construction activity tends to be limited to a seven-month period. Construction start-up occurs generally in April, building to a peak in July and August, and then tapering off in October.

Seasonality is not a significant factor in the Texas/Oklahoma area or the West Coast due to favorable weather conditions.

In the Northeast and North Central areas, the timing of the production of heads is directly related to the season of the year.

Capital Investment

Using the conventional manufacturing processes of pressing, spinning, and forging, it is estimated that an extremely large capital investment would be required for a new production facility. The investment would range from \$8 million to \$10 million.

Derived Demand

The demand for metal heads is a function of the demand for vessels incorporating heads. The demand for vessels is a function of the construction of new plants and equipment or a function of replacement of existing equipment. Historically the rate of construction activity in end-user industries has been a function of the economic climate in the United States.

For example, during 1969 to 1970 the economy was depressed contributing to the rather poor market for pressure vessels and metal heads.

Environmental

Recent ecological concerns have forced a reduced level of plant and equipment construction in two key end-user markets for vessels and heads: the petroleum and chemical industries. The reduced level of activity has been caused by two forces: large capital expenditures and lack of environmental and pollution control direction.

The petroleum industry will be required to build new facilities to manufacture more high-octane components to permit the reduction of lead additives in gasolines.

All industries that generate some form of pollution will be required to significantly reduce the quantities emitted to the atmosphere, the ground,

or into water. However, there has been a lack of specific guidelines on the maximum levels of permissible pollution from governmental agencies. This lack of direction has contributed to a "wait and see" attitude in the construction of plant facilities.

Competition

There is a high degree of competition among the limited number of head producers. Heads are purchased by fabricators on a bid system contributing to price cutting and the erosion of manufacturer profits.

Imported Steelplate

During the last decade, several domestic nonintegrated head producers have been purchasing steelplate from Japan and the European Common Market. These head producers have purchased foreign steel due to the favorable price differential as compared to the prices offered by domestic steelplate suppliers. Foreign steelplate used in the manufacture of U. S. heads may account for 10 to 25 percent of all plate used by American head producers.

SECTION VI

FUTURE IMPLICATIONS

Future implications for the custom metal heads market were obtained from knowledgeable engineering design personnel and from an analysis of secondary data including a review of construction activity for new plant and equipment. Certain trends become evident for fabricators and producers, for the head product mix, for end-user industries, and for growth potential.

Fabricators and Head Producers

- o Existing, efficient metal fabricators will increase in volume with existing plant and equipment; and the smaller, less efficient firms will have a reduced impact on the market.
- o Due to the high capital investment requirements for head production, no new competitive manufacturers will enter the market.
- o Existing producers will probably not expand existing plant and equipment because of the high cost of capital investment.
- o Imported steelplate will continue to account for about 20 percent of the total plate in head manufacturing usage, as long as the favorable price differentials remain and import quotas do not change.

Head Product Mix

- o There will be increases in the outside diameter and the rolled thicknesses of heads due to: (1) a need for controlling higher pressure and temperature requirements within vessels; and (2) the requirements for additional capacity and yield from existing systems.

- o There will be increases in usage of hemispherical heads since this type of head provides the most uniform distribution of internal pressures.
- o The complexity of custom heads will increase to accommodate new products developed by advancing technology.
- o The usage of more exotic metals will be increased to accommodate new technological processes.

End-User Industries

- o There will be a steady demand for vessels from the four principal end-user industries which are chemical processing, petrochemicals, petroleum refining, and electric utilities.
- o New complex undersea vessels with sophisticated metal heads will be required for the exploration of oil, gas, and for general research.
- o Demand will increase among utilities for power generating equipment with emphasis being placed on needs for vessels for nuclear plants.
- o There is a potential need for vessels in the coal gasification industry, for conversion of coal to gas and gasolines.
- o The petroleum industry will have a need for new vessels to manufacture more high octane gasoline to permit reduction of lead additives.
- o Pollution control demands by governmental agencies will require a significant investment in new equipment including pressure vessels. Planned spending by American industry in 1972 is \$4.9 billion up 51 percent from \$3.2 billion in 1971.¹⁰

¹⁰"Spending races to catch up to the need", Business Week, May 13, 1972, p. 77.

- o The demand from a growing economy will require periodic replacement of plant and equipment, and an attendant need for new vessels and heads.
- o The following industries will be potential increased users of heads and vessels in the next decade due to technological breakthroughs--food processing, water de-salination, pharmaceuticals, hydro-metallurgy, and synthetics.
- o The increasing importance of steel distributors, such as J. T. Ryerson and Company, as a component in either the distribution or the selling of metal heads, Over 20 percent of steel produced today passes through distributors on the way to fabricators and manufacturers.¹¹

Growth Potential

- o Expenditures for new plant and equipment from 1960 to 1971 showed an average annual percentage increase of 8.1 percent for all manufacturing, a 6.8 percent increase for the petroleum industry, and a 9.9 percent increase for the chemical industry (see Table III).
- o Although expenditures for new plant and equipment have been depressed during the 1968 - 1971 period, a pick up in the rate of construction is projected from 1972 to 1977.
- o Demand for steel for new plant and equipment construction is projected at 6 - 9 percent per year.¹²

¹¹"The Metal Service Center", Steel Service Center Institute, Cleveland Ohio, 1972.

¹²U. S. Industrial Outlook 1971, U. S. Department of Commerce, Washington, D. C. and F. W. Dodge Construction Outlook 1972, McGraw-Hill Information Systems Company, New York, October 1971.

- o Vessel design engineers believe that the market for custom vessels will grow approximately 6.4 percent per year.¹³
- 9 Although there has been a decline in the growth rate for vessels and metal tanks measured in constant sales dollars, over the past four years, the average annual growth rate from 1963 to 1970 was 6.4 percent per year.¹⁴
- o Based upon a derived demand for metal heads from vessel construction, the market for large, custom manufactured heads appears to have a potential growth rate of 6 percent per year yielding an increase in the market sales value from \$30 million in 1972 to \$40.2 million in 1977.

¹³Weighted average from telephone interviews to vessel design engineers (see Appendix B).

¹⁴See Table I.

TABLE III

**EXPENDITURES FOR NEW PLANT & EQUIPMENT
MANUFACTURING INDUSTRIES¹⁵
(Billions of Dollars)**

	<u>Chemical Industry</u>		<u>Petroleum & Coal Industry</u>		<u>All Manufacturing</u>	
	<u>Billion \$</u>	<u>Percent change year to year</u>	<u>Billion \$</u>	<u>Percent change year to year</u>	<u>Billion \$</u>	<u>Percent change year to year</u>
1960	1.55	32	2.89	4.7	15.09	18.1
1961	1.58	1.9	3.00	3.8	14.33	(5.1)
1962	1.56	(1.3)	3.12	4.0	15.06	5.0
1963	1.73	10.8	3.15	0.9	16.22	7.7
1964	2.08	20.2	3.59	14.0	19.34	19.2
1965	2.73	31.3	4.03	12.2	23.44	21.2
1966	3.26	19.4	4.70	16.6	28.29	21.5
1967	3.06	(6.2)	5.08	8.0	28.51	1.0
1968	2.83	(7.6)	5.25	3.3	28.37	(0.5)
1969	3.10	9.5	5.63	7.2	31.68	11.6
1970	3.44	9.6	5.62	(0.2)	31.95	0.8
1971 (pre)	3.45	0.2	6.00	6.7	30.21	(3.3)
Average annual percent charge		9.9		6.8		8.1

¹⁵Chemical Economics Handbook. Menlo Park: Stanford Research Institute, 1971, p. 219.2430F

COLORADO SEMINARY
UNIVERSITY OF DENVER
DENVER RESEARCH INSTITUTE

UNIVERSITY PARK • DENVER, COLORADO 80210

Industrial Economics Division



APPENDIX A: QUESTIONNAIRE TO FABRICATORS

May 5, 1972

Dear Sir:

The University of Denver Research Institute is conducting a study on the market for flanged and dished metal heads in the United States. We are a private, independent, non-profit research institute affiliated with the University of Denver.

The purpose of this survey on metal heads is to provide future direction to our Mechanical Sciences Division which has been active in the explosive forming of large heads for the aerospace industry. If the future domestic commercial market for heads proves attractive, the technology of explosive forming might be feasible to transfer to the American Metal Fabricating Industry.

We have attached a very short questionnaire that we would like you to complete and return to us. There are only 3 questions for you to answer requiring about five minutes of your time.

Your individual responses will be treated as completely confidential information, and no company names will be released. All results will be presented as totals in our survey. If you would like to receive a summary of the report, please check box in the bottom left hand corner of this page.

We have enclosed a postage-paid envelope for your use to return the survey to us as soon as possible. Thank you for your assistance.

Sincerely yours,

Eric F. Jaeckel
Industrial Economics Division

Gordon Milliken
Industrial Economics Division

() Yes, I would like a summary of report.

QUESTIONNAIRE

Your name _____ Title _____

Company name _____

Address _____

State _____ Zip _____

DENVER RESEARCH INSTITUTE--UNIVERSITY OF DENVER

QUESTIONNAIRE

This questionnaire applies only to metal heads purchased for the following applications:

Pressure Vessels	Nuclear Containment
Process Vessels	Storage Process Vessels
Cryogenic Vessels (over 3000 gallon capacity)	

- (1) How many metal heads with an outside diameter of over 60 inches and with a rolled thickness over 5/16 inches do you purchase on the average each year?

_____ Annual total unit volume

Insert in each space below your estimate of purchased unit volume of metal heads for each category of outside diameter and rolled thickness.

Outside Diameter	<u>Rolled Thickness</u>				
	<u>5/16 - 7/16</u>	<u>7/16 - 5/8</u>	<u>5/8 - 7/8</u>	<u>7/8 - 1 inch</u>	<u>over 1 inch</u>
60"-90"	_____	_____	_____	_____	_____
90"-120"	_____	_____	_____	_____	_____
120"-180"	_____	_____	_____	_____	_____
180"-240"	_____	_____	_____	_____	_____
Over 240"	_____	_____	_____	_____	_____

- (2) For metal heads with an outside diameter of over 60 inches and with a rolled thickness over 5/16 inches, what percent of your annual purchases is represented by each of the following types of metals:

_____ ASTM-A-285 or Equiv.	_____ Stainless Steel
_____ ASTM-A-515 or Equiv.	_____ Aluminum
_____ Other Carbon Steel	_____ Monel
_____ Nickel	_____ Clad Steels
_____ Other, Specify _____	

- (3) For metal heads with an outside diameter of over 60 inches and with a rolled thickness over 5/16 inches, what percent of your annual purchases is represented by the following shapes:

_____ Flanges & Dished, ASME	_____ Flanged & Dished, standard
_____ Hemispherical	_____ Conical
_____ Elliptical (2:1 ratio)	_____ Dished Only
_____ Flanged Only	_____ Other, Specify _____

DENVER RESEARCH INSTITUTE--UNIVERSITY OF DENVER

APPENDIX B: QUESTIONNAIRE TO ENGINEERING DESIGN FIRMS
TELEPHONE INTERVIEW GUIDELINE
TO CHIEF VESSEL DESIGN ENGINEER
AT ENGINEERING DESIGN FIRMS

Good Morning.

I am Eric J. Eckel from the University of Denver Research Institute, and we are conducting a survey on the market for flanged and dished metal heads in the United States. The purpose of our survey is to provide future direction to our Metallurgy Division which has been active in the explosive forming of large heads for the aerospace industry.

The questionnaire consists of 13 short questions that should only take about 10 minutes of your time. If this is inconvenient, may I call you back at a more appropriate time?

The questionnaire applies to all types of metal heads such as hemispherical, elliptical, flanged, and dished that are primarily used in the construction of specialty, custom pressure and process vessels. These are the larger size metal heads with an outside diameter of over 60 inches and a rolled thickness of over 5/16 inches.

PART I

NAME _____ TITLE _____

COMPANY NAME _____

ADDRESS _____

CITY _____ STATE _____ ZIP _____

1. Who in your company selects a fabricator to assemble a vessel/tank incorporating a metal head?

2. What states in the United States account for the majority of your vessel/tank projects?

3. What are the major current end user industries that purchase vessel/tanks incorporating metal heads?

4. What are the major uses of fabricated structures that use metal heads?

PART II

The following questions pertain to your estimate of the future market for metal heads with an outside diameter of over 60 inches and a rolled thickness of over 5/16 inches.

5. How would you describe the market for heads?

_____ Growing _____ Stable _____ Declining

(Go to Q 6 if you checked growing; go to Q 7 if stable; go to Q 8 if declining)

6. What annual rate of growth do you project for the head market?

_____ 1% _____ 2.5% _____ 5.0% _____ 7.5% _____ 10% _____ other, specify

Why do you feel that the market will grow?

7. Why do you project a stable market for heads?

8. What annual rate of decline do you project for the heads?

 1% 2.5% 5.0% 7.5% 10% other, specify

Why do you feel that the market will decline?

9. Over the next 10 years, what industries will become the major end users of vessels/tanks incorporating metal heads?

10. Why do you feel that these industries will be the major users?

APPENDIX C: PERSON INTERVIEWED: TELEPHONE OR PERSONAL

Manufacturers of Heads and Other Steel Products

Richard Agricola, Director of New Product Development, E. F. Industries, Inc., Louisville, Colorado

Tom Backus, Assistant to the Sales Manager, Commercial Shearing and Stamping Company, Youngstown, Ohio

Mr. Berger, Sales Manager of Head Department, Paul Mueller & Company, Springfield, Missouri

Mr. C. T. Colbourn, Head Product Manager, Phoenix Steel Company, Claymont, Delaware

Mr. Dienna, Corporate Economist and Manager of Commercial Market Research, The Lukens Steel Company, Coatesville, Pennsylvania

Richard Erb, Sales Manager, Orange County Machine Works, Orange, California

Thomas Harrison, Sales Manager for Heads, Hackney Iron and Steel Company, Dallas, Texas

Jerry Heminger, Commercial Research Division, U. S. Steel Corporation Pittsburgh, Pennsylvania

George Hopkins, Assistant Manager of Market Research, The Bethlehem Steel Company, Bethlehem, Pennsylvania

Richard Markovitz, Chief Engineer, Brighton Corporation, Cincinnati, Ohio

Dr. J. Mote, Engineering and Research Department, E. F. Industries, Inc., Louisville, Colorado

Mr. Phillips, District Sales Manager, United States Steel Corporation, Denver, Colorado

Mr. Valmer, Sales Manager of Heads, The Universal Head Company, Joliet, Illinois

Mr. Wesley, District Sales Manager, Republic Steel Corporation, Denver, Colorado

Fabricators

Mr. Edward Browning, Superintendent, Longero Inc., Denver, Colorado

Mr. Cronin, Director of Purchasing, National Annealing Box Company, Washington, Pennsylvania

Mr. Terry Deringer, Purchasing Agent, Power Generation Group, Westinghouse Electric Corporation, Tampa, Florida

Mr. John Everett, Design Engineer, Tank Car Division, General American Transportation Car, Sharon, Pennsylvania

Mr. W. R. Fickett, Estimating Manager, General Sales, Chicago Bridge and Iron, Oak Brook, Illinois

Mr. Franco, Purchasing Agent, Graver Tank and Manufacturing Company, East Chicago, Indiana

Jim Frese, Materials Manager, Babcock and Wilcox Company, Barberton, Ohio

Mr. D. E. Ginn, District Sales Manager, Pittsburgh, Des Moines Steel Company, Denver, Colorado

Mr. Jackson, Vice President of Manufacturing and Engineering, Eaton Metal Products Company, Denver, Colorado

Ray Moore, Purchasing Agent, National Tank and Manufacturing Company, Los Angeles, California

Mr. Neithercut, President, American Steel and Iron Works, Inc., Denver, Colorado

Mr. Rossetti, Vice President of Sales, Eaton Metal Products Company, Denver, Colorado

Chuck Schupp, Purchasing Agent, Manufacturing Division, Stearns-Roger, Englewood, Colorado

James Stroud, Director of Purchasing, Modern Welding Company, Inc., Owensboro, Kentucky

Mr. Swanson, District Sales Manager, Chicago Bridge and Iron Company, Denver, Colorado

Mr. Carl Williams, Work Order Manager, The Joseph T. Ryerson & Sons Company, Denver, Colorado

Elwood Williams, Manager of Purchasing Department, Thompson Pipe and Steel Company, Denver, Colorado

Mr. Williams, Purchasing Agent, Mosher Steel Company, Houston, Texas

Engineering Design Firms

Mr. Ambrosio, Senior Vessel Engineer, The Lummus Company, New York, New York

Mr. Baczewski, Chief Vessel Design Engineer, Blaw-Knox Chemical Plants, Inc., Pittsburgh, Pennsylvania

Mr. Curtis, Chief Pressure Vessel Designer, Refinery and Chemical Division, The Bechtel Corporation, San Francisco, California

Mr. Desai, Vessel Design Engineer, Monsanto-Enviro-Chem Systems, Inc., Chicago, Illinois

Bernard Erickson, Marine Vessel Designer, American Bridge Division, United States Steel Corporation, Pittsburgh, Pennsylvania

Mr. Evans, Vessel Designer, Apparatus Design Section, The C. F. Braun Company, Alhambra, California

Mr. Roy Howard, Chief Mechanical Engineer, Brown and Root, Inc., Houston, Texas

Mr. Leecoff, Chief Vessel Design Engineer, Catalytic Construction Company, Philadelphia, Pennsylvania

Mr. Miller, Vessel Design Purchase, Arthur McKee & Company, Cleveland, Ohio

Roger Reedy, Manager of Special Structures, Chicago Bridge and Iron Company, Oak Brook, Illinois

Jean M. Reese, Chief Vessel Design Engineer, Stearns-Roger, Denver, Colorado

Mr. Allan Wallace, Chief Vessel Engineer Design, The Badger Company, Inc., Cambridge, Massachusetts

Trade Associations, Periodicals, and Miscellaneous

Robert Atkinson, Executive Secretary, Forging Industry Association, Cleveland, Ohio

Jean Beeman, Secretary, American Metal Stamping Association, Cleveland, Ohio

Mr. Paul Bernard, Industry Division of the Census Department, Washington, D. C.

Mr. Earl Bratton, Executive Director, Steel Plate Fabricators Association, Hinsdale, Illinois

Forrest D. Clark, Project Engineer, Esso Research and Engineering Company, Florham Park, New Jersey

Mr. Jack Creek, Research Department, Iron Age Magazine, Philadelphia, Pennsylvania

Mr. Doxsey, Executive Director, Steel Service Center Institute, Cleveland, Ohio

Mr. Bradley Hoyt, Boiler and Pressure Vessel Group, The Pressure Vessel Institute, New York, New York

Jim Hughes, Statistical Division, American Iron and Steel Institute, Washington, D. C.

Mr. T. A. Kocis, Editor, The Association of Iron and Steel Engineers, Pittsburgh, Pennsylvania

Mr. Clem Labine, Marketing Manager, Chemical Engineering Magazine, New York, New York

Norm Lawson, Department of Commerce, Denver, Colorado

Mr. Linsee, Researcher, The Battelle Institute, Columbus, Ohio

Mr. Ernie Loeb, Industry Division of the Census Department, Washington, D. C.

Mr. Robert Nash, Special Services Manager, The Daily Journal Magazine, Division of F. W. Dodge, Denver, Colorado

Mr. Olds, Editor of Steel Facts, American Iron and Steel Institute, New York, New York

Mr. Ted Reiter, Marketing Manager, Industry Week Magazine, Cleveland, Ohio

Kurt Rothchild, Industrial Research Department, Metal Working News, New York, New York

APPENDIX D: BIBLIOGRAPHY

Books

U. S. Department of Commerce. Statistical Abstracts of the United States 1970. Washington, D. C.: Government Printing Office, 1970.

Spring, Harry M. Jr. Pressure Vessels for Industry. New York and London: McGraw Hill, Inc. 1947.

Pamphlets

American Iron and Steel Institute. Shipments of Steel Products by Market Classification, All Grades Including Carbon Alloys and Stainless. Washington, D. C.: 1971.

American Metal Stamping Association. Stamping Buyers Guide. Cleveland, 1972.

Bethlehem Steel. Bethlehem Flanged and Dished Spun Heads. Bethlehem, 1966.

Brighton Corporation. Tru-edge Tank Heads. Cincinnati, 1969.

Chicago Bridge and Iron Company. Heavy Wall Vessels. Oak Brook, 1972.

Commercial Shearing & Stamping Company. Pressed Metal Handbook. Youngstown, 1967.

Dun & Bradstreet, Inc. Construction Industry. New York, 1972.

E. F. Industries, Inc., "Market Investigation - Tanks and Pressure Vessels", unpublished proprietary memorandum, June 11, 1971.

Forging Industry Association. 1971-72 Forging Capability Chart. Cleveland, 1972.

Iron Age. National Analysis of Metal-working. Philadelphia: Chelton Publications, 1967-70.

Lukens Steel Company. Product Information. Coatesville, 1972.

McGraw-Hill Information Systems Company. F. W. Dodge Construction Outlook 1972. New York: McGraw-Hill, 1972.

McGraw-Hill Information Systems Company. Dodge Construction Statistics Bulletin. January - December, 1972.

Paul Mueller Company. Mueller Heads. Springfield, 1972.

Orange County Machine Works. Tank Heads. Orange, 1972.

Joseph W. Peckis, "Pressure Vessel Heads Market Survey", unpublished report from Denver Research Institute, January 15, 1970.

Phoenix Steel Corporation. Products, Flanged and Dished Heads. Claymont, (1971).

Phoenix Steel Corporation. 1971 Annual Report. Claymont, 1972.

Pittsburgh - Des Moines Steel Company. Engineering Fabrication and Construction Service. Pittsburgh, 1967.

Ryerson, Joseph T. & Sons. Ryerson Products in Stock Processing Services. Denver, 1972.

Standard and Poors New York Stock Exchange Reports. Bethlehem Steel. Vol. 39, No. 37, February 23, 1972.

Standard and Poors New York Stock Exchange Reports. Lukens Steel. Vol. 39, No. 22, February 1, 1972.

Standard and Poors American Stock Exchange Reports. Phoenix Steel. Vol. 7, No. 14, February 17, 1972.

Securities and Exchange Commission. Annual Report Pursuant to Section 13 or 15(d) of the Securities Exchange Act of 1934 - Lukens Steel Company. Washington, D. C., 1972.

Steel Plate Fabricators Association. Directory of Metal Plate Fabricators 1971-72. Hinsdale, 1972.

Steel Service Center Institute. The Metal Service Center, Cleveland, 1971.

Stearns-Roger Corporation. Purchasing Department Guide. Denver, 1971.

U. S. Department of Commerce. U. S. Industrial Outlook 1971. Washington, D. C.: Government Printing Office.

U. S. Department of Commerce. 1963, 1967 Census of Manufacturers. Washington, D. C.: Government Printing Office.

Periodicals

"The ENR 400", Engineering News Record, April 8, 1971, pp. 48-58.

F. D. Clark and S. P. Terni, Jr., "Thick-Wall Pressure Vessels", Chemical Engineering, April 3, 1972, pp. 112-116.

Kenneth M. Guthrie, "Estimating the Cost of High-Pressure Equipment", Chemical Engineering, December 2, 1968, pp. 144-148.

Richard E. Markovitz, "Choosing the Most Economical Vessel Head", Chemical Engineering, July 12, 1972, pp. 102-106.

"Slow growth shaping leaner, more efficient steel industry", Industry Week, February 21, 1972, pp. 53-54.

"Steel ekes out slight profits gain in 1971", Industry Week, February 7, 1972, pp. 61-63.

"Spending races to catch up to the need", Business Week, May 13, 1972, p. 77.

The Daily Journal, Denver, Colorado, Tuesday, March 28, 1972.

XII. EXPLOSIVE THERMOMECHANICAL PROCESSING

R. N. Orava

INTRODUCTION

One of the important factors associated with the practical application of high energy forming is the influence that it has on subsequent material behavior. Since some form of deformation processing would ordinarily be entailed in the fabrication of a component even if it were not produced by high energy techniques, the problem reduces to one of evaluating the influence of high energy forming relative to conventional forming on residual properties. Thereafter, one must decide whether detrimental effects, if any, would be acceptable in service, and if not, whether the design would accommodate such impairment in those circumstances where high energy processing has a distinct advantage over other fabrication methods.

A survey of terminal behavior from the viewpoint of relative material behavior following high energy or conventional forming was published in 1970¹. Although subsequent studies in this area have been limited, results have been reported on the effect of explosive forming on the tensile and fatigue properties of 2014 aluminum alloy², the stress corrosion cracking of 2014 aluminum in 3.5% NaCl³, the methanol cracking of unalloyed titanium (50A) and Ti-6Al-4V alpha-beta titanium alloy⁴, the tensile and fracture properties of HSLA steels^{5,6} and the deformation substructure and terminal properties of explosively-loaded thin-walled 304 stainless steel cylinders⁷. These findings and the results of the present investigation will be treated in a future publication⁸

Undoubtedly, much more information on the terminal characteristics of specific alloys is needed. However, there are several general areas of terminal

behavior in which the present state of knowledge is either inadequate or nonexistent. These include fracture toughness, elevated temperature short- and long-term (creep) properties, resistance to environmental crack propagation (K_{ISCC}), fatigue resistance, and thermal response (substructure recovery, and heat treatment characteristics). One aspect of terminal behavior which continues to be a perplexing problem is the lower stress corrosion resistance of 300-series stainless steels which have been explosively formed as opposed to conventionally formed. The reasons for the difference in stress corrosion behavior have not been resolved or methods examined to alleviate the problem. One observation which could have a bearing on the sign of the forming-rate sensitivity is the mode of fracture. Whereas the stress corrosion resistance of stainless steel, which exhibits transgranular cracking, is impaired by explosive forming¹, the resistance of 2014 aluminum alloy, unalloyed Ti, and Ti-6Al-4V, which fail intergranularly, is improved or, at worst, unaltered by explosive forming^{3,4}. A program is being initiated in this laboratory to investigate the mechanisms responsible for the impairment, and to examine methods whereby the problem could be remedied, perhaps by conventional prestrain, or preforming and/or postforming heat treatments, modification of forming rates, etc.

The purpose of the current investigation is two-fold: to generate additional data on terminal behavior and to examine the potential, if any, of thermomechanical processing (TMP) by the utilization of explosive forming as the deformation step in the treatment schedule.

Two alloys were selected for these studies -- 17-7 PH, a precipitation-hardenable semi-austenitic stainless steel, and Beta III, a beta-isomorphous titanium alloy hardened by alpha-phase precipitates. Thus, the principal factors which could contribute to TMP strengthening are substructure hardening, and the refinement and redistribution of precipitates relative to the thermally processed condition. In addition, any nucleation of precipitates on dislocations could conceivably delay substructure recovery and effect some microstructural stability.

It is known that 17-7 PH responds well to explosive forming and, in fact, exhibits enhanced ductility when forming velocities are in the range 700 to 800 fps^{9,10}, where the latter is the limiting velocity. Maximum uniform strains of 38% have been obtained⁹. This author is unaware of any published accounts of attempts to explosively form Beta III but its conventional cold formability¹¹ indicated that high energy forming of this alloy should present little difficulty.

The approach taken was to compare the effects of explosive TMP, conventional TMP, and thermal processing alone, on hardness, tensile properties, microstructure, and stress-rupture life. However, in view of the successful application of shock TMP, or shock-aging, on the mechanical properties and microstructural stability of nickel-base superalloys¹², some preliminary experiments were conducted on the age-hardening response of solution treated and shock-hardened 17-7 PH, Beta III, and 350 grade 18% Ni maraging steel (see Appendix).

Since this program is being continued and will be phased out as a graduate research project, this chapter is essentially a detailed report of the progress of this investigation to date.

EXPERIMENTAL DETAILS

Materials

The 17-7 PH stainless steel was obtained from Armco Steel Corporation, through the courtesy of Dr. J. L. Arnold, in the form of 0.080 in. thick sheet. The nominal composition is given below¹³:

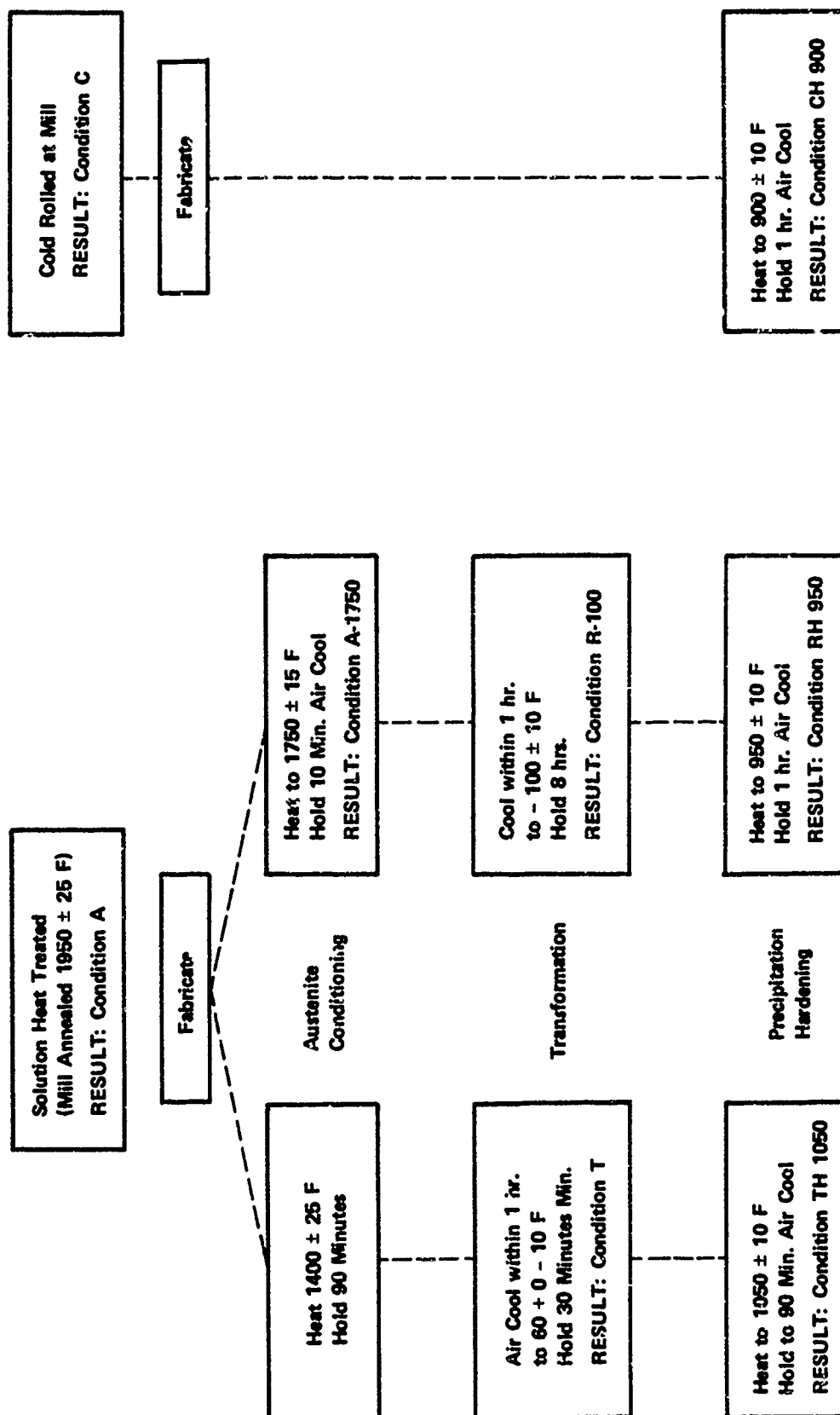
<u>Element</u>	<u>Wt. Pct.</u>
C	0.09 max
Mn	1.00 max
P	0.04 max
S	0.03 max
Si	1.00 max
Cr	16.00 - 18.00
Ni	6.50 - 7.75
Al	0.75 - 1.50

The standard thermal processing procedure for 17-7 PH steel is given in Table 1 and involves:

1. solution heat treatment (Condition A);
2. austenite conditioning to precipitate $M_{23}C_6$ ($Cr_{23}C_6$) and render the austenite less stable;
3. transformation to martensite, by cooling or cold working;
4. precipitation hardening, which serves as both a martensite temper and an aging treatment.

The sheet was received in Condition A. As shown in Table 1, the precipitation-hardened end product is normally reached from Condition A in one of three ways: the TH, RH or CH schedules. The CH condition has the highest

Table 1. Standard Heat Treatments for ARMCO 17-7 PH Stainless Steel



strength but lowest ductility. The TH schedule gives the lowest strengths (~200 ksi tensile) but highest ductility (~9% elongation). Tensile properties are reported with the results of TMP in the next section. The transformation temperature required to achieve Condition T and R-100 is governed by the stability of the austenite. Less carbide is precipitated during the 1750°F than 1400°F austenite conditioning anneal and accordingly, the M_s temperature is lower, requiring a lower transformation temperature. The amount of cold reduction applied to reach Condition C is 60% but 1/2 C and 3/4 C tempers are available where the reductions are 30% and 45% respectively. It should be noted that the TH schedule requires some modification when fabrication strains in Condition A are large. The austenite conditioning temperature is raised to 1550°F and the transformation temperature is 0°F, with a 4-hour hold. The precipitates which are believed to be primarily responsible for strengthening are of the BCC CsCl B_2 type^{14,15}, of composition (Ni, Fe, Cr) Al¹⁶. This tends to overage to the FCC $L1_2$ Cu_3Au form^{14,15}, of composition (Ni, Fe, Cr)₃Al¹⁶.

The Beta III titanium alloy was supplied by Colt Industries, through the courtesy of V. C. Petersen, in the form of 0.070-m. thick sheet. The following chemical analysis was provided:

<u>Element</u>	<u>Wt. Pct.</u>
C	0.01
N	0.012
O	0.112
Fe	0.05
H	0.0077
Mo	11.5
Sn	4.6
Zr	6.5

Thus, Beta III is nominally regarded as Ti-11.5Mo-6Zr-4.5Sn. This alloy has better toughness, elevated-temperature strength and stability, stress corrosion resistance and cold formability than the first developed, common beta alloy, Ti-13V-11Cr-3Al.¹¹

The sheet was received in a solution treated condition (1350°F, water-quenched) and contains some alpha phase. The standard aging temperatures range from 900 to 1100°F, for a time of 8 hr., depending upon the desired properties.

These aging temperatures cause the precipitation of HCP α phase, the major strengthener. Hexagonal ω phase precipitates at aging temperatures below about 800°F. Higher strengths are attainable with ($\beta + \omega$) than with ($\beta + \alpha$) structures, but ductility and toughness are drastically reduced. The primary deformation mode of Beta III is by mechanical twinning; slip and stress-induced orthorhombic martensite occur to a lesser extent¹⁷. Hexagonal martensite is apparently not a deformation product in the as-quenched condition¹⁸.

Explosive Forming and Shock Loading Procedures

Explosive forming of both 17-7 PH steel and Beta III titanium was accomplished by stretching a rigidly clamped workpiece in an open rectangular die, shown schematically in side view in Figure 1. The inside dimensions were 7 in. by 6-1/2 in. thereby accommodating a workpiece of the size illustrated in Figure 2. Attempts to form full-sized blanks, i.e., without a gage length, proved unsuccessful due to hold-down difficulties. This was

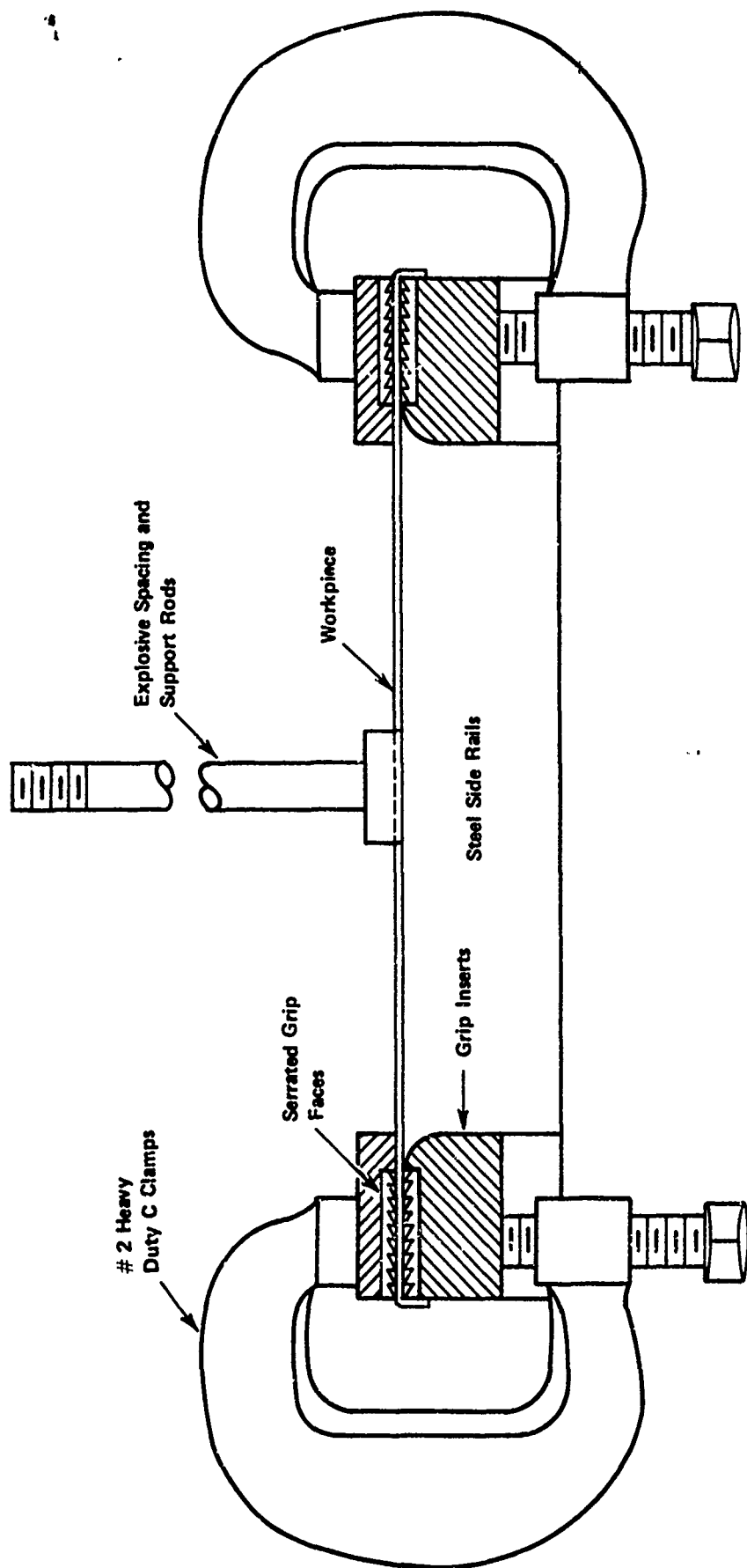


Figure 1. Schematic side view of rectangular explosive stretch forming die.

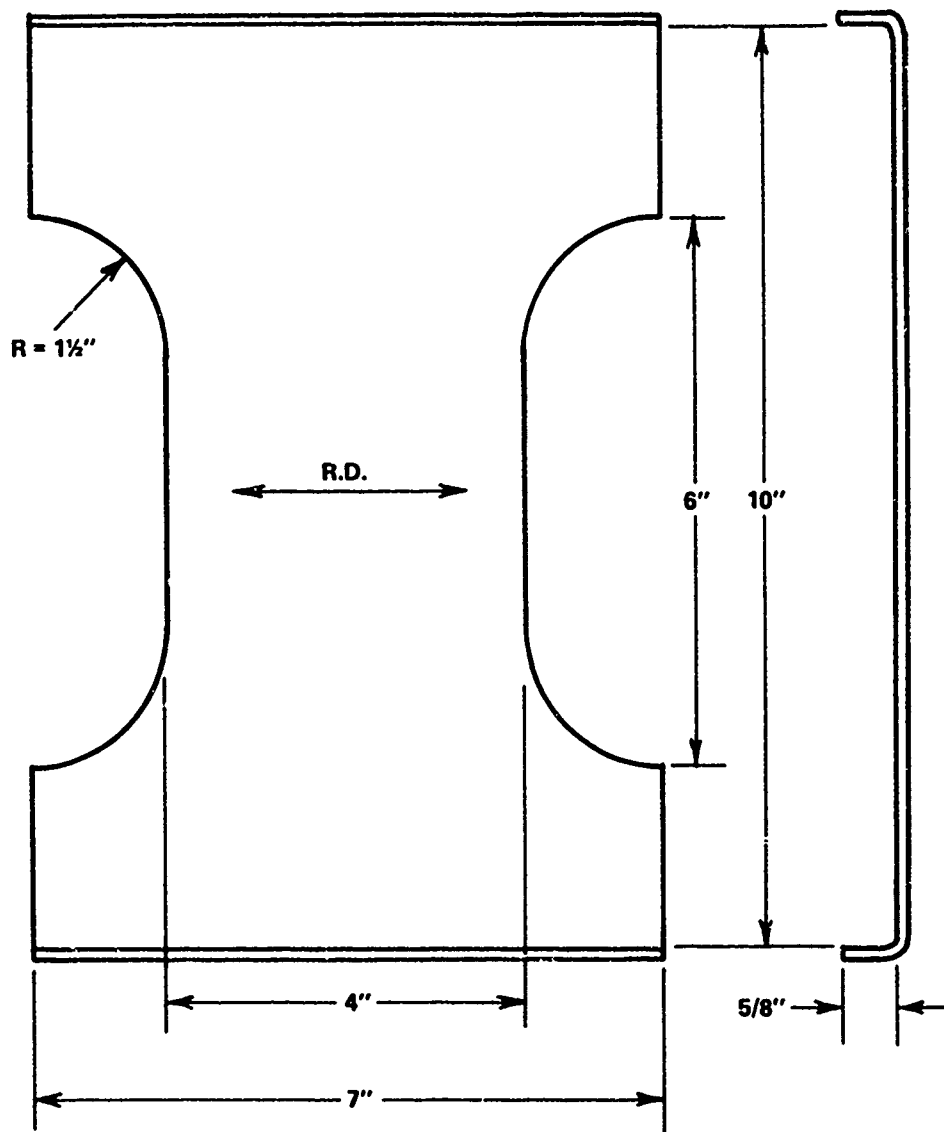


Figure 2. Explosive Stretch Forming Workpiece Configuration.

not improved substantially by attempts to inhibit pull-in through the introduction of bends at the ends of the sample or serrated grip faces. The final workpiece configuration was that in Figure 2, which could be successfully stretch formed providing the torque on the "C" clamp bolts was high enough (100 ft-lb. in this instance). It was also necessary that the bent ends were initially flush with the side surface of the die so that they would not be sheared off by impact with the die on detonation. A typical part formed in this manner is shown in Figure 3. This was produced by a multiple-shot sequence where one of the ends sheared off during the last shot. The significant advantages of the rectangular configuration as opposed to, say, a dome geometry, are the conservation of material and minimization of lateral curvature. Most of the formed blanks did have some lateral curvature due to side constraints. This could be alleviated by reducing the blank and gage width. However, one could no longer extract suitable tensile specimens from the formed product.

The explosive adopted for the forming operation was Primacord, a DuPont PETN-base variety, with a detonation velocity of $\sim 8000 \text{ msec}^{-1}$ and energy of detonation of $3320 \gamma \text{ in-lb/in}$ where $\gamma = \text{no. of grains/in.}$ Strands 4 in. long, of strength 100 or 200 gr./ft., were used. The Primacord was oriented parallel to the short dimension of the blank and located at a small distance from and directly over the center line of the blank (e.g., in Figure 1, normal to the page and above the die). The energy transfer medium was water.

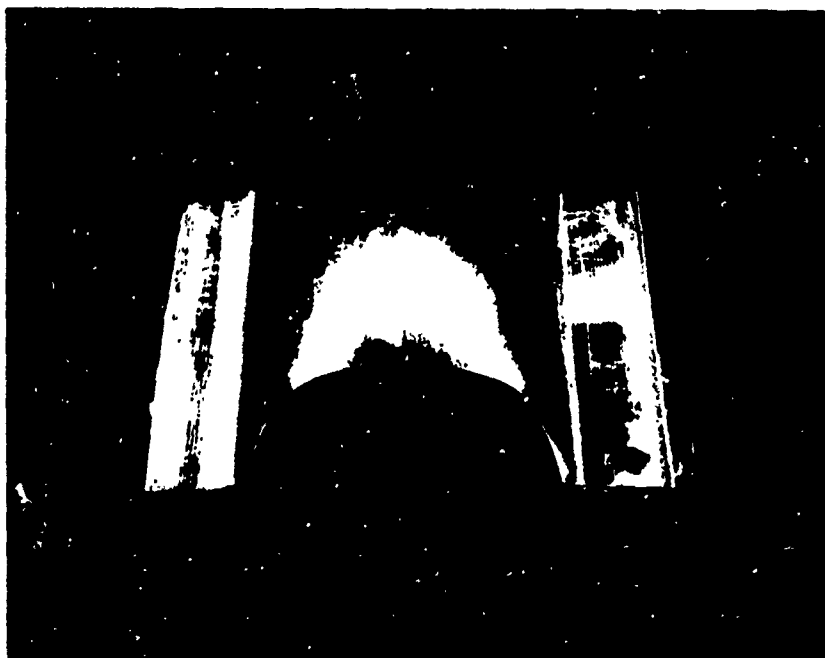


Figure 3. Explosively Stretch-Formed
17-7 PH Stainless Steel Blank.

The explosive charge requirements were estimated in the usual way from energy balance considerations¹⁹ assuming a standoff distance of 1 in. and explosive effectiveness of 0.5. Typical values of explosive weights, standoffs, and draw depths are given in Table 2.

Strains were measured from grids photographically transposed on the workpiece surface². Although lateral strains were small, they were taken into account in the calculation of effective forming strains. For property comparisons, material was multipass cold rolled to reductions corresponding to effective strains equivalent to those achieved by explosive forming. All strains are quoted as engineering or conventional values unless otherwise specified.

Shock loading was performed by utilizing a parallel-plate mousetrap configuration of the kind described previously^{12,20}, employing a copper driver plate and Detasheet C-2 explosive which has a detonation velocity of 7,380 msec⁻¹. The peak pressure of the planar shock wave in 17-7 PH was estimated to be 527 kbar, and in Beta III, 317 kbar. The corresponding true transient shock strains were estimated from stainless steel²¹ and titanium²¹ Hugoniot data to be 25.7 and 28.4%, respectively, using the relation²²

$$\epsilon_s = 4/3 \ln V/V_0.$$

Thermomechanical Processing Schedules

For 17-7 PH steel, explosive forming or cold rolling was inserted between solution treatment and austenite conditioning, between austenite

Table 2. Explosive Forming Parameters.

<u>Blank Number</u>	<u>Shot Number</u>	<u>Weight of Primacord (grains)</u>	<u>Standoff Distance (in.)</u>	<u>Final Draw Depth (in.)</u>
<u>(a) 17-7 PH</u>				
AX1	1	33	1-1/4	1-1/2
	2	66	1-5/8	
AX2	1	66	1-3/4	2-3/8
	2	133	2-1/8	
BX1	1	133	2	1-3/4
	2	133	1-3/4	
CX1	1	133	2-1/8	1-1/8
DX1	1	133	1-3/4	1-1/2
<u>(b) Beta III</u>				
AX1	5*	66	1-1/2	2-1/8
AX2	1	100	1-1/2	1/4 (failed)
AX3	3*	66	1-1/2	1-7/8
AX4	4*	66	1-1/2	1-1/2
AX5	2*	66	1-1/2	1-1/2
AX6	4*	66	1-1/2	1-5/8

* total number of shots; same conditions for each shot.

conditioning and transformation, between thermal transformation and precipitation hardening, and between Condition A and precipitation hardening. These are summarized in the tables of results.

For Beta III titanium, the cold working was conducted in the solution treated condition, where the solution treatment was either a mill treatment at 1350°F with a water quench (as-received material) or with an additional 1500°F anneal in this laboratory. These were followed by various aging treatments to effect precipitation of α or ω phase.

Testing Procedures

The terminal macrohardness was determined utilizing one of three hardness scales: Rockwell "C" or "B" for 17-7 PH: Rockwell "C" or DPH (10 kg load) for Beta III. These selections provided the best bases of comparison with previous work.

Tensile tests were conducted with an Instron Universal Testing Machine, at a strain rate of $3 \times 10^{-4} \text{ sec}^{-1}$ using specimens with a 1-inch gauge length.

Stress-rupture tests at constant load will be performed with a 12,000 lb. capacity Satec creep testing machine.

RESULTS AND DISCUSSION

17-7 PH Stainless Steel

A comparison of the hardness of explosively stretch-formed 17-7 PH steel with undeformed and cold-rolled stock, on the basis of equivalent effective strains, is given in Table 3. The nominal hardness values for Condition C (i.e., deformed Condition A) and CH 900 of Rc 43 and 49, respectively, correspond to 60% reduction by cold rolling. (With a conversion factor of $2/\sqrt{3}$ to account for the biaxial strain state, the effective engineering strain is 69.3%.) Rockwell hardness measurements were made to permit a direct comparison with the supplier's nominal values¹³, shown in the last column of the table. Normally, one would prefer to use scales such as Brinell or DPH which encompass the whole range of interest. The "C" scale readings below about 20 are less reliable than "B" values; they are included for continuity. Room-temperature tensile data for similar TMP schedules are listed in Table 4.

A number of points are noteworthy. Consider, firstly, the direct strengthening of metastable austenite (Condition A) by fabrication at different rates of strain. It is clear from an examination of the first set of hardness data in Table 3 for equivalent strains that explosive forming is less effective than conventional working by cold rolling in the hardening of solution treated 17-7 PH stainless steel. This trend is distinctly reversed when Condition A is explosively shock loaded to a peak

Table 3. Hardness Data for Undeformed, Cold-Rolled, and Explosively-Formed
17-7 PH Stainless Steel

Preforming History	Forming Method	Effective Forming Strain (%)	Postforming Heat Treatment	Average Hardness		Nominal Hardness (Rockwell)
				RB	Rc	
Condition A	UF CR	0	None	85.0	5.6	B85
		4.6	None	96.4	14.2	
	EF	14.0	None		30.7	C43
		23.3	None		31.4	
		50.8	None		41.5	
		4.6	None	91.5	10.6	
	ES	14.0	None		21.4	
		23.3	None		34.7	
Condition A	UF CR	0	Condition T		32.5	C31
		4.6	Condition T		32.3	
	EF	14.0	Condition T		30.2	
		4.6	Condition T		32.4	
		14.0	Condition T		30.2	
Condition A	UF CR	0	TH1050		42.9	C43
		4.6	TH1050		43.2	
	EF	14.0	TH1050		48.5	
		4.6	TH1050		42.6	
		14.0	TH1050		45.2	
Condition A	UF CR EF	0	A 1750	103.2	26.7	B85
		4.6	A 1750		26.3	
		4.6	A 1750		23.1	
Condition A	UF CR EF	0	A 1750	87.0		B85
		14.0	A 1750	82.9		
		14.0	A 1750	90.0		
	UF CR EF	0	R-100		35.2	C36.5
		4.6	R-100		33.9	
		4.6	R-100		34.8	
	UF CR EF	0	R-100		36.8	C36.5
		14.0	R-100		42.6	
		14.0	R-100		36.0	

Table 3 (Con't.)

Preforming History	Forming Method*	Effective Forming Strain (%)	Postforming Heat Treatment	Average Hardness		Nominal Hardness (Rockwell)
				RR	RC	
Condition A	UF	0	RH 950		48.7	C48
	CR	4.6	RH 950		48.3	
	EF	4.6	RH 950		46.9	
	UF	0	RH 950		47.5	C48
	CR	14.0	RH 950		49.8	
	EF	14.0	RH 950		48.8	
Condition A	UF	0	CH 900	88.8	7.5	C49
	CR	4.6	CH 900	97.8	17.7	
		14.0	CH 900		34.4	
		23.3	CH 900		34.0	
		44.0	CH 900		51.5	
		4.6	CH 900	93.9	11.8	
	EF	14.0	CH 900		25.2	C31
	ES	23.3	CH 900		40.2	
Condition T	UF	0	None		32.5	
	CR	4.0	None		33.6	
		23.3	None		38.6	
	EF	4.0	None		37.3	C43
	ES	23.3	None		39.2	
Condition T	UF	0	TH1050		42.9	
	CR	4.0	TH1050		46.4	
		23.3	TH1050		46.8	
	EF	4.0	TH1050		49.2	B85
	ES	23.3	TH1050		47.5	
A 1750	UF	0	None	87.0	6.4	
	CR	5.8	None	97.6	17.6	
	EF	5.8	None	89.5	8.7	

Table 3 (Con't.)

Preforming History	Forming Method*	Effective Forming Strain (%)	Postforming Heat Treatment	Average Hardness		Nominal Hardness (Rockwell)
				R _B	R _C	
A 1750	UF	0	R-100		36.8	C36.5
	CR	5.8	R-100		39.0	
	EF	5.8	R-100		39.0	
A 1750	UF	0	RH 950		47.5	C48
	CR	5.8	RH 950		48.1	
	EF	5.8	RH 950		46.7	
R-100	UF	0	None		36.8	C36.5
	CR	2.9	None		39.4	
	EF	2.9	None		42.0	
R-100	UF	0	RH 950		47.5	C48
	CR	2.9	RH 950		48.0	
	EF	2.9	RH 950		48.5	

* UF: unformed; CR: cold rolled; EF: explosively formed; ES: explosively shocked

Table 4. Room-Temperature Tensile Properties of 17-7 PH Stainless Steel Following Thermal Processing, Conventional TMP, or Explosive TMP.

<u>Forming History</u>	<u>Effective Forming Strain(%)</u>	<u>0.2% YS (ksi)</u>	<u>UTS (ksi)</u>	<u>Total Elong. (%)</u>	<u>R.A. (%)</u>
<u>(a) Condition A + Cold Work → Condition CH900</u>					
UF	0	52.0	137.1	38.8	52.7
CR	9.7	90.1	148.8	32.0	47.3
	12.9	106.3	159.6	30.0	49.1
	14.9	114.9	160.4	29.8	45.2
	23.3	107.9	158.2	29.2	40.4
EF	14.9	96.2	150.6	31.1	42.8
ES	23.3	131.7	169.4	21.5	42.2
Nominal	34.6	115	178	10	
	69.3	190	220	5	
<u>(b) Condition A + Cold Work → Condition TH1050</u>					
UF	0	181.8	194.9	6.5	27.0
CR	9.7	179.1	191.4	10.0	33.8
	12.9	185.9	194.7	6.1	33.0
EF	9.7	191.4	201.9	5.9	28.9
	12.9	187.4	199.1	8.1	36.4
Nominal	0	174.5	187.5	10.5	
	34.6	165.5	183.8	11.8	
<u>(c) Condition T + Cold Work → TH1050</u>					
UF	0	181.8	194.9	6.5	27.0
CR	2.8	192.6	197.9	3.8	19.0
EF	2.8	192.3	199.8	5.5	32.5
ES	23.3	203.1	205.8	3.2	28.2
Nominal	0	174.5	187.5	10.5	

Table 4. (Con't.)

<u>Forming History</u>	<u>Effective Forming Strain(%)</u>	<u>0.2% YS (ksi)</u>	<u>UTS (ksi)</u>	<u>Total Elong. (%)</u>	<u>R.A. (%)</u>
<u>(d) Condition Al750 + Cold Work → RH950</u>					
UF	0	211.4	222.3	6.9	31.4
CR	2.5	201.4	216.3	8.3	12.6
EF	2.5	140.1	193.5	11.4	34.6
Nominal	0	220	235	6	
<u>(e) Condition R-100 + Cold Work → RH950</u>					
UF	0	218.1	229.0	8.4	36.5
CR	2.9	183.3	216.1	11.5	35.5
EF	2.9	215.9	228.9	10.7	34.2
Nominal	0	220	235	6	

pressure of 527 kbar, yielding an engineering transient shock strain of 23.3%. The deformation of metastable austenite, characterized by Condition A, leads to the formation of martensite, the amount increasing with increasing strain. The observation of a negative strain-rate dependence of hardening when the primary contribution to strengthening is from a strain-induced transformation product is not an unexpected result. It has been shown that as the rate of deformation of metastable austenitic stainless steels increases, the amount of martensite formed decreases²³. This was clearly shown to be associated with an increase in specimen temperature on increasing the strain rate, an adiabatic heating effect. Thus, the effective M_d temperature is lowered by raising the deformation rate so that relatively less martensite is produced at equivalent strains. That this is the interpretation for the difference in the terminal hardnesses between explosively-formed and cold-rolled 17-7 PH was confirmed by surface-reflection X-ray diffractometry. From measurements of the relative intensities of (200) reflections²⁴, the percentage of martensite increased in the order: 12.1% reduction by explosive forming; an equivalent reduction by cold rolling; 44% reduction by cold rolling. While an examination of the microstructure does disclose some differences (Figure 4) its complexity does not unambiguously allow this distinction to be made optically. As a simple qualitative test, a small permanent magnet invariably attracted cold-rolled samples more strongly than those which were explosively formed to an equivalent strain, indicative of a substantially higher ferrite content in the former. The reason for the beneficial effect



(a) Cold Rolled to 12.1% Reduction



(b) Explosively Formed to 12.1% Reduction

Figure 4. Microstructure of 17-7 PH Stainless Steel
Fabricated in the Solution Treated Condition (A). 500X

of shock loading has not been resolved, but could reside in a higher volume fraction of martensite, and a denser substructure in both the austenitic and martensitic phases than in its explosively-formed or cold-rolled counterparts. This could be due to the fact that a martensitic shear transformation is a deformation mode which is a favorable alternative to ultra high-velocity slip at a plastic shock front in spite of significant adiabatic heating, and moreover, the rarefaction or release wave would serve to further work harden the martensite produced at the compression front.

As seen from both Tables 3 and 4, the preceding differences are retained when the material is aged at 900°F for 1 hour in order to convert to a fractional CH 900 condition. Accordingly, it was concluded that for an equivalent reduction, explosively stretch-formed and aged 17-7 PH has a lower strength than cold-rolled and aged 17-7 PH because of the presence of a smaller amount of tempered martensite. Conversely, the 22% increase in the yield strength and 7% increase in ultimate strength of the shocked and aged material, relative to that aged after rolling to a strain equivalent to the transient shock strain, clearly demonstrates the potential of shock-age strengthening. The improvement is further magnified when it is considered that residual dimensional changes resulting from shock loading can be kept below 2 or 3% by a suitable system which inhibits impact deformation.

The explosive forming findings are consistent with the terminal behavior in the as-deformed and fractional CH 900 conditions observed by Hendricksen et al.²⁵ (or see Ref. 1) for 17-7 PH prestrained statically and dynamically by uniaxial tension in the solution treated condition.

This author believes that these results should not be regarded as a detriment to the utilization of high energy forming as a fabrication technique. The negative dependence of the strain-induced martensitic transformation on deformation rate is well established. If the terminal properties do not meet design requirements then steps can be taken to improve the properties by lowering the forming temperature, or perhaps more practically, by applying some modified thermal processing procedure. Precisely what these heat treatment conditions should be has not been established. A decrease in the stability of the austenite by some austenite conditioning prior to high energy forming may be the solution if fractional or full CH 900 properties are deemed desirable.

Since CH 900 ductilities are so low, the TH and RH heat treatment sequences yield mechanical properties which are generally more attractive. While explosive forming in Condition A in comparison with rolling has a small detrimental effect on TH 1050 hardness, the reverse was true for the tensile properties. Therefore, one can reasonably regard the properties as being relatively forming-rate independent. As discussed previously, imparting conventionally a large amount of strain in Condition A prior to converting to TH 1050 requires a modification of the heat treatment schedule. It would appear that this modification is unnecessary for the forming strains examined (to 12.9%), particularly when Condition A is explosively formed.

In the latter case, the strengths are increased relative to thermally-processed control material by an average of 8% for yield and 3% for ultimate

strength in the strain range examined. Moreover, the ductility is raised slightly rather than falling off as might be expected. A comparison of Condition T and Condition TH 1050 hardnesses in Table 3 suggests that the property enhancement is a consequence of the 1050°F precipitation hardening treatment.

If one reaches the TH 1050 condition by cold working material in Condition T, then the hardness after explosive forming is raised about 15% over the undeformed control, and 7.5% over cold-rolled stock, for effective strains of only 4%. This TMP strengthening effect is also reflected by the strength properties in Table 4. Conventional and explosive TMP introduce roughly the same increase in the final strength levels. Whereas the former leads to substantial reductions in ductility, explosive forming leaves the ductility relatively unchanged from undeformed values.

It was observed that only a small amount of cold work (2.4% reduction) in Condition T raised the TH 1050 yield strength by 10 ksi. On a specific basis, a linear extrapolation to 10% strain would result in a 45 ksi strength increase. Unfortunately, one of the problems in explosive stretch forming in the high-strength martensitic condition is the instability or ductility limitation (a factor which also restricted forming in the R-100 condition). Conceivably, then, substantial beneficial effects could be realized if larger strains were introduced by a dynamic working technique which did not involve large tensile strain components. Consequently, some preliminary shock-aging experiments were also conducted where the material in Condition T was shock loaded to a pressure of 527 kbar, and thereafter aged at 1050°F for 90 minutes.

The as-shocked and TH 1050 hardnesses (Table 3) are only about 2% greater than those associated with cold-rolled material, but both fabrication methods lead to hardness values which exceed thermally-processed TH 1050 values by ~20%. Similarly, the yield strength of standard TH 1050 material is raised by ~21 ksi through shock-aging. This occurred at the expense of a 50% decrease in tensile ductility. However, this is little worse than the ductility reduction associated with a 2.4% cold reduction. Again, shock TMP tends to hold some promise for strengthening.

The influence of high energy forming in the Al750 condition on RH950 strengths led to some unusual results. For example, the yield strength after explosive TMP is 34% lower than that of the undeformed control material, and 30% lower than after conventional TMP by rolling to an equivalent strain. The decrease in ultimate strength is less severe, averaging 12%. These observations correspond to an average for two specimens. There is some indication from the hardness data for a different set of samples after the R-100 heat treatment, or after a further 950°F age to the RH950 condition, that these results might be anomalous. It is possible that the low-temperature transformation treatment of the tensile specimens was inadequate. It is definitely known that the discrepancy is due to an appreciable difference in the volume fraction of ferrite between cold-rolled and explosively-processed material. A further indication that the preceding effect may not be real is the fact that the explosive working in the R-100 condition before aging to RH950 did not significantly change the mechanical properties and, indeed, the

strength levels were appreciably higher than after conventional TMP. However, until additional experiments either confirm or negate these findings, it would be unwise to start with a history of A 1750 prior to explosive forming on the way to a final RH950 state.

In summary, the only two explosive TMP schedules which could introduce significantly poorer room-temperature mechanical properties than conventional TMP is the one which leads to a fractional CH900 condition, and one which involves explosive forming in the A1750 state and conversion thereafter to RH950. This latter must be regarded as a tentative conclusion subject to the results of additional tensile tests.

Beta III Titanium Alloy

While good cold formability is one of the attractions of Beta III, it had yet to be demonstrated that this would encompass high energy fabrication, and more specifically, explosive forming. Once initial hold-down problems were solved, it was shown that Beta III can be successfully either free-formed or stretch-formed. Large draw depths were attainable by permitting and controlling edge pull-in. Large material strains could be imparted by completely inhibiting edge pull-in. Such a stretch-forming operation (with 3 shots) yielded effective strains up to 27% (23.4% reduction) at the central region of the workpiece before pull-in caused the bent ends of the blank to shear off and preclude any additional forming.

This magnitude of forming strain is of some interest since the uniaxial instability strain in the transverse direction (i.e., the same orientation as

the direction of load application during stretch forming; see Figure 2) was measured to be 11.7%. The width of the blank sets up a state approaching plane strain and, accordingly, introduces a large positive normal stress component perpendicular to the stretch axis. Since a balanced biaxial tension would roughly double the instability strain, then the formability during stretch-forming should have been limited to strains of less than 23.4%. This suggests that there is a ductility enhancement at the high rates of strain characteristic of explosive forming (10^2 - 10^3sec^{-1}). This is consistent with the increase in uniform strain from 10 to 13% found by Wood for the Ti-13V-11Cr-3Al beta alloy under explosive biaxial forming conditions.⁹ What role the two deformation modes -- twinning and martensitic transformation -- play in raising or maintaining the effective transient work-hardening rate and, therefore, the instability strain at the high strain rates, is presently under study.

The first question which required an answer was whether Beta III could be explosively fabricated in the solution treated condition (in this case, as-received: 1350°F, W.Q.) without any adverse effects on the aged properties. The hardness data in Table 5 suggest that there is little TMP effect irrespective of working rate. However, the tensile properties clearly indicate that cold rolling prior to aging has a large beneficial influence on the ultimate strength, with a concomitant decrease in total elongation. Compared with cold rolling, explosive forming tends to be detrimental, although strength levels for the highest forming strain are only about 5% lower than for thermally-processed material.

Table 5. Hardness and Room-Temperature Tensile Properties of Unformed, Cold-Rolled, and Explosively Formed Beta III Titanium Alloy After Aging (900°F/8hr.)

<u>Forming History</u>	<u>Effective Forming Strain(1%)</u>	<u>Average Hardness (Rc)</u>	<u>0.2%ys ksi</u>	<u>UTS (ksi)</u>	<u>Total. Elong. (1%)</u>	<u>R.A. (%)</u>
UF (L)*	0	45.8	194.1	207.4	8.9	12.4
CR (T)	7.4	46.7	198.0	217.1	5.2	5.4
CR (L)	7.4	45.1	198.2	243.6	3.4	6.0
EF (L)	7.4	46.3	200.6	217.3	5.3	9.8
CR (T)	22.0	47.0	188.4	208.9	5.3	7.1
CR (L)	22.0	45.8	187.0	248.3	5.9	13.2
EF (L)	22.0	46.0	184.7	196.1	3.6	6.7

*L: longitudinal; T: transverse

The response of explosively formed and cold-rolled Beta III titanium to aging at several temperatures is being examined. Some of the more significant results are summarized in Table 6. The basis of comparison in (a) is the unstrained solution-treated (as-received) control material, and in (b) the undeformed but similarly aged stock. Although there is a distinct hardening effect due to prior working with all aging times and temperatures examined, the smallest influence of TMP occurs with the 900°F aging temperature which results in α -phase precipitation. The 900°F hardness data are consistent with the tensile properties in Table 5.

If one considers the results for 450°F and 700°F, which are conducive to the precipitation of ω phase, then a TMP strengthening effect becomes more evident. Whereas prior strain by cold rolling only marginally raised the hardness level on aging at 700°F, explosive forming led to an appreciable enhancement of hardening. A similar but more pronounced effect occurred for a longer aging time at 450°F. It should be noted that the as-formed hardness was generally lower after explosive forming than after conventional working. This is not inconsistent with previous findings for BCC metals.¹

When as-received material was shock loaded to 317 kbar, the final hardness averaged 31.2 Rc (279 DPH). This was essentially the same as the undeformed hardness (30.7 Rc). An equivalent amount of reduction by rolling gave a rolling-plane hardness of 32.8 Rc. The failure of Beta III to shock harden substantially when high peak pressures are applied can be explained on the basis of a pressure-induced phase transformation²⁶. Lower pressures

Table 6. Percentage Increase in Hardness (DPH) of Beta III Titanium Due to Aging After Forming to 10% Reduction in Thickness

<u>Forming History</u>	<u>4 Hr.</u>			<u>8Hr.</u>			<u>72 Hr.</u>
	<u>450°F</u>	<u>700°F</u>	<u>900°F</u>	<u>450°F</u>	<u>700°F</u>	<u>900°F</u>	<u>450°F</u>
<u>(a) Relative to the Undeformed, Solution Treated State</u>							
UD	18.3	51.8	52.1	21.6	59.0	60.3	23.5
CR	34.3	61.5	62.1	33.2	68.0	67.7	44.4
EF	33.6	75.2	58.2	33.6	78.4	64.9	56.7
<u>(b) Relative to the Undeformed, Aged State</u>							
CR	13.6	6.4	6.5	9.5	5.7	4.6	16.9
EF	12.9	15.4	4.0	9.8	12.2	2.9	26.9

in the region of 70 kbar should be more effective. Aging at 900°F and 700°F resulted in respective hardnesses of 46.2 and 49.6 Rc. These are a few percent larger than thermally-processed values and insignificantly different from rolling-plane hardnesses after conventional TMP.

The influence on rolling-plane Rc hardness of reduction by rolling up to 50% is illustrated in Figure 5. Utilization of this parameter indicates little work-hardening or TMP strengthening effect. These results are considered tentative at this time.

The interpretation of the preceding and other observations for Beta III is being sought, and forms the basis of a M.S. graduate research program being pursued currently by M. B. de Carvalho.

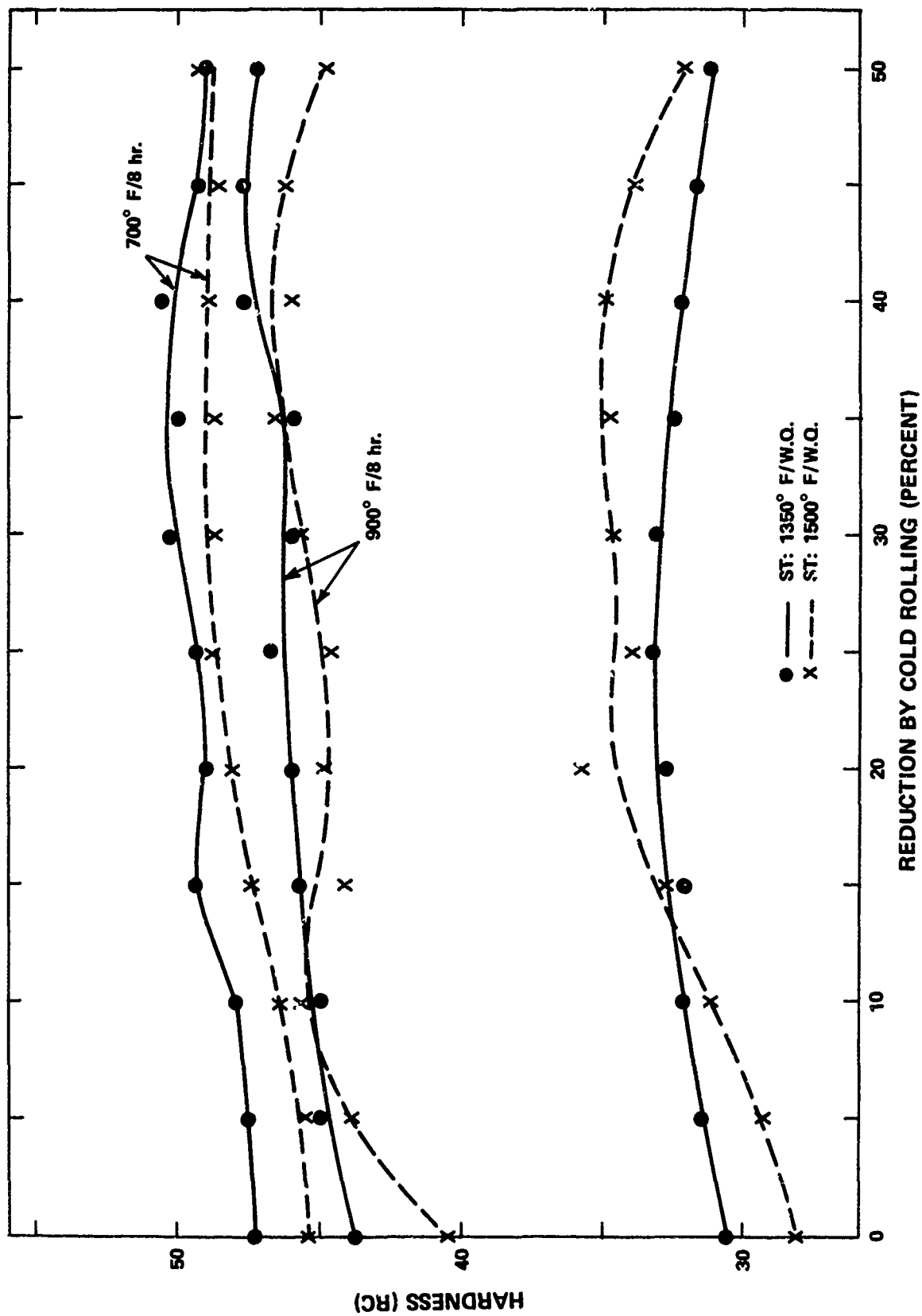


Figure 5. Effect of Reduction by Cold Rolling in Solution Treated Condition on AS-Rolled and Aged Hardness of Beta III

SUMMARY AND CONCLUSIONS

The results of this investigation and the conclusions drawn therefrom may be summarized as follows:

1. Precipitation-hardenable 17-7 PH stainless steel can be explosively formed successfully; attainable uniform forming strains and draw depths are expected to decrease with preforming history in the order: Condition A, Condition A1750, Condition T, Condition R-100.
2. Explosive forming may be inserted into a standard heat treatment schedule without significant room-temperature tensile property impairment under the following circumstances: when the initial state prior to working is Condition A or T converted after forming to TH 1050; Condition A or R-100 as the initial state, converted after forming to RH950. This holds for the effective forming strains examined, i.e., up to ~15%.
3. Explosive forming in Condition A or T prior to conversion to TH 1050 can lead to slightly improved tensile strengths with minimal, if any, ductility loss, as compared with conventional processing by cold rolling.
4. The aforementioned improvements are not considered sufficient to warrant the specific utilization of thermomechanical processing involving explosive forming for the specific purpose of strengthening 17-7 PH steel, at least for the schedules, strains, and properties (room-temperature hardness and tensile) reported herein. On the other hand, no adverse effects need be anticipated, except in the following instances.

5. Explosive forming in Condition A and aging at 900°F will not yield the expected properties achievable by an equivalent amount of deformation imparted at a lower rate. This can be attributed to the fact that the amount of martensite introduced by working decreases as the strain rate increases. A possible remedial measure is to condition the austenite prior to explosive forming so that it is less stable and more susceptible to a strain-induced martensitic transformation.
6. Until it can be shown otherwise, some caution must be exercised in the utilization of a combination of explosive working in Condition A1750 and standard heat treatment to Condition RH950.
7. Shock thermomechanical treatment, or shock-aging, has been shown to be a promising strengthening method for 17-7 PH stainless steel and is particularly attractive because residual dimensional changes can be kept small.
8. The inherent cold formability of Beta III titanium alloy renders it highly amenable to explosive or high energy forming. High strain rate deformation results in an enhancement of the uniform forming strain.
9. When Beta III titanium is aged at 900°F after explosive forming in the solution treated condition, one can expect the ultimate tensile strength to be appreciably less for low forming strains ($\sim 7\%$), and strength and ductility, in general, to be less for higher forming strains ($\sim 20\%$), than those for material thermomechanically processed conventionally to equivalent strains.

10. Preliminary findings indicate that shock-aging is not a viable method of strengthening Beta III titanium when peak pressures are high (e.g., ~ 300 kbar). This was tentatively attributed to a pressure-induced phase transformation.

REFERENCES

1. R. N. Orava and H. E. Otto, J. Metals 22(2), 17 (1970).
2. R. N. Orava, H. E. Otto, and R. Mikesell, Met. Trans. 2, 1675 (1971).
3. G. S. Whiting and R. N. Orava, "The Relative Effect of Explosive and Isostatic Forming on Stress Corrosion Cracking in 2014 Aluminum Alloy," Phase Report, Contract No. DA 12-066-AMC-266 (X), Center for High Energy Forming, University of Denver, Denver, Colorado, October (1969).
4. R. N. Orava and P. Khuntia, "The Relative Effect of Explosive and Isostatic Forming on Methanol Cracking in Titanium," Proc. 3rd Intl. Conf. of the Center for High Energy Forming, ed. A. A. Ezra, University of Denver, Denver, Colorado, p. 4.1.1 (1971).
5. H. E. Otto and R. Mikesell, "Terminal Properties of Explosively Formed High Strength Low Alloy Steels," source cited in Ref. 4, p. 4.2.1.
6. H. E. Otto, Chapter VI, this report.
7. L. E. Murr, J. V. Foltz, and F. D. Altman, Phil Mag. 23, 1011 (1971).
8. R. N. Orava, "Metallurgical Effects of High Energy Forming," invited paper, Conf. on Metallurgical Effects at High Strain Rates, Albuquerque, N. M., February (1973).
9. W. W. Wood, Product Engineering, p. 58, September (1963).
10. R. N. Orava, "Effect of Dynamic Strain Rates on Room-Temperature Ductility," Proc. 1st Intl. Conf. of the Center for High Energy Forming, ed. A. A. Ezra, University of Denver, Denver, Colorado, p. 7.5.1 (1967).
11. J. B. Guernsey, V. C. Petersen, and E. J. Dulis, Met. Progress 96 (5), 121 (1969).
12. R. N. Orava, "The Aging Response of Shock Deformed Nickel-Base Super-alloys," Contract No. N00019-71-C-0099, Naval Air Systems Command, Washington, D. C., Final Technical Report No. DRI 2592, University of Denver, Denver, CO, January (1972).
13. Product Data Bulletin S-30, "Armco 17-7 PH Precipitation-Hardening Stainless Steel Sheet and Strip," Armco Steel Corporation, Middletown, Ohio (1967).

14. H. C. Burnett, R. H. Duff, and H. C. Vacher, J. Res. Nat. Bureau Stds., 66C, 113 (1962).
15. J. C. Wilkens, R. E. Pence, and D. C. Perry, Advances in the Technology of Stainless Steels and Related Alloys, ASTM STP 369, p. 331 (1965).
16. H. L. Marcus, L. H. Schwartz, and M. E. Fine, Trans ASM 59, 468 (1966).
17. J. A. Feeney and M. J. Blackburn, Met. Trans. 1, 3309 (1970).
18. H. J. Rack, D. Kalish, and K. D. Fike, Mater. Sci. Eng. 6 181 (1970).
19. A. A. Ezra, J. Mater. 4 338 (1969).
20. H. E. Otto, "Shock Hardening of Aluminum Alloys," Phase Report, Contract No. DA 12-066-AMC-266(X), Center for High Energy Forming, University of Denver, Denver, Colorado, August (1968).
21. R. Kinslow, ed., High-Velocity Impact Phenomena, Appendix D, Academic Press (1970).
22. A. H. Holtzman and G. R. Cowan, in Response of Metals to High Velocity Deformation, ed. P. G. Shewman, and V. F. Zackay, Interscience, 447 (1961).
23. J. P. Bressanelli, and A. Moskowitz, Trans. ASM 59, 223 (1966).
24. H. R. Erard, Adv. in X-ray Analysis 7, 256 (1964).
25. E. K. Hendricksen, et. al. Symposium on Dynamic Behavior of Materials, ASTM STP 336, 104 (1964).
26. M. K. Koul and J. F. Breedis, The Science, Technology and Application of Titanium, ed. R. I. Jaffee and N. E. Promisel, Pergamon Press, 817 (1970).

APPENDIX TO CHAPTER XII
SHOCK THERMOMECHANICAL PROCESSING OF
350 GRADE MARAGING STEEL

R. H. Wittman and R. N. Orava

An investigation of the explosive welding of 350 grade maraging steel conducted previously by one of us (R.H.W.) had resulted in some improvement in the hardness, strength, and ductility of the alloy when it was aged after welding in the solution treated condition. The shock pressure and time of duration of the pressure pulse during explosive welding were unknown. However, stimulated by these findings, some preliminary experiments were carried out to evaluate the response of 350 grade maraging steel to TMP when the mechanical working is applied by explosive shock loading.

For simplicity, explosive shocking was accomplished by the tangential detonation of a 0.336 inch thick layer of Detasheet C explosive in contact with a 1/8-inch thick maraging steel plate in the solution treated condition. The sheet was supported by spall rails and a 1-inch thick steel anvil to promote flatness and prevent spallation. These explosive conditions are estimated to yield a peak shock pressure of 150 kbar. The peak pressure decays rapidly but the duration of pressure above 100 kbar is nevertheless approximately 1 μ s. This would correspond to a true transient shock strain within the range 6.8 to 11.8% based on Hugoniot data for mild steel.¹ It is most likely that the strain is much closer to the lower value, and one would estimate the average to be about 8%.

Room-temperature tensile tests were conducted in an Instron testing machine at a strain rate of $3 \times 10^{-4} \text{ sec}^{-1}$ using specimens with a 1-inch

gage length. The load axis was parallel to the original plate rolling direction. The data for the as-shocked and shock-aged alloy are shown compared with thermally-processed material in Table A.1. Percentage changes are given in Table A.2. There is a small shock-hardening effect at this shock pressure level, as reflected by the increase in ultimate tensile strength (engineering or true values) which is accompanied by a substantial reduction in total elongation. On the other hand, all of the aging treatments tend to produce a lower strength after shock loading as compared with undeformed material. However, these relative strength differences are not appreciable, and in fact, the hardness is slightly increased by shock-aging. Except for the duplex aging treatment, shock TMP also results in a reduction in tensile ductility which is especially large for the highest-strength condition (930°F/3 hr. age). In this case, the 50% decrease in elongation would have to be regarded as a serious detriment to shock-age strengthening of 350 grade maraging steel, at least for the strain level examined.

Conversely, there are good indications from the results of conventional TMP that higher pressure shock prestrains could lead to substantial strength, ductility, and toughness improvements. For example, Kula and Hickey² found that cold working prior to aging raised the final yield and ultimate strengths of 250 grade maraging steel roughly linearly at the rate of ~ 4 ksi/10% reduction. Although this was accompanied by a decrease in tensile elongation, the plane-strain fracture toughness (K_{IC}) values were always higher than for thermally-processed material, and peaked at ~ 20% reduction at a value ~ 5 ksi in greater than the standard. That this maximum coincided with an elongation minimum of little more than 1% illustrates the futility

of making any predictions of fracture toughness from the tensile data in Table A.1.

At this juncture, it would appear that any future work on the shock TMP, or indeed, explosive TMP, of 18% Ni maraging steels should be directed toward the application of higher shock pressures and strains. Moreover, payoffs are more likely with the grades lower than 350. It is conceivable that shock or explosive ausforming would prove fruitful but conventional ausforming has led to only minor strength improvements (e.g. Ref. 2) unless an appreciable amount of strain-induced martensite is produced.³

References

1. M. Van Thiel, ed., "Compendium of Shock Wave Data," Report No. UCRL-50108 (Vol. 1), Lawrence Radiation Laboratory, University of California, Livermore, CA, June (1966).
2. E. B. Kula and C. F. Hickey, Trans. TMS-AIME 230, 1707 (1964).
3. R. H. Bush, Trans. ASM 56, 885 (1963).

Table A.1. Mechanical Properties of Undeformed, Explosively Shocked, and Heat Treated 18% Ni 350 Grade Maraging Steel

Condition	0.2% YS (KSI)	UTS (KSI)	Elong. (%)	RA (%)	Hardness (Rc)
As-Received (Hot Rolled; Air Cooled from 1500°F)	144.6	158.9	9.83	65.7	35.2
As-Received and Shocked	140.5	172.5	6.74	68.5	36.0
As-Received, Plus 3 hr. at 930°F	349.5	354.8	4.75	28.4	56.5
As-Received, Shocked Plus 3 hr. at 930°F	340.2	341.0	2.36	22.5	57.5
As-Received, Plus 12 hr. at 850°F	356.3	358.5	4.19	32.5	58.5
As-Received, Shocked Plus 12 hr. at 850°F	347.0	348.8	3.28	31.0	59.4
As-Received, Plus 24 hr. at 350°F, and 6 hr. at 940°F	299.2	302.4	2.30	34.5	56.5
As-Received, Shocked Plus 24 hr. at 350° and 6 hr. at 940°F	295.9	297.1	2.69	36.5	57.8

Table A.2. Percentage Change* in Mechanical Properties
of 18% Ni 350 Grade Maraging Steel After
Shock TMP Relative to Thermal Treatment

<u>Treatment Schedule</u>	<u>0.2% YS</u>	<u>UTS</u>	<u>Elong.</u>	<u>RA</u>	<u>Hardness</u>
Unaged	- 2.8	+ 8.6	- 31.4	+ 4.3	+ 2.3
930°F/3 hr.	- 2.7	- 3.9	- 50.3	- 20.8	+ 1.4
850°F/12 hr.	- 2.6	- 2.7	- 21.7	- 4.6	+ 1.5
350°F/24 hr. + 940°F/6 hr.	- 1.1	- 1.8	+ 17.0	- 5.8	+ 2.3

*
$$\frac{\text{shock processed} - \text{thermally processed}}{\text{thermally processed}} \times 100\%$$

XIII. EXPLOSIVE POWDER COMPACTION

H. Otto

D. Witkowsky

T. McClelland

S. Stivers

INTRODUCTION

Explosives as an energy source for compacting powders is not a new concept. As early as 1900, low explosives were used to compact billets of ore concentrates.⁽¹⁾ Not until 1950, though, was metal powder compaction research initiated on a broader scale. The use of explosives as an energy source parallels the rapid growth of the powder metal industry during the past two decades. During the early stages of growth of the powder metal industry, the types and quality of metal powder available was limited to such materials as iron, copper base alloys and tungsten. It was not until three years ago that high quality aluminum alloy powders were available. As the number and quality of metal powders increased, the applications have increased.

Powder metallurgy has been used primarily to fabricate large numbers of close tolerance small parts such as gears and bearings for automotive and appliance applications. Conventional presses are used in which a straight draw can be used to eject the parts so limitations exist with respect to configuration. Press capacities are limited with respect to load unless heavy extrusion or forges are used for compaction. Again a limitation exists in that surface densities are higher than on the interior of the billet. Achievement of theoretical density in most cases is a function of the initial compaction plus the sintering operation. Even then some porosity is anticipated following sintering.

The use of large billets as forging and preforms is gaining acceptance since less waste occurs and forging or rolling operations are simplified.

Cast preforms have the disadvantage of non-uniform grain size and in most instances the grains are columnar and large which is detrimental to a forging operation. Powder preforms are being produced by several manufacturers that have the advantage of a uniform, small grain structure. Some porosity exists in the powder metallurgy preforms which is eliminated to some extent by the working operation.

Explosives generate extremely high pressures which can be utilized in producing high density compacts.^{2,3} Densities approaching theoretical can be achieved in several cases. In hard to compact metals and alloys such as the refractory metals explosive compaction can result in densities that are higher than can be achieved by conventional equipment and as such have more green strength which is beneficial for subsequent processing steps.

Composites have been made by high energy compacting filaments and whiskers such as boron, tungsten, silicon carbide, or alumina in titanium, nickel, aluminum, stainless steel, molybdenum or tungsten. Mechanical and diffusion bonding has been evident in these systems.⁴ The advantage of using explosives or high energy processes in metal matrix composites is the reduction of the intermetallic layer formed between the filament and matrix which is developed by most infiltration or diffusion bonding techniques. Feasibility for HERF process for compaction of composites was demonstrated by Battelle Northwest.⁵

The present program included three phases: (1) a study of the compaction parameters for steel powders; (2) development of a tungsten filament reinforced composite of steel; and (3) a study of compaction procedures for Udimet 700 powder. In the first phase basic parameters for compacting steel powders were developed for rolling and forging preforms. The properties of explosively

and conventionally compacted billets were compared to determine the relative merits of both processes. The second phase was concerned with developing a technique for making tungsten reinforced steel composites with eventual extension to superalloy composites. In the third phase Udimet 700 powder was compacted and sintered. The work on the Udimet 700 is in the preliminary stages of investigation and is a continuing effort.

COMPACTION OF ANCORSTEEL 1000 IRON POWDER

The program on compaction of iron powders was concentrated on the development of flat compacts. Ancorsteel 1000 atomized iron powder manufactured by the Hoeganaes Corporation was used in this study. Two lots of powder were used during the course of this investigation in which minor variations were present. The properties of the powders are presented in Table 1. Particles in both lots of powder were irregularly shaped which is beneficial to surface welding during compacting (See Figure 1).

Three different dynamites were used during this investigation so a correlation between energy of detonations could be made. The explosives were 40% Du Pont Red Cross Extra 60% Du Pont gelatin dynamite and Trojan SWP-5. The characteristics of the explosives are given in Table 2. In all of the experiments a ratio of weight of explosive to weight of iron powder was used. A comparison was made in the flat compact program with conventionally pressed iron powder.

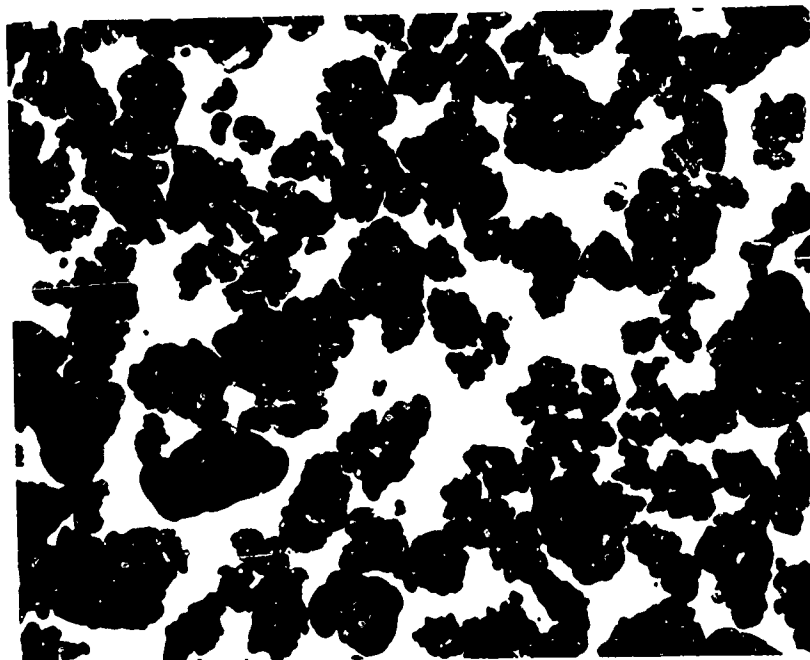


Figure 1. Photomicrograph of Ancorsteel 1000
Powders Showing Particle Shape

Table 1. Properties of Ancorsteel 1000 Iron Powder

Chemical Analysis

<u>Lot No.</u>	<u>Element, %</u>						
	<u>Fe</u>	<u>C</u>	<u>SiO₂</u>	<u>S</u>	<u>P</u>	<u>Mn</u>	<u>Cu</u>
29	99.2	< 0.015	0.05	0.013	< 0.01	0.21	0.10
83	99.2	< 0.015	0.05	0.018	0.012	0.18	0.095

Sieve Analysis

<u>Lot No.</u>	<u>Percent Retained in Each Mesh</u>							
	<u>60</u>	<u>80</u>	<u>100</u>	<u>140</u>	<u>200</u>	<u>230</u>	<u>325</u>	<u>- 325</u>
29	0	1.8	9.1	26.4	23.9	7.6	14.5	16.7
83	0	0.4	4.4	21.6	25.9	8.9	18.1	20.7

Physical Properties

<u>Lot No.</u>	<u>App Density, g/cc</u>	<u>Flow sec/50 g</u>	<u>Compressibility at 60,000 psi, g/cm³</u>	<u>Green Strength at 5.9 g/cm³, psi</u>
29	2.95	26.6	6.72 - 6.64	1680
83	2.86	24.6	6.71 - 6.64	1390

Table 2. Properties of Explosives Used in
Compaction Studies

<u>Explosive</u>	<u>Detonation Velocity, m/sec</u>	<u>Density, g/cc</u>	<u>Strength cal/g</u>	<u>Detonation Pressure, kbars</u>
40% Red Cross Extra	3100	1.29	720	61
60% Gelatin Dynamite	6000	1.44	780	94
SWP-5	3800	1.04	950	70

Experimental Procedures

The basic concept of this program was a picture frame arrangement containing the steel powder with cover plates on both sides and a supporting anvil below to sustain the blast. In the first few experiments a welded frame of 1 x 2-inch steel was used in which the compaction direction was through the 1-inch direction. Cover plates were cut from 1/4-inch steel plate. A compact size of 3 x 3 inches was used as the basic model. Steel foil was glued over the frame with epoxy so the powder area could be evacuated. The vacuum tube was pinched off just prior to detonation.

A plane wave detonator was used in the first experiments to eliminate to as great an extent as possible any differential in reflected shock waves from the shock wave arriving at different times at the lower cover plate. This system was complex and contained too many variables for a production technique so it was simplified.

First, the spall sails or picture frame did distort during loading and the welds would break. A simpler arrangement was made in which two 1/4-inch wall square steel pipe was pushed together. The inner pipe had internal dimensions of 3 x 3 inches and the outer pipe internal dimensions were 3-1/2 x 3-1/2 inches. On loading the momentum would be transferred to the outer pipe which would spall, leaving the inner pipe intact. The 1/4-inch cover plates were retained but the foil was eliminated. Evacuation of the powder area was found to be unnecessary for steel powder compaction so vacuum systems were eliminated. To prevent leakage of the fine powder, the seam between the cover plates and the inner wall of the pipe was filled with epoxy. In the initial tests, explosive was placed over the entire assembly which was again found to be unnecessary for steel powder compaction so vacuum systems were eliminated. To prevent leakage of the fine powder, the seam between

the cover plates and the inner wall of the pipe was filled with epoxy. In the initial tests, explosive was placed over the entire assembly which was again found to be unnecessary. In the final arrangement the box containing the explosive was the same size as the cover plates. The final assembly arrangement is shown in Figures 2 and 3. The explosive was packed in the cardboard container and the detonation system consisting of two diagonal strips of Detasheet was placed across the top. This arrangement aided in obtaining a more uniform detonation front.

Larger 6 x 6-inch billets were compacted using the original welded frame arrangement since large cross section square steel pipe was not available in the correct sizes. In both cases the length of the frame was varied to give billets of the desired thickness. Compact thicknesses of $1/4$, $1/2$, $3/4$ and 1 inch were made. For comparison purposes several billets were conventionally pressed at 30.5 tsi which is the recommended pressure for compaction of Ancorsteel powder. These compacts were 1-inch in diameter and $1/2$ -inch thick after pressing.

After compaction the density, hardness and diametral strength was determined. Problems were encountered in measuring the density by oil immersion mercury or bromobenzene displacement, and lineal analysis techniques. The method adopted for determining density was to coat the specimen from the compact with stearic acid and use water as the displacement media. The stearic acid prevented the water from entering any of the pores which would be disruptive to subsequent sintering operations. Stearic acid is a common binder in powder metallurgy and volatilizes at low temperature during sintering without reacting with the metal.

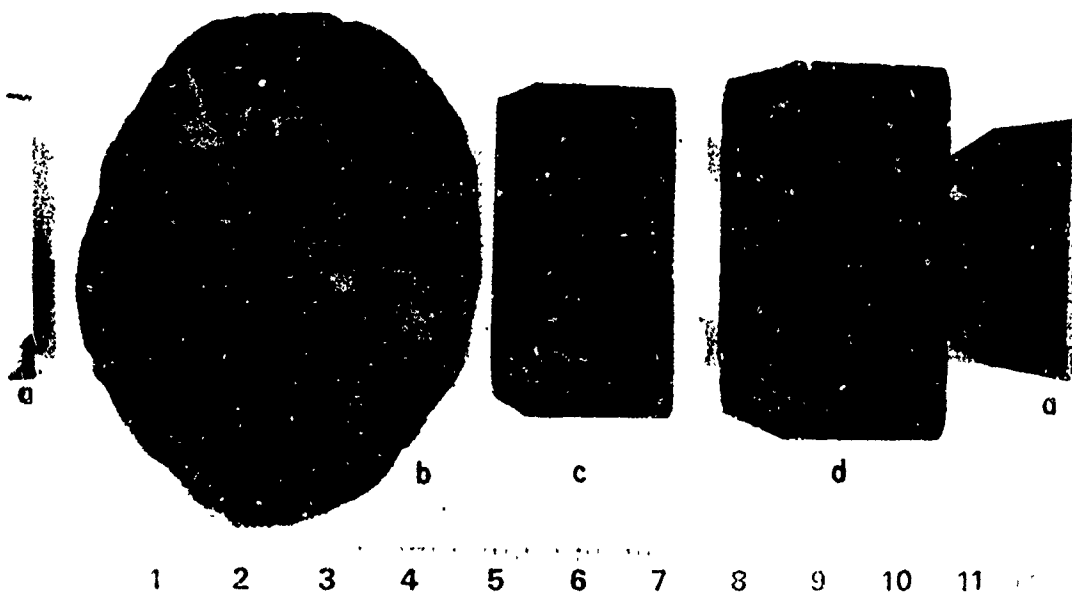


Figure 2. Dual Square Pipe Arrangement Showing a. Upper and Lower Cover Plates, b. Iron Powder, c. Inner Pipe, and d. Outer Pipe.

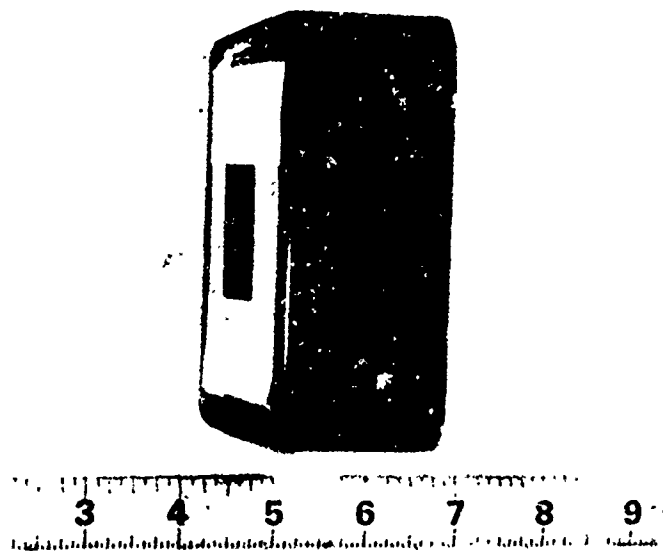


Figure 3. Assembled Dual Square Pipe Arrangement.

Brinell hardness tests were used which masked out some of the problems associated with small hardness penetrators hitting areas of high porosity. ASTM test B312⁶ for determining the strength of green compacts was not used since the specimens would have to be machined from the explosive compacts. This test is designed for conventionally pressed powders in which a standard die is used to prepare the specimens so the diameter is 0.5 inches and the thickness 0.25 inches. Although the green billets could be trepanned, a milling operation to give the desired thickness could influence the results or actually break the trepanned slugs. Therefore a diametral compression test was used as described by investigators at Max-Planck.⁷ In this test a right circular cylinder is compressed between two flat platens and the maximum tensile stress is developed normal to the loading direction. The maximum stress is then determined by the formula

$$\sigma_{\max} = \frac{2 P}{\pi D t}$$

where P = applied load at failure

D = specimen diameter

t = specimen thickness

Samples measuring 5/8-inches in diameter were trepanned from the compacts with the length of the cylinder normal to the compaction direction. The samples were taken along the diagonals of the 3 x 3-inch billets. Tests were conducted on the green compacts only to determine as compacted strengths.

Specimens of the compacts were sintered in gettered hydrogen so comparisons could be made with conventionally pressed compacts. In one set of experiments. the compacts were sintered at 2050°F, (the conventional sintering temperature for Ancorsteel) for varying periods of time. The second series of heat

treatments were conducted for one hour at temperatures varying from 800° to 2400°F.

Following the sintering treatments, metallographic examinations were conducted on specimens with the field of inspection normal to the compaction direction. Sintered specimens were rolled for comparison with conventionally compacted materials. These specimens were trepanned from the compacts and were the same size as used for the diametral tests.

EXPERIMENTAL RESULTS AND DISCUSSION

Typical 3 x 3-inch compacts of varying thickness are shown in Figure 4. As can be seen from an inspection of this photograph some dishing of the compacts was present as well as edge effects which became more pronounced as the thickness increased. Upsetting did occur which amounted to about 0.10 inches on an average with the maximum being about 2 percent of the average billet dimensions.

With the edge effects that were present, there was a variation throughout the green billets with respect to density, hardness and strength. Both the density and hardness data were treated statistically and as presented in Table 3 are the average of several samplings.

Densities varied between 93.9 and 98.7 percent of theoretical or a band of 4.8 percent of theoretical between maximum and minimum values. With the high densities and the small band in which they fell, comparisons of explosive loading ratio with the various properties were limited in several cases.

There were some trends that were observed with respect to density. At the lower loading ratio of 0.6 parts of explosive to 1.0 part of powder

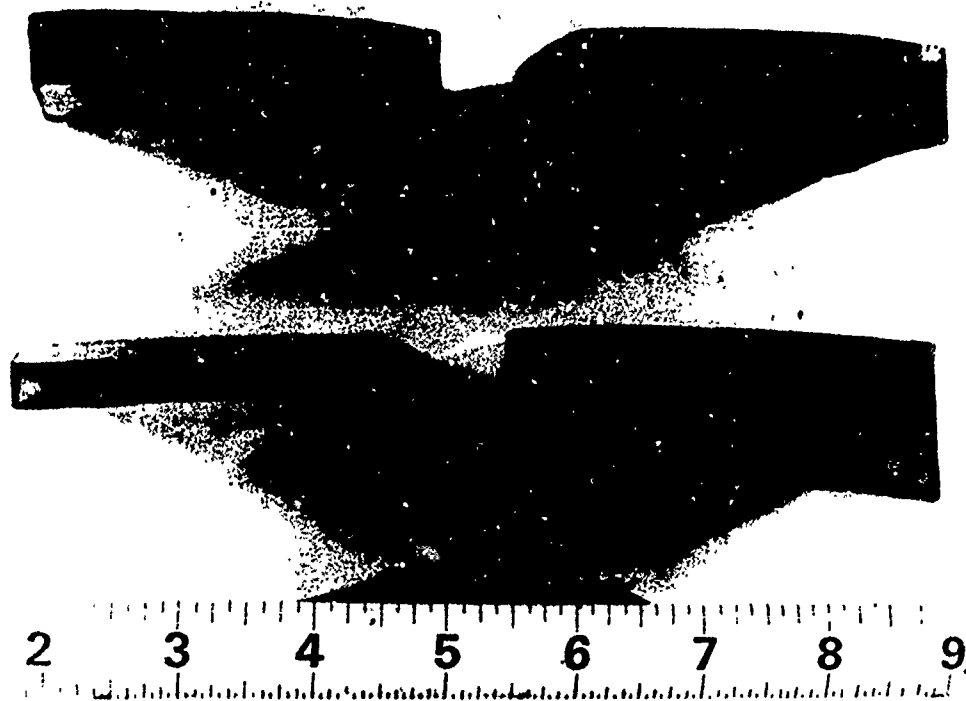


Figure 4. Ancorsteel Compacts Measuring 3 x 3 inches and Thicknesses of $1/4$, $1/2$, $3/4$ and 1 inch

Table 3. Average Properties of Green Explosively
Compacted Billets

Thickness (in.)	Weight Ratio of Explosive to Fe Powder	Sample Number	Percentage of Theoretical Density ^a (%)	Yield Point (psi)	Brinell Hardness	Percentage Reduction ^b (%)
<u>Du Pont Red Cross 40% Extra Dynamite</u>						
1/4 ^c	1.1:1	22	98.7	4593	160	2.0
	0.8:1	23	96.9	3572	146	1.6
	0.6:1	24	95.3	3367	140	1.9
1/2 ^c	1.1:1	12	98.3	5050	139	2.3
	0.8:1	11	98.1	6268	125	1.8
	0.6:1	10	94.8	4905	115	1.6
3/4 ^c	1.1:1	13	96.0	4151	119	3.2
	0.8:1	14	94.9	4154	112	2.9
	0.6:1	15	93.9	3480	111	2.0
<u>Du Pont 60% Gelatin Dynamite</u>						
1/2 ^c	1.1:1	16	98.3	4468	112	2.0
	0.8:1	17	97.1	4494	122	2.9
	0.6:1	18	96.1	3508	122	2.1
1 ^c	1.1:1	19	97.3	5682	145	4.3
	0.8:1	20	97.9	4876	126	3.6
	0.6:1	21	95.8	4473	108	4.5

Table 3 (Con't)

Thickness (in.)	Weight Ratio of Explosive to Fe Powder	Sample Number	Percentage of Theoretical Density ^a (%)	Yield Point (psi)	Brinell Hardness	Percentage Reduction ^b (%)
<u>6 in. x 6 in. Billets</u>						
1/4 ^d	1.1:1	29	96.7	5661	139	3.3
	0.8:1	30	95.8	3209	110	4.0
	0.6:1	31	96.2	2256	106	3.2
1/4 ^e	1.1:1	32	96.1	3046	98	7.7
	0.8:1	33	95.7	3690	100	6.9
	0.6:1	34	95.7	2852	103	4.8

^aMean measured corrections were of the order of $\pm 1.5\%$ of an experimentally-obtained value of 7.99.

^bPercentage reduction was defined as the strain at which a crack had propagated through the transverse sample in the thickness dimension.

^cThese billets measured 3 in. x 3 in.

^dDu Pont Red Cross 40% Extra Dynamite was used for these billets.

^eTrojan - U.S. SWP-5 was used for these billets.

by weight, it was apparent (See Figure 5) that the density decreased with increasing thickness of compact. Also, as the energy of the explosive increased the density increased. At a loading of 0.8 to 1.0 this trend was not observed. Using 40% dynamite at a loading of 1.1 to 1.0 did give the same general trend again with respect to thickness as did the 60% dynamite. However, using a 60% dynamite at the higher loading didn't have much effect as compared to using a lower energy dynamite up to compressing compacts 1/2-inch in thickness.

The relationship between hardness and loading rate was relatively good for the 3 x 3-inch compacts that had been compacted with the 40% dynamite. This relationship is shown in Figure 6. Hardness increased with increasing explosive loading with the hardness being a dependent upon the thickness. As the thickness increased the hardness decreased. With the 60% dynamite the hardness of the 1-inch thick billets increased whereas those of the 1/2-inch decreased. In making a comparison at the lowest loading ratio of 0.6 to 1.0 the same general trends were present for the hardness that prevailed for the density.

Results of the diametral tests did not correspond to the densities or hardness. Although the strength generally increased with increased amount of explosive, particularly at the lower loadings, there was no general trends with respect to billet thickness as can be seen by an inspection of Figure 7.

In scaling up the compact size to 6 x 6 x 1/4-inches the first observation was that the density remained fairly uniform irrespective of amount or type of explosive as an inspection of Table 3 indicates. All of the green densities were on the order of 96 percent of theoretical. Increasing the loading of the 40% dynamite did increase both the strength and the hardness as is shown

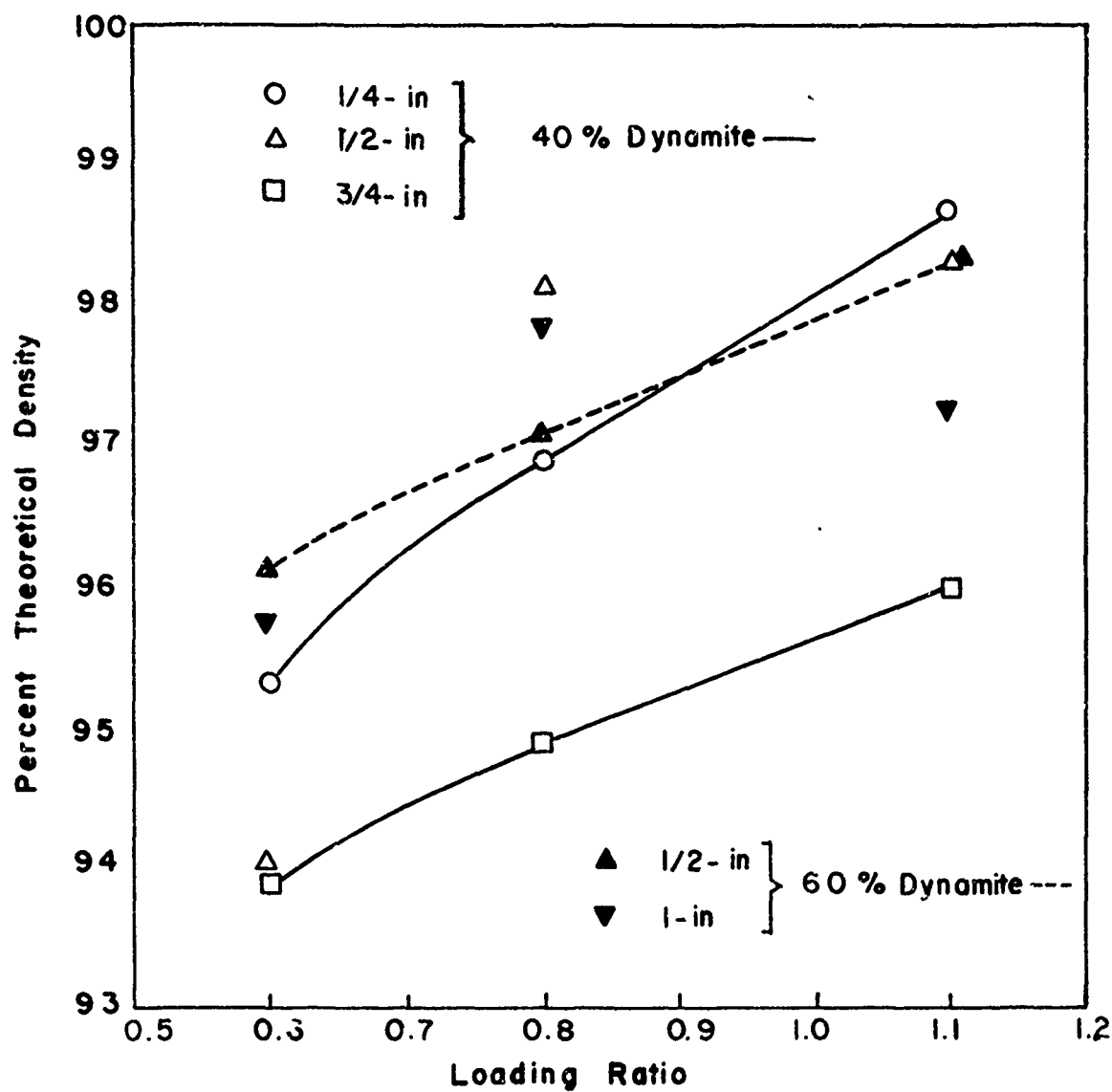


Figure 5. Percent Theoretical Density Obtained with 3 x 3 - inch Compacts as a Function of Loading Ratio of Explosive to Ancorsteel 1000 Powder.

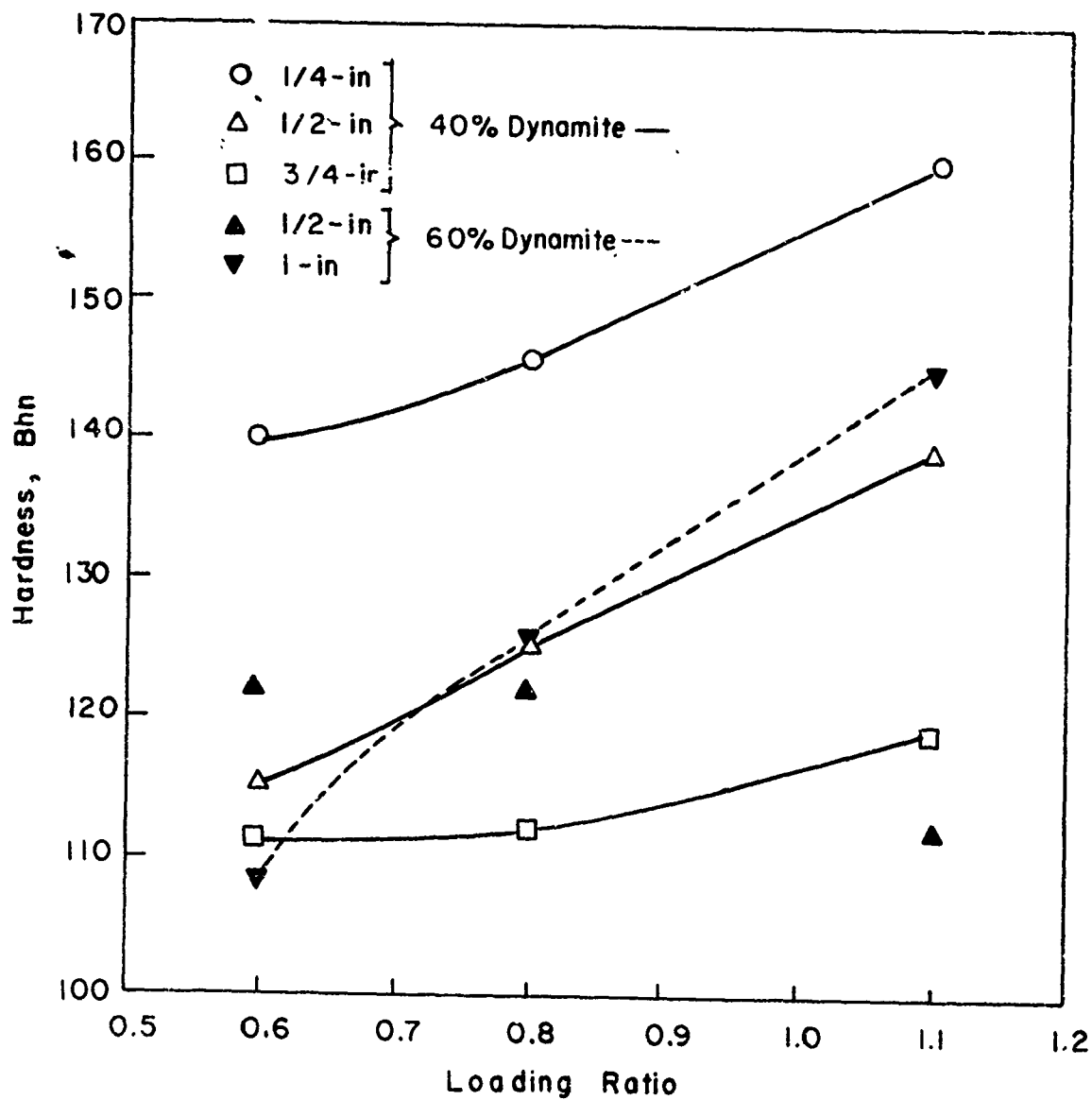


Figure 6. Hardness as a function of ratio of explosive to Annealed 1000 Powder for 2 x 3-Inch Compacts.

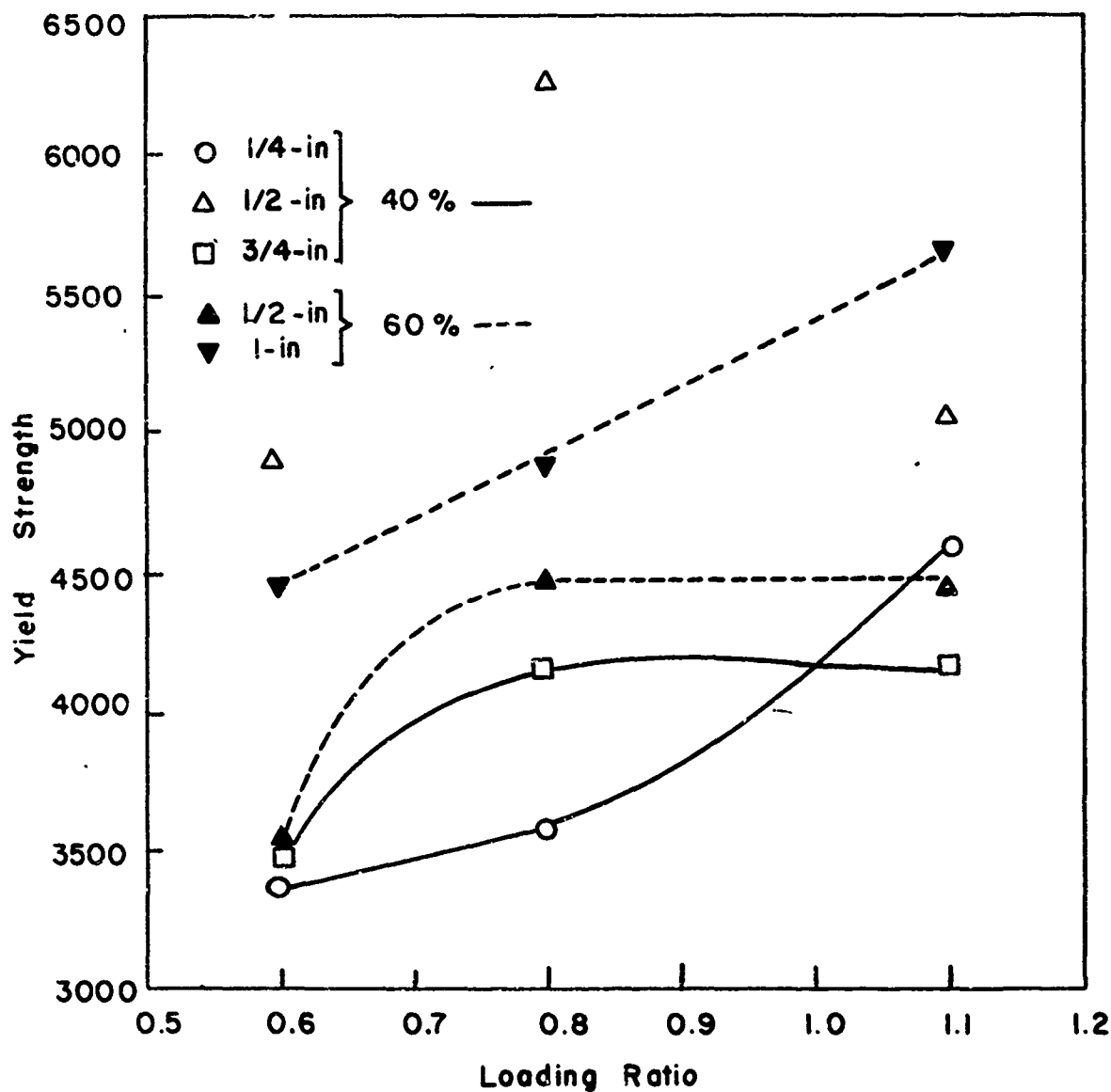


Figure 7. Diametral Yield Strength as a Function of Ratio of Explosive to Ancorsteel 1000 Powder for 3 x 3-inch Compacts.

in Figure 8. No correlation could be made with the billets compacted with Trojan SWP-5 powder.

In comparing the properties of the explosively compacted billets with compacts made by the conventional pressing at the recommended load of 30.5 tsi, several observations could be made. The average density of the conventionally pressed material was 84.8 percent of theoretical which was well below that obtained in any of the explosively loaded compacts.

The average hardness of the conventionally compacted Ancorsteel powder was 52 Bhn with the range being from 33 to 66 Bhn. A minimum hardness of 98 Bhn was noted in the explosively compacted powders with the maximum being 160. This was a two to threefold increase in hardness as would be anticipated by not only the higher densities but also the larger amount of strain introduced into the explosively compacted billets.

An average yield strength of 1615 psi was obtained for the conventionally compacted billets. A minimum of 2256 and a maximum of 6268 psi diametral yield strength was obtained by explosive compaction. The higher strengths can be related to the greater degree of compaction obtained by explosive compaction and would be a beneficial aspect in handling of green compacts.

The conventional sintering temperature for Ancorsteel 1000 compacts is 2050°F for one hour. A series of specimens from the 6 x 6 x 1/4-inch billets compacted with SWP-5 dynamite at an explosive to powder ratio of 0.8:1.0 were isothermally sintered in hydrogen for various periods of time. The results of the isothermal sintering treatments are presented in Table 4. The explosively compacted material had an original hardness of 100 Bhn, while that of a conventionally compacted billet was 40 Bhn. The change in hardness as a function of time at 2050°F is presented in Figure 9. A dramatic

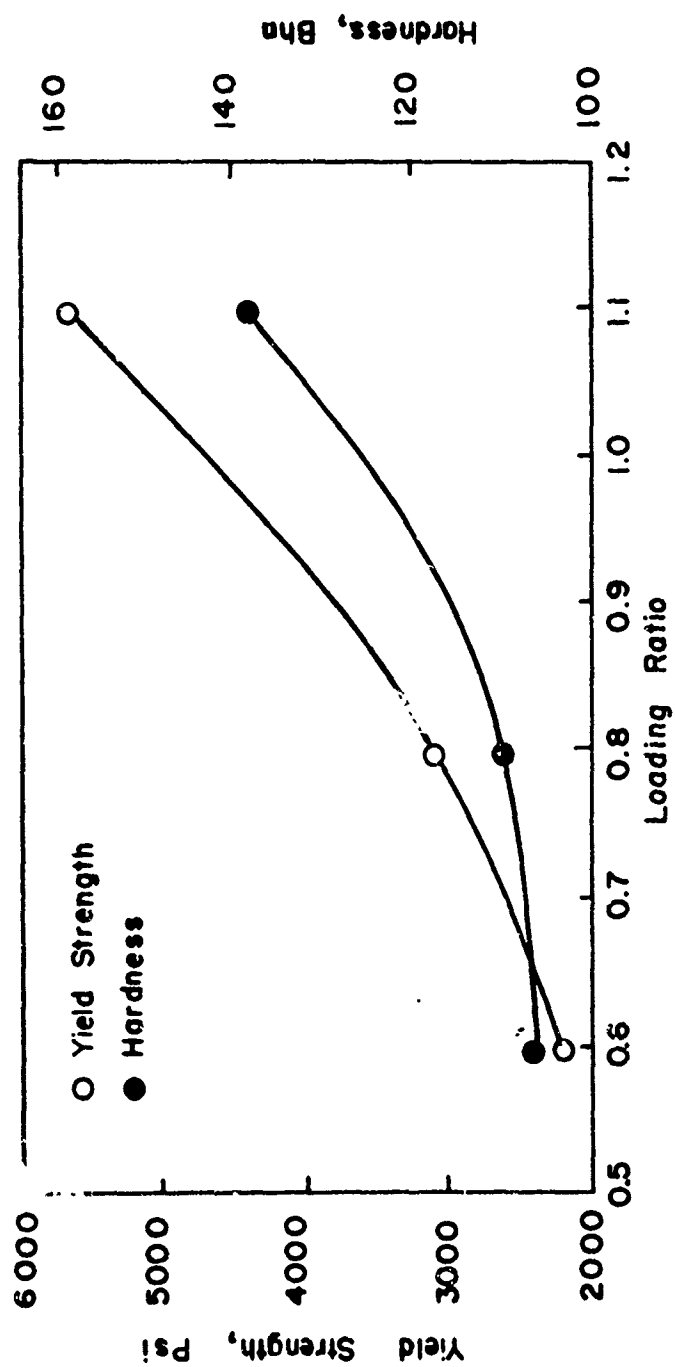


Figure 8. Hardness and Diametral Yield Strength for 6 x 6 x 1/4-inch Billets as a Function of Increasing Ratio of 40% Dynamite to Ancorsteel 1000 Powder.

Table 4. Physical Properties of Green and Sintered Iron Powder Billets Explosively and Conventionally Compacted

Weight Ratio of Explosive to Powder	Sinter ^c Time (hr.)	Percentage of Theoretical Density, Green (%)	Percentage of Theoretical Density, Sintered (%)	Difference Between Percentages of Green and Sintered Densities	Average Sintered Hardness, Bhn	Rolling Reduction ^a after Sintering, %
Billet 33, 6 in. x 6 in. x 1/4 in.						
0.8:1	0.25	96.3	95.5	- 0.8	67	16.4
	0.5	95.8	94.8	- 1.0	60	4.1
	0.75	96.7	96.1	- 0.6	63	18.2
	1.0	94.7	96.1	+ 1.4	75	4.0
	1.5	95.4	96.1	- 0.3	58	38.2
	2.0	96.5	96.0	- 0.5	62	9.4
	3.0	96.7	96.4	- 0.3	62	18.2
	6.0	95.4	96.3	+ 0.9	32	27.5
Conventional Compaction, 1 in. Diameter						
20.5 tsi	0.25	85.0	84.9	- 0.1	42	48.6
	0.50	86.0	85.8	- 0.2	43	52.4
	0.75	86.4	85.9	- 0.5	45	33.2
	1.0	85.5	83.1	- 2.4	42	20.7

Table 4 (Con't)

Weight, Ratio of SWP-5 Explosive to Fe Powder	Sinter ^c Time (hr.)	Percentage of Theoretical Density, Green (%)	Percentage of Theoretical Density, Sintered (%)	Difference Between Percentages of Green and Sintered Densities	Average Sintered Hardness, Bhn	Rolling Reduction after Sintering, % ^a
	1.5	84.7	84.5	- 0.2	41	50.5
	2.0	84.3	84.3	0	38	44.7
	3.0	84.9	83.4	- 1.5	39	53.4
	6.0	83.6	82.4	- 1.2	44	48.6
Hoeganaes Corporation Quality Control Tests						
Lot 29	0.5	85.1	85.0	- 0.1	--	10.5 ^b
Lot 83	0.5	85.1	85.1	0	--	7.2 ^b

^aPercentage reduction is measured at the time at which cracking has propagated through the sample in the thickness dimension.

^bThis figure is actually percentage elongation.

^cSintered at 2050°F.

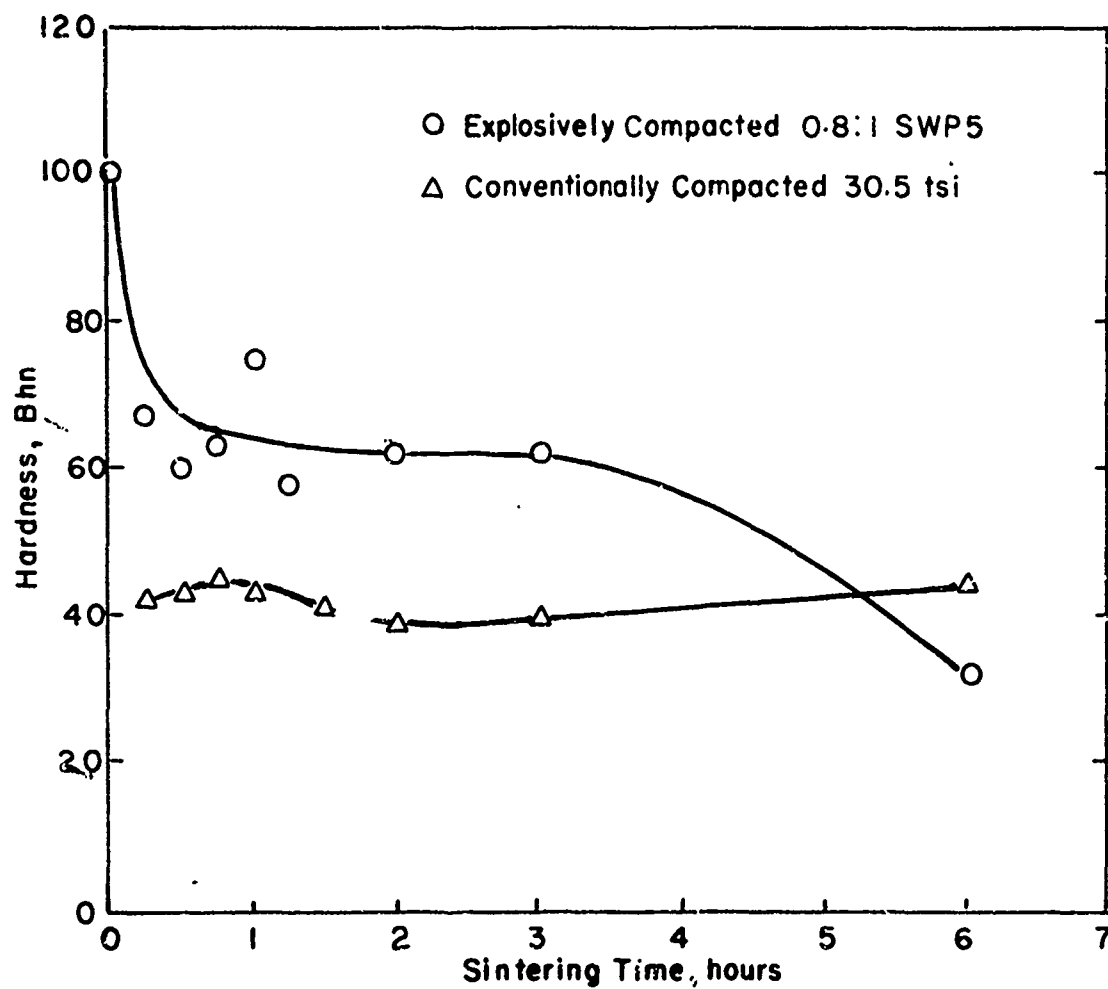


Figure 9. Hardness as a Function of Sintering Time at 2010°F for Explosively and Conventionally Compacted Ancorsteel 1000

drop in hardness is noted for the explosively compacted material after only 15 minutes at temperature after which a gradual decrease occurs up to 3 hours followed by a more rapid rate of decrease at 6 hours. The hardness of the conventionally compacted material does not show any dramatic change in hardness over the same period (6 hours).

Since one of the applications for the flat compacts is in rolling preforms, specimens were rolled after the isothermal sintering treatments to determine the amount of deformation the specimens would undergo. Figure 10 is a comparison of conventionally and explosively compacted specimens subjected to sintering at various times at 2050°F then cold rolled until cracked through the specimen. For both types of specimens a gradual increase in the amount of reduction in thickness occurs with increasing sintering times. The gradual increase in resistance to failure for the conventionally compacted specimens corresponds to the increase in hardness noted in sintering and the decrease in density (Table 4).

The explosively compacted specimens do not show any relationship between the decrease in hardness and the resistance to cracking during rolling. Also, the density of the explosively compacted specimens is relatively uniform throughout the various times at temperature. The indication is then that as the degree of sintering increases the resistance to failure also increases. The conventional compacted specimens are more resistant to failure since the density is considerably lower and thus able to sustain more deformation.

This is borne out by the metallographic examination carried out on the specimens sintered at 2050°F for various time periods and presented in Figures 11 through 16. In Figures 11 and 12 the as compacted specimens are shown. The conventionally compacted specimens have a great deal of porosity,

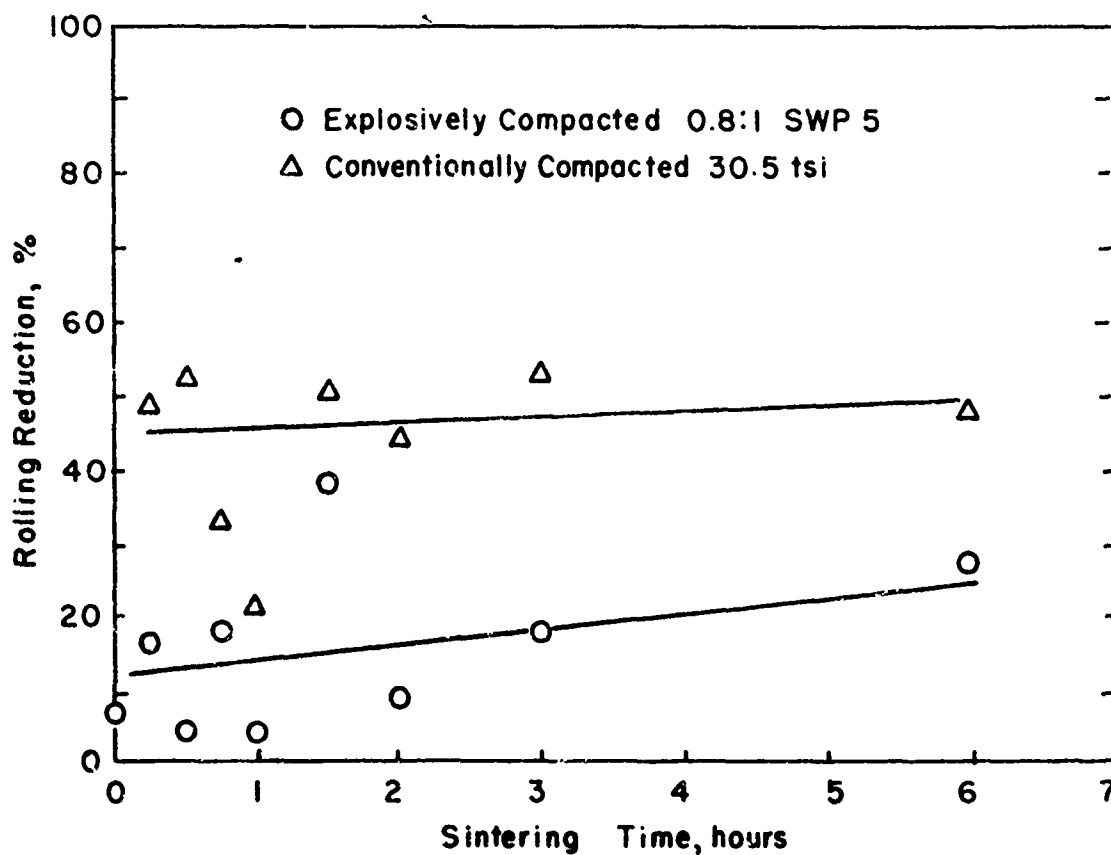
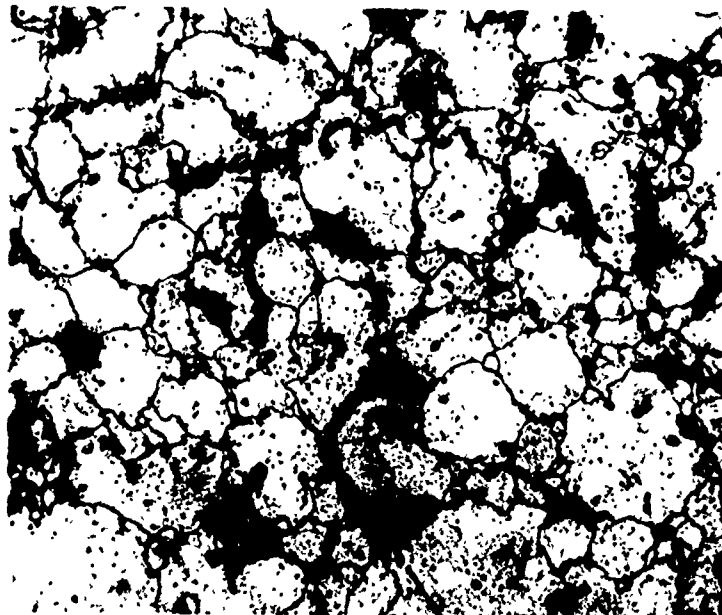


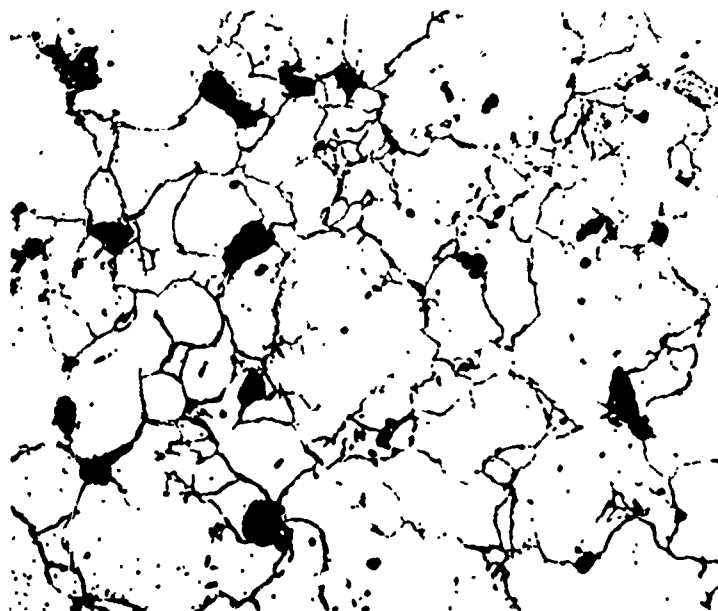
Figure 10. Results of Rolling Tests Relating Sintering Time at 2050°F to Amount of Reduction for Complete Cracking



As Polished

200X

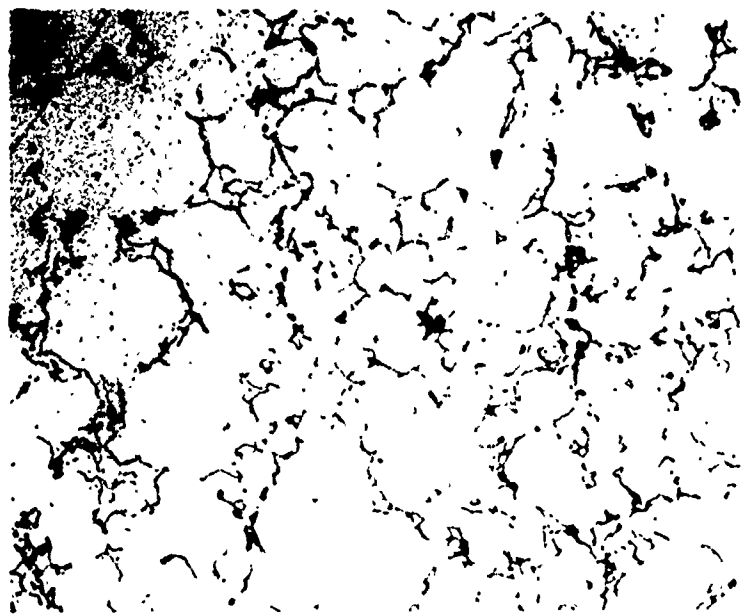
Figure 11. Green Conventionally Compacted Specimen
Showing Large Volume of Voids



As Polished

200X

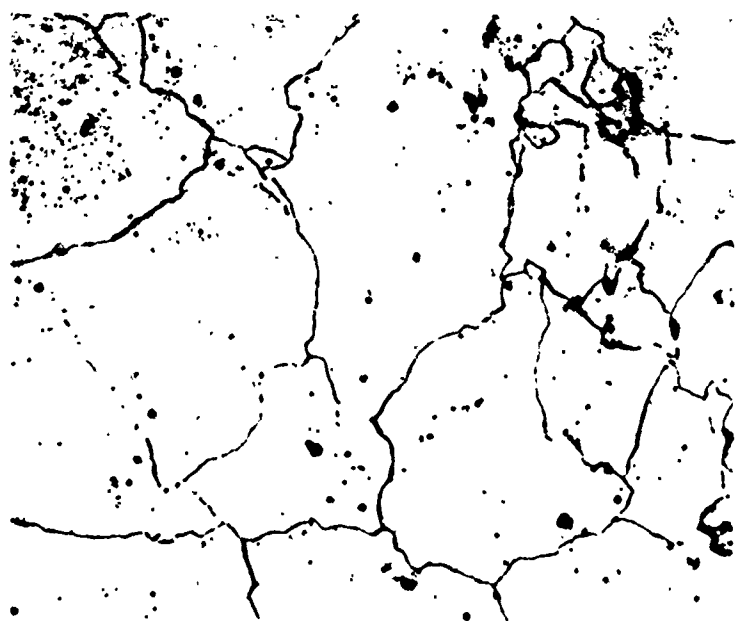
Figure 12. Green Explosively Compacted Specimen
Showing Relatively Small Amount of Porosity
(1.1:1 SWP-5)



As Polished

200X

Figure 13. Conventionally Compacted Specimen Sintered
One Hour at 2050°F



As Polished

200X

Figure 14. Explosively Compacted Specimen Sintered
One Hour at 2050°F (1:1:1 JWP-5)

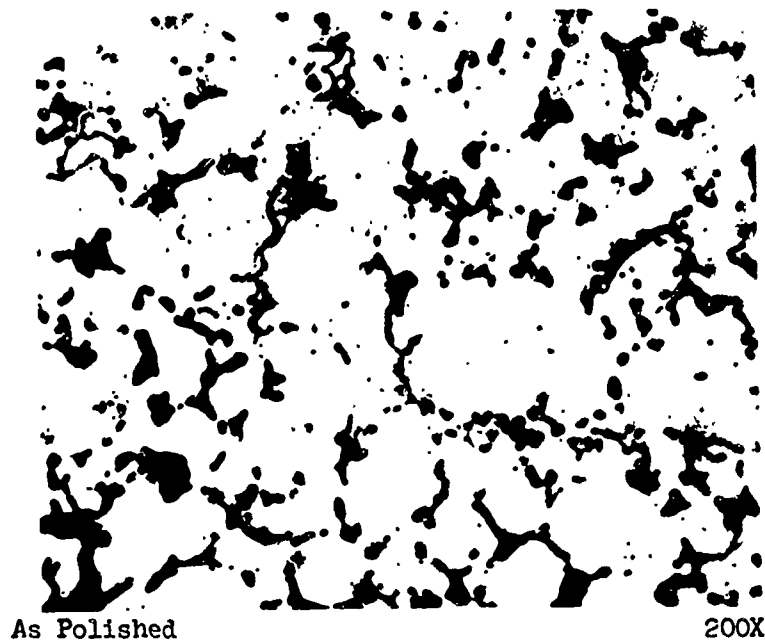


Figure 15. Conventionally Compacted Specimen Sintered
Twelve Hours at 2050°F

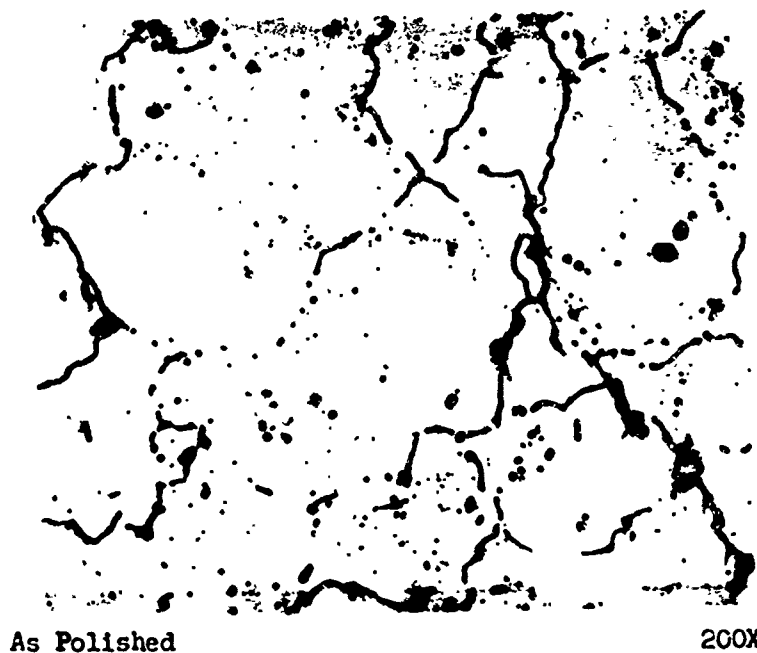


Figure 16. Explosively Compacted Specimen Sintered
Twelve Hours at 2050°F

whereas the explosively compacted specimens show relatively small amounts of porosity.

After sintering for one hour at 2050°F (Figure 15) the conventionally compacted specimen has developed coalescence of voids and started grain growth. In the explosively compacted material grain growth has progressed substantially more than in the conventionally compacted material. The hardness after one hour of the explosively compacted material is greater than the conventionally compacted specimens since annealing is not as great for the explosively compacted material. Also the porosity is lower. The finer grain size, greater porosity, and lower hardness of the conventionally compacted specimens allow greater deformation during rolling.

Sintering for greater periods of time at 2050°F does not substantially reduce the grain size of the explosively compacted specimens (See Figure 16). However, void collapse and coalescence does occur in the conventionally compacted Ancorsteel 1000 as is shown in Figure 15. The grain size is not substantially different than after one hour at 2050°F. The large amount of porosity in the conventionally compacted specimen allows greater deformation during rolling before the onset of cracking. The tests also show the sintering is essentially complete after one hour for the explosively compacted specimens with the main difference after that time being a gradual softening of the compact. After one hour at 2050°F grain bonding is still occurring in the conventionally compacted specimens still to be followed by void collapse and coalescence.

A series of sintering tests were conducted at various temperatures for one hour on both conventionally and explosively compacted specimens. In these tests the two explosive compaction conditions were used; (1) loading of

1/4-inch 6 x 6 compacts at a ratio 1.1:1 of SWP-5 to Ancorsteel powder and (2) a loading of 0.6:1. As can be seen from Table 3 very little difference was present in the green properties of the explosively loaded compacts.

The results of the isochronal sintering tests are presented in Table 5. For both types of compacts, explosive or conventional, there is an increase in hardness at a sintering temperature of 800°F. This can be attributed to a minor amount of grain bonding. As the temperature is increased the hardness decreases for both types of compacts as is shown in Figure 17. The hardness level is fairly stable after 1400°F for the conventionally compacted specimens. The hardness of the explosively compacted Ancorsteel still is decreasing up to about 2000°F.

Metallographic examinations at various temperatures do show that the explosively compacted specimens sinter more rapidly and at lower temperatures than the conventionally compacted specimens.

At a sintering temperature of 800°F very little difference is present between the as-compacted condition and after one 800°F for both types of compacts as a comparison of Figures 12 and 13 and Figures 18 and 19 shows. Sintering for one hour at 1400°F does result in some grain bonding of the conventionally compacted specimens as is shown in Figure 20. Actual grain coalescence and grain growth of the smaller particles has started at a temperature of 1400°F in the explosively compacted steel as an inspection of Figure 21 indicates. At 2050°F sintering is essentially complete in the explosively compacted specimens as mentioned previously. Grain bonding has occurred in the conventionally compacted specimens but void collapse and coalescence has not started to any great extent.

Table 5. Physical Properties of Green and Sintered Isochronally for One Hour
 Anomalous 1000 Iron Powder Billets Explosively and Conventionally
 Compacted

Weight Ratio of SWP-5 Explosive to Fe Powder	Sinter Temperature (°F)	Percentage of Theoretical Density, Green (%)	Percentage of Theoretical Density, Sintered (%)	Difference Between Percentages of Green and Sintered Densities	Average Brinell Sintered Hardness	Rolling Reduction after Sintering, % ^a
Billet 32, 6 in. x 6 in. x 1/4 in.						
1.1:1	800	96.3	93.4	- 2.9	139	5.9
	1000	96.9	94.6	+ 2.2	120	3.6
	1200	95.4	94.3	- 1.1	92	7.2
	1400	96.6	94.7	- 1.9	75	4.3
	1600	96.2	95.7	- 0.5	77	8.5
	1800	95.0	94.4	- 0.6	68	10.8
	2050	94.9	97.5	+ 2.6	54	18.5
	2200	97.5	96.9	- 0.6	55	16.5
	2400	97.1	96.4	- 0.7	64	42.5

Table 5 (Con't)

Weight Ratio of SWP-5 Explosive to Fe Powder	Sinter Temperature (°F)	Percentage of Theoretical Density, Green (%)	Percentage of Theoretical Density, Sintered (%)	Difference Between Percentages of Green and Sintered Densities	Average Brinell Sinter Hardness	Rolling Reduction after Sintering, % ^a
<u>Billet 3/4, 6 in. x 6 in. x 1/4 in.</u>						
0.6:1	800	97.0	95.7	- 1.3	131	5.5
	1000	95.5	94.9	- 0.6	124	7.1
	1200	97.3	95.3	- 1.5	84	7.1
	1400	96.3	94.5	- 1.8	64	9.8
	1600	97.2	95.9	- 1.3	73	11.1
	1800	96.6	96.1	- 0.5	76	20.8
	2050	95.1	96.6	+ 1.5	62	23.3
	2200	96.3	95.9	- 0.4	72	38.0
	2400	96.6	95.5	- 1.1	67	69.3

Table 5 (Con't)

Weight Ratio of SWP-5 Explosive to Fe Powder	Sinter Temperature (°F)	Percentage of Theoretical Density, Green (%)	Percentage of Theoretical Density, Sintered (%)	Difference Between Percentages of Green and Sintered Densities	Average Brinell Sintered Hardness	Rolling Reduction after Sintering, % ^a
<u>Conventional Compaction, 1 in. Diameter</u>						
30.5 tsi	800	83.2	82.0	- 1.2	64	0.5
	1000	83.4	82.5	- 0.9	44	1.0
	1200	82.4	81.1	- 1.3	40	6.0
	1400	82.8	80.4	- 2.4	37	13.4
	1600	84.5	81.8	- 2.7	40	36.1
	1800	85.2	83.7	- 1.5	39	43.9
	2050	85.5	83.1	- 2.4	42	20.7
	2200	83.3	80.4	- 2.9	34	42.6
	2400	84.1	80.6	- 3.5	35	53.5

^aPercentage reduction is measured at the time at which cracking has propagated through the sample in the thickness dimension.

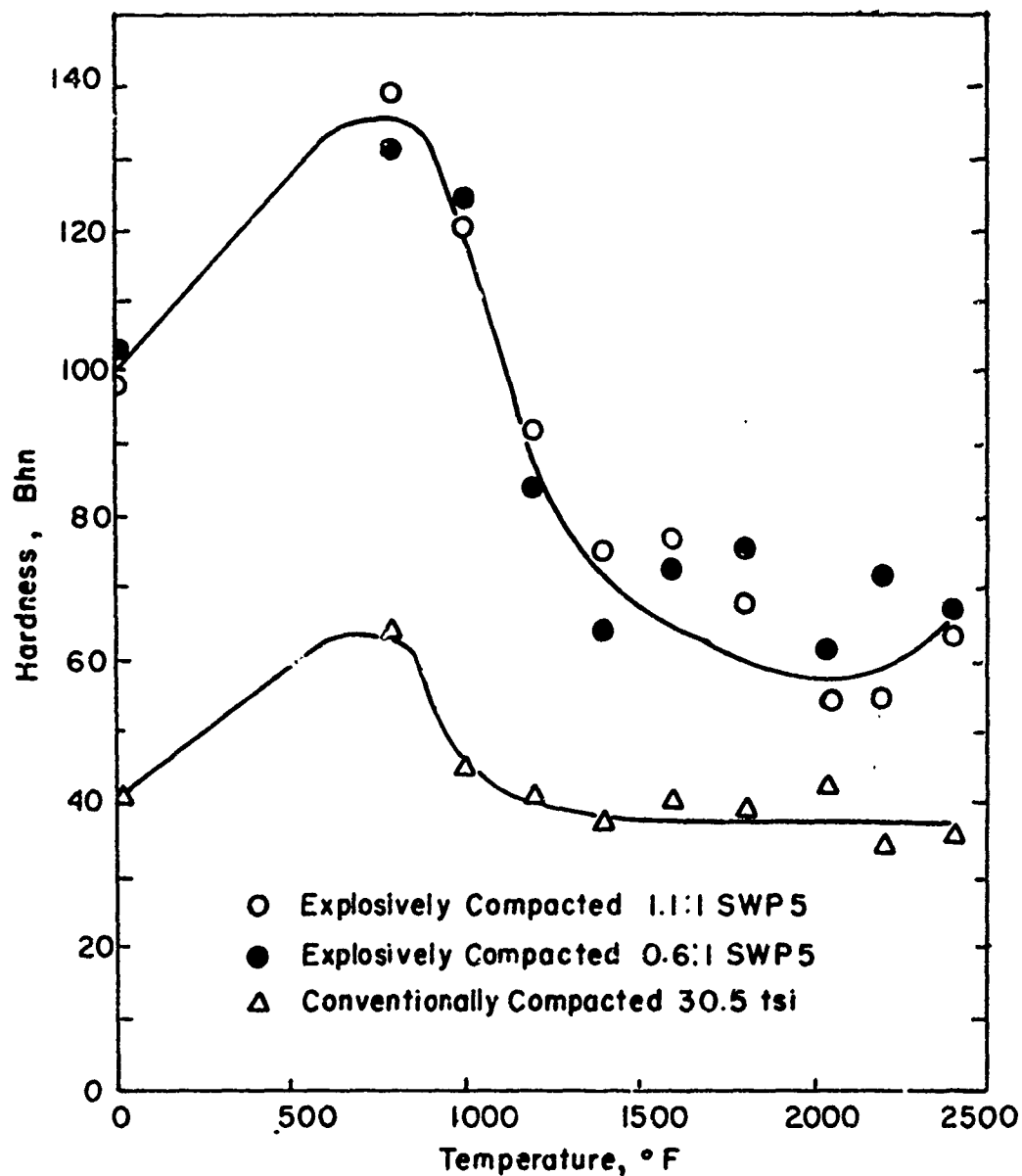
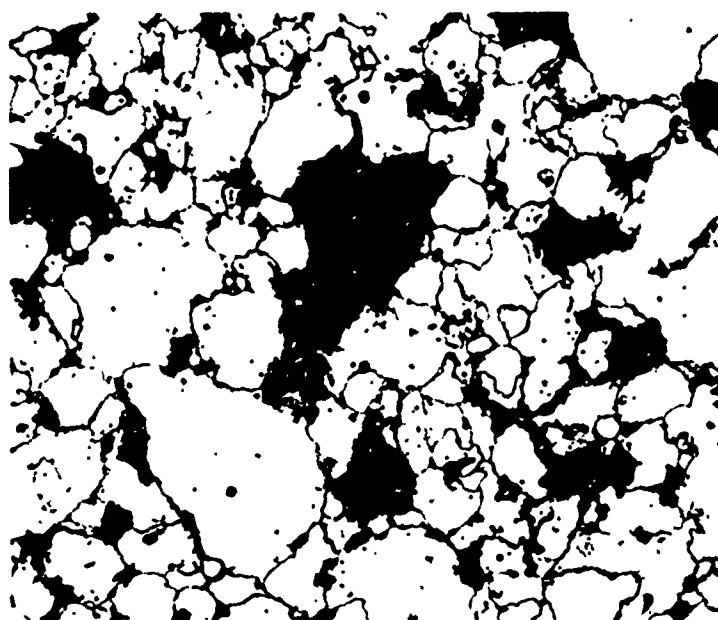


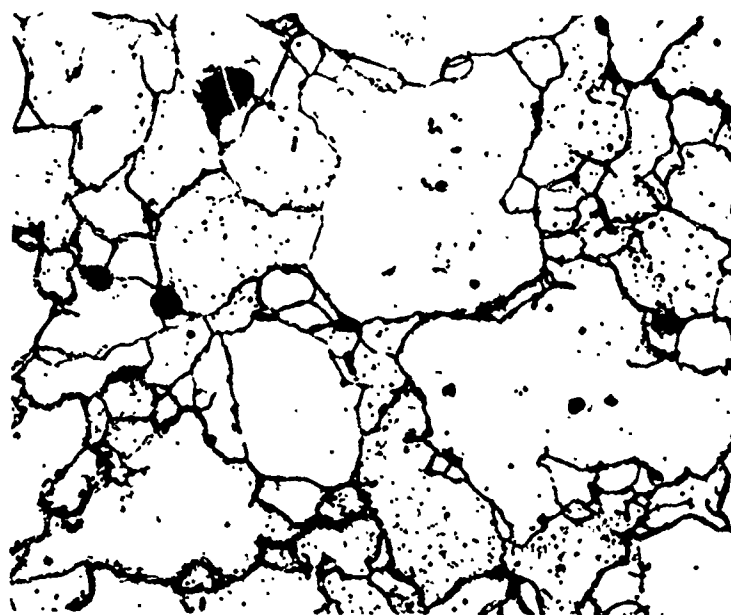
Figure 17. Hardness as a Function of Sintering Temperature for One Hour for Explosively and Conventionally Compacted Ancorsteel 1000



As Polished

200X

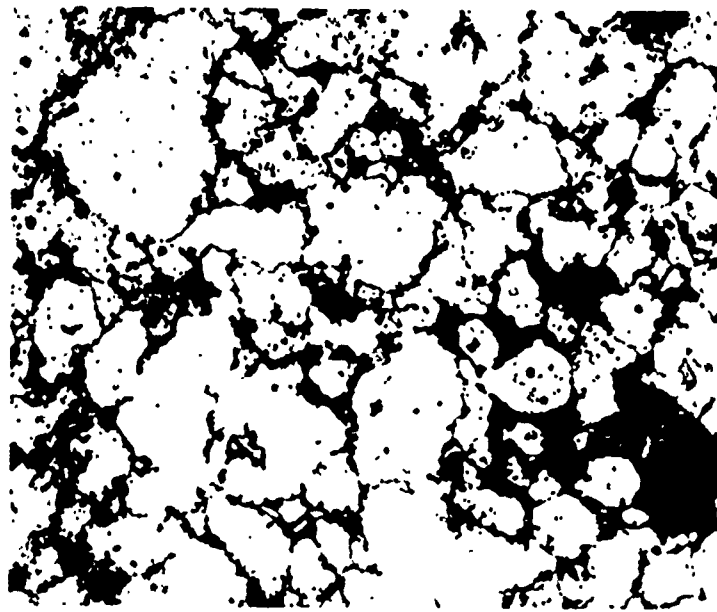
Figure 18. Photomicrograph of Conventional Compacted Ancorsteel after One Hour at 800°F



As Polished

200X

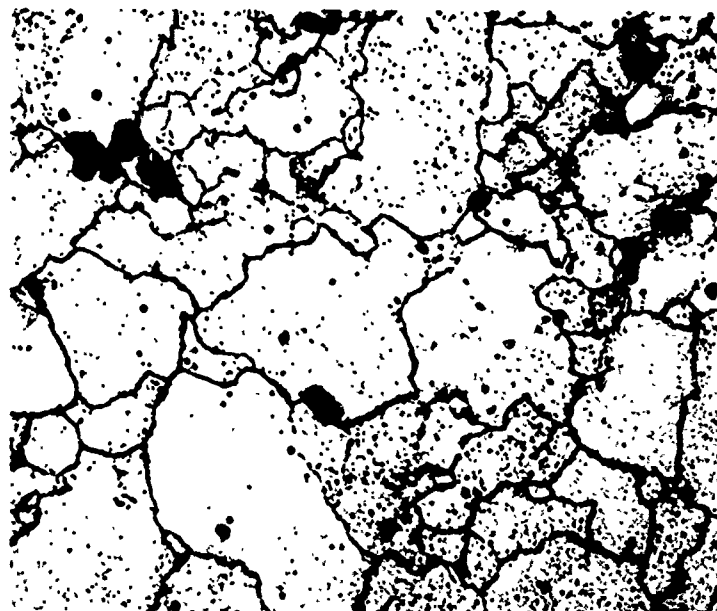
Figure 19. Photomicrograph of Explosively Compacted Ancorsteel after One Hour at 800°F



As Polished

200X

Figure 20. Photomicrograph of Conventionally Compacted Ancorsteel after One Hour at 1400°F



As Polished

200X

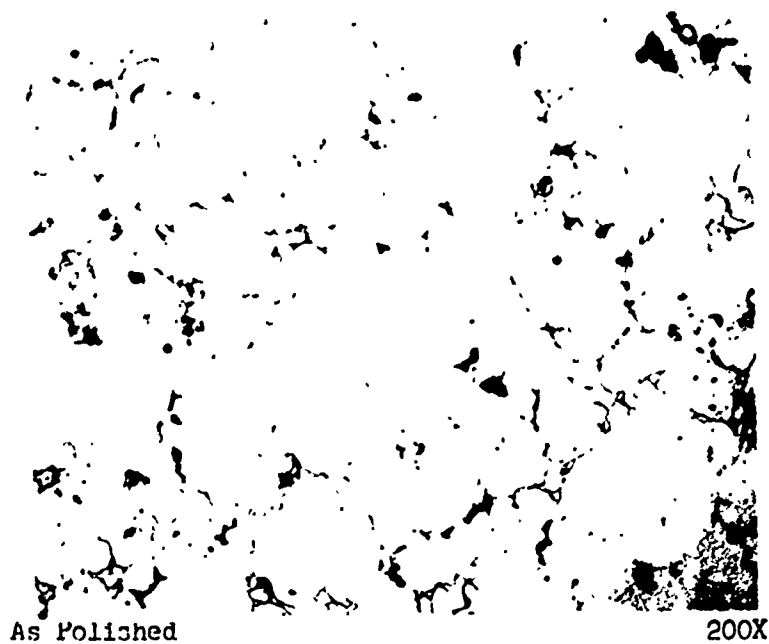
Figure 21. Photomicrograph of Explosively Compacted Ancorsteel after One Hour at 1400°F

Sintering at 2400°F for one hour results in further collapse and coalescence of the voids in the conventionally compacted specimens as is shown in Figure 22. Grain growth has progressed more in the explosively compacted Ancorsteel sintered at 2400°F as compared to the 2050°F counterpart (See Figure 23).

There is a difference in the response to cold rolling between an isothermal sintering treatment at 2050°F and an isochronal treatment. Figure 24 shows the percent reduction before cracking as a function of raising the sintering temperature. At a temperature of 2400°F very little difference is present irregardless of mode of compaction. Compacts sintered at 2200°F do show that the conventionally compacted steel has more resistance to failure during cold rolling than the explosively compacted steel. Again the lower initial hardness, smaller grain size and porosity would account for the fact that the conventionally compacted material can be subjected to greater deformation.

Conclusions

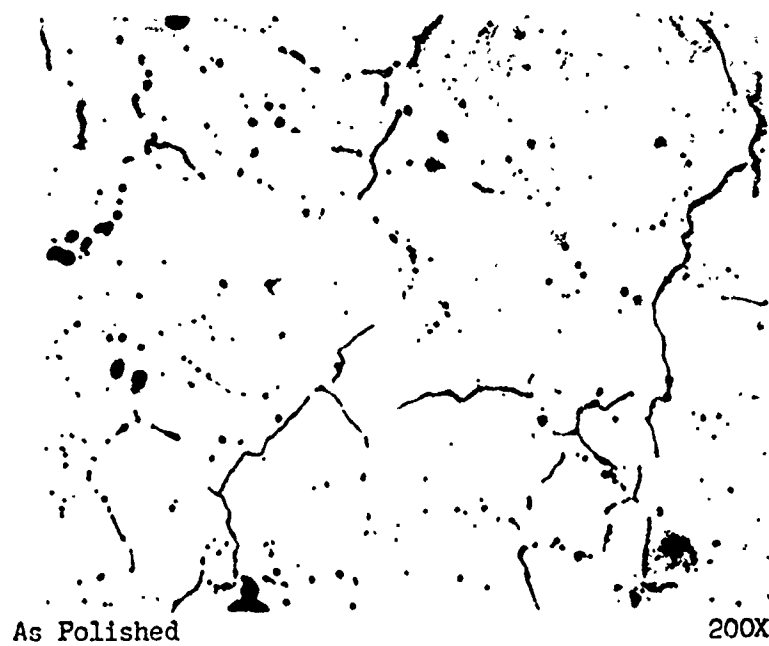
Explosive compaction of Ancorsteel 1000 iron powder results in much higher green densities than can be achieved by the standard pressing pressure of 30.5 tsi. Although there was some variation and scatter in the data, some general trends can be established. First with an increasing amount of explosive the density of the green compact will increase. The practical limitation on green density appears to be within 96 to 98 percent of theoretical. Hardness and strength of the green explosively compacted steel also increases with increasing amount of explosive. Using an explosive with higher energy of detonation also increased the hardness, density and strength at a given weight of explosive. In general the green hardness and strength of the explosive



As Polished

200X

Figure 22. Photomicrograph of Conventionally Compacted Ancorsteel after One Hour at 2400°F



As Polished

200X

Figure 23. Photomicrograph of Explosively Compacted Ancorsteel after One Hour at 2400°F

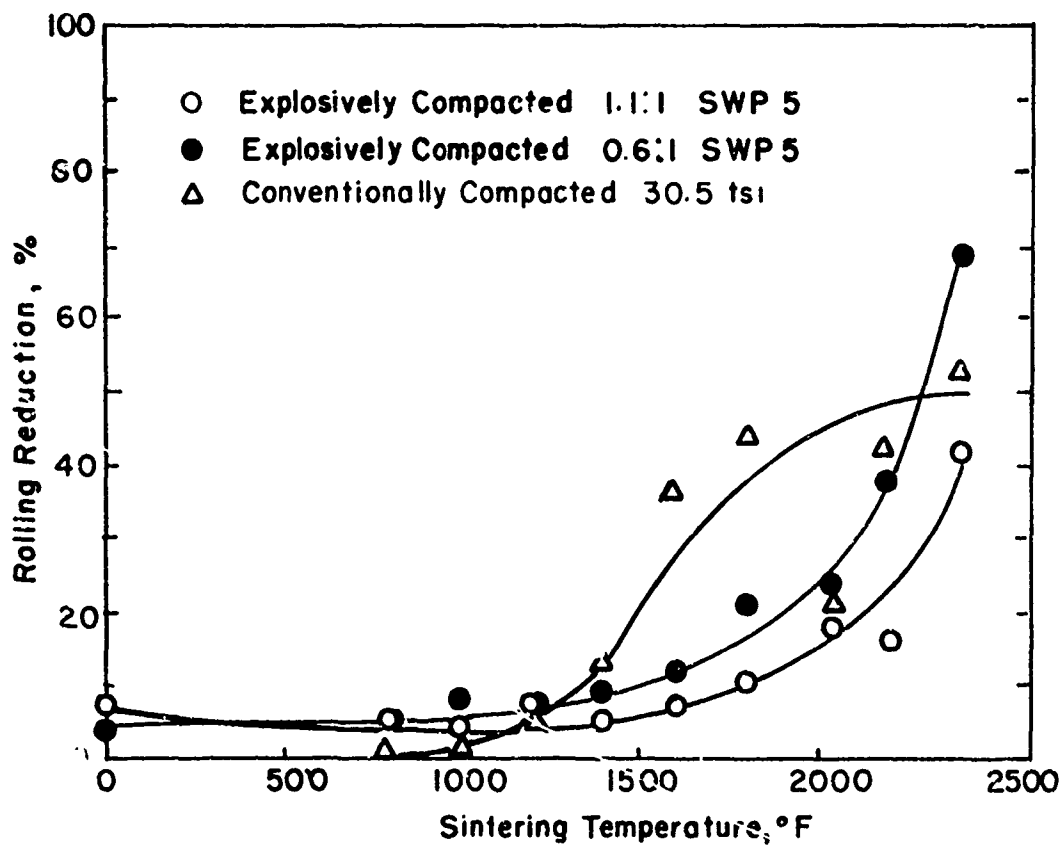


Figure 24. Effect of Sintering Temperature on the Ability of Conventionally and Explosively Compacted Ancorsteel 1000 to be Cold Rolled

compacts are considerably greater than that of conventionally compacted Ancorsteel 1000 iron powder.

The higher degree of grain bonding and higher density of explosively compacted Ancorsteel promotes a faster response to sintering with respect to grain growth and coalescence of voids at a given temperature. Sintering can occur at a lower temperature in explosively compacted Ancorsteel to achieve grain growth and porosity coalescence.

Explosive compaction introduces more strain hardening into the Ancorsteel than conventional pressing. This is manifested by the initial green hardness and the longer time required to reduce the hardness. Although the conventionally compacted specimens are more resistant to cracking during cold rolling, after sintering this situation can be attributed to the finer grain size, greater porosity and generally lower hardnesses of the conventionally compacted specimens. If a great deal of deformation is required after explosive compaction for a rolling preform, the sintering temperature can be raised to give results comparable to conventionally compacted specimens.

Explosive compaction of rolling preforms of Ancorsteel 1000 appears to be a feasible method of making large billets that have acceptable properties both in the green and sintered states.

DEVELOPMENT OF EXPLOSIVELY COMPACTED TUNGSTEN FILAMENT

REINFORCED STEEL COMPOSITES

This study was concerned with the development of procedures for making explosively compacted metal filament reinforced metal composites. The basic model that was selected was tungsten filaments and iron powder. Tungsten filaments are readily available and have high strength at elevated temperatures.

Ancorsteel 1000 iron powder was used. The properties of the iron powder were presented in the previous section. Du Pont 40% Red Cross Extra dynamite was used in this program. Again the characteristics of this explosive were presented in the previous section.

The ultimate aim of the program is to develop techniques for fabricating most any combination of filament-metal composite. The basic tungsten filament-steel powder composite has many variables and problems associated with it that in solving these problems can lead to numerous other systems. First, the difference in dynamic acoustic impedance of the two materials is large. Steel has an acoustic impedance on the order of 39×10^5 g/cm²/sec, whereas that of tungsten is on the order of 85×10^5 g/cm²/sec. This large disparity in acoustic impedance leads to rarefaction waves in the steel between layers that are tensile in nature and can be great enough to cause splitting or fracture of the compact.

Second, a disparity exists in the coefficient of linear thermal expansion of the two materials. The coefficients are 11.76 and 4.6 micro-in./in./°C for the steel and tungsten, respectively. On sintering the steel matrix expands at a rate of almost 2.5 times that of the tungsten. Again on sintering the stresses developed between the two metals can lead to problems of distortion and fracture.

Tungsten is relatively hard compared to the steel powder which allows flow around the tungsten filament but is not conducive to bonding. The high hardness of the tungsten which is indicative of high strength and low ductility can lead to cracking of the filament during compaction.

The problems associated with development of a compaction system for the tungsten-steel composite led to the selection of this system as a model.

Systems in which a similarity exists in dynamic physical and mechanical properties would be easier to work with, but eventually the type of problems presented above would have to be solved for composite systems.

Experimental Procedures

The experimental system used to date has consisted of a double piston arrangement into which is fitted a frame for holding the filaments. An exploded sketch of this system is shown in Figure 25. A sketch of the filament-powder frame is shown in Figure 26. This die was made from mild steel and is held together with four 1-inch diameter bolts.

The filaments are wound on two frames simultaneously and as each layer is finished the wires are glued with Duco cement. A spacer is inserted and then the next layer is wound. Spacings between the 0.005 inch wire have been 0.01 inch on the horizontal plane and 0.02 inches on the vertical plane. A micrometer screw is used to advance the wire the proper distance for each winding.

After the frame is wound, the bottom piston is inserted and positioned. The piston is glued in place using an epoxy resin. The desired amount of iron powder is added and the top piston inserted and glued in place. In some cases, the whole assembly is then vibrated to insure that the iron powder is around the wires. Various times and amplitudes have been used in the vibrating step of the operation.

Precompaction of the iron powder has been used in some instances to prevent segregation of the powder after vibration. Pressures of 25,000 to 50,000 psi have been used for precompaction. Experiments have been conducted in which neither vibration or precompaction was used.

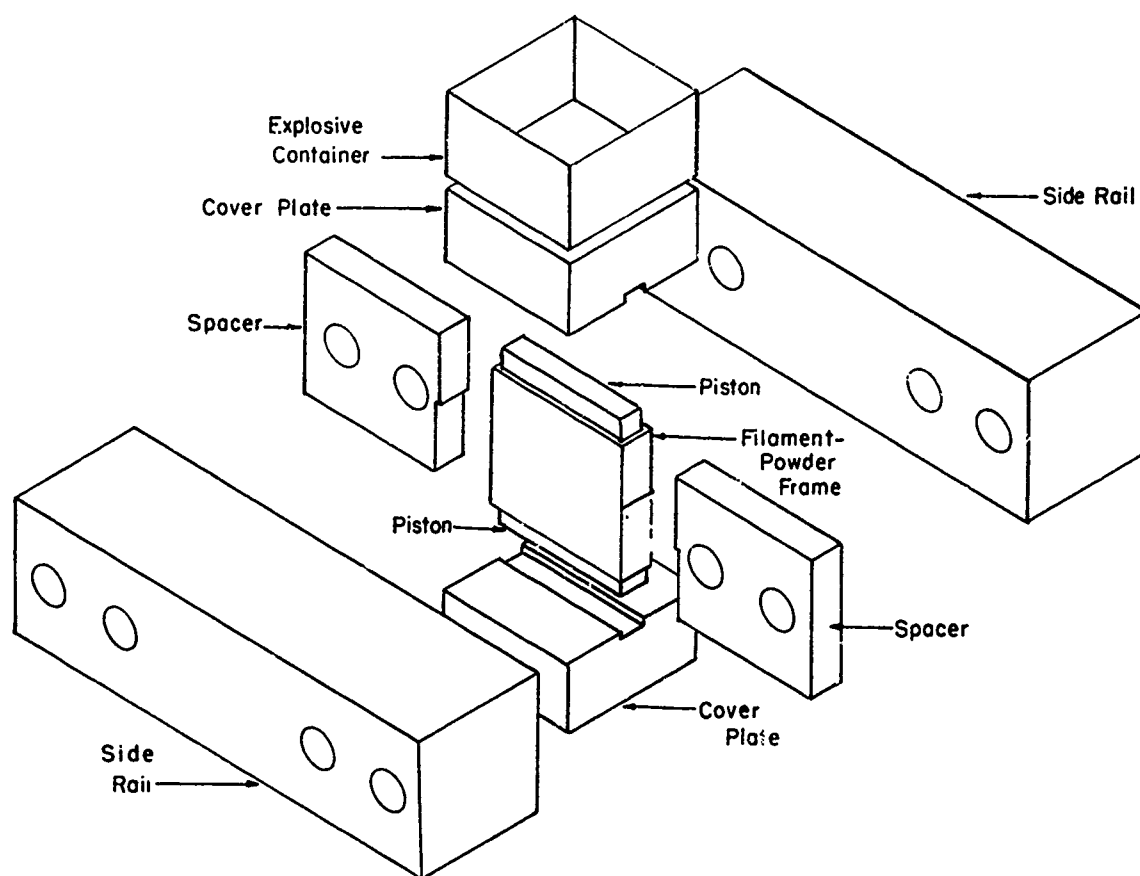


Figure 25. Sketch of Exploded View of Double Piston Arrangement Used to Compact Steel-Tungsten Composites

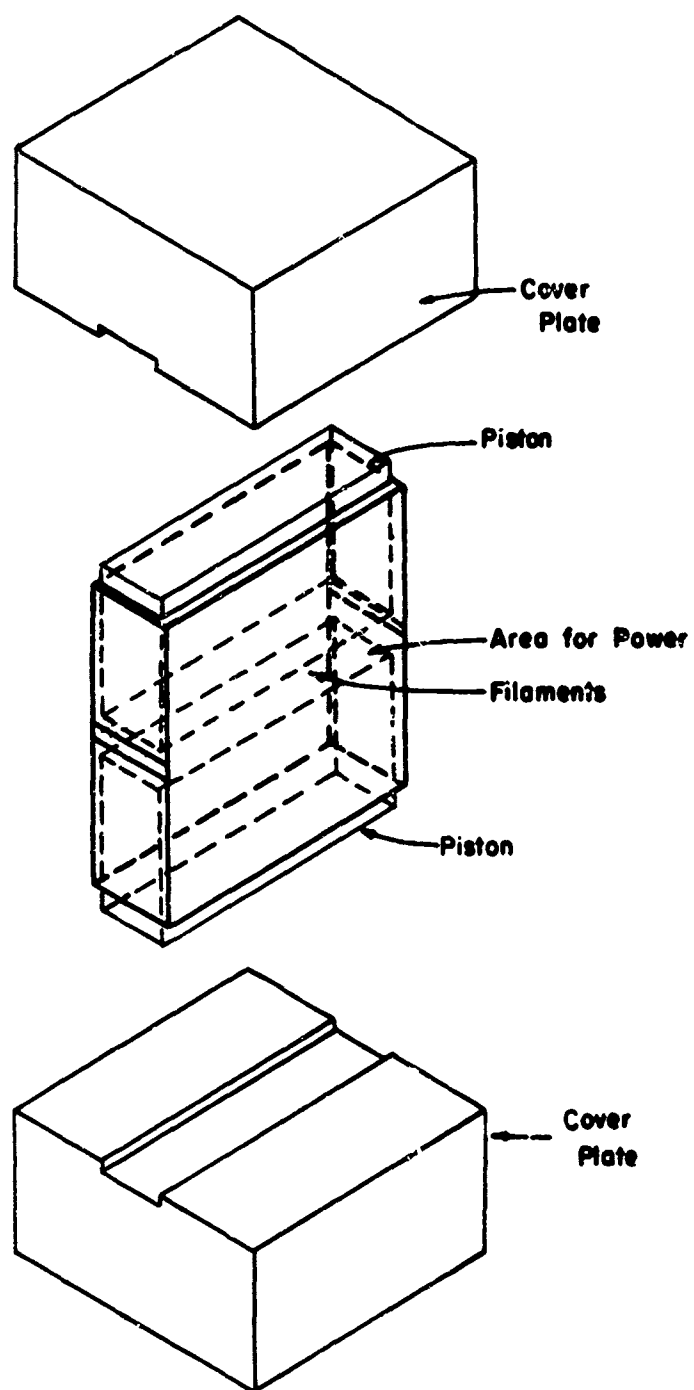


Figure 26. Schematic Sketch of Frame for Filament-Powder Arrangement

Although the die can be used as a double acting piston system, it can also be used as a single piston press. In the latter case the cover plate-piston is set on a heavy steel anvil to absorb the shock. The dynamite charge is placed in the cardboard container. A detasheet initiating system is used in which strips are laid along the diagonals on top of the dynamite. The charge is then initiated at the center. It is estimated that the actual pressure developed at the piston-powder interface is on the order of 10 kbars (150,000 psi).

After compaction, the die is disassembled and the compact removed for processing. Sintering of the composites has been conducted at 2050°F for one hour in hydrogen. Brinell hardness tests and density measurements have been conducted using the procedures mentioned previously.

Tensile tests have been conducted on sub-size tensile specimens with a one-inch gage length. The reduced section has measured 1/4 x 3/8 inches. The overall specimen length is on the order of three inches.

Metallographic and electron microprobe studies have been conducted to study the interface between the tungsten and the iron, both before and after sintering.

Experimental Results and Discussion

The main problem to date has arisen in splitting of the compact along the plane of one of the wire layers. In some cases this cracking has been quite pronounced while in others it is minimal. Splitting does not occur in compacts without the filaments so the fracture problem is associated with the compaction around the wire.

Since there is a large mismatch in the acoustic impedance between the tungsten and the steel, high carbon steel music wire was substituted for the

tungsten. Some cracking was still evident along the plane of the wire.

At the start of the program, both pistons were driven simultaneously to effect compaction. Since two compressive shock waves would meet at the center and be rarefacted as tensile waves a tensile stress would be set up at the center of the compact. Therefore, the approach was altered to drive one piston only which would eliminate the tensile rarefaction wave. Better results were obtained with a single accuated piston system. Experiments with steel music wire though were not substantially different from those with tungsten filaments, indicating that when fracture did occur it was not an impedance mismatch.

Precompaction and vibration of the powder was used in an attempt to distribute the powder uniformly around the wires and effect partial compaction. These procedures were used separately and together varying precompaction loads and vibration amplitudes and times. The technique that gave the best results was to simply tap the frame a few times to get the powder around the dies and then close the frame with no precompaction.

Several compacts were made without reinforcing to establish a base. These specimens were sintered for one hour at 2050°C prior to testing. After sintering the average density was 92% of theoretical and the average hardness was 63 Brinell. Average mechanical properties were (1) tensile strength - 23,200 psi; (2) 0.2% offset yield - 16,000 psi; and (3) elongation in 1 inch - 13%.

Two reinforced specimens were evaluated in which relatively good compaction was obtained. In one specimen the filament spacing was .025 inches apart in the horizontal plane and 0.015 inches apart in the vertical. Five layers of reinforcing wire were present. The volume fraction of wire in the

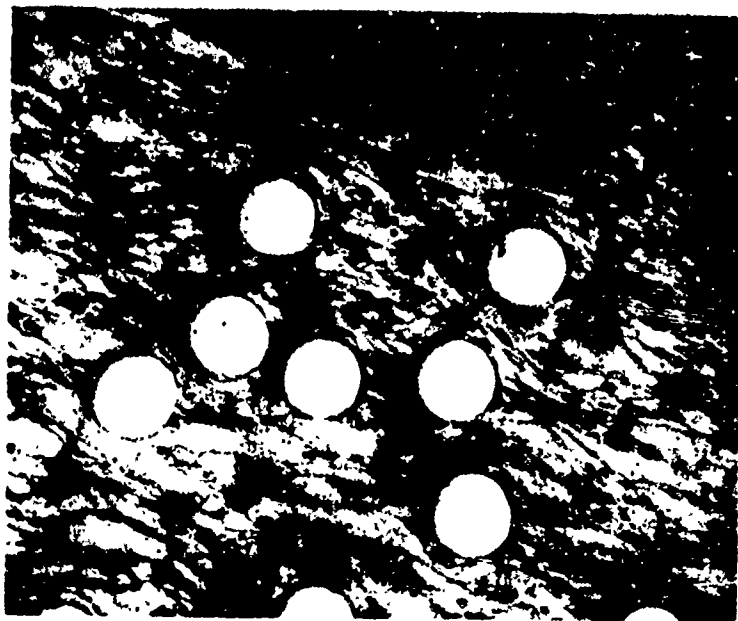
total cross section was 1.7 percent as the specimen was not machined to remove the excess iron. Another specimen with three layers of filament was also evaluated. In this specimen the wires were 0.01 inches apart in both the horizontal and vertical planes. The volume percent loading of 0.005 inch tungsten wire was the same as in the first specimen. These specimens were sintered for one hour at 2050°F prior to machining and testing.

After sintering the densities were 93 and 90 percent of theoretical with the average hardness being 55 Brinell. Average mechanical properties of these specimens were as follows: (1) tensile strength - 31,500 psi; (2) 0.2% offset yield strength - 18,300 psi; and (3) elongation in one inch - 30%.

The tungsten wire used in these experiments had a tensile strength of 360,000 psi. Using the law of mixtures at the volume percent loading in the above two specimens, the projected ultimate strength derived from the base specimens and the amount of reinforcing would be about 22,000 psi. The actual calculation is presented in Appendix A.

The average tensile strength was 31,500 psi which was above that predicted from the law of mixtures. This can be explained to a certain extent since the reaction between the tungsten and steel provides a bond as a result of sintering. On cooling from the sintering temperature the steel contracts more than the tungsten which puts the area adjacent to the fibers in compression. A finite tensile load is required to overcome this residual compression force.

Tungsten filament reinforced Ancorsteel 1000 composites have been studied by metallography and with the microprobe. Figure 27 is a photomicrograph of the as-compacted composite. There is no reaction between the tungsten filament and the steel as a result of compaction.



Nital Etch

100X

Figure 27. Tungsten Filament Reinforced Ancorsteel
1000 Composite after Explosive Compaction

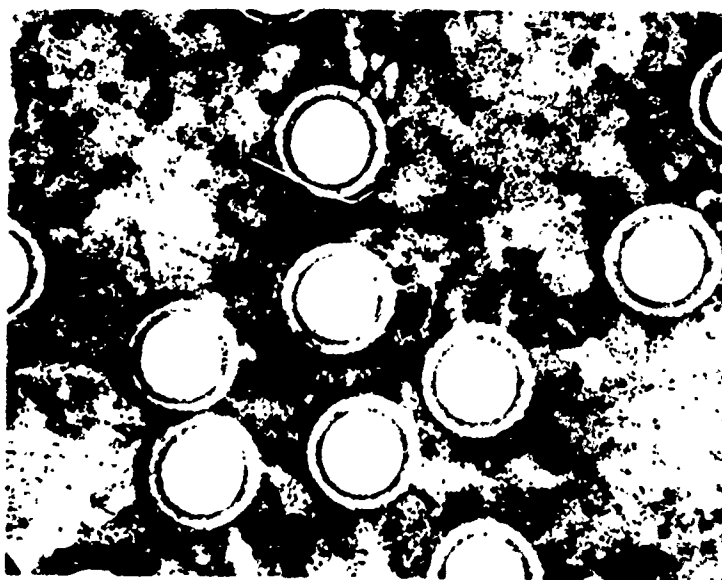


Figure 28. Tungsten Filament Reinforced Ancorsteel
1000 Composite after Sintering 1 Hour at 2000°F

After sintering for 1 hour at 2000°F a definite reaction zone is present, as is shown in Figure 28. Random analysis with the microprobe on the steel matrix indicated that a maximum of 3 a/o tungsten was present in the interface region after sintering. The tungsten concentration was highest in the matrix near the wires and decreased to near zero 50 to 75 microns from the wires. The 3 a/o tungsten is slightly into the two phase region, alpha iron plus ϵ hexagonal phase. Since the intermetallic ϵ phase is limited to a narrow region adjacent to the wires, it should not be detrimental to the strength of the alloy which is borne out by the tensile tests.

Conclusions

The work on the tungsten filament reinforced Ancorsteel 1000 composite is a continuing program and is not complete at the present time. Although the data presented to date are for composites with a minor volume percent of filaments, the tests would indicate that strong composites can be obtained.

The main problem is the cracking that develops preferentially along a plane of the wires. This problem is aggravated as the volume percent loading increases. This problem was originally present in one wire layer composites and is slowly being overcome as the procedures are refined. The use of a more massive die assembly helped considerably. Changes in the brace assembly have helped in alleviating cracking. End confinement of the wires appears to be a contributing cause and is under investigation at the present time.

This research has indicated that composite development by explosive compactions of powders appears feasible, but there are problems to be solved.

STUDIES WITH UDIMET 700

Udimet 700 is a high temperature superalloy used in gas turbines as a bucket material and in advanced jet engines for turbine wheels. The operational temperature ranges from 1400° to 1800°F and is suitable for short time service at temperatures to 2000°F. The alloy is used in the wrought condition. Fine grain structures are preferable, and one of the objectives of this program was to determine if the sintering operation on the compacted part would result in grain growth.

The Udimet 700 powder used in this program was supplied by Alloy Metals of Troy, Michigan. This powder was made by a grinding process as opposed to atomization. Specifications for the powder are presented in Table 6. As an inspection of Table 6 indicates, about one-half of the powder was greater than 325 mesh in size with the balance being -325 mesh.

Compaction and Sintering of Round Billets

In compacting the round bars thin wall steel tubing was used, as previously described for the Ancorsteel. The U-700 powder was pressed into the tubes so the bar length would be about 4.5 inches. In the first series of experiments the internal diameter of the tube was 1-4 inches. At a loading ratio of 1:1 of 40% Red Cross Extra dynamite to powder the center of the billet was not compacted.

In the next series of experiments tubing with an internal diameter of 0.9 inches was used and the length for the powder kept about the same. Explosive to powder ratios of 1, 1.5, and 2.0 were used. The powder at the center of the tube was compacted in these tests. At the highest loading some jetting was noted along the center of the rod. Circumferential cracks were

Table 6. Specifications on Udimet 700 Powder

Chemical Analysis

Element, %

<u>Al</u>	<u>B</u>	<u>C</u>	<u>Cr</u>	<u>Co</u>	<u>Fe</u>	<u>Si</u>	<u>Ti</u>	<u>Zr</u>	<u>Mo</u>	<u>O₂</u>	<u>Ni</u>
4.43	0.012	0.12	14.95	19.1	0.47	0.18	3.46	0.016	5.21	0.014	Bal.

Sieve Analysis

Mesh Size	+ 50	+ 60	+ 80	+ 100	+ 140	+ 325	- 325
Percent	0	0.4	2.8	2.4	20.9	24.1	49.8

present at several points along the billets. Several specimens were cut from these billets and the green density determined. The average respective densities were 7.72, 7.79 and 7.90 for loading ratios of 1, 1.5 and 2 or 97.5, 98.3 and 99.7 percent of theoretical density, respectively.

Specimens from the billets compacted at loading ratios of 1.5 and 2.0 were then sintered to obtain isochronal and isothermal relationships. The green density was determined for each specimen prior to heat treatment. Heat treatments were conducted in a gettered argon atmosphere at temperatures of 2050°, 2100°, 2150°, 2200° and 2300°F for periods of 1, 2, 4, 8 and 24 hours. The results of these experiments are presented in Table 7 with the exception of those for the 2300°F heat treatment. These data have been excluded since excessive oxidation occurred at this temperature.

At a temperature of 2050°F, some sintering occurred, but required eight hours or more to effectively start coalescence of the fine particles. Grain size was a function of the original particle size of the powders. Increasing the sintering temperature to 2100°F resulted in coalescence of the small grains after only an hour. This was true of all subsequent heat treatments at temperatures of 2100°F or higher.

Final densities irregardless of time at temperature were all in excess of 98 percent of theoretical. However, even the initial green densities were greater than 96.7 percent of theoretical, so changes in actual density were small. In all cases, with the exception of some of the specimens heat treated at 2050°F, an increase in density occurred as a result of sintering.

In Figure 29, in which the percent change in density as a result of sintering is presented as a function of time at temperature, it is noted that the greatest change occurs after two hours at temperature for each temperature

Table 7. Results of Sintering Experiments
With U-700 Compacts

<u>Time at Temperature, Hours</u>	<u>Original Density g/cc</u>	<u>Final Density g/cc</u>	<u>Percent Change</u>	<u>Percent Theoretical Density (Final)</u>
<u>2050°F</u>				
1	7.81	7.79	- 0.3	98.4
2	7.82	7.85	0.4	99.1
4	7.82	7.81	- 0.1	98.6
8	7.73	7.78	0.7	98.2
24	7.80	7.82	0.3	98.7
<u>2100°F</u>				
1	7.70	7.78	1.0	98.2
2	7.80	7.91	1.4	99.9
4	7.77	7.83	0.8	98.9
8	7.84	7.90	0.8	99.7
24	7.79	7.84	0.6	99.0
<u>2150°F</u>				
1	7.79	7.89	1.3	99.6
2	7.80	7.92	1.5	100.0
4	7.73	7.80	0.9	98.4
8	7.77	7.85	1.0	99.1
24	7.77	7.82	0.6	98.7
<u>2200°F</u>				
1	7.74	7.83	1.2	98.9
2	7.66	7.79	1.7	98.4
4	7.75	7.86	1.4	99.2
8	7.70	7.81	1.4	98.6
24	7.80	7.92	1.5	100.0

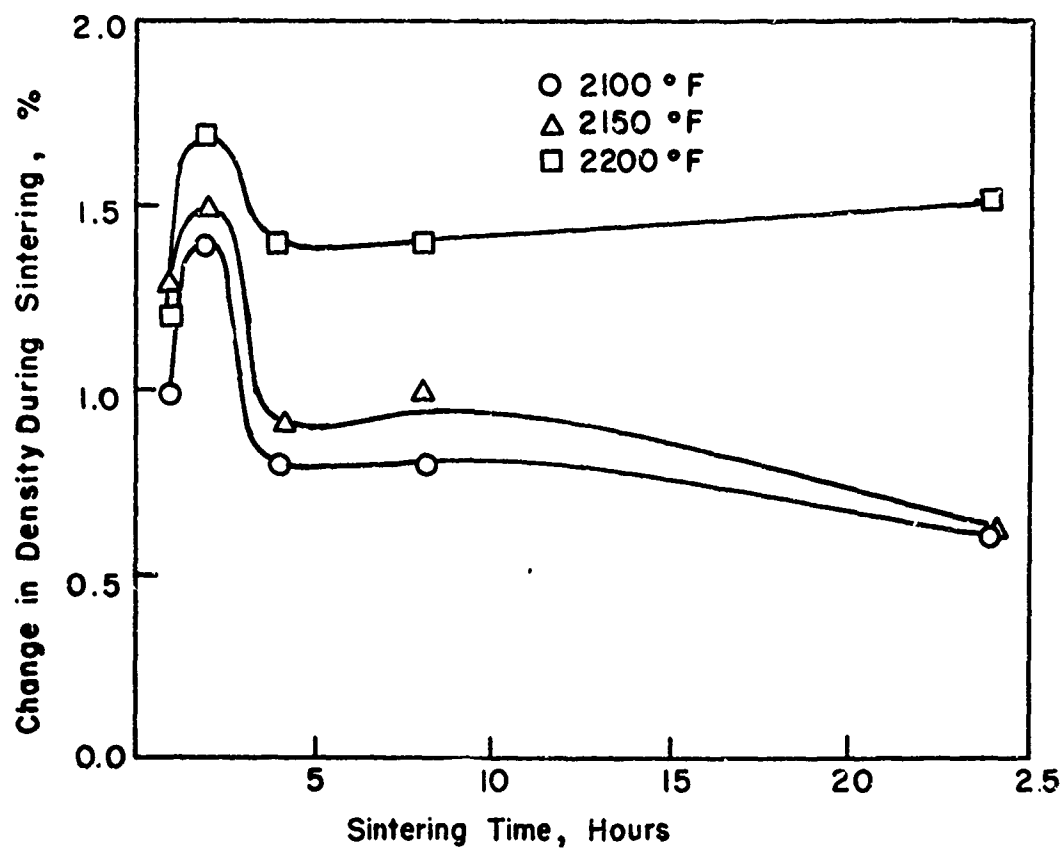


Figure 29. Change in Density in Sintered Udimet 700 Compacts as a Function of Time at Temperature

shown. A trend is present in that as the temperature is increased the change in density for a particular sintering time also increases. Since there was a variation in the initial and final densities, an isothermal plot of densities was not warranted.

Isochronal plots of the percent change in density as a function of temperature are presented in Figure 30. It is interesting to note that at sintering times up to two hours the percent density change increases with temperature at about the same rate. At sintering times of 8 and 24 hours the slope of the curve changes with very little change in density between temperatures of 2050 and 2150°F with a rapid percent change in density at a temperature of 2200°F. Intermediate between these is the isochronal curve at 4 hours which corresponds to the rate in percent density change up to 2150°F after which a rapid change occurs at a temperature of 2200°F.

Metallographic inspections were made of the sintered specimens. At a sintering temperature of 2050°F, the γ' precipitate common to solution heat treated U 700 is present in decreasing amounts up to sintering times of 2 hours. This type of structure is shown in Figure 31. After 2 hours at 2050°F a twinned structure develops which is still present after 24 hours as is shown in Figure 31. After 2 hours at 2050°F a twinned structure develops which is still present after 24 hours as is shown in Figure 32. The γ' precipitate is almost entirely gone after 4 hours at 2050°F. Coalescence of the fine grains around the larger particles is more pronounced as the time is increased.

At a temperature of 2100°F the amount of γ' precipitate present after 1 hour is about the same as that after 2 hours at 2050°F. Also the twins in the substructure have started to form after only 1 hour at temperature.

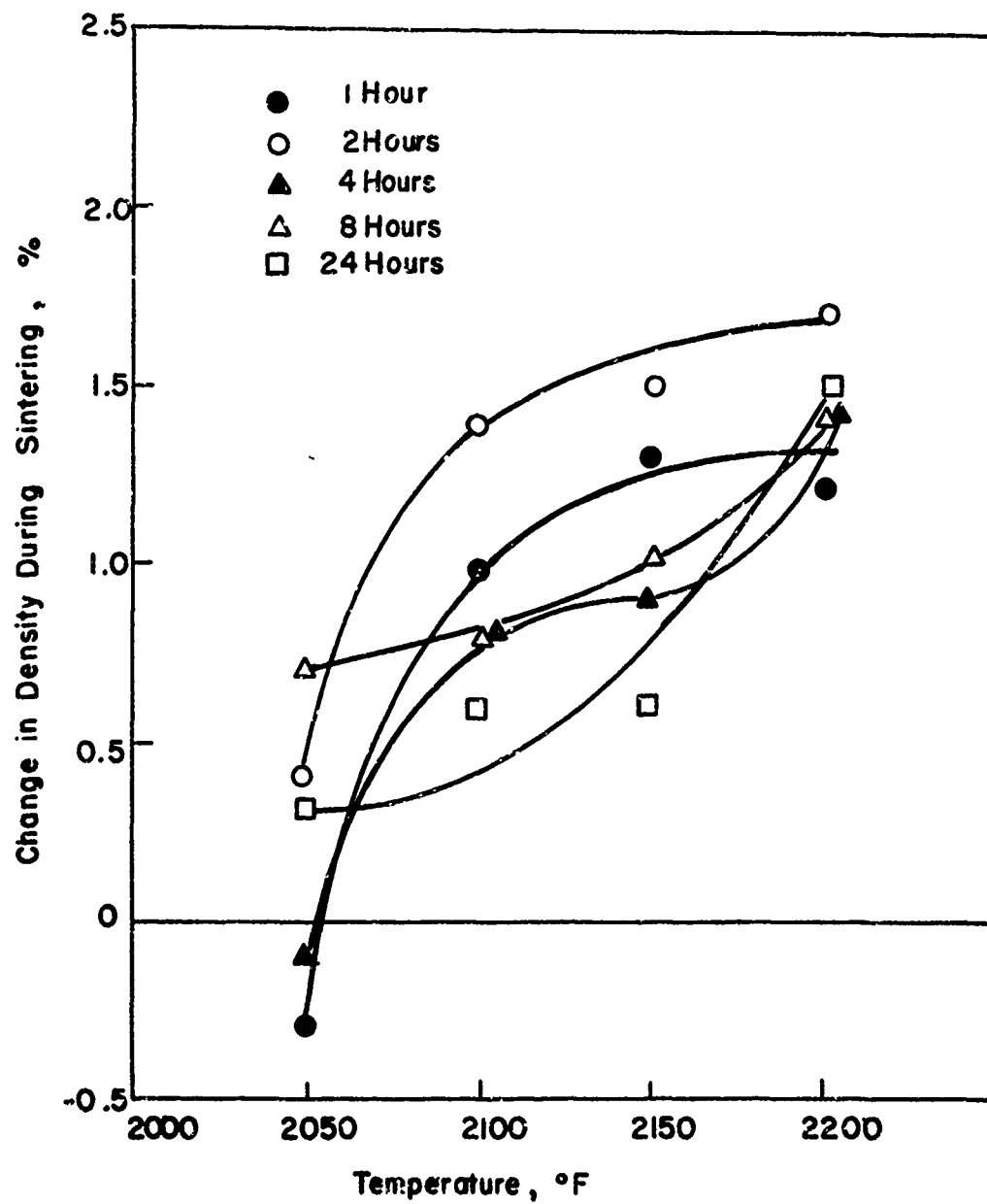


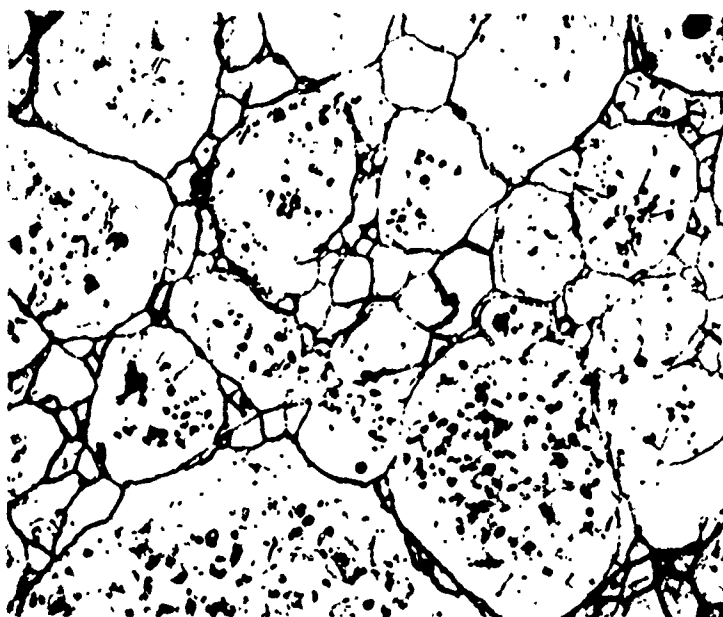
Figure 30. Change in Density in Sintered Udimet 700 as a Function of Varying Times and Temperatures



Oxalic Acid Etch

500X

Figure 31. Explosively Compacted U-700 Sintered for One Hour at 2050°F



Oxalic Acid Etch

500X

Figure 32. Explosively Compacted U-700 Sintered for 24 Hours at 2050°F

Coalescence of the fine grains has started after one hour, as shown in Figure 33, and gives the appearance of a peritectic type of structure. The amount of twinning does not increase perceptibly after 2 hours at temperature.

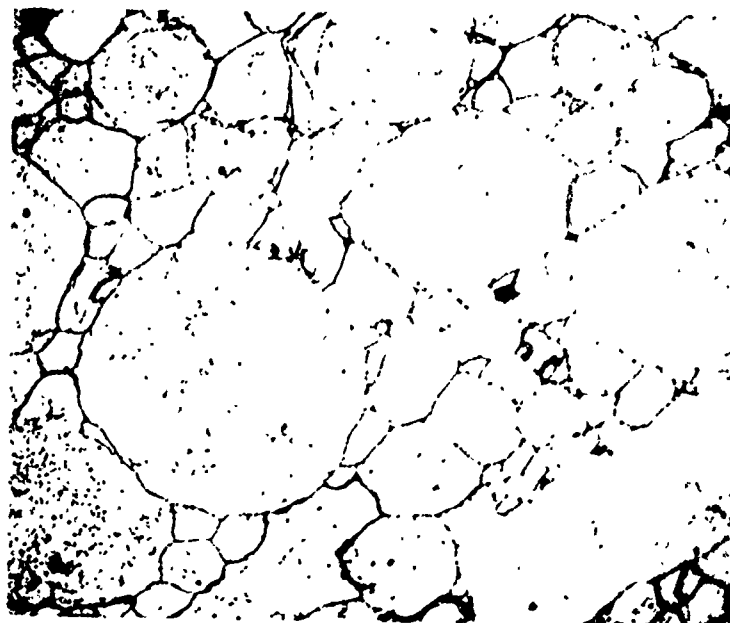
Very little difference is noted as a result of raising the temperature 50°F to 2150°F (See Figure 34). There is some growth and annealing of the twinned structure after 24 hours (See Figure 35). At a temperature of 2200°F the γ' precipitate is still present after 1 hour (See Figure 36). Coalescence of the fine grains has occurred to a greater extent after one hour than at lower temperatures for one hour. The twin structure is present after one hour. The size of the twins does increase with increasing time at 2200°F.

In all of the sintering tests on these compacts there is essentially no change in the size of the particles that are greater than 325 mesh. The fine particles do coalesce and give the appearance in several instances of a cored structure. The appearance of twins is related to mechanical work plus the annealing effect. Grinding plus the shock effect from explosive compaction can cause this structure.

Sintering for times in excess of about 8 hours is not warranted in most instances except at 2050°F in which at least 8 hours are required to start effective sintering. Sintering times of 2 to 4 hours at 2150° to 2200°F appears to give the best results based upon the metallographic examination.

One of the problems associated with production of round bars was cracking normal to the length of the billet. In the tests described above the as-received powder was used. Sintering tests indicated the main portion of the powder affected was the -325 mesh fraction.

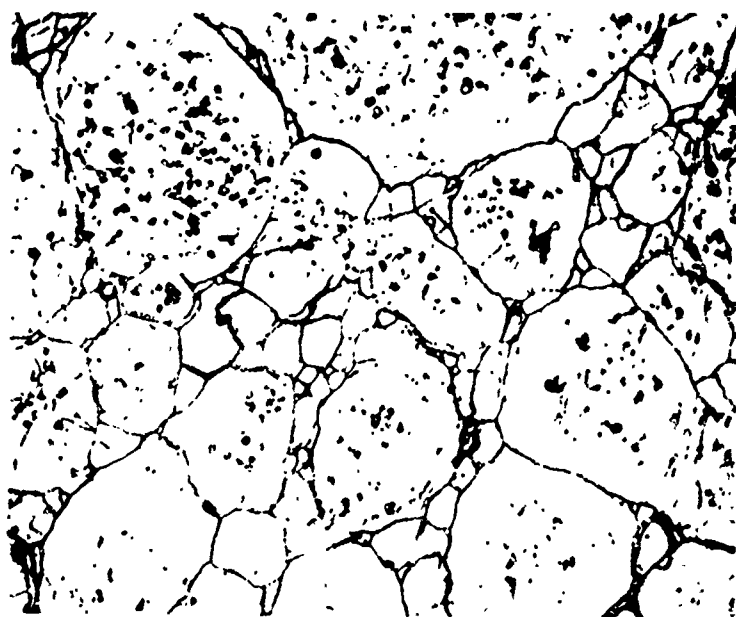
Tests were conducted using multiple explosive compaction steps with -325 mesh powder. In these tests cracking still occurred, although the extent



Oxalic Acid Etch

500X

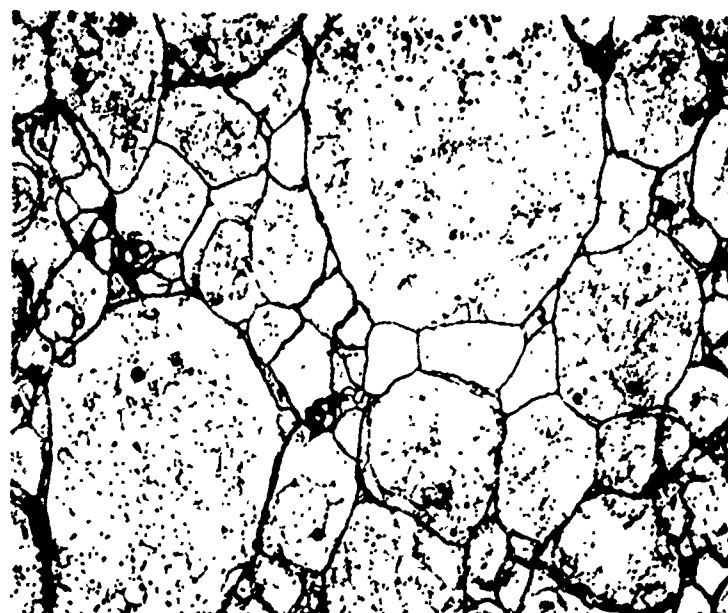
Figure 33. Explosively Compacted U-700 Sintered for One Hour at 2100°F



Oxalic Acid Etch

500X

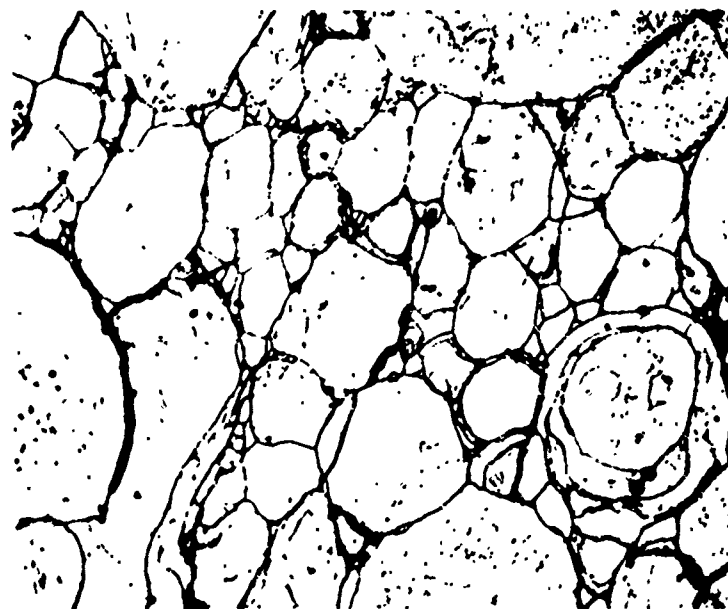
Figure 34. Explosively Compacted U-700 Sintered for One Hour at 2150°F



Oxalic Acid Etch

500X

Figure 35. Explosively Compacted U-700 Sintered for 2 1/2 Hours at 2150°F



Oxalic Acid Etch

500X

Figure 36. Explosively Compacted U-700 Sintered for One Hour at 2200°F

was not as great. In the next series, the powder was first annealed in hydrogen for 2 hours at 2000°F and furnace cooled. Using the annealed powder drastically reduced the propensity for cracking. Loading ratios of 1.6 and 1.8 gave relatively good billets without jetting of the center. These tests are a continuing effort.

Compaction of Flat Billets

The production of 3 x 3 inch billets similar to those produced for the Ancorsteel study indicated that the dual square pipe arrangement was inadequate since much higher loading ratios were required. At the higher loading ratios required the dual pipe spalled allowing the compact to upset and crack.

Use of 2 x 2 - inch steel spall rails and heavier pistons give better results. At the start of the experiments a 60% dynamite was used with 400 grams of U-700 being placed in the assembly. At loadings of 3000 and 5000 grams of dynamite, only pieces of the compact remained. Using annealed powder and a loading of 3500 grams of dynamite resulted in a compact without cracks, but poor compaction. Increasing the amount of dynamite to 4000 grams resulted in cracking of the composite.

In the next series of tests 40% dynamite was used. Rather than loading over the whole assembly the dynamite container was placed on top of the area to be compacted. The whole assembly was buried in sand to increase the energy transfer. With 1000 grams of dynamite to 400 grams of U-700 acceptable billets can be made, although the densities are low.

Again the production of the flat billets is a continuing study which is incomplete at this time.

BIBLIOGRAPHY

1. M. C. Noland et al., "High Velocity Metal Working," National Aeronautics and Space Administration, NASA SP-5062, p. 137-143, 1967.
2. J. Pearson, "The Explosive Compaction of Powders, ASTM Creative Manufacturing Seminars, 1961.
3. S. W. Porembka, "Explosive Compacting" Ceramic Age, 79, pp. 69-71, 1963.
4. L. W. Davis, "How Metal Composites are Made," Fiber Strengthened Composites, ASTM STP 427, 1967.
5. R. K. Robinson, "High Energy Rate Forming of Fibrous Composites," *ibid.*
6. Standard Method of Test for Green Strength of Compacted Metal Powder Specimens, ASTM Designation B 312-64 ASTM Standards, ASTM Philadelphia, 1971.
7. N. Claussen and J. Jahn, "Green Strength of Metal and Ceramic Composites as Determined by the Indirect Tensile Test," Powder Metallurgy International, 2, pp. 87-90, 1970.

APPENDIX A

Continuous Fiber Reinforced Composites and the Rule of Mixtures

The deformation of a composite containing uniaxially aligned continuous fibers when it is stressed parallel to the fibers may proceed in four stages:¹

1. Both fibers and matrix deform elastically.
2. The fibers continue to deform elastically, but the matrix deforms plastically.
3. Both the fibers and matrix deform plastically.
4. The fibers fracture followed by composite fracture.

Generally stage 2 occupies the largest portion of the stress-strain curve. This is particularly true when the fibers are brittle and show little or no plastic deformation.

For the purpose of discussion, assume the reinforcing fibers are continuous, uniform, unidirectional, uniformly dispersed in the matrix, and firmly gripped by the matrix so that no slippage can occur at the interface between fiber and matrix. This gives the equal strain relation

$$\epsilon_c = \epsilon_f = \epsilon_M \quad (1)$$

where ϵ_c = composite strain, ϵ_f = fiber strain, and ϵ_M = matrix strain.

The total load on the composite is shared between the fiber load, P_f , and the matrix load, P_M .

$$P_c = P_f + P_M \quad (2)$$

$$\sigma_c A_c = \sigma_f A_f + \sigma_M A_M \quad (3)$$

where σ represents the stress and A the area.

$$\sigma_c = \sigma_f \frac{A_f}{A_c} + \sigma_M \frac{A_M}{A_c} \quad (4)$$

and, since area fraction equals volume fraction in this case,

$$\sigma_c = \sigma_f V_f + \sigma_M V_M \quad (5)$$

This is the basic "Rule of Mixtures" equation.

For a composite containing more than a certain volume fraction, V_{min} , of continuous fibers, the ultimate strength is ideally reached at a total strain equal to the strain of the fibers at their ultimate tensile strength. The ultimate strength of the composite is then given by

$$\sigma_{cu} = \sigma_{fu} V_f + \sigma_{M\epsilon_f} (1 - V_f) \quad (6)$$

$$V_f \geq V_{min}$$

where σ_{fu} is the ultimate tensile strength of the fibers and $\sigma_{M\epsilon_f}$ is the matrix stress when the fibers are at fracture strain. For small values of V_f ($< V_{min}$), the behavior of the composite may not follow equation (6) because there is an insufficient number of fibers to effectively restrain the elongation of the matrix so that the fibers are rapidly stressed to the fracture point. If the fibers all break at the same stress, the composite will fail unless the remaining matrix can support the full composite stress. Therefore failure of all the fibers results in immediate composite failure only if

$$\sigma_{cu} = \sigma_{fu} V_f + \sigma_{M\epsilon_f} (1 - V_f) \geq \sigma_{Mu} (1 - V_f) \quad (7)$$

This defines a minimum volume fraction, V_{min} , which must be exceeded if the strength of the composite is to be given by equation (6).

$$V_{\min} = \frac{\sigma_{Mv} - \sigma_{M\epsilon_f}}{\sigma_{fu} + \sigma_{Mv} - \sigma_{M\epsilon_f}} \quad (8)$$

where σ_{Mv} is the ultimate matrix stress.

For the composite to have useful tensile properties, the composite ultimate strength must be greater than that of the matrix alone; i.e.

$$\sigma_{cu} = \sigma_{fu} V_f + \sigma_{M\epsilon_f} (1 - V_f) \geq \sigma_{mu} \quad (9)$$

This equation defines a critical volume fraction of fibers which must be exceeded for fiber strengthening.

$$V_{\text{crit}} = \frac{\sigma_{mu} - \sigma_{M\epsilon_f}}{\sigma_{fu} - \sigma_{M\epsilon_f}} \quad (10)$$

$$V_{\text{crit}} > V_{\min}$$

It should be noted that the rule of mixtures is a lower bound for composites in which there is good matrix-fiber bonding. This is due to the matrix inducing multiple necking in the fibers² and the matrix inhibiting the onset of necking. The fibers, in turn, can act as crack arresters for matrix cracks.

The strength of the composites as predicted by the law of mixtures was then calculated using the following data:

Steel: $\sigma_{Mu} = 23,200$

$\sigma_{M 0.2} = 16,100$

Tungsten $\sigma_f = 357,000$

Volume fibers = 0.017

$T_c = V_f \sigma_f + (1 - V) \sigma_{M 0.2} =$

$0.017 (357,000) + 0.983 (16,100)$

$\sigma_c = 21,900 \text{ psi}$

1. L. J. Broutman and R. H. Krock, "Principles of Composites and Composite Reinforcement," Modern Composite Materials, ed. Broutman and Krock, Addison-Wesley, 1967.
2. C. Schoene and E. Scala, "Multiple Necking Phenomena in Metal Composites," Met. Trans. 1, Dec. 1970.

XIV. EXPLOSIVE WELDING

S. H. Carpenter

R. H. Wittman

M. Nagarkar

INTRODUCTION

The basic goal of explosion welding research carried out at the University of Denver has been to advance the fundamental knowledge and applied technology leading to actual engineering application of the explosion welding process. While there are many areas of interest, care has been used to select problems which must be more fully understood to promote the use of explosion welding.

The most important and most difficult task in applying explosion welding to any application is the selection of the proper welding parameters to insure high quality welding. The term welding parameters is used to describe the variables the welding engineer has at his disposal in any engineering application. The most common welding parameters include: the type and amount of explosive, method of detonation, weld geometry and support tooling. Of equal importance is a knowledge of the material properties and how the material properties relate to the explosion welding process. Establishment of criteria to select the proper welding parameters has been a subject of continuing investigation since the beginning of the ¹ Center for High Energy Forming. During the past year an intensive program has been conducted to incorporate the important material properties into the welding parameters. The concept has been to use an energy balance by determining the important energy absorbing mechanisms in the explosion welding process. Of principal importance has been the determination of which material properties limit the application of the explosion welding process and to determine the thickness limitations. The results of this investigation will not be present in this report since a phase report will be released in the near future.

Of equal importance with the welding parameters is a knowledge of how the fabricated weld will perform under service conditions. Data presented at the Third International Conference of the Center for High Energy Forming² indicated that one must investigate weld properties as a function of thermal treatments. Data from an explosion welded copper-nickel composite showed significantly enhanced diffusion across the weld interface over that measured in a conventionally roll bonded copper-nickel composite. This effect could lead to serious deterioration of material properties in many metal systems. Important in the reported data is the fact that the enhancement of the diffusion occurs at temperatures above the recrystallization temperature of both metals in the couple. The high temperature indicates that a thermally stable defect structure probably exists along the interface of the explosion weld at temperatures above the recrystallization temperature. It is a well known fact that an explosion weld is characterized by very intense plastic deformation along the weld interface. The plastic deformation is considerably greater than that occurring in more conventional solid state bonding operations. It is believed that the intense plastic deformation must be responsible for the formation of some type of thermally stable defect structure along the weld interface. If this is indeed the case, one must consider the effects of thermal treatments both before and after the welding operation. To fully understand this problem, the effects of the thermal treatments on the explosion welding of aluminum, nickel, and steel have been investigated. To better characterize the defect structure work on the copper-nickel system has been continued.

METALLURGICAL INVESTIGATION OF EXPLOSION WELDED COPPER-NICKEL COMPOSITES

As stated earlier, previously reported work on explosion welded copper-nickel composites indicates that diffusion across the weld interface is significantly enhanced at high temperatures (above 750°C) over that observed in a conventional roll bonded composite. Work during the past year has been directed towards verifying the reported results and to provide a basic understanding of them. Repeated experiments have proven beyond doubt that an enhancement of the diffusion process occurs in explosively welded samples of copper-nickel at high temperatures. Experiments using a symmetrical weld geometry to give a smooth weld interface have shown the effect is a result of the explosion welding process and is not a result of the unique ripple interface.

To fully understand why the enhanced diffusion occurs one must be able to characterize the defect structure along the weld interface. To do this it is necessary to observe some property which will change with change in structure or be able to use transmission electron microscopy for direct observation. In this investigation it was decided to monitor changes in the electrical resistivity across the interface as a function of temperature along with transmission microscopy. Transmission microscopy for this system was exceedingly difficult due to problems in sample preparation. Normal chemical etching practices commonly used in thinning samples could not be used due to the composite nature of the samples. In order to prepare samples it was necessary to design and construct an ion bombardment machine. In this apparatus argon atoms are first ionized

and then accelerated through a high voltage toward the weld interface. As the high energy ions impinge on the weld sample they sputter off atoms without changing the substructure of the specimen. Using this machine any weld combinations can be thinned for observation in the electron microscope. At present samples are now being thinned and the substructure along the weld interface is being investigated with the electron microscope. The structures observed are being compared with the previous diffusion data and the new electrical resistivity data. This investigation is the basis for a doctoral thesis in the metallurgy department and will be fully reported in a phase report during the coming year.

A PRELIMINARY INVESTIGATION OF NICKEL, STEEL, AND NICKEL/STEEL EXPLOSION WELDING

A thorough investigation of the explosion welding and heat treatment response of nickel, ferritic steel, and nickel-steel combinations was initiated in an effort to develop a more general understanding of the explosion cladding behavior of corrosion resistant alloys to ferritic steel. Nickel 200 was selected to represent the cladding alloy because it is a face centered cubic metal that has strong work hardening tendencies, typical of most cladding alloys. Furthermore the explosive shock behavior and general metallurgy of nickel is well characterized. A-515 Grade 70 steel was chosen as the ferritic alloy because it closely resembles several pressure vessel steels and has been the subject of other investigations at high strain rates during the ARPA program. The alloy has relatively good impact properties, moderate yield, and tensile strength and will respond to heat treatment. It is, therefore, a better choice for study than so-called "mild steel" of the AISI 1018 variety, although the explosion weldability of most low alloy, moderate strength ferritic steels should be essentially the same.

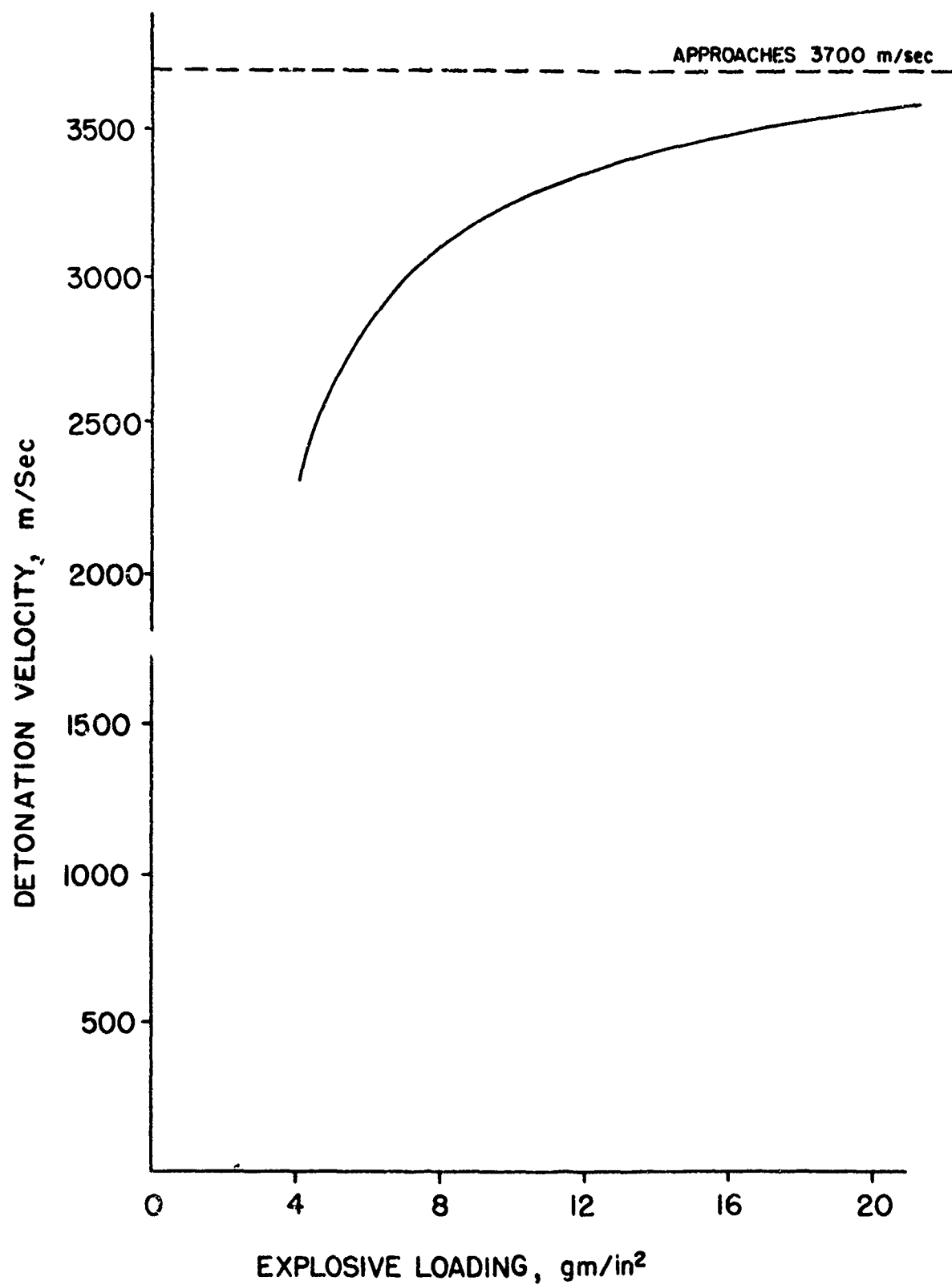
Initially a great deal of thought was given to the choice of an explosive for this study. What is the most suitable or commonly used cladding explosive? Investigation reveals that about as many explosives are being used as there are explosion welders. However, it will be recognized that almost every organization uses some type of low velocity dynamite for parallel geometry cladding. Therefore, for this study a dynamite was chosen that has proven to have useful handling characteristic, low velocity,

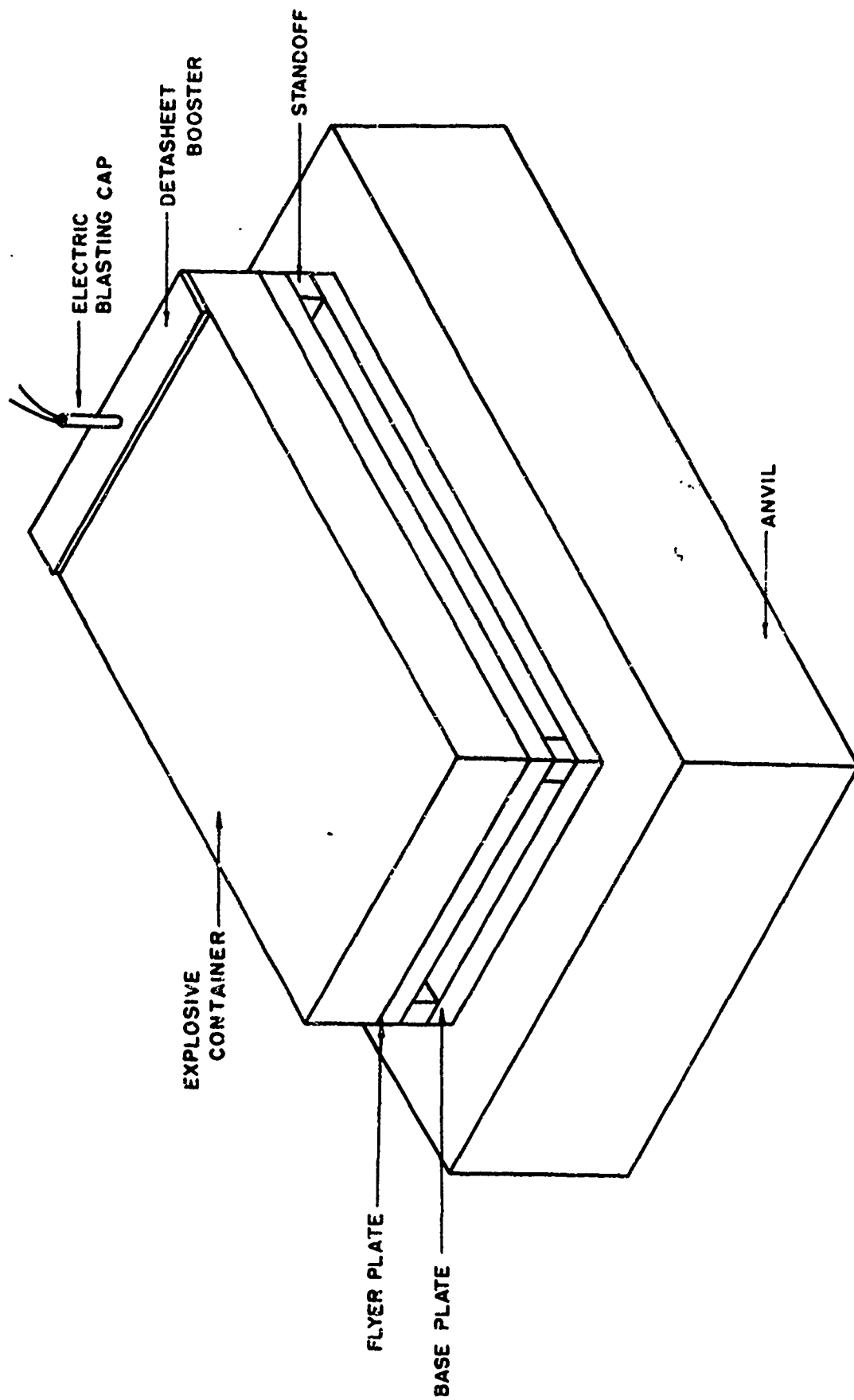
and unusually high heat of detonation. Other explosives with similar detonation velocity characteristics can be expected to yield similar results, if the explosive loading is modified to compensate for different heat of detonation properties. The explosive, known as DBA-10HV, is produced by IRECO Chemical Company of Salt Lake City. It is supplied as two non-explosive ingredients that can be safely mixed to form a slurry just prior to use. The explosive has a high heat of detonation, will propagate in 1/4 in. thick layers and maintains a uniform density. The detonation velocity-loading curve is shown in Figure 1.

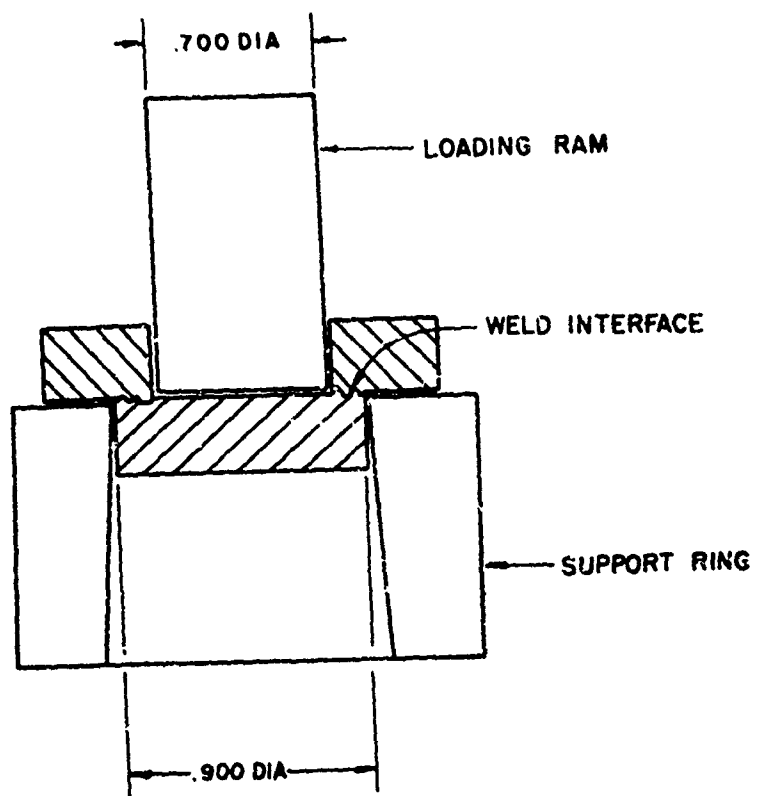
The nickel and steel welding studies are only partially completed at this time. The nickel-steel welding will not begin until the individual welding studies are completed. Preliminary experiments have already produced interesting results.

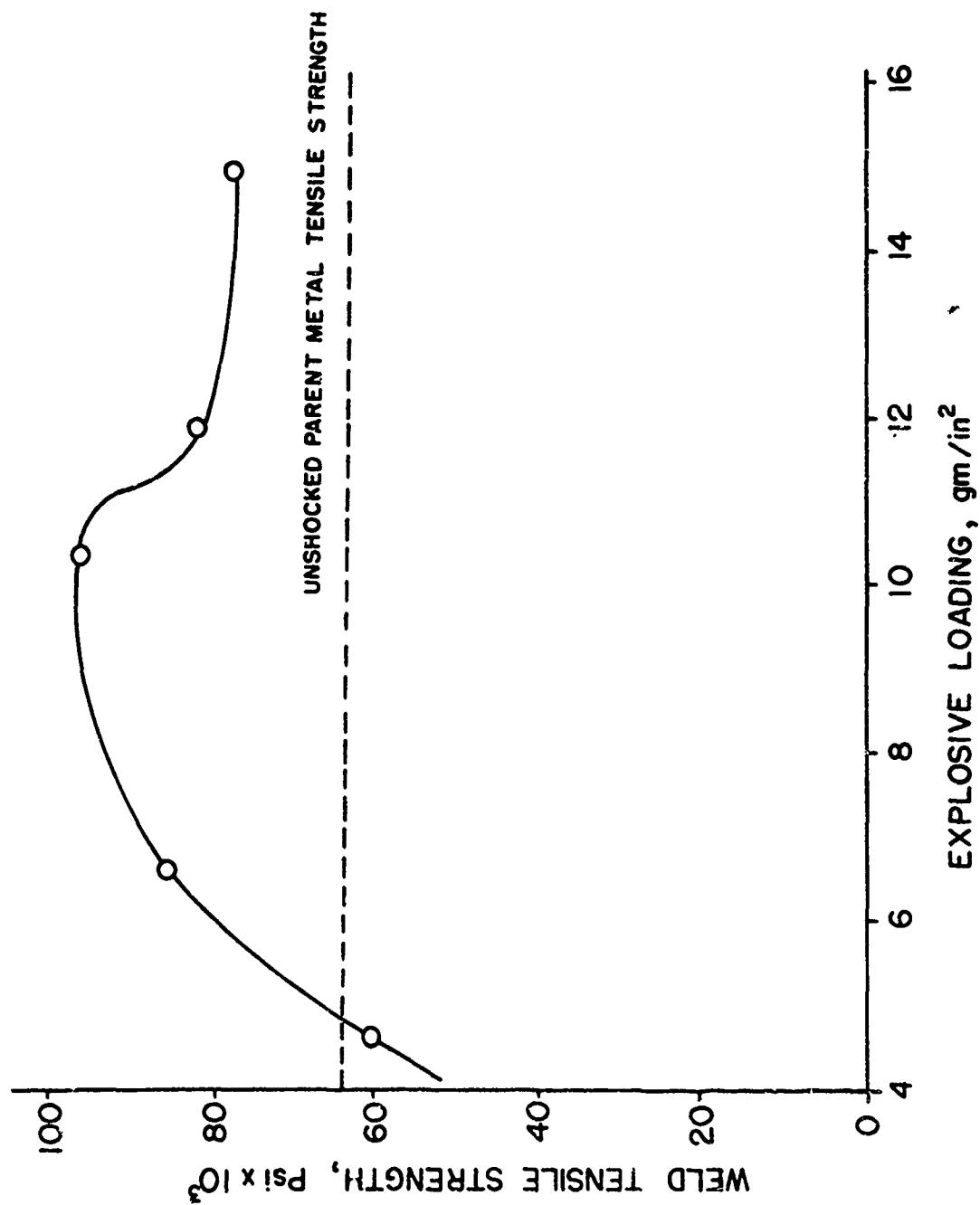
Nickel

Nickel 200 plate 3/16 in. thick was explosion welded to itself on a 4-in. thick steel anvil using a 3/32 uniform standoff and various explosive loadings of DBA-10HV. The specimen configuration is shown in Figure 2. Two tensile samples of the type shown in Figure 3 were cut from each welded plate. Test results are shown in Figure 4. The weld tensile strength exceeds the parent nickel strength in four of the five loading conditions. The fractures in all but the 4.6 g/in.² loading had a cup-cone appearance and did not occur in the weld interface. Hardness surveys indicate the increased strength is due to a combination of shock impact and strain hardening in the vicinity of the weld interface. Mechanical twins are









visible under the microscope for varying distances on either side of the weld interface. The microstructure also reveals a consistent pattern of weld structure. At the lowest explosive load condition there is little wave structure, only direct bond and elongated regions of solidified melt. As the loading increases the wave pattern becomes more pronounced and regular until the highest load of 14.9 g/in.². At that condition considerable interfacial melting has occurred and the wave pattern is poorly defined. Weld defects in the form of solidification voids are numerous. In this metal, however, weld strength does not seem to be strongly affected by the presence of the spherical voids. Other, less ductile cladding alloys might exhibit a much larger strength reduction and failure in the bond interface. Photomicrographs of the weld interface at various explosive loadings are shown in Figures 5 through 8.

Steel

Initial results for steel welding were not as successful but very informative. A-515 grade 70 steel, 1/4 in. thick, was explosion welded on a 4-in. thick steel anvil using a 1/8 in. uniform standoff and various explosive loadings of DBA-10HV. The specimen configuration is the same as shown in Figure 2. Tensile samples of the type shown in Figure 3 were cut from the welded plates at 1/4, 1/2, and 3/4 of the plate length, measured from the explosive initiation point. Tensile test results are shown in Figure 9. The weld tensile strength greatly exceeds the parent metal strength over much of the loading range. It was observed, however, that driving a chisel into the interface would result in rather easy plate separation. Microscopic examination of the interface shows the probable

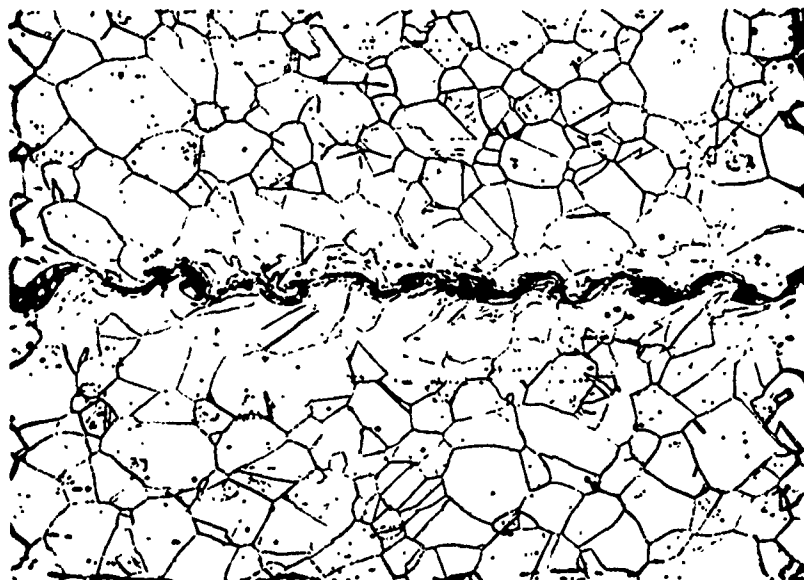


Figure 5. Nickel Explosion Welded Interface.
 6.7g/in² of IRECO DBA-10HV Explosive and
 3/32 in. Standoff. 100X Magnification.

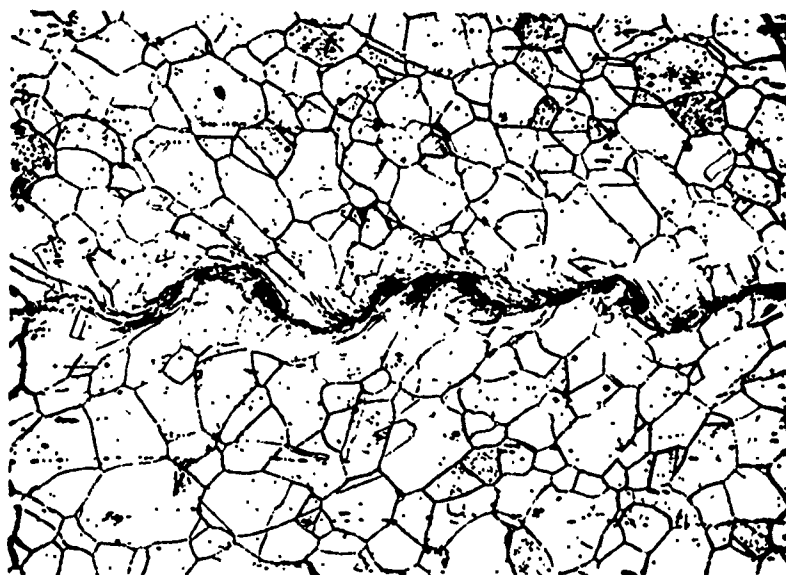


Figure 6. Nickel Explosion Welded Interface.
 10.3g/in² of IRECO DBA-10HV Explosive and
 3/32 in. Standoff. 100X Magnification.

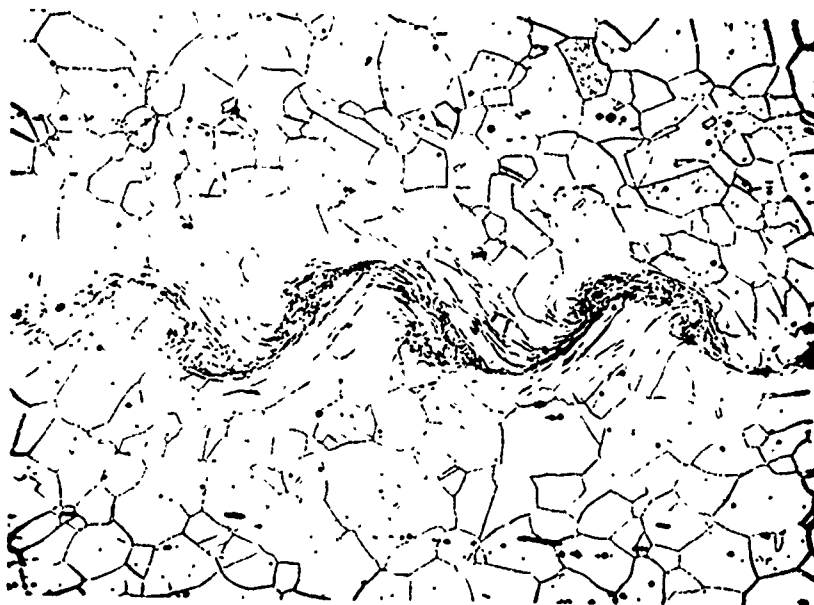


Figure 7. Nickel Explosion Welded Interface.
 11.8g/in² of IRECO DBA-10HV Explosive and
 3/32 in. Standoff. 100X Magnification.

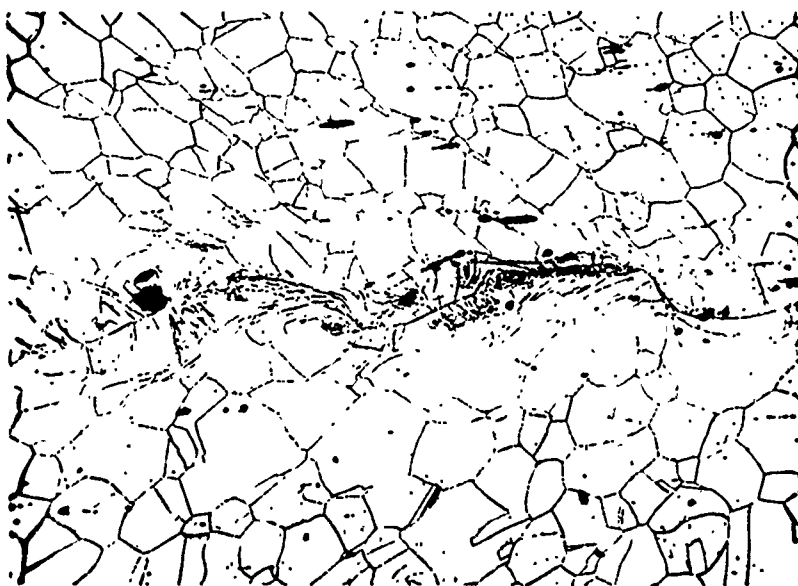
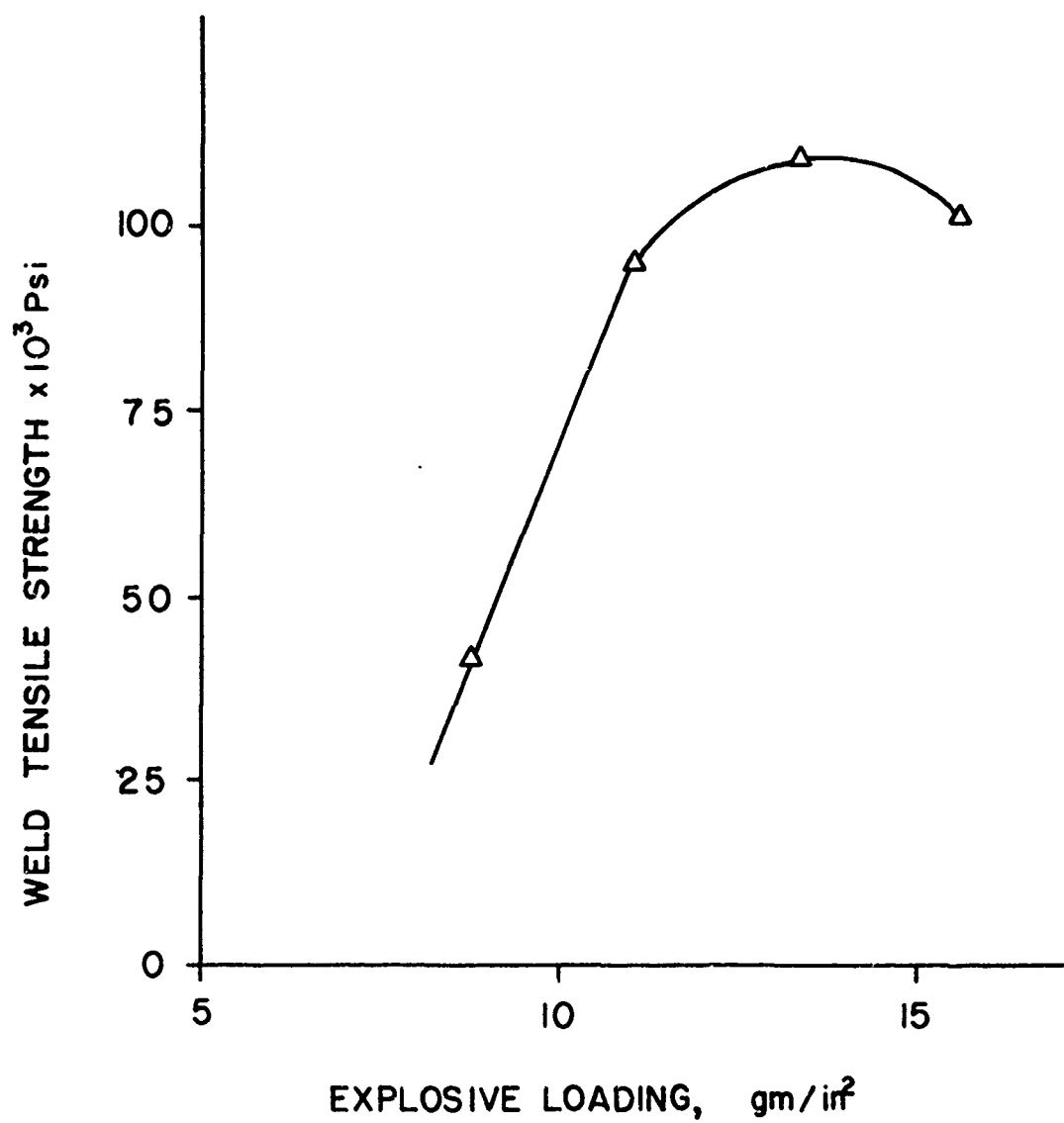


Figure 8. Nickel Explosion Welded Interface.
 14.9g/in² of IRECO DBA-10HV Explosive and
 3/32 in. Standoff. 100X Magnification.



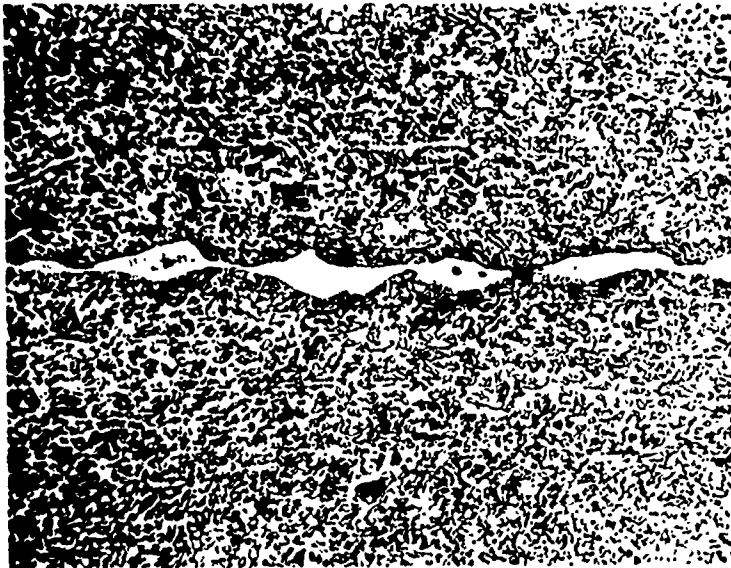


Figure 10. A-515 Steel Explosion Weld Interface.
 13g/in² IRECO DBA-10HV Explosive and 1/8 in. Standoff
 100X Magnification.



Figure 11. A-515 Steel Explosion Weld Interface.
 13g/in² IRECO DBA-10HV Explosive and 1/4 in. Standoff
 100X Magnification.

reason. A light phase is observed along the interface in all welded samples. A typical example is shown in Figure 10. This phase is found to be hard; the Knoop hardness number being equivalent to R_c 50 to 60. Undoubtedly this light phase is martensite that has formed when the interfacial layer has melted, solidified and rapidly cooled to near room temperature. The high weld tensile strength reflects the high strength of the martensitic structure and the low chisel strength reflects the notch sensitivity and lack of ductility.

Further explosion welding trials at the 13g/in^2 load and $1/4$ inch and $3/8$ inch standoffs indicate a departure from the continuous band of melt to a discontinuous melt structure and a better defined wave pattern. A typical microstructure at the $1/4$ inch standoff is shown in Figure 11. Much additional work will be necessary to identify optimum parallel welding parameters for this system before proceeding to the nickel-steel explosion welding.

•

THE EFFECT OF EXPLOSIVE LOADING AND HEAT TREATMENT ON
THE MECHANICAL PROPERTIES OF 6061 ALUMINUM ALLOY EXPLOSION WELDS

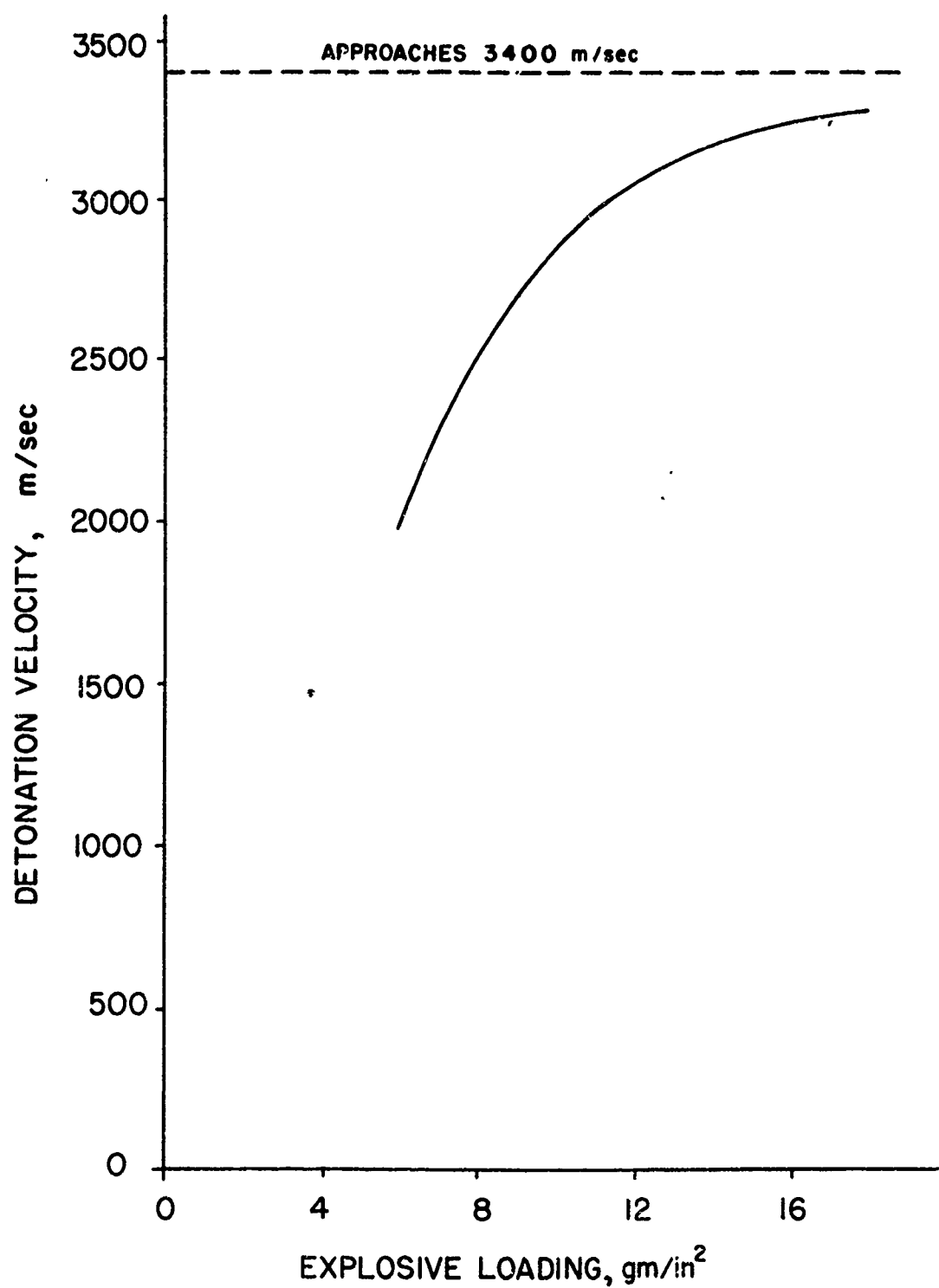
Precipitation hardened aluminum alloys are a convenient vehicle for the study of explosion weld effects. These alloys in the optimum precipitation (T6) condition have high tensile strengths relative to the annealed (O) condition. The solution treated (T4) condition and the (T6) condition can be sharply modified by relatively low temperatures. The recovery of cold work is also affected by relatively low temperatures. In general, the mechanism of strengthening involves precipitate-dislocation and to some extent point defect interactions, all of which are subject to modification by explosive shock, high strain rate flow and moderate temperatures that accompany explosion welding. Precipitation hardened aluminum alloys are difficult to fusion weld. The characterization of their explosion weldability and resulting properties should contribute to applications development. Additionally, information about the combined effects of shock pressure and high strain rate flow should result from the determination of explosion welding effects on properties and microstructure.

Aluminum alloy 6061 was used exclusively in this study because of its widespread commercial use and the relative ease with which explosion welding can be achieved (relative to 2000 and 7000 series alloys). All explosion welding was accomplished using 1/4 in. thick by 6 in. wide by 12 in. long specimens saw cut from commercial plate stock. A uniform standoff of 1/8 in. was used in all cases. The parallel aluminum plates were supported by a 4 in. thick steel anvil during welding. The explosive, du Pont Red Cross 40 percent extra dynamite, was detonated parallel

to the 12 in. plate length. The explosive was contained in a posterboard box in direct contact with the flyer plate surface. The detonation velocity of the dynamite on aluminum as a function of explosive loading is shown in Figure 12. The explosion welding configuration is shown in Figure 2. Surface condition was standardized by dipping the rolled plate finish into a hot caustic solution and washing in water until a smooth bright metal appearance resulted.

The initial task was the determination of optimum explosive loading conditions for 6061 alloy in the annealed (O), solution treated (T4), and precipitation hardened (T6) condition. Previous work had shown the 1/8 in. standoff (1/2 the flyer plate thickness) to be near optimum for 6061 alloy using the Red Cross 40 percent dynamite. Therefore, standoff was not included in the present weld parameter optimization. It should be realized, however, that optimum weld strength is probably not a single valued function but can be obtained with numerous explosive, explosive loadings and standoff combinations. The parameter optimization represents a particular solution to a general problem.

Parallel 6061 aluminum plates were explosion welded in the (O), (T4), and (T6) condition using the technique described above and explosive loadings ranging from 6g/in.² to 14g/in.² of Red Cross 40 percent dynamite. Four tensile samples of the type shown in Figure 3 were cut from the welded plates. Two tensile specimens were removed at 1/2 and 3/4 of the plate length measured from the initiation end. These samples were tested on a 60,000 pound capacity Tinius Olsen machine. The maximum load (usually the fracture load) was recorded and divided by the bond area (.25in.²)



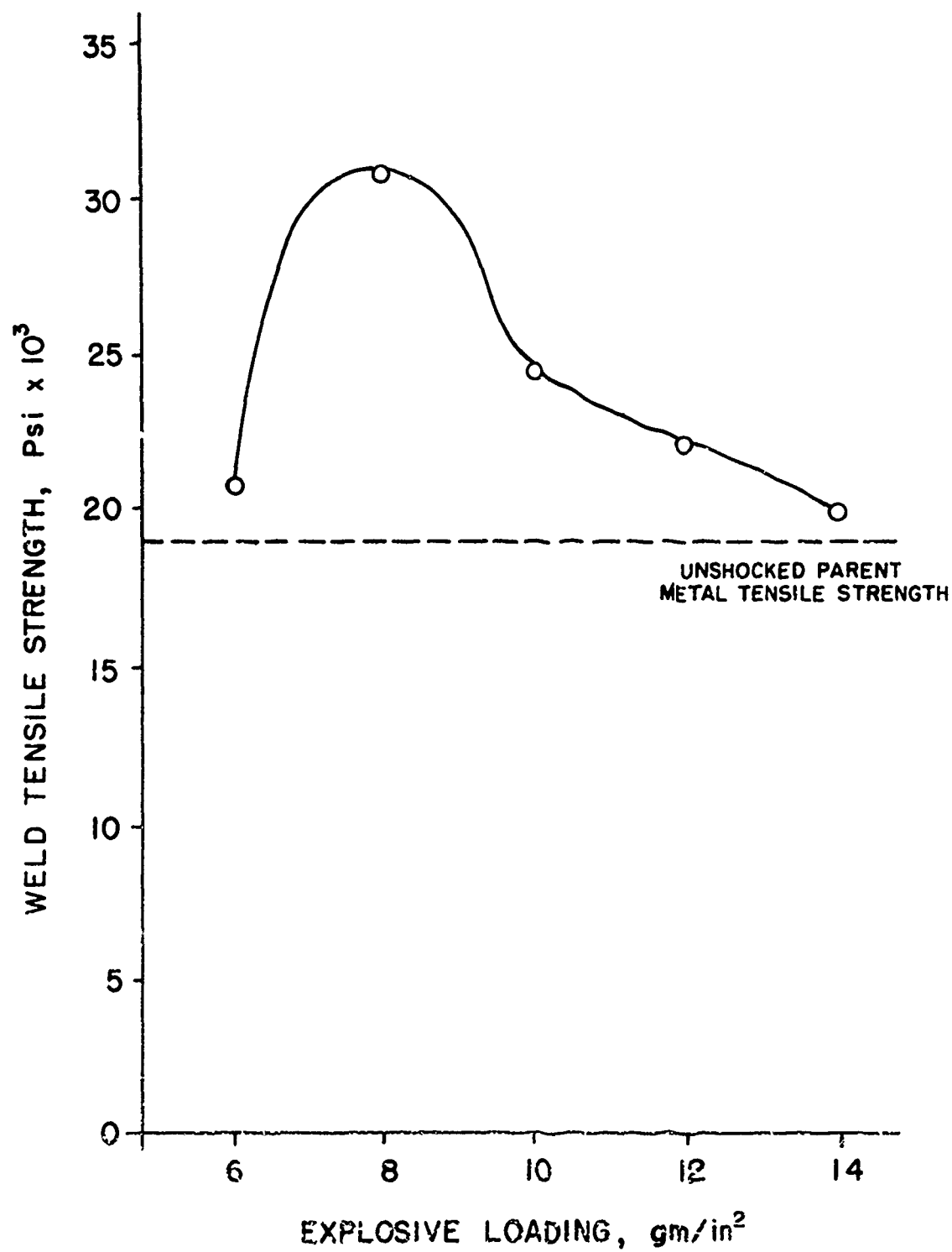
to determine the weld tensile strength. The average weld tensile strength for each explosive loading and initial heat treatment is graphically displayed in Figures 13, 14, and 15.

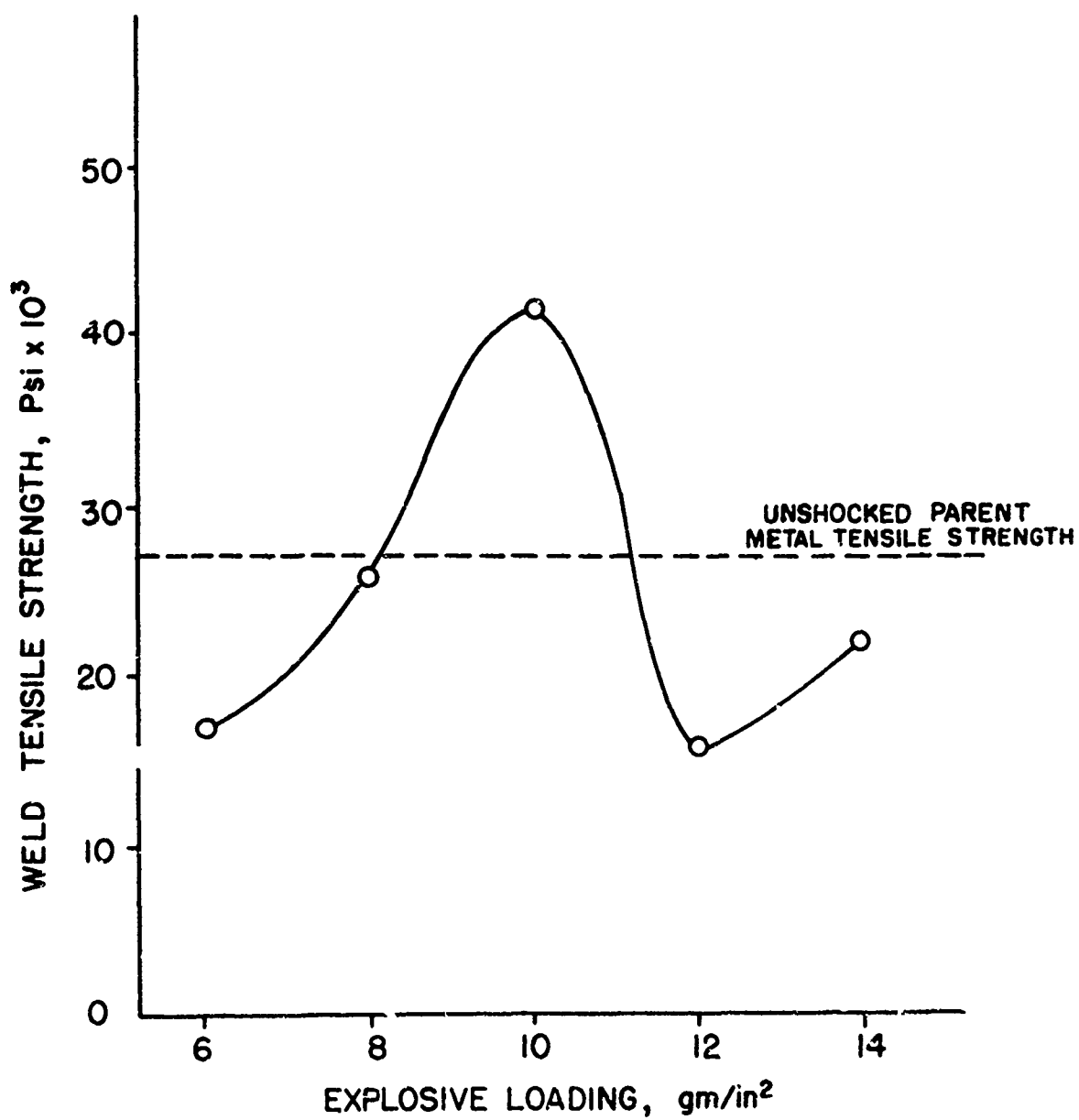
Perhaps the most striking feature of the weld tensile data is the degree to which the strength can exceed parent metal tensile strength. The high weld strength is not a function of the unique test geometry, although the parent metal strengths shown were derived from 2 in. gauge length tensile specimens. The weld tensile specimen when cut from homogeneous plate has been shown to give results identical to those of conventional plate tensile specimens. Hardness tests show a considerable increase in hardness near the weld interface and to a lesser degree at the flyer plate surface. Final interface and surface hardness were about the same for all explosive loadings. Typical results are listed in Table I.

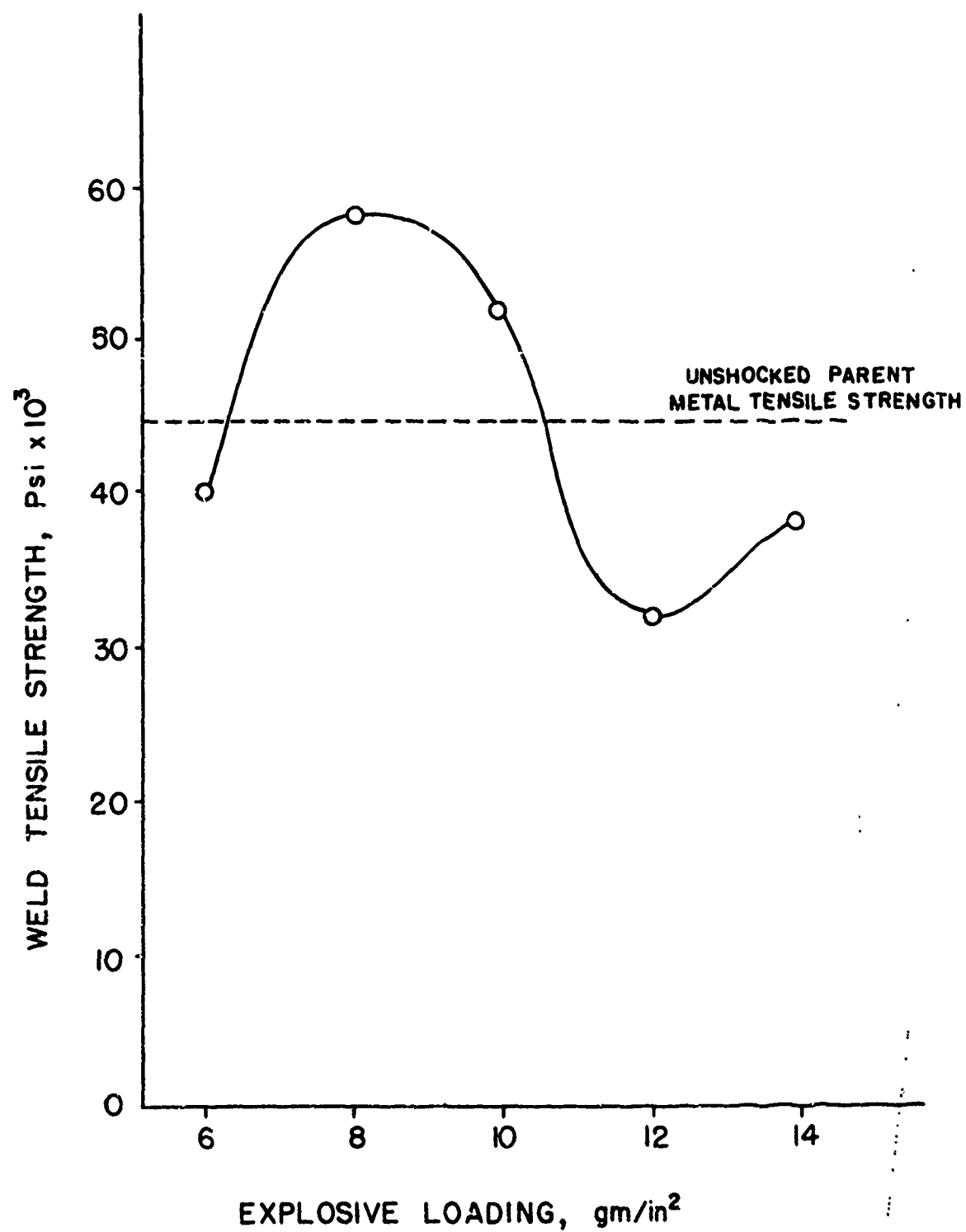
Table I. Brinell Hardness of Explosion Welded
6061 Aluminum Alloy

<u>Initial Weld Condition</u>	<u>Initial Hardness</u>	<u>Surface Hardness</u>	<u>Interface Hardness</u>
Annealed (O)	38	48	60
Solution Treated (T4)	55	94	90
Hardened (T6)	90	110	118

In the case of the 6061-O condition, the increase in hardness and strength must reflect the shock wave strengthening and local work hardening that accompany the formation of the wavy interface. The extreme local flow can be seen in Figure 16. The tensile strength which is a measure of the







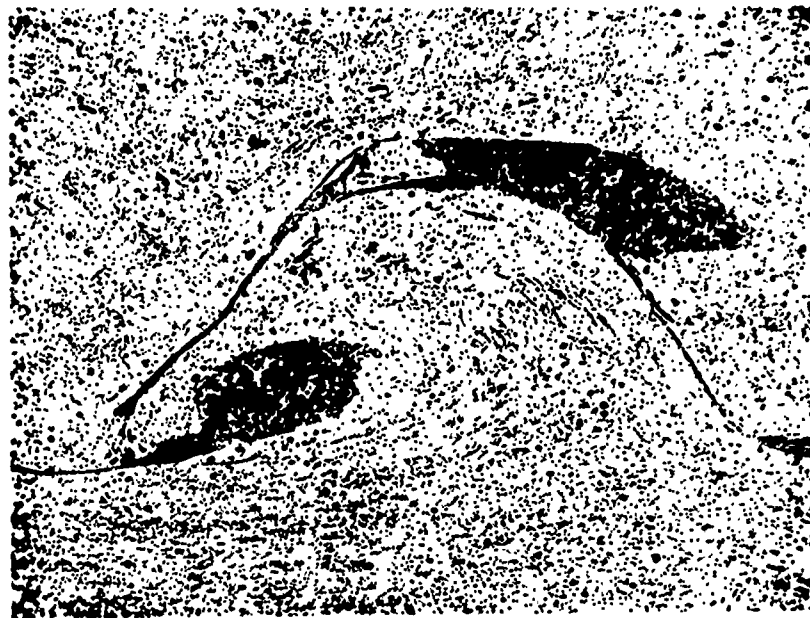


Figure 16. 6061-T6 Aluminum Explosion Weld Interface.
8g/in² of Red Cross 40% Dynamite and 1/8 in. Standoff.
100X Magnification.

Large Dark Regions are Porous Solidified Melt Pockets
that have been overetched by the HF-H₂O Reagent.

strength in the vicinity of the weld interface by virtue of the test specimen design, therefore, reflects the strength of that deformation region. Reduction of strength below the maximum attainable for the deformation strengthened state is attributable to defects along the weld interface. These defects become more populous at the higher explosive loads. One or all of the following types of defects are observed at the interface of the (O), (T4), (T6) welds:

1. Melt pocket solidification voids.
2. Hot tears associated with melt solidification and thermal contraction.
3. Cracks attributable to shear strains resulting from extreme flow gradients.

The fracture surface was not associated with the weld interface at the 6, 8, and 10g/in.² explosive loadings used with the (O) condition. The fracture occurred at 45° to the tensile axis in these specimens. At the 12 and 14g/in.² load fracture occurred along the wavy interface at 90° to the tensile axis. The weld tensile strengths were very consistent from specimen to specimen regardless of the fracture behavior.

The 6061-T4 results were not as consistent. There was considerable scatter in the weld tensile strengths. Most of the explosive loading conditions were by necessity repeated several times; each repeat having about as much scatter from point to point in one plate as the last. Some test values (both high and low) were discarded as being non-typical. For example, at the 10g/in.² loading one specimen failed at 48,000 psi and one failed at 10,000 psi. Similar scatter was observed in all but the highest explosive

load ($14/\text{in.}^2$) condition. In every case fracture occurred along the wavy interface at 90° to the tensile axis of the (T4) specimens. The relationship between this fracture pattern and microstructure is not clear at the present time. A typical as-welded microstructure is shown in Figure 17. The general form of the weld tensile strength curve is believed to represent typical results that can be expected at the various explosive load conditions. Perhaps other parameter combinations would yield more consistent results.

Examination of the hardness data in Table I and subsequent microhardness data indicates that precipitation hardening due to the heat produced during welding of the (T4) alloy is more responsible for the hardness and strength increase than combined shock and work hardening. Note the surface hardness is higher than the interface hardness which may indicate the interfacial region has actually been overaged. The number of weld defects are observed to increase at both the $12\text{g}/\text{in.}^2$ and $14\text{g}/\text{in.}^2$ explosive loadings; thus probably being the major contributor to reduced weld strength as hardness data is generally the same for all explosive load conditions.

The (T6) aluminum alloy welds exhibited both high strength and consistent results from plate to plate and point to point within a single welded plate. At the $8\text{g}/\text{in.}^2$ and $10\text{g}/\text{in.}^2$ explosive load conditions the tensile fracture occurred outside the weld zone. The fracture surface was inclined at 45° to the tensile axis. At the other load conditions failure occurred along the wavy interface at 90° to the tensile axis. The increase in weld tensile strength above parent metal strength is due



Figure 17. 6061-T4 Aluminum Explosion Weld Interface.
10g/in² of Red Cross 40% Dynamite and 1/8 in. Standoff.
100X Magnification.

primarily to deformation (shock and flow) hardening as comparison of hardness and strength data would indicate. Reduction in strength below the maximum attainable can be attributed to the three types of weld defects listed previously. Microhardness profiles indicate little evidence of local annealing due to heat generated in the weld interface. Parent metal hardness is maintained to within a few thousands of an inch from solidified melt pockets. A typical microstructure showing the extreme flow deformation pattern is shown in Figure 18.

In an effort to learn more about the effect of explosion welding on the properties and structure of 6061 alloy and to develop heat treating information useful in product applications, explosion welds of maximum weld tensile strengths for the (O), (T4), and (T6) initial conditions were subjected to isochronal anneals at temperatures up to 775°F. The weld tensile strength and Brinell hardness of the annealed samples were determined and compared to unshocked parent alloy and to cold rolled alloy subjected to the same isochronal annealing schedule.

Using the weld tensile strength-explosive loading data, a series of explosion welds were made to obtain maximum as-welded strength for use in isochronal annealing. The explosion welds were made using the techniques described previously. An explosive loading (Red Cross 40 percent dynamite) of 8g/in.² was used for the (O) and (T6) initial condition and 10g/in.² for the (T4) initial condition. A total of 54 tensile samples were cut from the welded plates. The as-welded strength was first determined for each plate. Plates which had weld strengths less than expected were rejected for use in isochronal annealing in the present study. However,

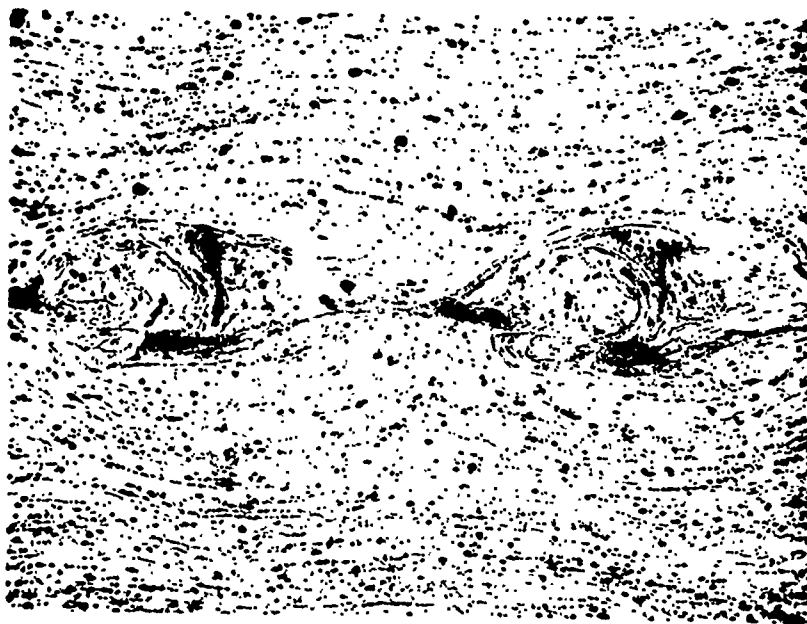
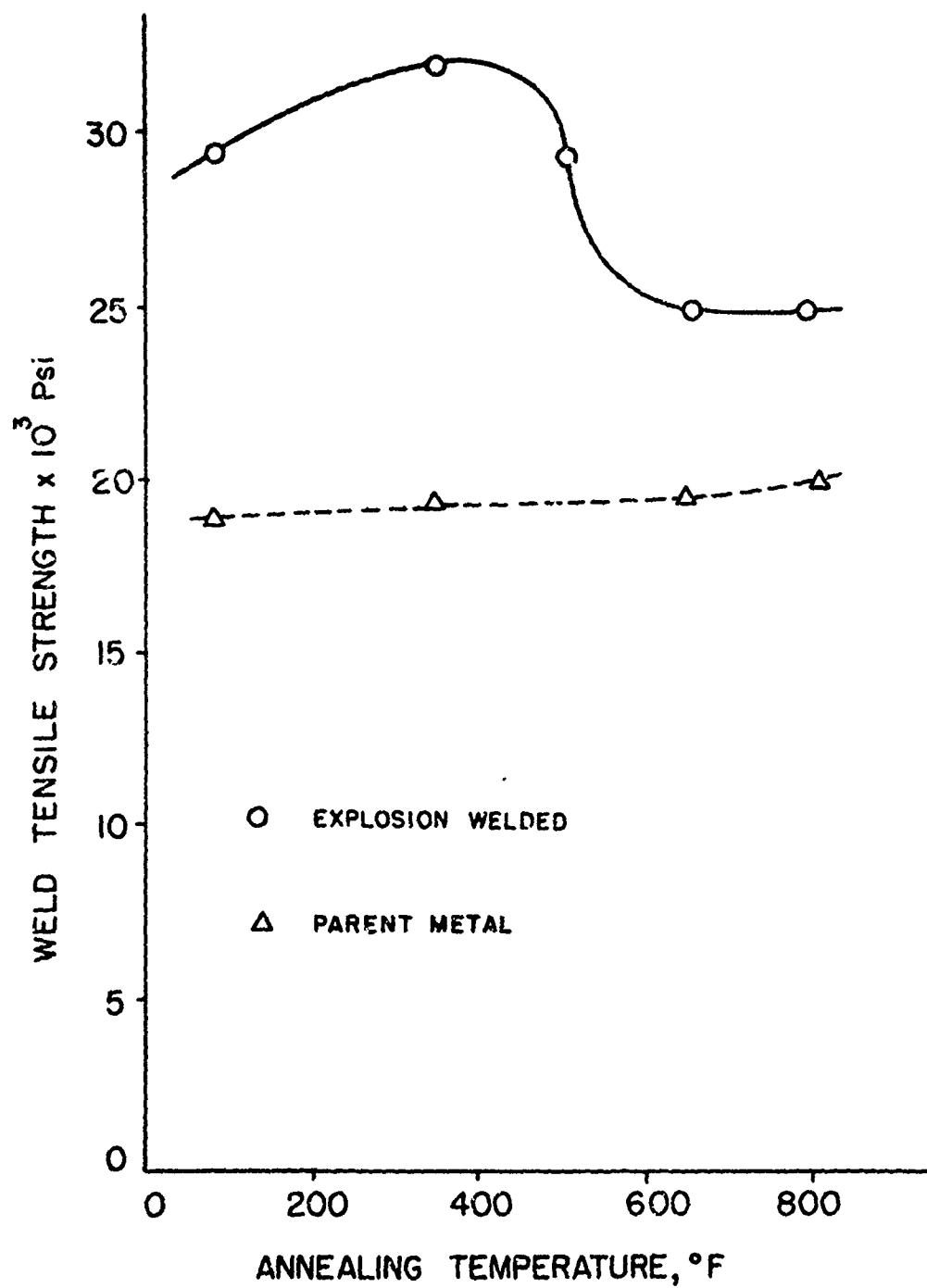


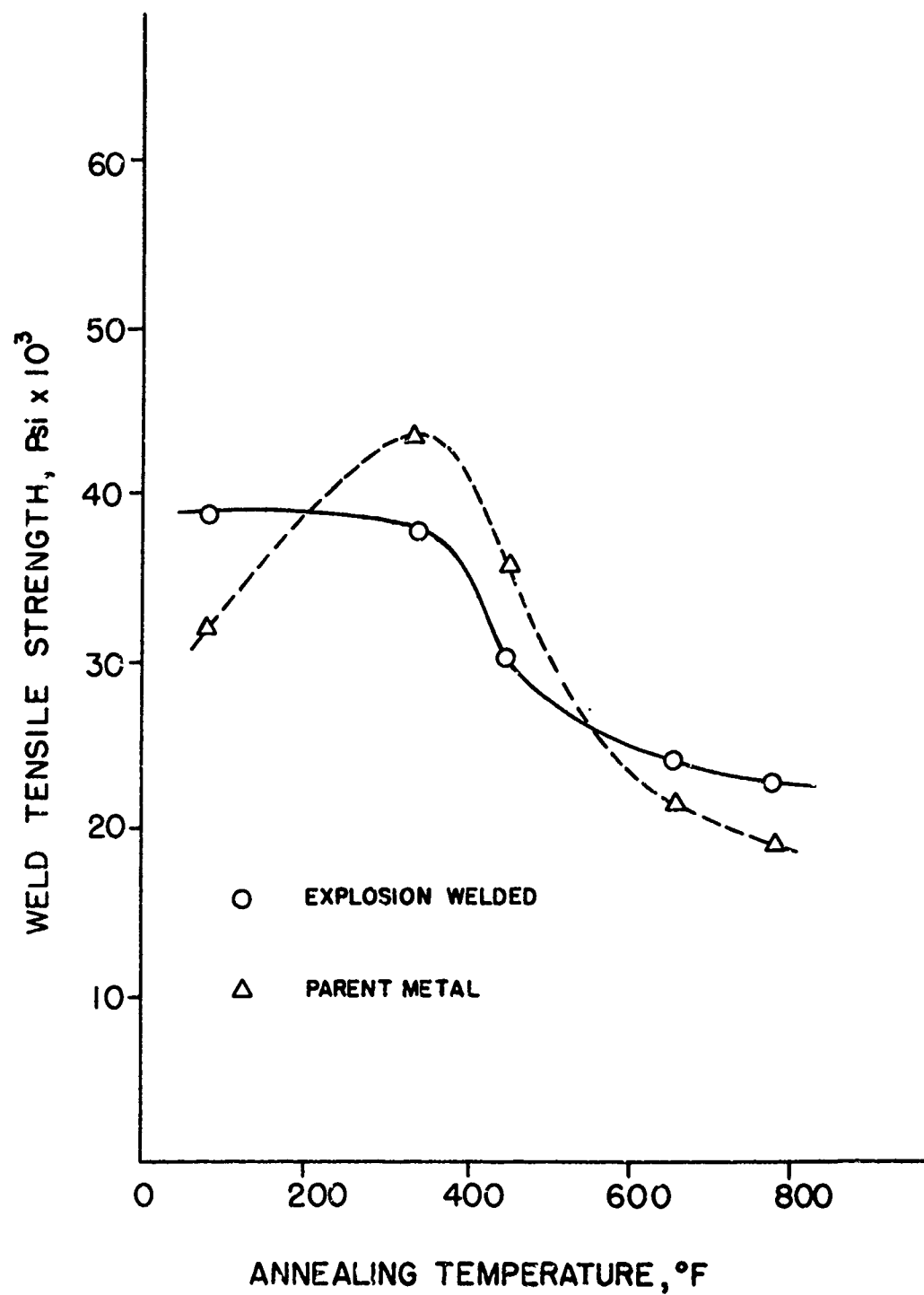
Figure 18. 6061-T6 Aluminum Explosion Weld Interface.
8g/in² of Red Cross 40% Dynamite and 1/8 in. Standoff.
100X Magnification.

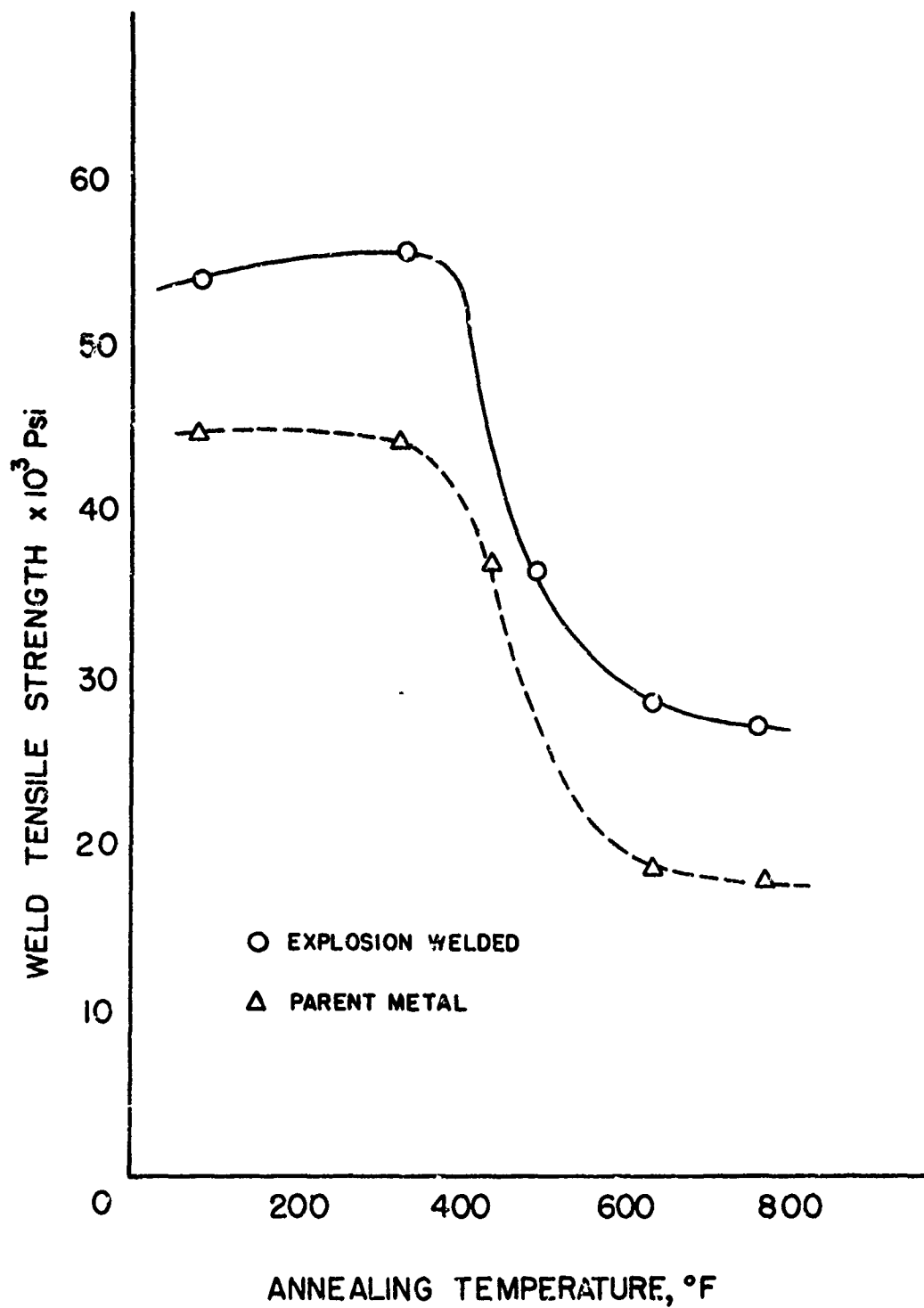
the effect of heat treatment on non-optimum welds will be considered during continued investigation.

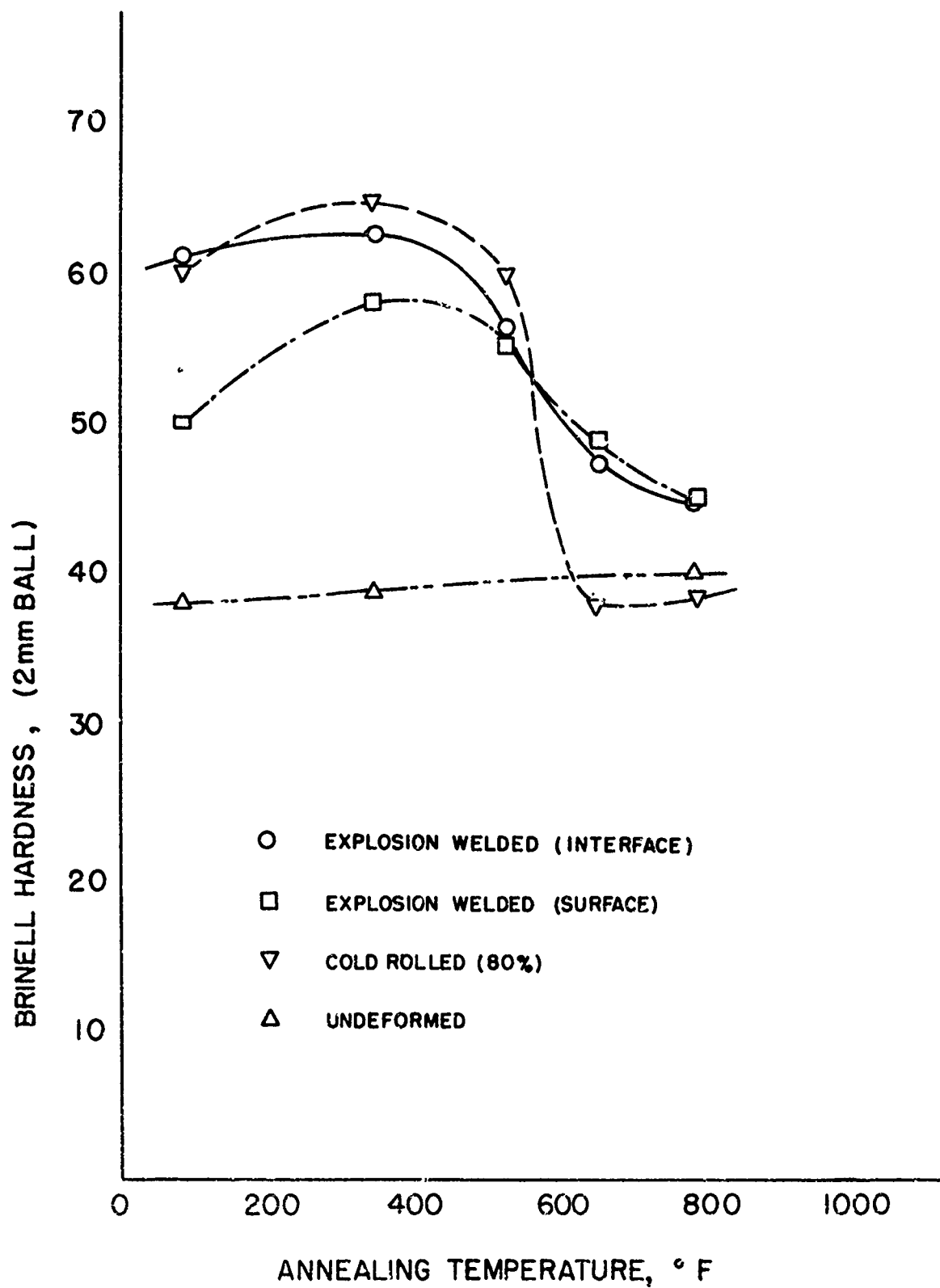
The explosion welded interface and plate surface Brinell hardness was determined for the (O), (T4), and (T6) initial condition. Then 6061 alloy plates in the same initial heat treatment were cold rolled to the approximate hardness of the corresponding explosion welded alloy condition. These plates were used to compare strength and hardness recovery of the conventionally deformed condition with the high strain rate deformation of explosion welding. In addition, samples of undeformed 6061 alloy in the (O), (T4), and (T6) initial condition were prepared for inclusion in the isochronal annealing sequence.

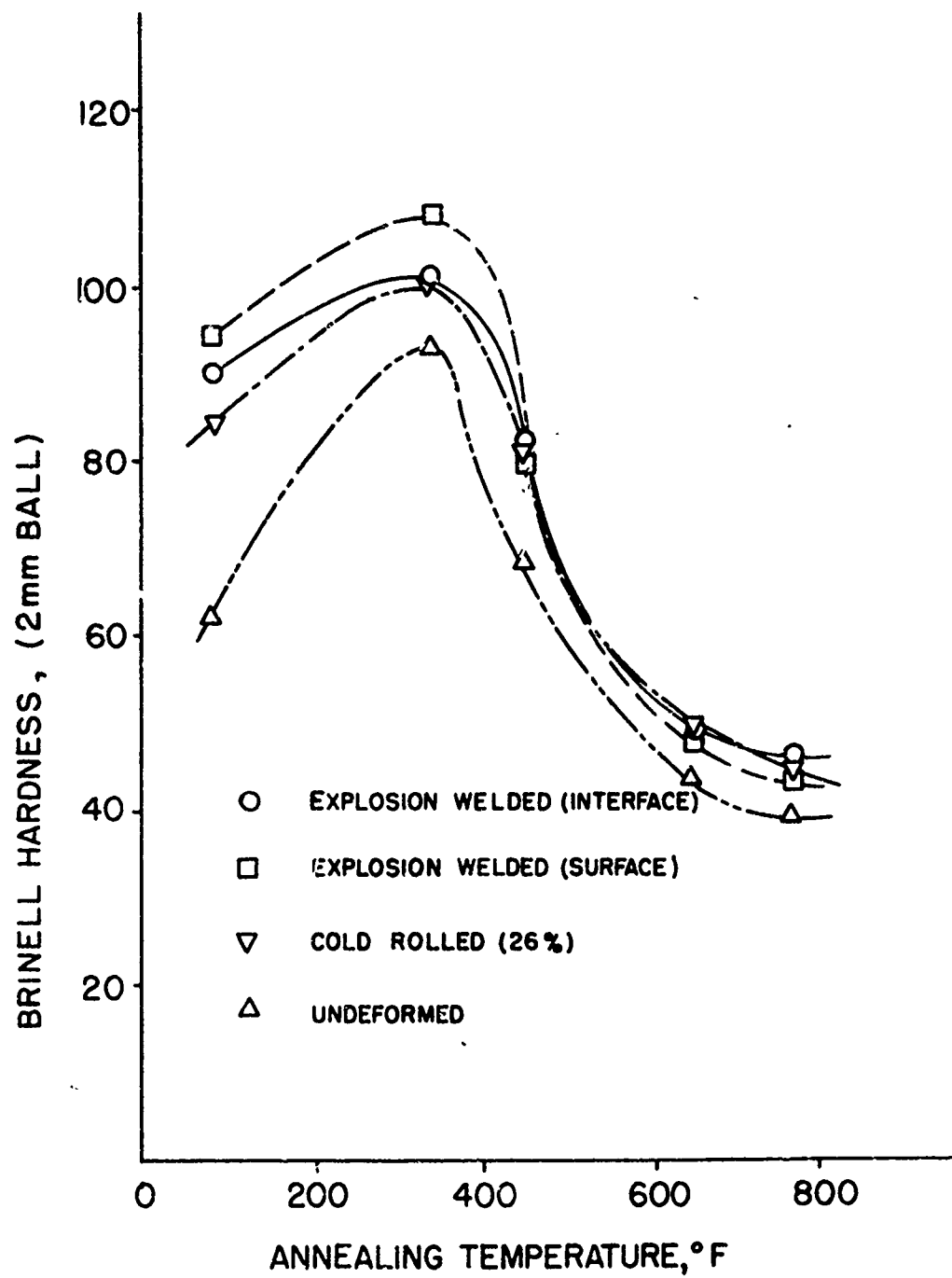
Annealing of the explosion welded, cold rolled, and undeformed aluminum alloy was conducted in an air atmosphere, electric muffle. The annealing time was three hours at temperatures of 350°F, 450°F or 500°F, 650°F, and 775°F. Tensile samples of the type shown in Figure 3 were prepared for each annealing condition and tested on a Tinius Olsen machine. The maximum load was recorded and ultimate tensile strengths were calculated for the .25/in.² tensile samples. Brinell hardness data was taken at the surface and interface of each welded and annealed sample and at the surface of each cold rolled and undeformed sample. The weld tensile strength data for various annealing temperatures and initial heat treatments is displayed in Figures 19, 20, and 21. The Brinell hardness data for the different annealing temperatures and sample conditions is shown in Figures 22, 23, and 24. Photomicrographs of the as-welded interface of the (O), (T4), (T6) initial condition are shown in Figures 16, 17, and 18. Photomicrographs of the weld interface after 650°F heat treatment are shown in Figures 25, 26, and 27.

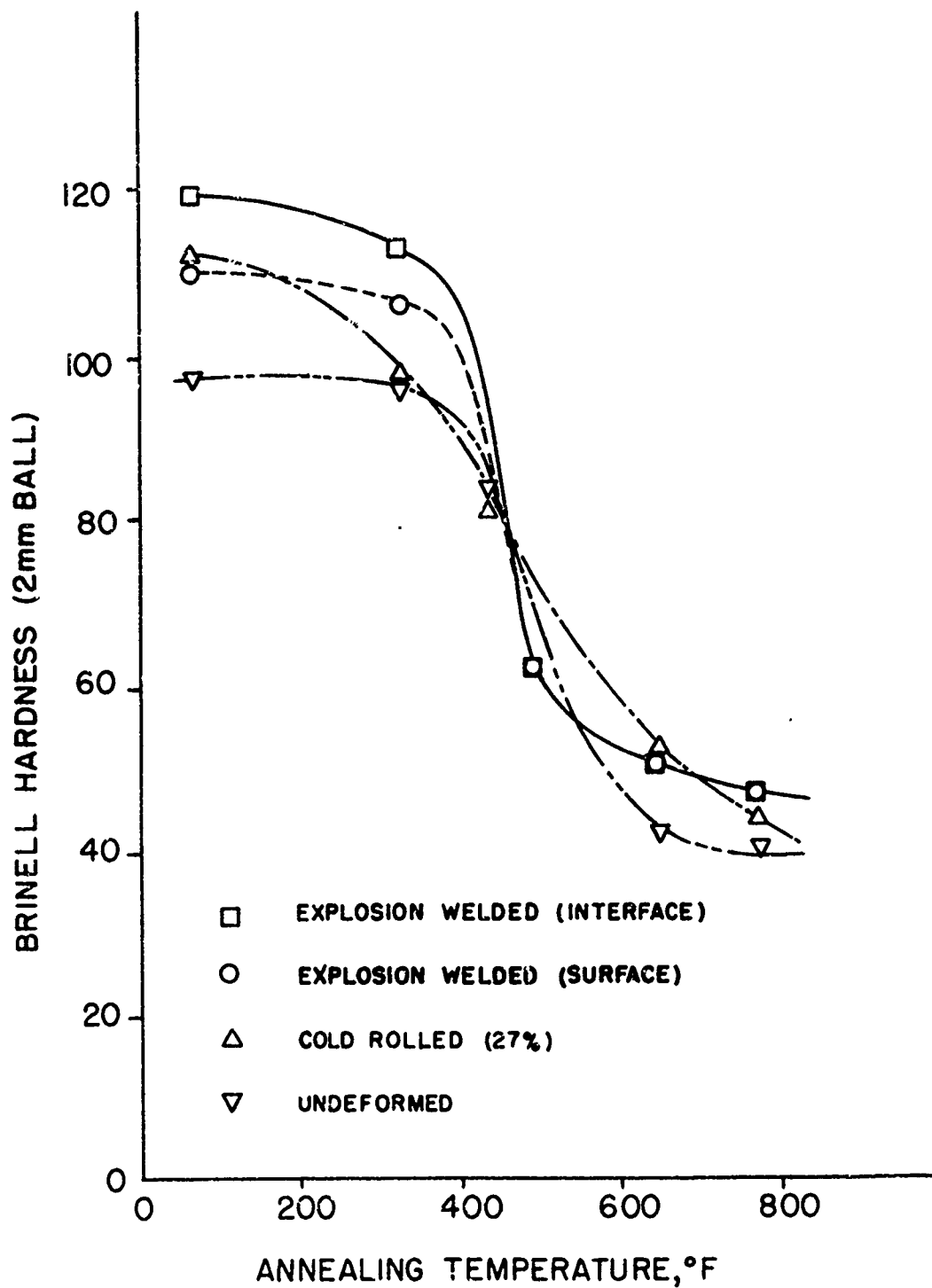












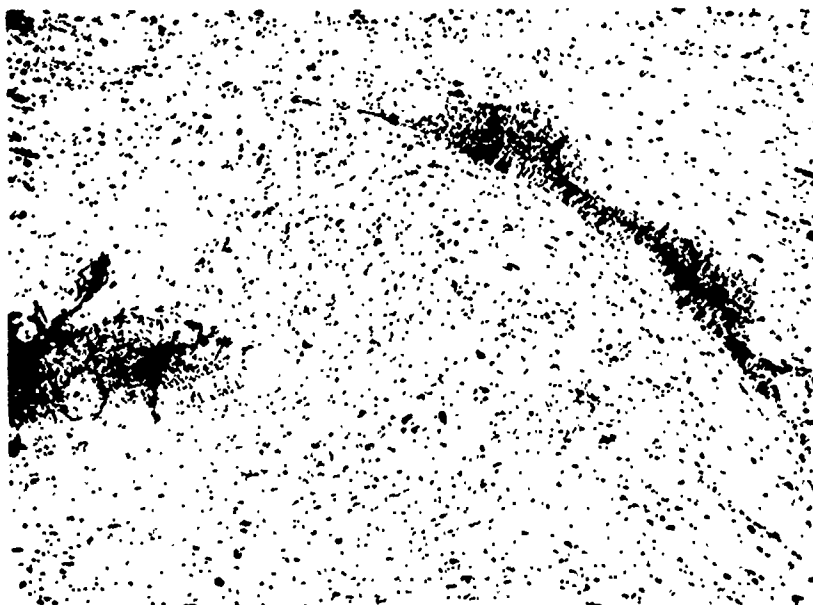


Figure 25. 6061-O Aluminum Explosion Weld Interface after Annealing at 650°F for 3 hr. Welded using 8g/in² Red Cross 40% Dynamite and 1/8 in. Standoff.

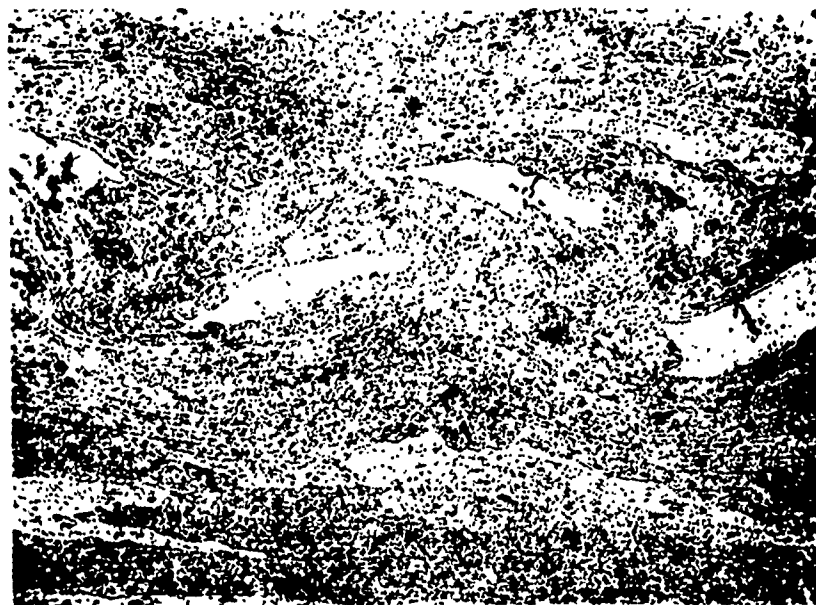


Figure 26. 6061-T4 Aluminum Explosion Weld Interface after Annealing at 650°F for 3 hr. Welded using 10g/in² Red Cross 40% Dynamite and 1/8 in. Standoff.



Figure 27. 6061-T6 Aluminum Explosion Weld Interface
after Annealing at 650°F for 3 hr. Welded using
8g/in² Red Cross 40% Dynamite and 1/8 in. Standoff.

Examination of the hardness and tensile strength results after annealing reveal several effects of interest. Perhaps the most practical result at the present time is the observation that fracture occurs after some plastic extension when the annealing temperature equals or exceeds the 450° or 500°F value. After the 350°F heat treatment and in the as-welded condition, fracture occurred abruptly with no observable plastic extension even when the failure was at 45° in parent metal. At or above the 450°F temperature restoration of ductility occurs either by recovery of cold work and/or by overaging the the (T4) or (T6) condition. In applications where weld ductility is most important a low temperature, anneal may be necessary for best performance. For example, Figure 21 indicates that a 450°F anneal would yield a weld tensile strength equivalent to the unshocked, unannealed 6061-T6 tensile strength. A 500°F anneal would sacrifice only 22 percent of the parent metal tensile strength while gaining a large amount of weld ductility.

A second point of interest is the higher strength and hardness after annealing in the 650°F to 775°F range as compared to either cold rolled or undeformed alloy. The tensile strength of the 6061-T6 alloy after annealing at 650°F and 775°F was approximately 50 percent higher than undeformed 6061-T6 annealed at the same temperatures. A smaller increase in weld tensile strength over undeformed parent metal strength was noted for the (T4) and (O) condition. The Brinell hardness does not reflect the weld tensile strength improvement except for the (O) weld condition. Additional examination of the microstructure will be needed to determine the cause of this behavior.

It was expected 6061 alloy in the (T4) condition, with greater ductility than the (T6) condition, would have greater explosion weldability. If so, then it would be simple to heat treat the explosion welded (T4) condition to the (T6) condition. However, Figure 23 indicates the strength and hardness after annealing at 350°F for three hours do not respond in a parallel manner. The hardness increases to 108 Brinell indicative of high base metal strength while the weld tensile strength remains constant during the same heat treatment. This would indicate that weld defects play the dominant role in determining weld tensile strength, not the increased plate strength developed by post weld heat treatment. Apparently welding in the (T4) condition and subsequent strengthening by heat treatment is not a feasible method of producing a (T6) weld strength condition.

The explosion weldability of 6061 alloy is maximum in the annealed condition. High joint strengths can be produced over a wide range of explosive loadings. It is likely that many other explosive, explosive loading, and standoff combinations would produce equally good results. Heat treatment after welding in the (O) condition is of no benefit since the as-welded ductility is adequate. In the (T6) condition 6061 aluminum alloy is much more sensitive to explosive loading conditions. Welds exceeding parent metal strength with ductile fracture behavior can be achieved over a range of explosive loadings that would be practical to achieve with Red Cross 40 percent dynamite or similar explosive compositions. Heat treatment after welding at a temperature of approximately 500°F will sacrifice some weld strength but greatly increase weld ductility. The 6061-T4 alloy is the most difficult to explosion weld. Only a narrow range of explosive

loadings can produce parent metal strength. The normal scatter in granular explosive detonation behavior, combined with the thermal and mechanical instability of the (T4) condition, make this alloy the least weldable of the three conditions evaluated.

Examination of weld strengths, hardness data, and microstructures indicate that melt solidification structure is the major factor determining weld strength in the (T4) and (T6) condition. The (O) condition and the nickel weld strength reported in the preceding section are primarily affected by work hardening. The steel weld strength at one series of impact conditions was controlled by a thermally produced phase transformation. These observations clearly indicate the importance of metallurgical and physical characteristics in determining explosion weldability.

REFERENCES

1. S. H. Carpenter, R. H. Wittman, and R. J. Carlson, "The Relationship of Explosive Welding Parameters to Material Properties and Geometry Factors," Proceedings of First International Conference of the Center for High Energy Forming, Estes Park, Colo. 1967.
2. S. H. Carpenter, and M. Nagarkar, "The Effects of Explosive Welding on the Kinetics of Metallurgical Reactions," Proceedings of the Third International Conference of the Center for High Energy Forming, Vali, Colo. 1971.

APPENDIX A

Papers and Publications by the Center Staff On Explosive Fabrication and Related Effects

Ezra, A. A. and Kulkarni, S. B., "The Design and Analysis of Explosive Forming Thin Shell Dies." To be presented at the Thirteenth International Machine Tool Design and Research Conference, Birmingham, England, Sept. 1972.

Kaplan, M. and Kulkarni, S. B., "An Investigation of the Edge Pull-in in Explosively Formed Domes." To be presented at the Thirteenth International Machine Tool Design and Research Conference, Birmingham, England, Sept. 1972.

Kaplan, M., Glick, H., Knight, R. E., D'Souza, V., and Howell, W., "The Radial Piston Approach to the Dynamic Autofrettage of Thick Walled Forging Dies." To be presented at the Thirteenth International Machine Tool Design and Research Conference, Birmingham, England, Sept. 1972.

Carpenter, S. H., Wittman, R. H. and Carlson, R. J., "The Relationship of Explosive Welding Parameters to Material Properties and Geometry Factors." Proceedings 1st International Conference of the Center for High Energy Forming, 1.2.1 (1967).

Carpenter, S. H. and Otto, H. E., "Explosive Welding of Lead to Steel." Trans. AIME, 1866, 239 (1967).

Carpenter, S. H., "Theory and Application of Explosive Welding," ASTME Creative Manufacturing Engineering Program, Chicago, 1969, Paper No. AD69-108.

Carpenter, S. H., "Dislocation Damping of Explosively Shocked Polycrystalline Copper." Phil Mag, 17, 855 (1968).

Carpenter, S. H. and Nagarkar, M., "The Effects of Explosive Welding on the Kinetics of Metallurgical Reactions." Proc. 3rd International Conference, Center for High Energy Forming, (1971).

Carpenter, S. H., Wittman, R. H., and Otto, H. E., "Explosion Welding Research at the University of Denver." Proc. Eleventh International Machine Tool Design and Research Conf., Birmingham, England, Sept. 1970.

Ching, L. K., and Weese, J. A., "The Explosive Forming of Rings." Proceedings 2nd International Conference of the Center for High Energy Forming, 1969.

Ezra, A. A., "The Use of Scale Models in Explosive Forming." 2nd International Symposium on High Energy Rate Metal Working, Prague, Sept. 1966.

Ezra, A. A., "Explosive Metal Forming," High Velocity Metal Working Seminar, Midwest Research Institute, Kansas City, Missouri, ASTRA, 1-46 (1966).

Ezra, A. A. and Malcolm, M., "An Investigation of the Effect of Explosive Stand-off Distance on the Forming of Metal Blanks." Proceedings 1st International Conference of the Center for High Energy Forming, June 1967, Vol. 2, pp. 6.4.1-6.4.20 (1968).

Ezra, A. A., "The Outlook for High Energy Forming." Frontiers in Metalworking, The Second Symposium on Methods of Materials Selection, University of Florida, Gainesville, Florida, (1967). To be published in Metals Progress.

Ezra, A. A., "Overcoming Barriers in R&D Coupling." Office of Aerospace Research Report, OAR 69-0005, March 14, 1969.

Ezra, A. A., "Explosive Forming of Metals." Proc. CIRP (International Conf. Manufacturing Technology, Ann Arbor, Mich., Sept. 25-28, 1967). Published by American Society of Tool and Manufacturing Engineers, Dearborn, Mich., 775-799, (1967).

Ezra, A. A., "Advances in the Theory of Explosive Metalworking." ASTM Fall Meeting, Atlanta, Ga., Sept. 29-Oct. 4, 1968, Journal of Materials, J.M.L.S.A., Vol. 4, No. 2 (1969).

Ezra, A. A., "Principles and Procedures for the Explosive Forming of Large Domes from Flat Blanks." Technical paper presented at ASTM Engineering Conference. Published by American Society of Tool and Manufacturing Engineers, Dearborn, Mich., No. MF69-186 (1969).

Ezra, A. A. and Adams, J. E., "The Explosive Forming of Ten Feet Diameter Aluminum Domes." Proc. 1st International Conference of the Center for High Energy Forming, June 1969, Vol. 1, pp. 3.2.1-3.2.75 (1968).

Ezra, A. A. and Peterson, H. C., "Interaction of an Underwater Shock Wave with a Deforming Circular Plate." Proc. 2nd International Conf. of the Center for High Energy Forming, June 1969, Vol. 1, pp. 3.1.1-3.1.-12 (1969).

Gilbert, L. E. and Lawrence, W. N., "Design of Electromagnetic Swaging Coils." Proc. 2nd International Conference of the Center for High Energy Forming (1969).

Harding, J., Kulkarni, S. B., and Ezra, A. A., "The Explosive Punching of Metals." Proc. 2nd International Conference of the Center for High Energy Forming, June 1969, Vol. 2, pp. 8.4.1-8.4.30 (1969).

Hardee, P., "Explosive Forming with Vented Dies." Proc. 3rd International Conference of the Center for High Energy Forming, 1971.

Hoggatt, C. R. and Recht, R. F., "Stress-Strain Data Obtained at High Rates Using an Expanding Ring." Presented at 1969 SESA Spring Meeting, Philadelphia, Pa., May 13-16, 1969, Experimental Mechanics, Oct. (1969).

Hoggatt, C. R., Orr, W. R. and Recht, R. F., "The Use of an Expanding Ring for Determining Tensile Stress-Strain Relationships as Functions of Strain Rate." Proc. 1st International Conference of Center for High Energy Forming (1967).

Hoggatt, C.R. and Recht, R. F., "Stress-Strain Data Obtained at High Rates Using an Expanding Ring." Experimental Mechanics 9, #10, Oct. (1969).

Hoggatt, C. R. and Recht, R. F., "Dynamic Stress-Strain Relationships Determined from Expanding Ring Experiments." Proc. 2nd International Conference of Center for High Energy Forming, June 1969.

Howell, W., "Explosive Welding of Pipeline Joints." Proc. 3rd. International Conference of Center for High Energy Forming, 1971.

- W. Howell, "Explosive Strengthening of Forging Dies," Ibid.
- W. Howell and A. R. Dowling, "Explosive Punching of High Strength Steel," 2nd Int'l. Conf. of Center for High Energy Forming, 1969.
- M. Kaplan and H. Boduroglu, "Lateral Flange Instability in the Formation of Domes," Proc. 3rd Int'l. Conf. of Center for High Energy Forming, 1971.
- W. N. Lawrence, "Scale Modelling Calculations for Electromagnetic Forming," Proc. 2nd Int'l. Conf. of Center for High Energy Forming, 1969.
- S. Mahajan, "The Inhibition of Shock Twinning in Prestrained Armco Iron," Proc. 1st Int'l. Conf. of Center for High Energy Forming, 7.7.1 (1967).
- S. Mahajan, "Twins and Complementary Twins in Shock Hardened Iron," Phil. Mag. 19, 199 (1969).
- S. Mahajan, "Shock-Induced Substructural Changes in Prestrained Iron," phys. stat. Vol. 33, 291, (1969).
- S. Mahajan, "Twins and Anti-Twins in Polycrystalline Armco Iron," presented at Fall Meeting of AIME, Cleveland, Oct. (1967).
- S. Mahajan, "Interactions Between Slip Dislocations and Deformation Twins in FCC Metals," presented at Fall Meeting of AIME, Cleveland, Oct. (1967).
- S. Mahajan, "The Early Stages of Shock-Induced Recrystallization in Prestrained Armco Iron," presented at Annual Meeting of AIME, New York, Feb. (1968).
- R. P. Mikesell, "The Fatigue Behavior of Formed 2014 Aluminum," Proc. 2nd Int'l Conf. of Center for High Energy Rate Forming, 1.3.1, June 1969.
- R. N. Orava, "The Effect of Dynamic Strain Rates on Room Temperature Ductility," 1st Int'l Conf. of Center for High Energy Forming, 7.5.1 (1967).
- R. N. Orava, "The Influence of Strain Rate on Room Temperature Ductility," presented at Fall Meeting of AIME, Cleveland, Oct. (1967).
- R. N. Orava, "The Effect of Strain Rate on Plastic Instability, presented at 2nd Int'l. Conf. on Strength of Metals and Alloys, Pacific Grove, Ca., Aug. 30 - Sept. 4, 1970.
- R. N. Orava and H. E. Otto, "Discussion of the Effect of Explosive Forming on Fatigue Properties," Met. Res. Stds. 8, 45, April (1968).
- R. N. Orava and H. E. Otto, "The Effect of High Energy Rate Forming on the Terminal Properties of Aluminum Alloys," Proc. 2nd Int'l. Conf. of Center for High Energy Forming, 1.2.1 (1969).
- R. N. Orava, R. M. Mikesell, G. S. Whiting and H. E. Otto, "Tensile and Fatigue Properties of Explosively and Conventionally Formed 2014 Aluminum Alloy," Met. Trans. 2, 1675-1682, June (1971).

R. N. Orava and H. E. Otto, "The Effect of High Energy Rate Forming on the Terminal Characteristics of Metals--A Review," J. Metals 22, 17-31, Feb. (1970).

R. N. Orava and G. S. Whiting, "Relative Effects of Explosive and Isostatic Forming on Stress Corrosion Cracking in 2014 Aluminum Alloys," Fall Meeting AIME, Cleveland, No. 1970.

R. N. Orava and H. E. Otto, "Effect of Explosive Forming on the Properties of Titanium and Its Alloys," presented at Plastic Deformation Section, Metals Congress (1970).

R. N. Orava, H. E. Otto and R. P. Mikesell, "Tensile and Fatigue Properties of Explosively and Conventionally Formed 2014 Aluminum Alloys," Met. Trans. 2, 1675, (1971).

R. N. Orava and P. Khuntia, "The Relative Effects of Explosive and Isostatic Forming on Methanol Cracking in Titanium," Proc. 3rd Int'l. Conf. of Center for High Energy Forming (1971).

H. E. Otto and R. Mikesell, "The Shock Hardening of Structural Metals," Proc. 1st Int'l Conf. of Center for High Energy Forming, 7.61. (1967).

H. E. Otto, "Shock Hardening of Aluminum Alloys," Invited paper presented at 1969 WETEC Conf., ASM Tech. Paper W9-14.4.

H. E. Otto, "Shock Hardening of Aluminum Alloys," Metals Eng. Quart. 11, 62, (1971).

H. E. Otto and R. P. Mikesell, "Terminal Properties of Explosively Formed High Strength Low Alloy Steels," Proc. 3rd Int'l Conf. of Center for High Energy Forming (1971).

H. E. Otto and S. Carpenter, "High Energy Rate Swaging of Aluminum Pipe Connectors," Ibid.

A. G. Thurman and A. A. Ezra, "The Analysis and Design of Explosive Forming Facilities," Ninth Int'l Machine Tool Design and Research Conf., Birmingham, England (1968).

G. A. Thurston, "Plastic Strains in Circular Blanks Formed in Ellipsoidal Dies," Proc. 1st Int'l Conf. of Center for High Energy Forming, (1967).

G. A. Thurston with R. J. Harris, "Plastic Deformation of a Circular Membrane under Pressure," Developments in Mechanics, Vol. 5, Proc. of 11th Midwestern Mechanics Conf., Iowa State University Press, Ames, Iowa, pp. 669-684, Aug. (1969).

G. A. Thurston, "On the Effect of Edge Pull-In on the Explosive Forming of Domes," Proc. 7th Int'l. Conf. Advances in Machine Tool Design, Birmingham, England, Sept. 1966, Pergamon Press, New York, 129-143 (1967).

L. F. Trueb, "Lattice Defects in Explosion Shocked Nickel After Thermal Recovery," Proc. 2nd Int'l. Conf. of Center for High Energy Forming, 1.1.1, June 1969.

L. F. Trueb, "Explosive Metallbearbeitung," Neue Zürcher Zeitung, Technik, No. 571, 17-18, Sept. (1969)

L. F. Trueb, "An Electron Microscope Study of Thermal Recovery Processes in Explosion Shocked Nickel," J. Appl. Physics 40, 2976-2887, (1969).

L. F. Trueb, "Thermal Recovery Processes in Shocked Nickel," Proc. 27th Meeting of Electron Microscopy Society of America, St. Paul, Minn., ed. C. J. Arceneaux, Claitor's Publishing, Baton Rouge, La., 198-199 (1969).

L. F. Trueb and B. Hill, "Resistance to Corrosion and Stress Corrosion Cracking of Explosion Bonded Stainless to Steel Clads," Corrosion 25 (1) 23-29 (1969) and Proc. 1969 NACE Conf., Houston, Tex., Paper #75, 1-8 (1969).

L. F. Trueb, "Microstructural Effects of Heat Treatment on the Bond Interface of Explosively Welded Metals," Met. Trans. 2, 145-153 (1971).

G. S. Whiting, "Stress Corrosion Behavior of Explosively and Isostatically Formed 2014 Aluminum Alloy," M. S. Thesis, University of Denver, Aug. (1969).

V. R. Winchell, "High Pressure Bonding Within the Mo-Cu and Cr-Cu Alloy Systems," Ph.D. Thesis, University of Denver, June (1970).

R. H. Wittman, "Criteria for the Selection of the Explosion Welding Process," presented at ASTM Mid-Atlantic Engineering Conf., ASTM Paper No. AD69-820 (1969).

R. H. Wittman, "Explosion Bonding of Tubes to Tubesheets," Annual Winter Meeting ASME (Invited Paper), (1969).

C. Yin, "The Strengthening and Twinning of Explosively Formed HY80 Steel," M. S. Thesis, University of Denver (1970).

P. S. Yu and J. D. Mote, "X-Ray Measurements of Shock-Induced Stacking Faults in Copper and Alpha Brass," presented at Fall Meeting of AIME, Cleveland, Oct. (1967).

P. S. Yu, "X-Ray Measurements of Shock-Induced Stacking Faults in Copper and Alpha Brass," Ph.D. Thesis, University of Denver (1967).

Beck, W. A., and Rudy, J. F., "Production of Explosive Formed Five Foot Diameter Aluminum Domes," Proc. 1st Int'l Conf. of the Center for High Energy Forming, June 1967, Vol. 1, 3.4.1 - 3.3.24.

Borema, D. D., "Dynamic Strain Measurements During Explosive Forming," 2nd Int'l. Conf. of the Center for High Energy Forming, June 1969, Vol. 1, pp. 3.2.1 - 3.2.14.

Borema, D. D., "Strain Measurements Upon Blank and Die During Explosive Forming," 3rd Int'l. Conf. of the Center for High Energy Forming, July 1971, pp. 4.4.1 - 4.4.15.

Shuford, D. M., "The Chemical Milling of Explosively Formed Ten Foot Diameter Aluminum Domes," Proc. 1st Int'l. Conf. of the Center for High Energy Forming, June 1967, Vol. 1, 3.3.1 - 3.3.31.

Shuford, D. M., "Effect of Explosive Forming on Chemical Milling," Proc. 2nd Int'l. Conf. of the Center for High Energy Forming, June 1969, Vol. 1, 2.1.1 - 2.1.27.

Snyder, J. T. and Mote, J. D., "Fabrication of Joints on Rocket Propellant Tanks Using Explosive Bonding Methods," Society of Manufacturing Engineers, Technical Paper AD71-211, (1971).

APPENDIX E

Students Earning Advanced Degrees Supported by the Center for High Energy Forming

Department of Mechanical Sciences and Environmental Engineering

<u>Student</u>	<u>Degree</u>	<u>Date</u>	<u>Title of Thesis</u>
R. Harris	M.S.	1968	Numerical Solution for Membrane Deformation in the Hydrostatic Bulge Test
L. Ching	M.S.	1968	Response of Cylindrical Structures to Explosive Loads
L. Gilbert	M.S.	1968	Analysis and Design of Electro-magnetic Forming Coils
M. Malcolm	M.S.	1968	An Experimental Procedure for Determining Characteristics of Shock Waves from Underwater Explosion
G. Ney	M.S.	1969	Design of Cylindrical Explosive Forming Dies
P. Hardee	M.S.	1971	Explosive Forming with Vented Dies
R. Aderohunmu	M.S.	1971	Optimization of Explosive Forming of Tank Ends
S. Kulkarni	Ph.D.	1971	Prediction of Edge Pull-in In Explosively Formed Domes
H. Boduroglu	Ph.D.	1971	Lateral Flange Instability in the Formation of Domes

Department of Metallurgy and Materials Science

C. Yin	M.S.	1970	Strengthening and Twinning of Explosively Formed HY80 Steel
G. Whiting	M.S.	1969	Stress Corrosion Behavior of Explosively and Isostatically Formed 2014 Aluminum Alloy

Dept. of Metallurgy and Materials Science (Cont.)

D. Witkowsky	M.S.	1972	A Comparison of Conventional and High Energy Rate Metal Powder Compaction Utilizing Ancorsteel 1000 Iron Powder
J. Krupar	M.S.	1969	The Effect of Velocity of Forming on the Passivation of 304 L/C Stainless Steel
P. Yu	Ph.D.	1967	X-ray Measurements of Shock Induced Stacking Faults in Copper and Alpha Brass
V. Winchell	Ph.D.	1970	High Pressure Bonding within the Molybdenum-Copper and Chromium-Copper Alloy Systems

APPENDIX C

Graduate Students of the University of Denver Presently Working on Center for High Energy Forming Research Programs Expected to Finish Between 1972 and 1974

<u>Name of Student</u>	<u>Degree Expected</u>	<u>Department</u>
V. D'Souza	Ph.D.	Mechanical Sciences and Environmental Engineering
S. Aku	Ph.D.	Mechanical Sciences and Environmental Engineering
G. Rowell	Ph.D.	Mechanical Sciences and Environmental Engineering
A. Eriksen	M. S.	Mechanical Sciences and Environmental Engineering
A. Teotia	M. S.	Mechanical Sciences and Environmental Engineering
M. Nagarkar	Ph.D.	Metallurgy and Materials Science
D. Witkowsky	Ph.D.	Metallurgy and Materials Science
T. McClelland	Ph.D.	Metallurgy and Materials Science
R. Mikesell	Ph.D.	Metallurgy and Materials Science
R. Wittman	M.S.	Metallurgy and Materials Science
S. Stivers	M.S.	Metallurgy and Materials Science
M. de Carvalho	M.S.	Metallurgy and Materials Science